Dynamic Thermal Response of Buildings Resulting From Heating And Cooling Interruptions

by

GEORGE FADLO BOUFADEL

DISSERTATION submitted to the Faculty of the

Virginia Polytechnic Institute and State University

in partial fulfillment of the requirements for the degree of

DOCTOR OF PHILOSOPHY

in

MECHANICAL ENGINEERING

APPROVED:

WILLIAM C. THOMAS, Chairman

J. ROBERT MAHAN

WILLIAM H. MASHBURN

DOUGLAS J. NELSON

ROBERT P. SCHUBERT

ADRIAN G. SZELESS

OCTOBER, 1987

Blacksburg, Virginia

Dynamic Thermal Response of Buildings Resulting From Heating And Cooling Interruptions

by

GEORGE FADLO BOUFADEL

WILLIAM C. THOMAS, Chairman

MECHANICAL ENGINEERING

(ABSTRACT)

Transient modelling of heat fluxes and temperatures in structures was conducted to examine the effect of various characteristics on the temperature response during unusual operating and extreme weather conditions. The analytical model was validated using published experimental data and numerical results from well-known computer codes.

The effect of including radiation heat transfer between interior surfaces, using the Mean Radiative Temperature method, on the temperature response was investigated and found to be negligible for a typical commercial building and a house during winter and summer power outages.

The effect of thermal mass in the interior and exterior walls on the inside temperature drift after an HVAC system cutoff or a power outage was presented. The inside air temperature response curve is presented for different wall (exterior or interior) constructions of buildings. The effect of insulation position in exterior walls was also shown for several R values. The effect of exterior wall emissivity, sky temperature, outside vertical convective coefficient, furnishings, and ground temperature on the interior temperature response during winter and summer power outages were examined for buildings.

The effect of infiltration on the temperature drift in buildings was investigated during winter and summer power outages. Restarting the HVAC after the power outage was examined during both seasons for typical buildings.

Outside temperature profiles exceeding the 97.5 design temperature criterion were used to study the effect of extreme weather on the interior temperature of buildings with the HVAC system operating.

Acknowledgements

I am deeply indebted to my advisor Dr. William C. Thomas for his invaluable guidance and encouragement throughout this research. It was a great pleasure to work with him, in particular, to take part in the many sessions and discussions.

Many thanks are due to the members of my committee, Professors J. R. Mahan, D. J. Nelson, W. H. Mashburn, R. P. Schubert, and A. G. Szeless for their help and suggestions.

I appreciate the friendship of many students at VPI, in particular,

and many others.

I wish to dedicate my work to my parents

Table of Contents

NOMENCLATURE **1**

GREEK SYMBOLS 2

1. INTRODUCTION **5**

2. BACKGROUND **9**

CONDUCTION--WALLS 10

CONDUCTION--FLOOR SLABS 13

INFILTRATION 14

INTERNAL LOADS 18

RESPONSE FACTORS OF ROOMS AND BUILDINGS 19

ENERGY ANALYSIS CODES 21

CLIMATIC DATA AND SIMULATIONS 26

3. THERMAL RESPONSE FACTOR METHOD **29**

LAPLACE TRANSFORMATION 31

TRANSMISSION MATRIX 36

SUPERPOSITION PRINCIPLE AND RESIDUE THEOREM 40
INVERSION TO THE TIME DOMAIN 46
CHARACTERISTICS OF THE RESPONSE FACTORS 51
HIGHER-ORDER RESPONSE FACTORS 64
CHARACTERISTICS OF THE HIGHER-ORDER RESPONSE FACTORS 69
ROOTS AND RESPONSE FACTORS OF TYPICAL WALLS 76
VALIDATION OF THE TRFM 76

4. SINGLE ZONE MODEL 81
HEAT TRANSFER THROUGH SLAB-ON-GRADE FLOORS 81
INFILTRATION 88
GENERATED LOADS 92
SURFACE ENERGY BALANCES 93
SURFACE ENERGY BALANCES OF WINDOWS AND DOORS 102
ROOM ENERGY BALANCE 105
NBS TEST HOUSES 116
VALIDATION OF THE PROPOSED MODEL 122

5. MULTIZONE MODEL 129
SOLAR LOAD 129
INFILTRATION LOAD 130
EXTERIOR WALLS AND ROOF 130
SLAB-ON-GRADE SURFACE TEMPERATURES 133
OUTSIDE WINDOWS AND DOORS 135
INTERIOR ROOMS 136
ROOM ENERGY BALANCE 149
MULTIZONE ANALYSIS IN BUILDINGS 152
IMAGINARY WALLS 153

U-SHAPED BUILDINGS 154
HOUSES 155
HEATING AND COOLING LOADS 157
INTERNAL RADIATION IN ROOMS 158
INTERNAL MASS (FURNISHINGS) IN THE ROOM 162
VALIDATION OF THE MULTIZONE MODEL 163

6. RESULTS AND DISCUSSIONS 178
HOUSTON HOUSE SIMULATIONS 179
WILLIAMS HALL SIMULATIONS 181
EFFECTS OF BUILDING PARAMETERS 192
INFRARED RADIATION 194
EXTERIOR WALL EMISSIVITIES 194
SKY TEMPERATURE 195
MRT RADIATION 200
WALL MASS 203
EXTERIOR AND INTERIOR WALL MASS OF THE HOUSE 203
EXTERIOR WALL MASS OF THE BUILDING 207
EXTERIOR WALL RESISTANCE 210
INTERIOR WALL MASS OF THE BUILDING 213
INSULATION POSITION IN EXTERIOR WALLS 213
FURNISHINGS INSIDE ROOMS 216
INFILTRATION UNCERTAINTIES 222
EXTERIOR WALL VERTICAL CONVECTIVE COEFFICIENTS 232
GROUND TEMPERATURE 235
97.5 PERCENT DESIGN TEMPERATURE 239

7. CONCLUSIONS AND RECOMMENDATIONS 251

8. REFERENCES 254

APPENDIX A INVERSION TO THE TIME DOMAIN 261

APPENDIX B ROOTS AND RESPONSE FACTORS OF TYPICAL WALLS 272

APPENDIX C VALIDATION OF THE TRFM 308

APPENDIX D SOLAR LOAD 316

APPENDIX E INFILTRATION LOAD 332

APPENDIX F MRT METHOD 339

VITA 342

List of Illustrations

Figure 1. Path of Integration in the Inversion Formula 41

Figure 2. Trapezoidal (solid lines) or Triangular (dashed lines) Pulses 44

Figure 3. Typical Multilayer Wall 52

Figure 4. Typical Roof 56

Figure 5. Flow Diagram of the Response Factors Computer Code 78

Figure 6. Ground Temperature Distribution below a House on a Flat Terrain for (a) January and (b) July Months 83

Figure 7. Side and Top View of the Slab 84

Figure 8. Temperature and Heat Flux Nomenclature of the slab 89

Figure 9. Typical Multilayer Wall 97

Figure 10. Typical Window with Energy Loads on Both Surfaces 103

Figure 11. Typical Single Room Structure 106

Figure 12. Calculated and Measured Room Temperatures of the Insulated Lightweight Wood Frame House During the Winter (February) season 124

Figure 13. Calculated and Measured Room Temperatures of the Uninsulated Masonry House During the Winter (February) season 125

Figure 14. Calculated and Measured Room Temperatures of the Log House During the Winter (February) season 126

Figure 15. Calculated and Measured Room Temperatures of the Insulated Masonry (outside mass) House During the Spring (April) season 127

Figure 16. Numbering Scheme for the Rooms on Each Floor, N and M rooms in the x and y direction, respectively 137

Figure 17. Numbering Scheme for the Rooms and Floors, N and M rooms in the x and y direction, respectively 138

Figure 18. Interior Room Numbering 140

Figure 19. Interior Flux Directions Employed in the Analysis 144

Figure 20. Nomenclature Employed in the Multizone Model 150

Figure 21. Floor Plan of the Houston Test House 165

Figure 22. Measured Interior, Exterior, and Attic Temperature Profiles 166

Figure 23. Total Hemispherical Solar Profile (measured and calculated) 167

Figure 24. Comparison of the Calculated and Measured Sensible Cooling Loads for the Houston Test House 170

Figure 25. Comparison of the Calculated and Measured Sensible Cooling Loads for the Houston Test House 171

Figure 26. Comparison of the Calculated and Measured Sensible Cooling Loads for the Houston Test House 172

Figure 27. Calculated and Measured Attic Temperatures 173

Figure 28. Calculated and Measured Attic Temperatures 174

Figure 29. Calculated and Measured Attic Temperatures 175

Figure 30. Calculated and Measured Indoor Temperatures of the Houston Test House 177

Figure 31. Outside Summer and Winter Temperature Profiles 180

Figure 32. Interior Temperature Profile of the Houston House During a Summer Power Outage 182

Figure 33. Interior Temperature Profile of the Houston House During a Winter Power Outage 183

Figure 34. Floor Plan of Williams Hall, All Three Floors Have The Same Floor Plan . . . 184

Figure 35. Room Numbering of Williams Hall Employed in the Computer Code 186

Figure 36. Solar Profiles For July 1, Blacksburg, VA 189

Figure 37. Solar Loads Transmitted Through the Windows (Williams Hall) 190

Figure 38. Interior Temperatures of Williams Hall During a Winter Power Outage, First Floor 191

Figure 39. Interior Temperatures of Williams Hall During a Summer Power Outage, First Floor 193

Figure 40. Effect of Exterior Wall Emissivity on the Interior Temperature of the Building During a Summer Power Outage, Third Floor 196

Figure 41. Effect of Sky Temperature on the Interior Temperature of the House During A Winter Power Outage 198

Figure 42. Effect of Sky Temperature on the Interior Temperature of the Building During A Winter Power Outage, Third Floor 199

Figure 43. Temperature Response of the House With and Without Interior Radiation .. 201

Figure 44. Temperature Response of the Building With and Without Interior Radiation, Third Floor 202

Figure 45. Effect of Thermal Mass on the Temperature Response of the House During a Summer Power Outage 206

Figure 46. Effect of Thermal Mass on the Temperature Response of the House During a Winter Power Outage 208

Figure 47. Effect of Exterior Wall Mass on the Temperature Response of the Building During a Summer Power Outage, First Floor 211

Figure 48. Effect of Exterior Wall Mass on the Temperature Response of the Building During a Winter Power Outage, First Floor 212

Figure 49. Effect of Interior Wall mass on the Temperature Response of the Building During a Summer Power Failure, Third Floor 214

Figure 50. Effect of Interior Wall mass on the Temperature Response of the Building During a Winter Power Failure, Third Floor 215

Figure 51. Effect of the Insulation's Location on the Temperature Response of the House During a Summer Power Failure 218

Figure 52. Effect of the Insulation's Location on the Temperature Response of the House During a Winter Power Failure 219

Figure 53. Effect of the Insulation's Location on the Temperature Response of the Building During a Summer Power Failure, Third Floor 220

Figure 54. Effect of the Insulation's Location on the Temperature Response of the Building During a Winter Power Failure, Third Floor 221

Figure 55. Effect of Furnishings on the Interior Temperature of the House During a Winter Power Outage 223

Figure 56. Effect of Furnishings on the Interior Temperature of the Building During a Winter Power Outage, Third Floor 224

Figure 57. Temperature Response of the House With and Without Infiltration 226

Figure 58. Infiltration Loads of the South Side Room in the House 227

Figure 59. Temperature Response of the House With and Without Infiltration 228

Figure 60. Temperature Response of Room 36 (North Side) With and Without Infiltration, First Floor 230

Figure 61. Temperature Response of Room 26 (Central Room) With and Without Infiltration, Third Floor 231

Figure 62. Temperature Response of Room 36 (North Side) With and Without Infiltration, First Floor 233

Figure 63. Effect of the Outside Convective Coefficient on the Interior Temperature of the House During a Winter Power Outage 234

Figure 64. Effect of the Ground Temperature at a depth of 1 m on the Interior Temperature of the Building, First Floor 237

Figure 65. Restarting the AC With an Initial House Temperature of 38 C 238

Figure 66. Restarting the Heater With an Initial House Temperature of 5 C 240

Figure 67. Outside Temperature Profiles for a Winter Season 242

Figure 68. Outside Temperature Profiles for a Summer Season 243

Figure 69. Interior Temperature Profiles of the House During a Winter Season 244

Figure 70. Interior Temperature Profiles of the Building During a Winter Season, First Floor 246

Figure 71. Characteristic Equation B of a 0.2 ft (0.061 m) of Insulation 274

Figure 72. Root Distribution of Wall 1. 276

Figure 73. Root Distribution of Wall 2. 277

Figure 74. Root Distribution of Wall 3. 278

Figure 75. Root Distribution of Wall 4. 279

Figure 76. Root Distribution of Wall 5. 280

Figure 77. Characteristic Equations A and B of Wall 1 282

Figure 78. Characteristic Equations A and B of Wall 2 283

Figure 79. Characteristic Equations A and B of Wall 3 284

Figure 80. Characteristic Equations A and B of Wall 4 285

Figure 81. Characteristic Equations A and B of Wall 5 286

Figure 82. Solution of the Energy Balances of a Roof [71] 314

Figure 83. Solution of the Energy Balances of a Roof (present work) 315

Figure 84. Solar Path and Variable Nomenclature 317

Figure 85. Definition of Solar Angles 318

Figure 86. MRT Network for a Gray Surface. 340

List of Tables

Table 1. Material Description of the Typical Roof 57

Table 2. Root Distribution for the Typical Roof 58

Table 3. Response Factors for the Typical Roof 59

Table 4. Response Factors 73

Table 5. Response Factors 74

Table 6. Response Factors 75

Table 7. Overall Heat Transfer Coefficient for the Typical Roof 77

Table 8. Average Outside Air Temperatures [32] 86

Table 9. Coefficients Used in the LBL Infiltration Model [36] 91

Table 10. Heat Generated by People [26] 94

Table 11. Nomenclature Used in the Single Room Model 108

Table 12. Description of the NBS Test Houses 118

Table 13. Description of the Walls of the Houston Test House [82] 168

Table 14. Description of the Walls, slab, windows, and doors of Williams Hall 185

Table 15. Layer Description of the Four Walls Used in the Simulations 204

Table 16. Layer Description of the Three Walls Used in the Simulations 209

Table 17. Layer Description of Exterior Walls of the House With different Insulation Location 217

Table 18. Summary of Test Cases for the Houston House, Summer Season 247

Table 19. Summary of Test Cases for the Houston House, Winter Season 248

Table 20. Summary of Test Cases for Williams Hall, Summer Season 249

Table 21. Summary of Test Cases for Williams Hall, Winter Season 250
Table 22. Description of the Five Walls 275
Table 23. Response Factors X for Wall 1 287
Table 24. Response Factors Y for Wall 1 288
Table 25. Response Factors Z for Wall 1 289
Table 26. Response Factors X for Wall 2 290
Table 27. Response Factors Y for Wall 2 291
Table 28. Response Factors Z for Wall 2 292
Table 29. Response Factors X for Wall 3 293
Table 30. Response Factors Y for Wall 3 294
Table 31. Response Factors Z for Wall 3 295
Table 32. Response Factors X for Wall 4 296
Table 33. Response Factors Y for Wall 4 297
Table 34. Response Factors Z for Wall 4 298
Table 35. Response Factors X for Wall 5 299
Table 36. Response Factors Y for Wall 5 300
Table 37. Response Factors Z for Wall 5 301
Table 38. Response Factors for the Multilayer Roof 309
Table 39. Description of the Multilayer Wall [12] 310
Table 40. Heat Flux Calculations for the Periodic Heat Transfer Problem 311
Table 41. Exterior Surface Temperature Using the TRFM and Finite Difference 313
Table 42. Solar Variables, Northern Hemisphere 320
Table 43. Solar Variables, Southern Hemisphere 321
Table 44. Window Coefficients, Single Glazed 326
Table 45. Window Coefficients, Double Glazed 329
Table 46. Infiltration Coefficients and Exponents 333
Table 47. Pressure Correction Factors 337

NOMENCLATURE

A	area, m^2
A	transmission matrix element, Eq. 3.36
B	transmission matrix element, Eq. 3.36
C	thermal capacitance, $W/m^2.C$
C	transmission matrix element, Eq. 3.36
C	coefficient of flux histories, Eq. 3.107, dimensionless
$\overline{CR}$	common ration, Eq. 3.89, dimensionless
D	transmission matrix element, Eq. 3.36
F	use factor of lights, dimensionless
g	gravitational acceleration, 9.8 m/s^2
H	height of the structure, m
h	door or hallway height, m
h	convective heat transfer coefficient, $W/m^2.C$
h	nonlinear radiation coefficient, Eq. 4.17, $W/m^2.C$
K	matrix, Eq. 3.67
k	thermal conductivity, $W/m.C$
k	maximum number of floors, Chapter 5

L effective leakage area, Eq. 4.7, m^2

N maximum number of rooms in the x direction

N limit of response factors summation

n layer number

P maximum number of rooms in the y direction

Q heat flow, W

q heat flux, W/m^2

$\bar{q}$ Laplace transforms of the heat flux

R thermal resistance, $m^2.C/W$

R fraction of leakage on horizontal surfaces, dimensionless

T temperature, C or K

t time, s or h

U overall heat transfer coefficient, $W/m^2.C$

V outside wind speed, m/s

W width of the structure, m

w door or hallway width, m

X response factor, $W/m^2.C$

x length, m

Y response factor, $W/m^2.C$

Z response factor, $W/m^2.C$

GREEK SYMBOLS

α thermal diffusivity, m^2/s

α angle of tilt from vertical, degrees

α solar absorptivity, dimensionless

β root, Eq. 3.69, dimensionless

δ pulse width, h

δ time increment, h

ε emissivity, dimensionless

γ wall solar azimuth angle, degrees

θ angle of incidence, dimensionless

θ change in temperature, Eq. 3.55, C

$\overline{\theta}$ Laplace transform of θ

ρ mass density, kg/m^3

ρ solar reflectivity, dimensionless

σ Stefan-Boltzmann constant, $J/s.m^4.K^4$

τ solar transmittance, dimensionless

τ time step, h

φ solar azimuth angle, degrees

φ pulse function, dimensionless

SUBSCRIPTS

1 inside surface of a multilayer wall

a attic space

c ceiling

d door

e east side

f floor

g ground

h horizontal

i layer number, response factor number, or room number

j room number

k wall side

ℓ	response factor order
n	outside surface of a multilayer wall
n	north side
o	outside or ambient
r	room
s	slab
s	south side
s	sky
v	vertical
w	window
w	west side

1. INTRODUCTION

Reducing energy consumption and improving the efficiency of heating, ventilating, and air-conditioning (HVAC) systems has encouraged engineers and designers to use computer-based calculations and analyses extensively. Several computer codes have evolved to calculate loads and provide information to design highly efficient heating and cooling systems. Examples of codes are NBSLD, BLAST-2, TARP, DOE-2, and TRACE. A problem that has not received much attention, however, is the determination of the response of various buildings to controlled or uncontrolled HVAC system shut-down, including loss of power. The question has long been posed on how long it would be before the inside temperature drops or rises to a dangerous or, at least, an uncomfortable level during a power outage. Resolving this question was the primary driving force behind this research. Most of the HVAC programs available in the private and public domains determine the cooling or heating loads based on a set internal temperature. This analysis determines the internal temperatures in a structure and their response to different mechanisms for a specified heating or cooling rate. (In most cases, a complete interruption is assumed, i.e., the rate is set to zero.)

Analytical transient modeling of heat transfer in buildings was performed to predict the temperature on all wall surfaces and interior room air temperatures. Most of the significant parameters were included in the transient analysis. These parameters are infiltration, con-

duction, internal mass, internal generation, solar load, radiation inside each room, emission to the sky by the outside walls and windows, and convective fluxes by all surfaces to the outside or inside air. A supporting computer code to implement the analysis accommodates multi-room and -floor commercial and residential buildings. The new model is validated with experimental data (based on projects carried out by the National Bureau of Standards) and numerical results obtained from well-known computer codes (NBSLD, DOE-2, and BLAST-2) published in the American Society of Heating, Refrigerating, and Air-Conditioning Engineers (ASHRAE) Transactions.

A study was conducted to examine the effect of various characteristics on the temperature response during summer or winter power outages. These characteristics are the exterior wall emissivities, sky temperature, exterior wall convective coefficients, ground temperature, wall masses in the structure, positioning of insulation in exterior walls, and furnishings in the rooms. The effect of including radiation between interior surfaces (using the Mean Radiative Temperature [MRT] method) on the temperature response was also investigated for a typical commercial building and a house. The primary dependent variables are the wall surface and inside air temperatures for each room in the building. Energy balances are used to obtain the expressions for these temperatures. A set of equations, equal to the number of unknown temperatures, is solved iteratively at every time step.

A transient one-dimensional heat conduction model, based on the transfer function method (TFM, also known as the thermal response factor method, TRFM) using response factors, is used for all walls, ceilings, and the floor slab.

For large structures, the infiltration to each room is calculated using a pressure distribution model. The static pressure in each room is calculated iteratively for a prescribed external pressure field based on ambient wind, building height, flow coefficients, and flow areas. The results are used to determine infiltration rates in individual spaces. For small structures,

the Lawrence Berkeley Laboratory (LBL) model is used to calculate infiltration. This infiltration is calculated based on the assumption of constant pressure in the structure.

All outside surfaces allow for nonlinear boundary conditions. In addition to a convective flux to the outside air, an arbitrary solar flux, and a conduction flux to the inside surface, a radiative flux to the sky is accommodated. An energy balance is performed on both surfaces of all walls to obtain an expression for their surface temperatures. Inside surfaces have a convective flux to the inside air, a conduction flux through the wall, and a radiative flux to the other walls of that room. Room temperatures are determined from energy balances on the room air.

The windows are treated similar to outside walls for convection and infrared radiation except that heat flux calculations assume steady-state conditions. Following ASHRAE procedures, the transmittance, absorptance, and reflectance are calculated for each window. The solar flux absorbed by the window is taken into account in the outside surface energy balance. The solar gain through each window is included in the corresponding room air energy balance. Quasisteady-state flux equations are also used for doors. Solar and infrared radiation heat transfers are neglected for outside door surfaces since the area is a small portion of the overall area of the building envelope.

Individual rooms are taken into consideration as separate zones, resulting in a room-to-room analysis. This aspect of the formulation provides freedom in simulations and comparisons. The supporting code has no limitations on the number of rooms per floor and the number of floors. It is recognized, however, that computer memory and computational time could become a critical factor for extremely large buildings.

The "temperature response" is defined as the drift of the interior temperature when an interruption occurs over the next day or two. This temperature response consists of a curve

representing the drop (winter application) or rise (summer application) of the interior temperature.

A background review of the research in this field is presented in Chapter 2. In Chapter 3, the thermal response factor method is developed. Comparisons with numerical and analytical results are presented. In Chapter 4, the single zone model is introduced and validated with experimental data. In Chapter 5, the multi-room and -floor model is formulated. Validations with experimental data and published numerical results are presented. In Chapter 6, results and discussions are presented. Finally, Chapter 7 contains the conclusions from this research.

2. BACKGROUND

Transient thermal analysis of buildings is being studied by designers, engineers, and government agencies with the objective of achieving maximum efficiency in sizing heating, ventilating, and air-conditioning (HVAC) equipment. Conduction heat transfer through walls, roofs, and floor slabs constitutes a large percentage of the total heat transfer from buildings. The need to determine accurately the conduction and various parameters affecting the heat transfer in buildings brought on an extensive research effort by the United States Department of Energy, ASHRAE, and numerous HVAC companies.

The following literature review includes papers used in this research and others presented as general background. A review of research conducted on the "conduction through walls" is given initially. The thermal response factor method [12-15], used in this research, is given in that section. A review of the "conduction through floor slabs" is also given, including the analysis by Kusuda and Beam [32] used in this thesis. Various infiltration models are examined along with the models from references 36, 49, and 52, used in this research. A background review of research conducted on "internal loads, response factors of rooms and buildings, energy analysis codes, and climatic data simulations" is also given. Papers used in this research from these topics are noted in their corresponding sections.

CONDUCTION--WALLS

The thermal response factor method (TRFM), also known as the transfer function method (TFM), has recently evolved for analyzing the transient conduction through multilayer walls, floors, and roofs. This method is used in the present analysis. The advantage of using the TRFM over other well known solutions, such as the finite-difference method, is in the reduction of computational time and storage it provides. Once the so-called response factors are calculated (a full description and derivation of the TRFM is given in Chapter 3) for a given multilayer wall and time step, they remain constant throughout the calculations. Also, small time and space increments are required in the finite-difference method in order to insure stability and convergence. In the TRFM method, large time increments (one hour) can be used and accuracy is maintained in the calculations. In the present analysis, the inside and outside surface temperatures are only needed. These temperatures are calculated using the TRFM while for the finite-difference method, other temperatures in the slab are given and not used.

The TRFM is based on the transient one-dimensional heat conduction equation for single homogeneous slabs but applies to multilayer composite slabs. The superposition principle and the residue theorem are employed in the TRFM.

In the TRFM, the heat conduction equation was first solved using the lumped parameter approximation of resistor-capacitor circuits on analog computers [1-8]. In 1967, Mitalas and Arseneault [9] contributed significantly to the accuracy of the TRFM by not using the lumped resistance and capacitance concept. Instead, they solved the heat conduction equation for multilayer walls in the Laplace domain. A high-speed digital computer was used to invert numerically the Laplace transform matrix to the time domain. Later, Stephenson and Mitalas [10] introduced the use of the TRFM in HVAC calculations. They stressed the use of a digital computer to calculate the response factors of walls and the cooling loads for buildings. In 1968, Mitalas [11] carried out the analysis for nonlinear boundary conditions on walls. He

explained the iteration sequence needed to solve for the coupled inside and outside surface temperatures.

In 1969, Kusuda [12] laid out the complete derivation of the TRFM. He extended the calculations of response factors to multilayer structures of various curvatures (cylindrical and spherical) and semi-infinite mediums. His comprehensive analysis included the explanation of how to apply the TRFM to nonlinear boundary conditions. A complete mathematical analysis of the TRFM is presented in Chapter 3.

In the TRFM, many terms (at least 50) are required in the summation of response factors. Peavy [13,14] introduced higher order response factors. He was able to reduce the number of response factors required in the summation by approximately 1/3. This work made the TRFM more practical and efficient to use. A comprehensive mathematical analysis of the higher order response factors, along with the original order response factors, is presented in Chapter 3.

Finding the roots of the characteristic equation of the Laplace transformed solution to the heat conduction equation is needed in the TRFM. The traditional method was to iterate for these roots (poles) taking small steps in a marching procedure. In 1984, Hittle and Bishop [15] introduced an improved root-finding procedure for the TRFM. This modification is also presented in Chapter 3.

The fluxes are linearly related to the product of temperatures and response factors. If the temperatures and corresponding fluxes were known, the system of equations could be solved to determine the response factors. Pederson and Mouen [16] set up the experimental apparatus to measure temperatures and fluxes on both sides of a given wall in their attempt to determine the response factors of walls experimentally. They were not successful because any slight inaccuracy in temperature, present in experimental measurements, would lead to an almost 100 percent change of response factors.

In 1971, Stephenson and Mitalas [17] introduced response factors based on the the z-transform. The authors claimed that this type of response factor is more efficient in terms of computer running time and storage. Mitalas and Arseneault [18] wrote the Fortran code to calculate the response factors for a multilayer wall using the z-transform technique. Mitalas [19] examined extensively the z-transfer function method with applications to multilayer walls and roofs for cooling or heating load calculations. The original TRFM, however, remained the standard method for calculating response factors of multilayer walls.

Sherman, et al. [20] and Codon, et al. [21] introduced a simplified model that characterizes the dynamic thermal performance of a wall on the basis of the measured surface temperatures and heat fluxes. The model uses a set of "simplified thermal parameters" (STP) to characterize the thermal performance of walls from a measured temperature history.

Burch, et al. [22] investigated the effect of wall mass on the heating and cooling loads of residential buildings. The heating and cooling loads, wall transmission, indoor temperature, and humidity were measured for six test buildings. These measurements were taken during a winter heating season, an intermediate heating season, and a summer cooling season. No reductions in heating energy attributable to wall mass were observed during the winter heating season. During the intermediate heating and the summer cooling seasons, significant reductions in HVAC loads attributable to wall mass were observed.

Burch, et al. [23, 24] examined the effect of wall mass on annual heating and cooling loads of single family residences for five selected climates using the TARP computer program. The authors used the data from ref. [22] and the TARP program to compare the results. For the winter season, the TARP program predicted cumulative space heating loads within a root mean square (RMS) average of 11 percent. For the summer period, the TARP program predicted cumulative space cooling loads within a RMS average of 25 percent. They also presented their simulations for a typical house and a high solar gain house. The presence of interior wall mass caused the typical house to approach a static high-mass limit that coincided

with the steady-state theory. Under such a condition, wall mass was found to have only a small effect on annual space heating and cooling.

Burch, et al. [25] studied the effect of thermal mass on night temperature setback savings. For the four experimentally tested buildings, a reduction in the balance-point temperature was found as the effect of the night temperature setback. The computer simulations using the TARP program indicated that the heavyweight test buildings had smaller setback savings than the lightweight test buildings. Also, the addition of interior wall mass for a typical house provided a small decrease in the annual setback savings.

The TRFM [12-15] is used in this research. Data given in references 22 through 25 are used in Chapter 4 to validate the single zone model.

CONDUCTION--FLOOR SLABS

The conduction heat transfer through floor slabs constitutes a large portion of the conduction heat transfer in buildings. Several procedures for determining the heat transfer through slabs are given in the ASHRAE Handbook of Fundamentals [26-28]. Coefficients for calculating the loss through the center and the perimeter of the slab are obtained from Wang's finite element computer program [29]. McQuiston and Parker [30], a widely used reference for HVAC calculations, used the same methods as given in references 26 through 28.

In 1982, Mitalas [31] examined extensively the heat loss through basements. He calculated the heat transfer rate in terms of the distance from exterior walls. He introduced equations that determine the maximum and total basement heat loss over the heating season. Analytical results and experimental data were used to develop a set of factors needed in the calculations. Mitalas presented these factors for 26 cases.

Kusuda and Beam [32] introduced a simplified method for determining seasonal heat loss from uninsulated slab-on-grade floors. Their procedure is based on an average earth temperature and the inside room temperature. According to Kusuda and Beam, Mitalas' solution [31] showed a larger time lag effect, resulting in lower winter floor heat loss and higher summer floor heat loss (than did Green's function and Delsante's Fourier Transform solutions).

Yard, Morton-Gibson, and Mitchell [33] developed a method for calculating the monthly and annual heat loss from basement walls and floors. The average heat loss is calculated using overall wall and floor conductances and the representative ground temperature.

Perry, Cunningham, and Scessa [34] presented an analysis of the heat losses through residential floor slabs using a finite-element method. They showed the effects of the outdoor air temperature, deep soil temperature, and thermal conductivity of the underlying soil on the heat losses through slabs. The study showed that for an uninsulated slab, 60 percent of the total heat losses occurs through the region lying within three feet of the slab edge.

Kusuda and Achenbach [35] introduced an equation to calculate the ground temperature in terms of the depth, location, time of the year, and ground thermal properties. They also calculated earth temperatures and thermal diffusivities for selected stations in the United States.

Data given by Kusuda and Beam [32] are used along with the TRFM to calculate the conduction heat transfer through the floor slab.

INFILTRATION

Infiltration is the uncontrolled flow of outside air through leakage areas in structures. Controlling the infiltration is essential in reducing the HVAC system size needed in buildings.

Grimsrud, Modera, and Sherman [36] presented the long-term field validation results of an air infiltration model obtained by experimental measurements in a mobile infiltration test unit. This model is known as the Lawrence Berkeley Laboratory (LBL) model. In addition, they compared the model predictions with measured infiltration data from three unoccupied test houses. Hour-by-hour or long-term average infiltration in structures is calculated using the wind speed, outdoor temperature, and site parameters. Of the single cell models validated by the the Air Infiltration Center (AIC) [37] with experimental data, the best overall results were obtained using the LBL model. In the ASHRAE Handbook of Fundamentals [26-28], leakage areas and pressure coefficients for typical building components are given. The model is dependent on the shielding around the structure, leakage area exposed to the wind, wind measurements away from the structure, and the stack effect. The authors validated the model using the Mobile Infiltration Test Unit (MITU). For an entire 34 day data set, the half-hour infiltration predictions had an accuracy of 35 percent, the daily infiltration predictions were within 20 percent, and the weekly infiltration predictions were within 10 percent.

Liddament and Allen [37] compared and validated several mathematical models of air infiltration. These were three models from the United States of America (USA), four from the United Kingdom (UK), and one model each from Canada, Netherlands, and Norway. In their presentation, certain models were referred to as 'single-cell' models since the interior of the building was assumed to be at a uniform pressure. For the 'multi-cell' models, the interior of the building was divided into different pressure regions interconnected by leakage paths.

The Building Services Research and Information Association [38] (UK) developed a multi-cell model to predict ventilation rates and air movement in buildings. The building under consideration is divided into a set of nodes, interconnected by air flow paths. The maximum permissible number of nodes is 135 and the maximum number of interconnections to any node is 20. This model was tested against experimental data and was found that as long as the input conditions were adequately specified, it was consistent within 25 percent.

The National Research Council of Canada [39, 40] introduced a model to calculate the air flow and pressure differences in buildings depending on the outside wind speed, stack effect, and the inside air handling. The building is represented by a series of interconnected vertically stacked compartments. The leakage areas are specified for each external wall, floors, and the interconnecting walls, enabling air to pass from every compartment or cell to the adjacent cells (vertically and horizontally). A limitation of this model is the assumption of constant 24 C (75 F) interior temperature. When the same input data to the previous model [38] was used, the computed results of the two models were close to each other.

The IG-TNO Institut Voor Milieuhygiene en Gezondheidstechniek [41] (Netherlands) developed a multi-cell model to predict room pressures, air flows between the rooms, and flows across exterior walls. The building is characterized by a network in which each connection is described by two pairs of integers. The first pair represents the path from that node while the other pair of integers represents the path to the node. The model can accommodate up to 20 rooms and 25 connections for each room. The effects of window opening and natural wind pressure fluctuations are included in the calculations. This model produced good results for one of the specific houses that was tested.

Oscar Faber Partnership (SWIFIB) [42] (UK) introduced a model to calculate air flow through buildings. The building is considered a 'multi-cell' network in which individual rooms are represented as nodes. Cracks and ventilation ducts are represented by connecting paths. The stack pressures, wind pressures, and mechanical ventilation are taken into consideration in the calculations. The pressure and mass flow rate of each individual room (node) are calculated. This model is used to calculate air infiltration contributed by component leakage only. Good agreement between calculated and measured air infiltration in the Lawrence Berkeley Laboratory test unit was observed.

The British Gas Company (UK) [43, 44] introduced a model (VENT) to predict the individual room and whole house flow rates. This model is dependent on the external pressure distrib-

ution, the internal and external temperatures, and the leakage distribution. The inclusion of the turbulent correlation parameter, contained in this model, resulted in a marginal increase above the measured air infiltration throughout the entire data range.

The Norwegian Building Research Institute (ENCORE) [45] (Norway) developed a 'single-cell' model for calculating air infiltration based on the flow balance approach. This model is used to calculate mean hourly rates of ventilation throughout the heating or cooling season. The model is dependent on external air temperature, wind speed and direction, terrain category, leakage area, building geometry, number of exhaust ducts, and type and capacity of each exhaust duct. This model was assessed against six sets of data. Good results were obtained for wind speeds of less than 2 m/s. For higher wind speed, the calculated air infiltration rate tended to be greater than the measured rate.

The Gas Research Institute/Institute of Gas Technology [46] (USA) developed a 'single-cell' simulation model for residential buildings. The characteristics of the structure, its heating system, wind effects, stack effects, and weather conditions are used in the model to calculate the infiltration and chimney flow rates.

The Building Research Establishment [47] (UK) introduced a model relating air infiltration rate for any given set of conditions to the leakage characteristics of the building as determined by a pressurization test. Despite the simplicity of this model, consistently accurate predictions were achieved using the experimental data.

The Reeves, McBride, and Spesy model [48] (USA) is a 'single-cell' model. The infiltration through the building envelope, depending on the height of the building for the stack effect, the inside and outside temperatures, the wind speed, and the crack characteristics are calculated. This model differs from those previously investigated. It is applied to buildings after tracer gas measurements of air infiltration have already been made.

An ASHRAE task group on energy calculations in buildings was formed in 1975. They presented procedures [49] for building heat transfer algorithms (solar loads, infiltration, etc.). The multi-cell infiltration model developed by Sander and Tamura [50, 51] was recommended by the ASHRAE task group. The infiltration is calculated based on the pressure difference across the building envelope. This model is used in the current research. A complete description of this model is presented in Appendix E.

Balcomb and Yamaguchi [52] examined the heat distribution by natural convection in buildings and houses. According to Balcomb et al., experimental results from several buildings showed convective heat flow of 1000 to 2000 Btu/h (293 to 586 W) between rooms driven by temperature differences of 3 to 5 F (5.4 to 9 C). They added that convection through single doorways was found to be the major mechanism for heat distribution from the sun space to the rest of a solar home, accounting for transfer of 16.3 million Btu during one 6 month winter season.

The LBL infiltration model [36] is used in this research for small structures. The pressure distribution model [50, 51] is used for large structures. The parametric equation given by Balcomb and Yamaguchi [52] is used to predict natural convection through interior doors and hallways.

INTERNAL LOADS

Kimura and Stephenson [53] presented a theoretical study on the effects of lights on the cooling load in buildings. Their analysis showed that the cooling load associated with the power input to lights depends on the convective heat transfer coefficients at the ceiling and floor surfaces, the thermal resistance of the ceiling, the proportions of the input power that are dissipated upward and downward from the light fixture, and the heat storage capacity of the floor slab.

Barakat and Sander [54] derived "utilization factors" for internal gains using hour-by-hour computer simulation with actual weather data for 11 Canadian locations. Determination of internal gain loads such as people, appliances, lights, and hot water were estimated from occupant use data. The authors presented practical equations to calculate the seasonal internal gain utilization factor for houses, apartments, schools, and offices.

The internal loads generated by lights, people, and equipment are calculated in this research using ASHRAE procedures [26-28].

RESPONSE FACTORS OF ROOMS AND BUILDINGS

Application of response factors was extended to rooms and buildings for HVAC calculations. The following review is given as general background information. None of the papers listed in this section were directly used in this research. Mitalas and Stephenson [55] introduced response factors for rooms to determine their dynamic thermal characteristics for HVAC applications. An energy balance was performed on the room air. A matrix that includes the inside wall surface temperatures as unknowns was solved to obtain the room response factors. This analysis is applicable only for constant room air temperature.

Muncey, Spencer, and Gupta [56] introduced a method for thermal calculations of buildings using the so-called total building response factors. In large massive buildings, these response factors are needed for as long as 10 days. To reduce the data bank necessary to store the total building response factors, they introduced a method in which they retained only the last six hours as the affecting parameters.

Kusuda [57] applied time series analysis for obtaining building thermal response factors which are basically regression coefficients of single room buildings. The primary assumption imposed upon this technique is that the building thermal loads are a linear function of various

excitation parameters such as outdoor temperature, solar radiation, internal heat generation, and the indoor temperature.

Sonderegger [58] investigated the determination of thermal response of buildings based on their equivalent thermal parameters (ETP). This method consists of data oriented techniques that infer the ETP's of a particular building by multiple correlation of indoor temperature and weather parameters. According to the author, a set of ETP's was established for a residential townhouse by means of a simple single thermal mass model.

Wilson, Colborne, and Ganesh [59] introduced the determination of thermal parameters of an occupied house by means of steady-state and dynamic analyses of its data. The authors presented steady-state and dynamic model equations along with the parameters computed from measurements of temperatures and other weather parameters. The steady-state model yielded reliable estimates for the building load coefficient and balance point temperature. The dynamic model yielded an estimate of the thermal capacitance of the house in addition to the ETP's yielded by the steady-state model.

Crawford and Woods [60] introduced a new procedure for deriving the dynamic system model of a building from its actual performance data. The variables used in this procedure are divided into outputs, controlled inputs, and disturbances. The system output variables are the indoor conditions such as dry bulb temperature and relative humidity. Controlled inputs are the variables used to control the building systems such as the electrical consumption of a heat pump or the rate of outdoor ventilation air. Disturbances to the system are defined as any uncontrolled inputs such as ambient weather conditions or internal loads. The mathematical representation of the model for a single controlled input, output, and an arbitrary number of disturbances was expressed with an autoregressive moving average (ARMA) model developed by Franklin and Powell [61] in 1980. The authors modified the original equation and introduced the dynamic system model of buildings based on their actual performance.

Harrison, Hansen, and Zelenski [62] developed a model transfer function for an air-conditioned room for the investigation of short-term transient response. An energy balance was performed on the room air and the resulting differential equation was expressed in the form of a transfer function and added the lumped capacitance effects of furniture and walls. The authors solved the corresponding differential equation and introduced the room transfer function. This paper was exploratory in nature and was introduced with the purpose of stimulating interest for this type of modeling.

The Analog Computer Method has been used to determine the interior temperature in houses. Walls, roofs, doors, etc., are simulated by resistances and capacitances and coupled to the inside room temperature. This method was introduced by Nelson in 1965 [63]. In 1976, Kaya [64] developed an analytical model for a single zone assuming no heat transfer by radiation inside the zone and neglecting the storage effects of the structure. Later, D.P. Mehta [65, 66] solved the problem analytically with the HVAC system turned off.

ENERGY ANALYSIS CODES

The advent of digital computers has stimulated interests in their use for HVAC calculations. Designers are relying heavily on the use of computers as a mean of performing the large number of calculations required in determining heating and cooling loads for buildings. Currently, few large programs and numerous PC type programs are available for engineers and designers. A listing of the large programs is given next. The BLAST (Building Loads Analysis and System Thermodynamics) program was developed by the US Army Construction Engineering Research Laboratory (CERL)[67]. The DOE-2 program was developed by the Department of Energy [68-70]. The TRACE (Trane Air Conditioning Economic Computer Program) was developed by the TRANE Company. The NECAP (NASA Energy/Cost Analysis Program) was developed by NASA in 1974. The NBSLD (National Bureau of Standards Load Determi-

nation Program) was developed by Kusuda at NBS [71]. The TARP (Thermal Analysis Research Program) was developed by Walton at NBS [72].

Yuill and Phillips [73] used the BLAST program to predict the energy consumptions of two office buildings. They compared the calculated energy consumption with the consumptions indicated by the utility bills. The energy usage of the first building was predicted to be 90 percent of that measured. In building 2, the predicted electricity consumption was within 1 percent of that measured, as was the winter gas consumption.

Diamond and Hunn [74] verified the DOE-2 computer program using seven commercial buildings. The buildings were a restaurant, a single-floor office building, a retail store, a hospital, a multi-floor office building, a school, and a solar-heated and -cooled building. They compared the calculated energy consumption to the utility monthly metered data. The comparison of predicted vs. measured energy use on a monthly basis showed significantly higher deviations than the annual comparisons of all buildings.

Alreza and Hovander [75] developed an hourly building energy simulation model for microcomputers. They claimed their model has the same basic capabilities of large programs such as the DOE-2. They used their model to calculate the energy consumption in 36 commercial buildings.

Diamond, Capiello, and Hunn [76] validated the DOE-2 program using four commercial buildings. The four buildings were single- and multi-floor office buildings, a retail store, and a restaurant. One of the conclusions was that considerable scatter in results of monthly energy calculations can be expected among expert users of building energy analysis computer programs such as DOE-2.

Robertson and Christian [77] compared four computer models with experimental data from test buildings in Northern New Mexico. The experimental study, called the Southwest

Thermal Mass Study (SWTMS), was performed at Tesuque Pueblo, New Mexico, to evaluate the effect of envelope thermal mass on the heating energy consumption of conventional residential buildings. The DOE-2.1A, BLAST, DEROB, and DOE-2.1B computer codes were used for the comparisons. For the midwinter, the DOE 2.1B simulation was the closest to the measurements with 6 percent lower values followed by the BLAST and DEROB with 10 percent lower values, and the DOE 2.1A with 18 percent lower result. For the late winter, the BLAST predicted 2 percent lower cumulative heating load, the DOE 2.1B predicted 8 percent lower, and the DOE 2.1A had 12 percent lower data. For the spring season, the cumulative predicted heating load was 13 percent higher for Blast, 13 percent lower for the DOE 2.1A, 61 percent higher for the DOE 2.1B, and 86 percent lower for the DEROB than the measured load.

Sorrell, Luckenbach, and Phelps [78] presented a validation study to determine the accuracy of the DOE 2.1B, EMPS 2.1, and TARP in predicting the hourly energy use of residential structures. Accuracy in predicting absolute energy use for a typical residential structure was 5 to 20 per cent for a one to three days period. The computed results were generally in better agreement for longer time periods. The uncertainty in predicting the energy consumption was due to the inability to model the building and in the accuracy of the models themselves. The DOE 2.1B was more accurate for frame and/or low mass structures, at least for residential size buildings. The models predicted the relative hourly energy use or load profile of residential buildings to within 10 to 20 percent

Yuill [79] verified the performance of the BLAST program in simulating single family houses. Another objective was to detect and eliminate errors in the descriptions of houses prepared for use with BLAST. At the University of Alberta, researchers conducted thermal measurements on six houses of identical geometry and different thermal characteristics for testing the thermal performance of these houses. Yuill used data from two houses to conduct his validation of the BLAST program. The deviations between the BLAST predictions and the measured building performance were 3 to 12 percent. Yuill concluded that the BLAST program could satisfactorily model houses in different climates.

Burch, Peavy, and Powell [80] compared the predicted hourly heating and cooling requirements for an instrumented wood-framed townhouse using the NBSLD computer program and the measured data. An instrumented four bedroom townhouse was exposed to simulated winter and summer temperature conditions inside an environmental chamber. During the tests, the activities of a six member family were simulated and the inside temperature of the test house was maintained at approximately 75 F (24.2 C). Hourly heating and cooling input energies were measured and compared with corresponding computer predicted values. The calculated results underpredicted the experimental data by an average range of 33 percent for the first 12 hours and overpredicted the measured data by almost 33 percent for the remaining 12 hours of the day. The cooling test revealed a closer prediction by the NBSLD to the measured data with a range of 10 percent difference.

Kusuda and Bean [81] used a one-room high-mass test building, designed for a hot and dry desert climate, and tested it in the National Bureau of Standards environmental chamber under simulated cycles representing typical summer sol-air temperature profiles. The NBSLD calculation results were compared with measured hourly cooling loads and indoor temperature under simulated steady periodic outdoor sol-air temperature cycles. The authors attributed the poor agreement between the measured and calculated thermal performance data to the excessive amount of moisture released from the masonry structure during the daytime warm-up period when the air-conditioner was off. They concluded that night cooling is more energy efficient than 24-hour cooling, at least under the desert-type climate condition used in their study.

Kusuda, Pierce, and Bean [82] compared the measured hourly cooling loads and the attic temperature of a Houston test house with those determined by the NBSLD, DOE-2, and BLAST programs. The weighting factor approach appeared to show a more pronounced time lag effect in the cooling requirements after the peak cooling hours than the NBSLD/BLAST approach. The observed values tend to fall between the two approaches.

Borresen [83] presented four simplified dynamic room models. He showed that the choice of the simplification level employed depends on how closely the long-term responses and steady-state values fit the actual room response.

Sullivan, et al. [84] examined a procedure to reduce the number of required parametric computer runs in creating and expanding a data base. Their objective was to minimize the cost of performing annual building energy simulations. Through the use of numerous building energy simulations using both the DOE-2.1 and BLAST energy analysis computer programs, they showed that the form of the relationship between residential building thermal loads for varying configuration parameters is independent of climatic location.

Hackner, Mitchell, and Beckman [85] introduced a model to determine an optimal control strategy. Their objective was to determine operating strategies for HVAC systems that incorporate system dynamics and interactions and potentially reduce energy usage. A simulation of the entire HVAC system was performed to compare the system energy use under various control strategies. They concluded that the dynamic HVAC operating strategies can be identified through simulation techniques. This provides a procedure for exploring the control strategy options. They showed that a 3 to 4 percent energy savings can be achieved with a system operating under dynamic control as opposed to a system in which control decisions were made on an hourly basis. Using an optimal control strategy, an overall energy use reduction of 8.7 percent (to the current strategy) is possible. Compared to operation with fixed set points, a reduction of 19 percent is possible.

Goldman [86] presented measured results of energy conservation retrofits in residential buildings. He presented a complete history of the retrofit energy savings in houses. Attic, wall, floor insulation, and storm windows were successful in most single-family electric space heated homes. Achieved savings were typically 20 to 30 percent of pre-retrofit space heating energy use. Also, the average investment in multifamily buildings is approximately $700/unit, far lower than the $1350 average expenditure in single-family residences.

Lau, Beckman, and Mitchell [87] developed computer models for a chilled water plant to study the energy conservation potential of control strategies intended for a minicomputer control system. Their primary objective was to identify computer control strategies to reduce the cost of electricity consumed by the chilled water plant of a large commercial facility. This study pointed out that the actual outside air supplied was inconsistent with the supposed values which is often the case in many plants and buildings.

Peavy, Powell, and Burch [88] measured the dynamic heat transfer in an experimental masonry building and compared the data to the NBSLD computer program as part of the validation of that program. The building was located inside a large environmental chamber at the National Bureau of Standards which allowed flexibility in monitoring and simulating different outside weather conditions. When the measured data were compared to the NBSLD predicted values, it was shown that when the inside room was thermostatically controlled, this program predicted the maximum and daily average heating loads. Therefore, the authors presented their recommendation that this program is capable of predicting these loads and can be used to size equipments for HVAC purposes. Also, for five heating tests, the largest difference between computed maximum heating loads and measured values was 8 percent and the average difference was 4.3 percent.

The data presented by Burch, et al. [80] are used in Chapter 4 to validate the single room model. The data given by Kusuda, et al. [82] are used in Chapter 5 to validate the multizone model.

CLIMATIC DATA AND SIMULATIONS

Hittle [89] presented a new combined deterministic and stochastic model for climate variable studies. The calculations of heating or cooling loads of buildings with constant inside room temperature and a sinusoidal outside air temperature was presented. Hittle claimed to

account for the stochastic (random) variation in weather data by applying series analyses techniques in order to separate the deterministic periodic behavior in the data from its stochastic behavior.

Thomas and Reed [90] compared effective sky temperature models in their analysis of infrared irradiance on collector thermal performance. The models by Berdahl, Bliss, and Swinbank predicted sky temperature ehich were close to each other. The model presented by Whillier predicted the sky temperature higher then those calculated using the other models.

Haghighat, Unny, and Chandrashekar [91] examined the stochastic boundary condition on exterior walls. They introduced a new formulation that presented solar radiation as a sum of average values and stochastic fluctuations. The energy balance equation thereby reduces to a stochastic differential equation, the solution of which represents the performance characteristic.

Richard [92] introduced a new "Duration Design Temperature" that accounted for the duration of extreme weather. He based his analysis on the season's representation. For the cooling season, the data base was June through September. For the heating season, the data base was December through February.

Kusuda and Ishii [93] presented hourly solar radiation values for eighty different locations in the United States and Canada. The Liu and Jordan method for calculating incidence hourly solar radiation on a surface of any tilt and orientation under "average" conditions was modified and used. Average hourly incidence total radiation on eight primary vertical and horizontal orientations for each month of the year and for each 80 locations in the United States and Canada were computed. They also calculated the sol-air temperature for glass for each of these locations.

As presented earlier, a large interest lies in determining the thermal characteristics of buildings. Tye and Spinney [94] presented 81 different materials for which they measured the specific heat along with the density and moisture content. They determined the heat capacity using an adiabatic calorimeter [95] technique with an accuracy of 5 percent. This technique provides results at any desired temperature within the approximate range -180 to 400 C. For the lower density materials, some additional measurements by a drop calorimeter technique [96] were included to serve as a confidence check on the basic adiabatic method.

The thermal response factor method (TRFM), derived by Kusuda [12] is presented next along with the modification introduced by Peavy [13]. A validation of the TRFM with published exact and numerical solutions is also given.

3. THERMAL RESPONSE FACTOR METHOD

The thermal response factor method (TRFM) will be developed for single and multilayer homogeneous slabs. The TRFM was originally derived by Kusuda [12] in 1969. In this chapter, Kusuda's derivation is presented with little modification. The TRFM is a one-dimensional heat conduction method based on the transient heat conduction equation for single homogeneous layer slabs but applies to multilayer composite slabs. Laplace transforms and the superposition principle are both employed in the TRFM. The final heat conduction equation for the multilayer wall is based on the so-called response factors of that wall and the inside and outside surface temperatures. These response factors are calculated for the wall materials (conductivity, density, specific heat, and thickness of each layer) and specified time step. Peavy [14] improved the TRFM by introducing modified response factors. The number of response factors needed for accurate calculations were decreased significantly using his modification. On the average, the number of response factors were decreased by a factor of about three. An improved procedure to determine some important roots of the TRFM was presented by Hittle [15] in 1984.

Kusuda's derivation of the TRFM is presented next along with the modifications introduced by Peavy and Hittle. Several examples are given for single and multilayer slabs under linear and nonlinear boundary conditions (convective, fixed temperature, adiabatic, and com-

bined solar load and infrared radiation emitting boundaries). Comparisons with the well-known finite-difference scheme and other known analytical solutions are also given.

One-dimensional heat conduction through a single homogeneous layer (i) of a multilayer slab is governed by

$$\frac{\partial^2 T(x,t)}{\partial x^2} = \frac{1}{\alpha_i} \frac{\partial T(x,t)}{\partial t} \tag{3.1}$$

where

$$\alpha_i = \frac{k_i}{\rho_i C_{pi}} \tag{3.2}$$

In the present analysis, k, ρ , and C_p are assumed constant for each layer. Imposing the initial and boundary conditions,

$$\begin{aligned} T(x, 0) &= T_m = Constant \\ T(x_i, t) &= T_i(t) \\ T(x_{i+1}, t) &= T_{i+1}(t) \end{aligned} \tag{3.3}$$

The heat flux at any position x and time t is given by

$$q(x,t) = -k_i \frac{\partial T(x,t)}{\partial x} \tag{3.4}$$

Applying the Laplace transform to Eqs. 3.1, 3.3, and 3.4 is a common approach to the solution.

LAPLACE TRANSFORMATION

Introducing the nomenclature $\theta(x,t) = T(x,t) - T_m$ and substituting into Eqs. 3.1 and 3.3

$$\frac{\partial^2\theta(x,t)}{\partial x^2} = \frac{1}{\alpha_i}\frac{\partial\theta(x,t)}{\partial t} \tag{3.5}$$

$$\begin{aligned}\theta(x, 0) &= 0\\ \theta(x_i, t) &= \theta_i(t)\\ \theta(x_{i+1}, t) &= \theta_{i+1}(t)\end{aligned} \tag{3.6}$$

Using the Laplace transform property

$$L\left[\frac{\partial f(t)}{\partial t}\right] = sF(s) - f(t)\big|_{t=0} \tag{3.7}$$

For the present analysis, applying Eq. 3.7 to the right hand side of Eq. 3.5

$$L\left[\frac{1}{\alpha_i}\frac{\partial\theta}{\partial t}\right] = \frac{1}{\alpha_i}\left[s\bar{\theta} - \theta\big|_{t=0}\right] = \frac{1}{\alpha_i}s\bar{\theta} \tag{3.8}$$

where $\bar{\theta}$ is the Laplace transforms of θ

$$\bar{\theta}(x,s) \quad = \quad L\left[\theta(x,t)\right] \tag{3.9}$$

Applying the Laplace transform to Eq. 3.5, transforms it to an ordinary differential equation

$$\frac{d^2\bar{\theta}(x,s)}{dx^2} = \frac{1}{\alpha_i}s\bar{\theta}(x,s) \tag{3.10}$$

Transforming the boundary conditions

$$\begin{aligned} \bar{\theta}(x_i, s) &= \bar{\theta}_i(s) \\ \bar{\theta}(x_{i+1}, s) &= \bar{\theta}_{i+1}(s) \end{aligned} \tag{3.11}$$

The Laplace transform of the heat flux equation (Eq. 3.4) is

$$\bar{q}(x,s) = -k_i \frac{d\bar{\theta}(x,s)}{dx} \tag{3.12 - a}$$

where

$$\bar{q}(x,s) = L\,[q(x,t)] \tag{3.12 - b}$$

The solution of Eq. 3.10 is

$$\bar{\theta}_i(x_i,s) = A_i \cosh(x_i \sqrt{s/\alpha_i}) + B_i \sinh(x_i \sqrt{s/\alpha_i}) \tag{3.13}$$

where A_i and B_i are arbitrary constants. Substituting into Eq. 3.12-a

$$\bar{q}_i(x_i,s) = -A\,k_i \sqrt{s/\alpha_i} \sinh(x_i \sqrt{s/\alpha_i}) - B\,k_i \sqrt{s/\alpha_i} \cosh(x_i \sqrt{s/\alpha_i}) \tag{3.14}$$

The coefficients A_i and B_i are determined by substituting the boundary conditions into Eqs. 3.13 and 3.14 and solving simultaneously for these constants. Layer 1 is used to solve for A and B. For the first layer (i = 1)

$$\begin{aligned} x_i &= 0\ ,\ \bar{\theta}_i = \bar{\theta}_1\ ,\ \bar{q}_i = \bar{q}_1 \\ x_{i+1} &= \Delta x\ ,\ \bar{\theta}_{i+1} = \bar{\theta}_2\ ,\ \bar{q}_{i+1} = \bar{q}_2 \end{aligned} \tag{3.15}$$

Substituting into Eqs. 3.13 and 3.14,

$$
\begin{aligned}
\bar{\theta}_1(s) &= A \\
\bar{\theta}_2(s) &= A\cosh(\Delta x\sqrt{s/\alpha}) + B\sinh(\Delta x\sqrt{s/\alpha}) \\
\bar{q}_1(s) &= -Bk\sqrt{s/\alpha} \\
\bar{q}_2(s) &= -Ak\sqrt{s/\alpha}\sinh(\Delta x\sqrt{s/\alpha}) - Bk\sqrt{s/\alpha}\cosh(\Delta x\sqrt{s/\alpha})
\end{aligned}
\tag{3.16}
$$

Solving for A and B in terms of $\bar{\theta}_2(s)$ and $\bar{q}_2(s)$

$$
\begin{aligned}
A &= \frac{\theta_2(s) - B\sinh(\Delta x\sqrt{s/\alpha})}{\cosh(\Delta x\sqrt{s/\alpha})} \\
B &= \frac{-\bar{q}_2(s) - Ak\sqrt{s/\alpha}\sinh(\Delta x\sqrt{s/\alpha})}{k\sqrt{s/\alpha}\cosh(\Delta x\sqrt{s/\alpha})}
\end{aligned}
\tag{3.17}
$$

Defining, for simplicity, the following variables:

$$
\begin{aligned}
\Gamma &= k\sqrt{s/\alpha} \\
C &= \cosh(\Delta x\sqrt{s/\alpha}) \\
S &= \sinh(\Delta x\sqrt{s/\alpha})
\end{aligned}
\tag{3.18}
$$

Equation 3.17 becomes

$$
\begin{aligned}
A &= \frac{\bar{\theta}_2(s) - BS}{C} \\
B &= \frac{-\bar{q}_2(s) - A\Gamma S}{\Gamma C}
\end{aligned}
\tag{3.19}
$$

Substituting A into B in the above equation,

$$
B = -\frac{\bar{q}_2(s)}{\Gamma C} - \frac{\Gamma S}{\Gamma C}\left[\frac{\bar{\theta}_2(s) - BS}{C}\right] \tag{3.20}
$$

or

$$B = -\frac{\bar{q}_2(s)}{\Gamma C} - \frac{S\,\bar{\theta}_2(s)}{C^2} + \frac{B\,S^2}{C^2} \tag{3.21}$$

Solving for B

$$B\left[\frac{C^2 - S^2}{C^2}\right] = -\frac{\bar{q}_2(s)}{\Gamma C} - \frac{S\,\bar{\theta}_2(s)}{C^2} \tag{3.22}$$

However,

$$C^2 - S^2 = \cosh^2(\Delta x\sqrt{s/\alpha}) - \sinh^2(\Delta x\sqrt{s/\alpha}) = 1 \tag{3.23}$$

Substituting Eq. 3.23 into 3.22 and solving for B

$$B = -\frac{\bar{q}_2(s)\,C}{\Gamma} - S\,\bar{\theta}_2(s) \tag{3.24}$$

Substituting Eq. 3.24 into 3.19 leads to

$$A = C\,\bar{\theta}_2(s) + \frac{S\,\bar{q}_2(s)}{\Gamma} \tag{3.25}$$

Substituting back the original coefficients

$$A = \cosh(\Delta x\sqrt{s/\alpha})\,\bar{\theta}_2(s) + \frac{\sinh(\Delta x\sqrt{s/\alpha})}{k\sqrt{s/\alpha}}\,\bar{q}_2(s) \tag{3.26}$$

$$B = -\sinh(\Delta x\sqrt{s/\alpha})\,\bar{\theta}_2(s) - \frac{\cosh(\Delta x\sqrt{s/\alpha})}{k\sqrt{s/\alpha}}\,\bar{q}_2(s) \tag{3.27}$$

Therefore, the solution in the Laplace domain for layer 1 is

$$\bar{\theta}_1(s) = A_1 \bar{\theta}_2(s) + B_1 \bar{q}_2(s) \tag{3.28}$$

$$\bar{q}_1(s) = C_1 \bar{\theta}_2(s) + D_1 \bar{q}_2(s) \tag{3.29}$$

where

$$\begin{aligned} A_1 &= \cosh(\Delta x_1 \sqrt{s/\alpha_1}) \\ B_1 &= \frac{1}{k_1\sqrt{s/\alpha_1}} \sinh(\Delta x_1 \sqrt{s/\alpha_1}) \\ C_1 &= k_1\sqrt{s/\alpha_1} \sinh(\Delta x_1 \sqrt{s/\alpha_1}) \\ D_1 &= \cosh(\Delta x_1 \sqrt{s/\alpha_1}) \end{aligned} \tag{3.30}$$

Using the general notation, the above solution is applicable to any layer i

$$\bar{\theta}_i(x_i,s) = A_i \bar{\theta}_{i+1}(x_{i+1},s) + B_i \bar{q}_{i+1}(x_{i+1},s) \tag{3.31}$$

$$\bar{q}_i(x_i,s) = C_i \bar{\theta}_{i+1}(x_{i+1},s) + D_i \bar{q}_{i+1}(x_{i+1},s) \tag{3.32}$$

where

$$\begin{aligned} A_i &= \cosh(\Delta x_i \sqrt{s/\alpha_i}) \\ B_i &= \frac{1}{k_i\sqrt{s/\alpha_i}} \sinh(\Delta x_i \sqrt{s/\alpha_i}) \\ C_i &= k_i\sqrt{s/\alpha_i} \sinh(\Delta x_i \sqrt{s/\alpha_i}) \\ D_i &= \cosh(\Delta x_i \sqrt{s/\alpha_i}) \end{aligned} \tag{3.33}$$

and

$$\Delta x_i = x_{i+1} - x_i \tag{3.34}$$

Rewriting Eqs. 3.31 and 3.32 in a matrix form,

$$\begin{bmatrix} \bar{\theta}_i \\ \bar{q}_i \end{bmatrix} = \begin{bmatrix} A_i & B_i \\ C_i & D_i \end{bmatrix} \begin{bmatrix} \bar{\theta}_{i+1} \\ \bar{q}_{i+1} \end{bmatrix} \tag{3.35}$$

TRANSMISSION MATRIX

The matrix

$$\begin{bmatrix} A_i & B_i \\ C_i & D_i \end{bmatrix} \tag{3.36}$$

is know as the "Transmission Matrix."

The determinant of the transmission matrix is equal to one, i.e.,

$$\begin{vmatrix} A_i & B_i \\ C_i & D_i \end{vmatrix} = \cosh^2(\Delta x_i \sqrt{s/\alpha_i}) - \sinh^2(\Delta x_i \sqrt{s/\alpha_i}) = 1 \tag{3.37}$$

The thermal resistance, R, and thermal capacitance, C, are defined for layer i by

$$R_i = \frac{\Delta x_i}{k_i} \quad ; \quad C_i = \Delta x_i \, \rho_i \, C_{pi} \quad ; \quad R_i \, C_{pi} = \frac{\Delta x_i^2}{\alpha_i} \tag{3.38}$$

Thus, the transmission matrix for a single layer (using layer 1 for example) in terms of the resistance and capacitance is

$$\begin{bmatrix} A_1 & B_1 \\ C_1 & D_1 \end{bmatrix} = \begin{bmatrix} \cosh\sqrt{sR_1C_1} & \dfrac{R_1}{\sqrt{sR_1C_1}}\sinh\sqrt{sR_1C_1} \\ \dfrac{\sqrt{sR_1C_1}}{R_1}\sinh\sqrt{sR_1C_1} & \cosh\sqrt{sR_1C_1} \end{bmatrix} \tag{3.39}$$

For a lightweight slab or a convective air film, $C_1 \rightarrow 0$ and elements of the transmission matrix are

$$\begin{aligned} &\cosh\sqrt{sR_1C_1} \rightarrow 1 \\ &\frac{\sqrt{sR_1C_1}}{R_1}\sinh\sqrt{sR_1C_1} \rightarrow 0 \end{aligned} \tag{3.40}$$

By L'hospital's rule, limit as $C_1 \rightarrow 0$

$$\frac{R_1}{\sqrt{sR_1C_1}}\sinh\sqrt{sR_1C_1} \rightarrow R_1 \tag{3.41}$$

which leads to the following important relation for lightweight slabs or convective air films:

$$\begin{bmatrix} A_1 & B_1 \\ C_1 & D_1 \end{bmatrix} = \begin{bmatrix} 1 & R_1 \\ 0 & 1 \end{bmatrix} \tag{3.42}$$

Rearranging Eq. 3.31 for a general layer and solving for the heat flux transform on surface $i+1$ in terms of the temperatures,

$$\bar{q}_{i+1}(x_{i+1},s) = \frac{1}{B_i}\bar{\theta}_i - \frac{A_i}{B_i}\bar{\theta}_{i+1} \tag{3.43}$$

Substituting into Eq. 3.32 and solving for the heat flux at surface i,

$$\bar{q}_i(x_i,s) = \frac{D_i}{B_i}\bar{\theta}_i - \left[\frac{A_iD_i - C_iB_i}{B_i}\right]\bar{\theta}_{i+1} \tag{3.44}$$

Noting that

$$[A_iD_i - C_iB_i] = \begin{vmatrix} A_i & B_i \\ C_i & D_i \end{vmatrix} = 1.0 \tag{3.45}$$

Eq. 3.44 becomes

$$\bar{q}_i(x_i,s) = \frac{D_i}{B_i}\bar{\theta}_i - \frac{1}{B_i}\bar{\theta}_{i+1} \tag{3.46}$$

Rewriting Eqs. 3.46 and 3.43 in matrix form gives the heat flux equations, at either surface of the layer, in terms of the surface temperature transforms

$$\begin{bmatrix} \bar{q}_i \\ \bar{q}_{i+1} \end{bmatrix} = \begin{bmatrix} \frac{D_i}{B_i} & -\frac{1}{B_i} \\ \frac{1}{B_i} & -\frac{A_i}{B_i} \end{bmatrix} \begin{bmatrix} \bar{\theta}_i \\ \bar{\theta}_{i+1} \end{bmatrix} \tag{3.47}$$

Application of Eq. 3.35 to all layers gives

$$
\begin{bmatrix} \bar{\theta}_1 \\ \bar{q}_1 \end{bmatrix} = \begin{bmatrix} A_1 & B_1 \\ C_1 & D_1 \end{bmatrix} \begin{bmatrix} \bar{\theta}_2 \\ \bar{q}_2 \end{bmatrix}
$$

$$
\begin{bmatrix} \bar{\theta}_2 \\ \bar{q}_2 \end{bmatrix} = \begin{bmatrix} A_2 & B_2 \\ C_2 & D_2 \end{bmatrix} \begin{bmatrix} \bar{\theta}_3 \\ \bar{q}_3 \end{bmatrix}
$$

$$
\begin{bmatrix} \bar{\theta}_3 \\ \bar{q}_3 \end{bmatrix} = \begin{bmatrix} A_3 & B_3 \\ C_3 & D_3 \end{bmatrix} \begin{bmatrix} \bar{\theta}_4 \\ \bar{q}_4 \end{bmatrix} \qquad (3.48)
$$

$$
\vdots \quad \vdots \quad \vdots \quad \vdots
$$

$$
\begin{bmatrix} \bar{\theta}_{n-1} \\ \bar{q}_{n-1} \end{bmatrix} = \begin{bmatrix} A_{n-1} & B_{n-1} \\ C_{n-1} & D_{n-1} \end{bmatrix} \begin{bmatrix} \bar{\theta}_n \\ \bar{q}_n \end{bmatrix}
$$

The above matrix equations for an (n-1) multilayer homogeneous slab can be written in the form

$$
\begin{bmatrix} \bar{\theta}_1 \\ \bar{q}_1 \end{bmatrix} = \begin{bmatrix} A & B \\ C & D \end{bmatrix} \begin{bmatrix} \bar{\theta}_n \\ \bar{q}_n \end{bmatrix} \qquad (3.49)
$$

where the overall transmission matrix is

$$
\begin{bmatrix} A & B \\ C & D \end{bmatrix} = \begin{bmatrix} A_1 & B_1 \\ C_1 & D_1 \end{bmatrix} \begin{bmatrix} A_2 & B_2 \\ C_2 & D_2 \end{bmatrix} \cdots \begin{bmatrix} A_{n-1} & B_{n-1} \\ C_{n-1} & D_{n-1} \end{bmatrix} \qquad (3.50)
$$

since

$$
\begin{vmatrix} A & B \\ C & D \end{vmatrix} = \begin{vmatrix} A_1 & B_1 \\ C_1 & D_1 \end{vmatrix} \begin{vmatrix} A_2 & B_2 \\ C_2 & D_2 \end{vmatrix} \cdots \begin{vmatrix} A_{n-1} & B_{n-1} \\ C_{n-1} & D_{n-1} \end{vmatrix} = (1) \,.\, (1) \ldots .(1) = 1 \qquad (3.51)
$$

Similarly, Eq. 3.49 can be expressed in terms of the inner and outer surface temperatures.

$$\begin{bmatrix} \bar{q}_1 \\ \bar{q}_n \end{bmatrix} = \begin{bmatrix} \frac{D}{B} & -\frac{1}{B} \\ \frac{1}{B} & -\frac{A}{B} \end{bmatrix} \begin{bmatrix} \bar{\theta}_1 \\ \bar{\theta}_n \end{bmatrix} \tag{3.52}$$

Equation 3.52 is the desired solution in the Laplace domain for surface heat fluxes in terms of the surface temperatures. In order to invert back to the time domain, the functional form of the boundary temperature profiles needs to be specified. Since these boundary temperatures are ultimately used to represent measurements in the form of tabular data, a continuous function in the form of trapezoidal "pulses" is convenient for representing and interpolating the surface temperature. The approach for representing the boundary temperatures is developed in the next section. After determining the temperature profile on each surface, the residue theorem for the inversion of the Laplace transform is applied to Eq. 3.52 to obtain the heat flux in the real time domain at each surface.

SUPERPOSITION PRINCIPLE AND RESIDUE THEOREM

The inversion formula for a known Laplace transform function $\bar{F}(s)$ of a function F(t) is

$$F(t) = \frac{1}{2\pi j} \int_{\gamma - j\infty}^{\gamma + j\infty} e^{st} \bar{F}(s)\, ds = \frac{1}{2\pi j} \int G(s)\, ds \tag{3.53}$$

where $j = \sqrt{-1}$. The integration is to be performed in the complex s plane along the infinite line $x = \gamma$, as shown in Fig. 1. The constant γ is chosen so that all singularities of F(s) lie to the left of the line $x = \gamma$. In this instance, the integral in Eq. 3.53 is evaluated using the contour integration of complex variable functions and results from the residue theorem.

The residue theorem [97] applied to a function G(s) around a contour C is

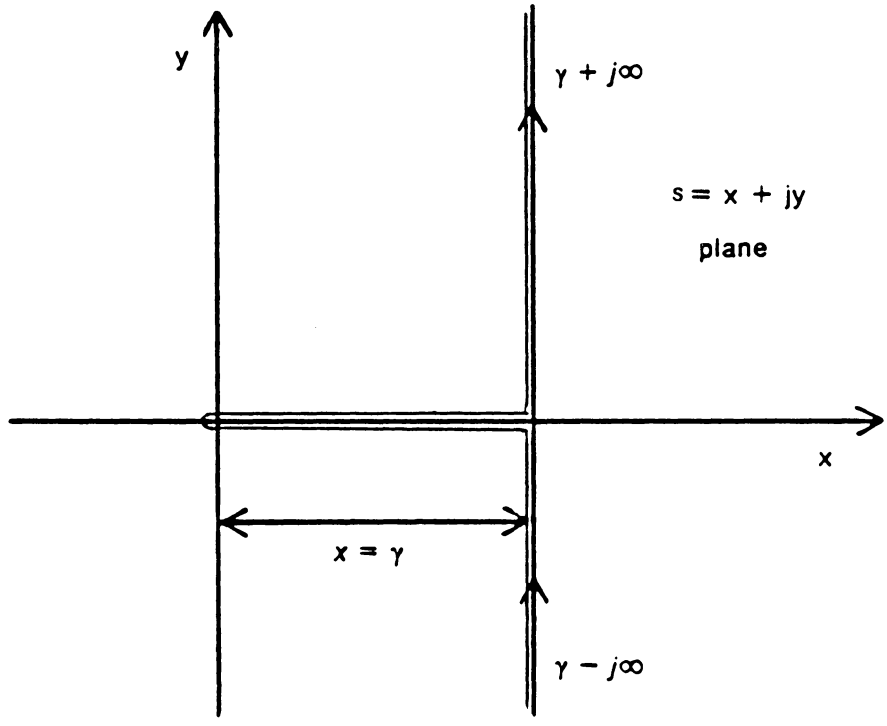

Figure 1. Path of Integration in the Inversion Formula

$$\frac{1}{2\pi j}\int_C G(s)ds \quad = \quad \sum_{k=1}^{N} res(s_k) \qquad (3.54 - a)$$

where k refers to the poles. Equation 3.53 becomes

$$F(t) = \frac{1}{2\pi j}\int_C G(s)ds \quad = \quad \sum_{k=1}^{N} res(s_k) \qquad (3.54 - b)$$

where G(s) is a complex variable function that is analytic inside the region under consideration except at poles located at s_1, s_2, s_3 , etc. Also, $res(s_1)$, $res(s_2)$, $res(s_3)$, etc., denote the residues of the integrand G(s) at these poles. The function G(s) is said to be analytic at a point s_0 in the complex plane if it has a single value and a derivative in some neighborhood of the point $s = s_0$. A pole is an isolated singularity because the function is not analytic at that point. For example, the function g(s) = 1/s has a pole at s = 0, irrespective of the direction in which the point is approached.

Before applying the residue theorem to invert back to the time domain, one useful principal which will be applied needs to be discussed. The superposition principle is used to obtain the temperature profiles of both wall surfaces, taken as

$$\theta = T - T_m \cong \sum_{i=0}^{\infty} \theta_i(t_i) \qquad (3.55)$$

Extending this representation for the boundary surface temperatures of the slab

$$\begin{aligned} \theta_1 &= T_1 - T_m = \sum_{i=0}^{\infty} \theta_{1,i}(t_i)\ \varphi(t_i) \\ \theta_n &= T_n - T_m = \sum_{i=0}^{\infty} \theta_{n,i}(t_i)\ \varphi(t_i) \end{aligned} \qquad (3.56)$$

where $\theta_{k,i}$ are amplitudes at time t = i δ for the boundary surfaces. In Eqs. 3.55 and for the remainder of this chapter, i denotes the time coordinate of the pulse. (Earlier, i was used to denote the layer number.) The time interval of the pulses is δ. The functions $\varphi(t_i)$ are defined for the interval $0 < t_i < a\delta$ where a is the width of the pulse at the base.

The trapezoidal or triangular pulses which correspond to a=2 or a base of 2δ will be used. They are suited to model well the temperature profiles at the boundaries, as shown in Fig. 2. This representation is a piecewise linear fit to temperatures at discrete times. The triangular pulse is represented by

$$\varphi(t_i) = \begin{cases} 0 , & t_i \leq 0 \\ \dfrac{t_i}{\delta} , & 0 < t_i \leq \delta \\ 2 - \dfrac{t_i}{\delta} , & \delta < t_i \leq 2\delta \\ 0 , & t_i > 2\delta \end{cases} \tag{3.57}$$

as shown in Fig. 2.

Adjustment of the time relating the pulses in the summations to the real time coordinate t, taken at δ intervals, in the original differential equation is now given. By substituting Eqs. 3.56 and 3.57 back into the original differential equation, it is found that they are valid for θ_i (i=1, 2, 3, etc.) provided that

$$t_i = t - i\delta \tag{3.58}$$

where t is the original time coordinate at δ intervals and t_i is the time coordinate corresponding to the θ_i pulse.

Equation 3.57 is the pulse function in the real time domain. The Laplace transform of the triangular pulse function is

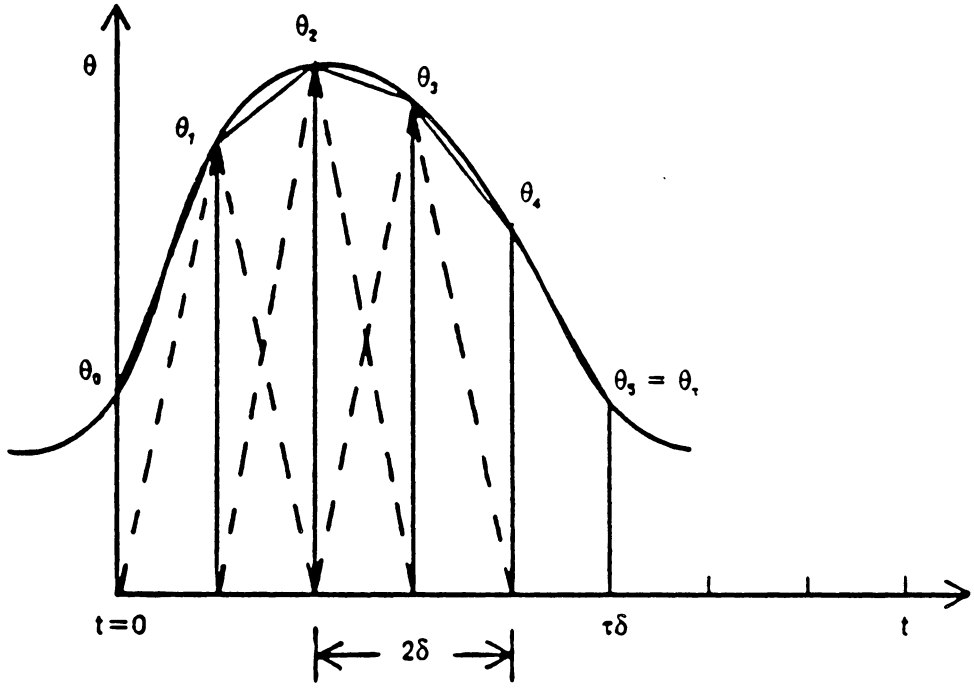

Figure 2. Trapezoidal (solid lines) or Triangular (dashed lines) Pulses

$$\bar{\varphi}(t_i) = \begin{cases} \dfrac{1}{\delta s^2} , & 0 < t_i \leq \delta \\ \dfrac{1}{\delta s^2}(1 - 2e^{-s\delta}) , & \delta < t_i \leq 2\delta \\ \dfrac{1}{\delta s^2}(1 - e^{-s\delta})^2 , & t_i > 2\delta \end{cases} \tag{3.59}$$

and the Laplace transforms of Eq. 3.56 is

$$\begin{aligned} \theta_1 &= \sum_{i=0}^{\infty} \bar{\varphi}\ \theta_{1,i}(t - i\delta) \\ \theta_n &= \sum_{i=0}^{\infty} \bar{\varphi}\ \theta_{n,i}(t - i\delta) \end{aligned} \tag{3.60}$$

Substitution into Eq. 3.52 leads to

$$\begin{bmatrix} \bar{q}_1 \\ \bar{q}_n \end{bmatrix} = \bar{\varphi} \sum_{i=0}^{\infty} \begin{bmatrix} \dfrac{D}{B} & -\dfrac{1}{B} \\ \dfrac{1}{B} & -\dfrac{A}{B} \end{bmatrix} \begin{bmatrix} \theta_{1,i}(t - i\delta) \\ \theta_{n,i}(t - i\delta) \end{bmatrix} \tag{3.61}$$

Expressing the Laplace Transform flux relation for each temperature pulse, gives

$$\begin{bmatrix} \bar{q}_{1,i} \\ \bar{q}_{n,i} \end{bmatrix} = \bar{\varphi} \begin{bmatrix} \dfrac{D}{B} & -\dfrac{1}{B} \\ \dfrac{1}{B} & -\dfrac{A}{B} \end{bmatrix} \begin{bmatrix} \theta_1(t - i\delta) \\ \theta_n(t - i\delta) \end{bmatrix} \tag{3.62}$$

Equation 3.62 can now be inverted from the Laplace domain using the residue theorem. Equation 3.62 can be expressed as

$$\begin{bmatrix} \bar{q}_{1,i} \\ \bar{q}_{n,i} \end{bmatrix} = \begin{bmatrix} \bar{X}_i & -\bar{Y}_i \\ \bar{Y}_i & -\bar{Z}_i \end{bmatrix} \begin{bmatrix} \theta_1(t - i\delta) \\ \theta_n(t - i\delta) \end{bmatrix} \tag{3.63}$$

where

$$\begin{aligned} \bar{X}_i &= \bar{\varphi}\,\frac{D}{B} \\ \bar{Y}_i &= \bar{\varphi}\,\frac{1}{B} \\ \bar{Z}_i &= \bar{\varphi}\,\frac{A}{B} \end{aligned} \tag{3.64}$$

Equation 3.63 is of the form

$$\begin{bmatrix} \bar{q}_{1,i} \\ \bar{q}_{n,i} \end{bmatrix} = \bar{K}_i \begin{bmatrix} \theta_1(t - i\delta) \\ \theta_n(t - i\delta) \end{bmatrix} \tag{3.65}$$

Inverting it back into the time domain will lead to a similar equation form, i.e.,

$$\begin{bmatrix} q_{1,i} \\ q_{n,i} \end{bmatrix} = K_i \begin{bmatrix} \theta_1(t - i\delta) \\ \theta_n(t - i\delta) \end{bmatrix} \tag{3.66}$$

where

$$K_i = \begin{bmatrix} X_i & -Y_i \\ Y_i & -Z_i \end{bmatrix} \tag{3.67}$$

INVERSION TO THE TIME DOMAIN

The inversion of the $\bar{K}_i$ matrix is carried out by inverting its elements. (Reference 97 is recommended for a more detailed explanation of this residue theorem application.)

$$L^{-1}[\bar{X}_i] = X_i = \lim_{s \to 0} \frac{d}{ds}\left[\frac{s^2\bar{\varphi}De^{st_i}}{B}\right] + \sum_{k=1}^{\infty}\left[\frac{\bar{\varphi}De^{st_i}}{\frac{dB}{ds}}\right]_{s=-\beta_k}$$

$$L^{-1}[\bar{Y}_i] = Y_i = \lim_{s \to 0} \frac{d}{ds}\left[\frac{s^2\bar{\varphi}e^{st_i}}{B}\right] + \sum_{k=1}^{\infty}\left[\frac{\bar{\varphi}e^{st_i}}{\frac{dB}{ds}}\right]_{s=-\beta_k} \qquad (3.68)$$

$$L^{-1}[\bar{Z}_i] = Z_i = \lim_{s \to 0} \frac{d}{ds}\left[\frac{s^2\bar{\varphi}Ae^{st_i}}{B}\right] + \sum_{k=1}^{\infty}\left[\frac{\bar{\varphi}Ae^{st_i}}{\frac{dB}{ds}}\right]_{s=-\beta_k}$$

where the β 's are the roots (poles) of the following equation:

$$B(s = -\beta_k) = 0 \ , \qquad k = 1, 2, ..., \infty \qquad (3.69)$$

In Eq. 3.68, the residues are being summed over all the poles, s=0 and $s = -\beta_k$, k=1, 2, 3, etc., to satisfy the residue theorem. Inversion of Eq. 3.68 is presented in Appendix A. The results are

Response Factors X :

$$X_0 = \left[\frac{D}{B} + \left(\frac{1}{\delta B}\right)\left(\frac{dD}{ds}\right) - \left(\frac{D}{\delta B^2}\right)\left(\frac{dB}{ds}\right)\right]_{s=0} + \sum_{k=1}^{\infty}\left[\left(\frac{e^{-\beta_k\delta}}{\delta\beta^2}\right) \quad \frac{D}{\frac{dB}{ds}}\right]_{s=-\beta_k}$$

$$X_1 = \left[\frac{D}{\delta B^2} - \left(\frac{1}{\delta B}\right)\left(\frac{dD}{ds}\right)\right]_{s=0} + \sum_{k=1}^{\infty}\left[\left(\frac{(1 - 2e^{\beta_k\delta})e^{-2\beta_k\delta}}{\delta\beta^2}\right) \quad \frac{D}{\frac{dB}{ds}}\right]_{s=-\beta_k} \qquad (3.70)$$

$$X_i = \sum_{k=1}^{\infty}\left[\left(\frac{(1 - e^{\beta_k\delta})^2 e^{-(i+1)\beta_k\delta}}{\delta\beta^2}\right) \quad \frac{D}{\frac{dB}{ds}}\right]_{s=-\beta_k} \qquad i = 2, 3, 4, ...$$

Response Factors Y :

$$Y_0 = \left[\frac{1}{B} - \left(\frac{1}{\delta B^2}\right)\left(\frac{dB}{ds}\right)\right]_{s=0} + \sum_{k=1}^{\infty}\left[\left(\frac{e^{-\beta_k\delta}}{\delta\beta^2}\right) \quad \frac{1}{\frac{dB}{ds}}\right]_{s=-\beta_k}$$

$$Y_1 = \left[\frac{1}{\delta B^2}\right]_{s=0} + \sum_{k=1}^{\infty}\left[\left(\frac{(1-2e^{\beta_k\delta})e^{-2\beta_k\delta}}{\delta\beta^2}\right) \quad \frac{1}{\frac{dB}{ds}}\right]_{s=-\beta_k} \qquad (3.71)$$

$$Y_i = \sum_{k=1}^{\infty}\left[\left(\frac{(1-e^{\beta_k\delta})^2 e^{-(i+1)\beta_k\delta}}{\delta\beta^2}\right) \quad \frac{1}{\frac{dB}{ds}}\right]_{s=-\beta_k} \qquad i = 2, 3, 4, \ldots$$

Response Factors Z :

$$Z_0 = \left[\frac{A}{B} + \left(\frac{1}{\delta B}\right)\left(\frac{dA}{ds}\right) - \left(\frac{A}{\delta B^2}\right)\left(\frac{dB}{ds}\right)\right]_{s=0} + \sum_{k=1}^{\infty}\left[\left(\frac{e^{-\beta_k\delta}}{\delta\beta^2}\right) \quad \frac{A}{\frac{dB}{ds}}\right]_{s=-\beta_k}$$

$$Z_1 = \left[\frac{A}{\delta B^2} - \left(\frac{1}{\delta B}\right)\left(\frac{dA}{ds}\right)\right]_{s=0} + \sum_{k=1}^{\infty}\left[\left(\frac{(1-2e^{\beta_k\delta})e^{-2\beta_k\delta}}{\delta\beta^2}\right) \quad \frac{A}{\frac{dB}{ds}}\right]_{s=-\beta_k} \qquad (3.72)$$

$$Z_i = \sum_{k=1}^{\infty}\left[\left(\frac{(1-e^{\beta_k\delta})^2 e^{-(i+1)\beta_k\delta}}{\delta\beta^2}\right) \quad \frac{A}{\frac{dB}{ds}}\right]_{s=-\beta_k} \qquad i = 2, 3, 4, \ldots$$

where X_0 , Y_0 , and Z_0 are evaluated at the end of the time step δ. At the end of the time step 2δ, X_1 , Y_1 , and Z_1 are evaluated. At the end of the time step 3δ, X_2 , Y_2 , and Z_2 are evaluated, etc.

Using Eq. 3.61, the fluxes at the inner and outer surfaces of the slab can be calculated. Using the notation,

$$t = \delta\,\tau \qquad (3.73)$$

The new time coordinate becomes

$$\begin{aligned} \theta_1(t - i\delta) &\rightarrow \theta_1(\tau - i) \\ \theta_n(t - i\delta) &\rightarrow \theta_n(\tau - i) \end{aligned} \tag{3.74}$$

Substituting Eq. 3.74 into 3.61 leads to

$$\begin{bmatrix} q_1(\tau) \\ q_n(\tau) \end{bmatrix} = \sum_{i=0}^{\infty} \begin{bmatrix} X_i & -Y_i \\ Y_i & -Z_i \end{bmatrix} \begin{bmatrix} \theta_1(\tau - i) \\ \theta_n(\tau - i) \end{bmatrix} \tag{3.75}$$

where

$$\begin{aligned} \theta_1(\tau - i) &= T_1(\tau - i) - T_m \\ \theta_n(\tau - i) &= T_n(\tau - i) - T_m \end{aligned} \tag{3.76}$$

The summation in Eq. 3.75 is from zero to infinity. In computer applications, however, it is more convenient to start the summation at one and end at a limit N. Therefore, the following notation is introduced:

$$\begin{bmatrix} q_1(\tau) \\ q_n(\tau) \end{bmatrix} = \sum_{i=1}^{N} \begin{bmatrix} X_i & -Y_i \\ Y_i & -Z_i \end{bmatrix} \begin{bmatrix} T_1(\tau + 1 - i) - T_m \\ T_n(\tau + 1 - i) - T_m \end{bmatrix} \tag{3.77}$$

The response factors are now shifted forward one subscript (X_0 is now redefined as X_1 , X_1 is now X_2, etc.). Therefore, the redefined response factors are summarized as follows:

Response Factors X :

$$X_1 = \left[\frac{D}{B} + \left(\frac{1}{\delta B}\right)\left(\frac{dD}{ds}\right) - \left(\frac{D}{\delta B^2}\right)\left(\frac{dB}{ds}\right)\right]_{s=0} + \sum_{k=1}^{N}\left[\left(\frac{e^{-\beta_k\delta}}{\delta\beta^2}\right) \quad \frac{D}{\frac{dB}{ds}}\right]_{s=-\beta_k}$$

$$X_2 = \left[\frac{D}{\delta B^2} - \left(\frac{1}{\delta B}\right)\left(\frac{dD}{ds}\right)\right]_{s=0} + \sum_{k=1}^{N}\left[\left(\frac{(1-2e^{\beta_k\delta})e^{-2\beta_k\delta}}{\delta\beta^2}\right) \quad \frac{D}{\frac{dB}{ds}}\right]_{s=-\beta_k}$$

$$X_i = \sum_{k=1}^{N}\left[\left(\frac{(1-e^{\beta_k\delta})^2 e^{-i\beta_k\delta}}{\delta\beta^2}\right) \quad \frac{D}{\frac{dB}{ds}}\right]_{s=-\beta_k} \qquad i = 3, 4, 5, \ldots$$

Response Factors Y :

$$Y_1 = \left[\frac{1}{B} - \left(\frac{1}{\delta B^2}\right)\left(\frac{dB}{ds}\right)\right]_{s=0} + \sum_{k=1}^{N}\left[\left(\frac{e^{-\beta_k\delta}}{\delta\beta^2}\right) \quad \frac{1}{\frac{dB}{ds}}\right]_{s=-\beta_k}$$

$$Y_2 = \left[\frac{1}{\delta B^2}\right]_{s=0} + \sum_{k=1}^{N}\left[\left(\frac{(1-2e^{\beta_k\delta})e^{-2\beta_k\delta}}{\delta\beta^2}\right) \quad \frac{1}{\frac{dB}{ds}}\right]_{s=-\beta_k} \qquad (3.78)$$

$$Y_i = \sum_{k=1}^{N}\left[\left(\frac{(1-e^{\beta_k\delta})^2 e^{-i\beta_k\delta}}{\delta\beta^2}\right) \quad \frac{1}{\frac{dB}{ds}}\right]_{s=-\beta_k} \qquad i = 3, 4, 5, \ldots$$

Response Factors Z :

$$Z_1 = \left[\frac{A}{B} + \left(\frac{1}{\delta B}\right)\left(\frac{dA}{ds}\right) - \left(\frac{A}{\delta B^2}\right)\left(\frac{dB}{ds}\right)\right]_{s=0} + \sum_{k=1}^{N}\left[\left(\frac{e^{-\beta_k\delta}}{\delta\beta^2}\right) \quad \frac{A}{\frac{dB}{ds}}\right]_{s=-\beta_k}$$

$$Z_2 = \left[\frac{A}{\delta B^2} - \left(\frac{1}{\delta B}\right)\left(\frac{dA}{ds}\right)\right]_{s=0} + \sum_{k=1}^{N}\left[\left(\frac{(1-2e^{\beta_k\delta})e^{-2\beta_k\delta}}{\delta\beta^2}\right) \quad \frac{A}{\frac{dB}{ds}}\right]_{s=-\beta_k}$$

$$Z_i = \sum_{k=1}^{N}\left[\left(\frac{(1-e^{\beta_k\delta})^2 e^{-i\beta_k\delta}}{\delta\beta^2}\right) \quad \frac{A}{\frac{dB}{ds}}\right]_{s=-\beta_k} \qquad i = 3, 4, 5, \ldots$$

In Eq. 3.77, the flux subscript 1 means the inner surface and n the outer surface or vice versa depending on the coordinate taken when calculating the response factors. That is, once a direction is decided, it should be retained throughout the analysis. T_m is the initial temperature

of the slab at time t = 0. Derivation of this method in the literature (references 13 through 15) is sometimes presented with T_m taken as zero.

CHARACTERISTICS OF THE RESPONSE FACTORS

Important properties of response factors are presented next. It should be noted here that the directions of the fluxes as given in Eq. 3.75 are q_1 is positive when pointing *away* from surface 1 and q_n is positive when pointing *toward* surface n (Fig. 3).

The steady-state heat transfer through a slab is

$$q = U(T_1 - T_n) \cdot \tag{3.79}$$

The steady-state heat flux equations are equal when represented in the same direction as the TRFM fluxes.

$$q_1 = q_n = U(T_1 - T_n) \tag{3.80}$$

Setting $T_m = 0$ in Eq. 3.75

$$\begin{bmatrix} q_1(\tau) \\ q_n(\tau) \end{bmatrix} = \sum_{i=1}^{N} \begin{bmatrix} X_i & -Y_i \\ Y_i & -Z_i \end{bmatrix} \begin{bmatrix} T_1(\tau + 1 - i) \\ T_n(\tau + 1 - i) \end{bmatrix} \tag{3.81}$$

Since Eqs. 3.80 and 3.81 have the same directions, they can be equated at the steady-state condition

$$\begin{aligned} q_1 = U\ (T_1 - T_n) &= \sum_{i=1}^{N} [X_i T_1 - Y_i T_n] \\ q_n = U\ (T_1 - T_n) &= \sum_{i=1}^{N} [Y_i T_1 - Z_i T_n] \end{aligned} \tag{3.82}$$

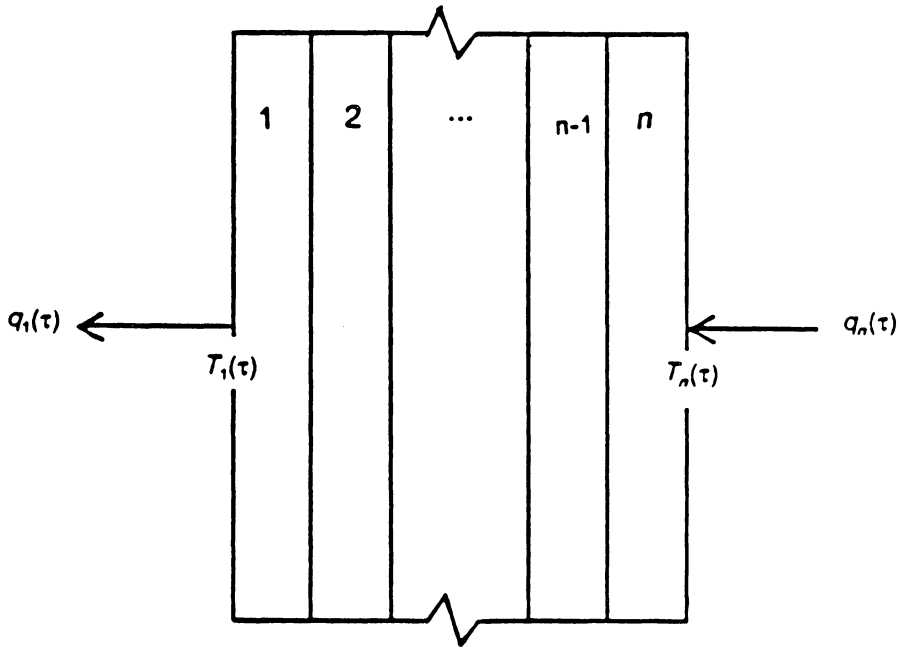

Figure 3. Typical Multilayer Wall: the direction of heat fluxes is shown

Further expansion leads to

$$\begin{aligned} U\,T_1 - U\,T_n &= \sum_{i=1}^{N} X_i T_1 - \sum_{i=1}^{N} Y_i T_n \\ U\,T_1 - U\,T_n &= \sum_{i=1}^{N} Y_i T_1 - \sum_{i=1}^{N} Z_i T_n \end{aligned} \tag{3.83}$$

Hence, the first characteristic of the response factors, which will prove later to be a valuable check on whether or not the response factors have been calculated correctly, is given by

$$\sum_{i=1}^{N} X_i = \sum_{i=1}^{N} Y_i = \sum_{i=1}^{N} Z_i = U \tag{3.84}$$

The second characteristic is determined from examining the response factors X_i, Y_i, *and* Z_i, for i = 3, 4, 5, etc.

$$\begin{aligned} X_i &= \sum_{k=1}^{N} \left[\left(\frac{(1 - e^{\beta_k \delta})^2 e^{-i\beta_k \delta}}{\delta \beta^2} \right) \frac{D}{\frac{dB}{ds}} \right]_{s=-\beta_k} && i = 3, 4, 5, \ldots \\ Y_i &= \sum_{k=1}^{N} \left[\left(\frac{(1 - e^{\beta_k \delta})^2 e^{-i\beta_k \delta}}{\delta \beta^2} \right) \frac{1}{\frac{dB}{ds}} \right]_{s=-\beta_k} && i = 3, 4, 5, \ldots \\ Z_i &= \sum_{k=1}^{N} \left[\left(\frac{(1 - e^{\beta_k \delta})^2 e^{-i\beta_k \delta}}{\delta \beta^2} \right) \frac{A}{\frac{dB}{ds}} \right]_{s=-\beta_k} && i = 3, 4, 5, \ldots \end{aligned} \tag{3.85}$$

The response factors with i $\geq$ 3 (Eq. 3.85) can be written in the following form:

$$X_i = \sum_{k=1}^{N} g_{k,1} \lambda_k^i$$
$$Y_i = \sum_{k=1}^{N} g_{k,2} \lambda_k^i \qquad (3.86)$$
$$Z_i = \sum_{k=1}^{N} g_{k,3} \lambda_k^i$$

where

$$\lambda_k = e^{-\beta_k \delta} \quad ; \quad g_{k,1} = \left[\frac{(1 - e^{\beta_k \delta})^2}{\delta \beta^2} \; \frac{D}{\frac{dB}{ds}} \right]_{s=-\beta_k}$$
$$g_{k,2} = \left[\frac{(1 - e^{\beta_k \delta})^2}{\delta \beta^2} \; \frac{1}{\frac{dB}{ds}} \right]_{s=-\beta_k} \quad ; \quad g_{k,2} = \left[\frac{(1 - e^{\beta_k \delta})^2}{\delta \beta^2} \; \frac{A}{\frac{dB}{ds}} \right]_{s=-\beta_k} \qquad (3.87)$$

The following characteristic is observed: the response factors X_i, Y_i, *and* Z_i decrease on the order of $e^{-\delta\beta_1}$ at large values of i. Since $g_{k,1}$, $g_{k,2}$, *and* $g_{k,3}$ do not change with i and only $\lambda_k^i = e^{-i\beta_k\delta}$ changes with i, it is apparent that this common factor, or ratio, for all three response factors is affecting their values by the same amount as i is increased. Therefore, the second characteristic of response factors is that they all have the same common ratio for large values of i.

$$\frac{X_{i+1}}{X_i} = \frac{Y_{i+1}}{Y_i} = \frac{Z_{i+1}}{Z_i} = e^{-\delta\beta_1} \quad , \quad i > M \qquad (3.88)$$

The parameter M is usually larger than 15.

A brief examination of the numerical values of Eqs. 3.84 and 3.88 for a typical multilayer wall is shown next. A typical roof is used for the numerical example. The roof has a suspended ceiling with an air space, insulation, concrete, and roofing (felt and pitch slab). A sketch of the roof is shown in Fig. 4. In Table 1, the material description is presented with the

numerical values of the thickness, conductivity, density, and thermal capacity of each layer. The roots (β_k) and the response factors (X_i, Y_i, *and* Z_i) were calculated using a Fortran code, discussed later in this chapter, implementing the previous formulations. These roots and response factors are presented in Tables 2 and 3, respectively. The overall heat transfer coefficient was calculated from Table 1. Using Table 3 and the first characteristic of the response factors (Eq. 3.84), the overall heat transfer coefficient of the roof is

$$U = 0.6050088$$

$$\sum_{i=1}^{50} X_i = 0.6050088$$

$$\sum_{i=1}^{50} Y_i = 0.6050020$$

$$\sum_{i=1}^{50} Z_i = 0.6051014$$

The above numerical example gives an indication on how many response factors are needed to obtain the steady-state solution.

As noted above, the number of response factors used to satisfy the steady-state condition in the example was 50. This number is the limit in the summation of response factors used to satisfy Eq. 3.84. The suggested method of determining N is given next. For i > 1 and at every step i, the response factors are added (X_i is added separately, as well as Y_i *and* Z_i) and compared to each other and to the overall heat transfer coefficient. If Eq. 3.84 is essentially satisfied for all response factors, N is large enough. If Eq. 3.84 is not satisfied, the addition of response factors is continued. Therefore, Eq. 3.84 is used to insure steady-state simulation and to determine the number of response factors needed. There is no assurance, however, to whether the individual response factors are correct. That is, it is possible to sum the response factors and satisfy Eq. 3.84 but still have wrong individual response factors.

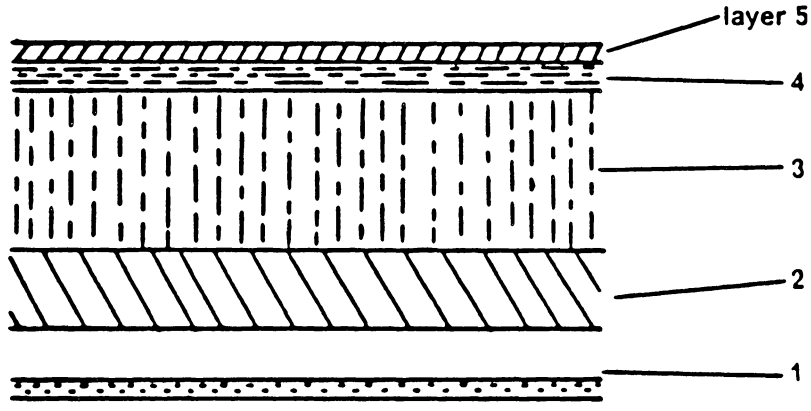

1 Suspended ceiling

2 Insulation

3 Concrete

4 Felt

5 Pitch slab

Figure 4. Typical Roof

Table 1. Material Description of the Typical Roof

DESCRIPTION OF LAYERS	LAYER No.	ΔX (m)	k (W/m.C)	ρ (kg/m^3)	C_p (kJ/kg.C)
Suspended Ceiling R = 0.36 m^{2}C / W	1	---	---	---	---
Insulation	2	0.051	0.0433	208.2	1.34
Concrete	3	0.102	1.7307	2243	0.84
Felt	4	0.02	0.191	1121	1.675
Pitch Slag	5	0.013	1.436	881	1.67

Table 2. Roots Distribution for the Typical Roof

k	B_k
1	0.238336556
2	1.333489115
3	3.499668506
4	6.038898336
5	11.813352109
6	14.807240054
7	22.534247015
8	27.338218867
9	32.176455395
10	44.160260026
11	50.429367947
12	65.172980117
13	68.709522427
14	83.485695006
15	91.656553189
16	113.211048122
17	121.737458504
18	147.260123544
19	155.732537630
20	173.776321939
21	193.017521293
22	208.492185917
23	235.641036630
24	256.420919639
25	282.646241346

Table 2. (continued)

k	β_k
26	306.358697286
27	332.807620691
28	342.473377576
29	384.524345865
30	393.506382080
31	444.704574234
32	453.975245522
33	488.604233029
34	512.168862801
35	541.102739107
36	580.276431432
37	614.425144442
38	652.375201251
39	673.697286942
40	723.371080783
41	735.180817192
42	805.297408701
43	819.356747809
44	892.142325171
45	909.380719291

Table 3. Response Factors for the Typical Roof

i	X_i W/m².C	Y_i W/m².C	Z_i W/m².C
1	0.21933432900	0.00011032508	3.30513212390
2	-0.08202804840	0.00512731738	-1.66661355443
3	-0.01813065000	0.01463976435	-0.33432617911
4	-0.00572015903	0.01646823722	-0.25534051235
5	-0.00226624717	0.01438020478	-0.20015315287
6	-0.00119540493	0.01170407624	-0.15746717247
7	-0.00078634868	0.00932058430	-0.12401176189
8	-0.00057859624	0.00737000190	-0.09769706473
9	-0.00044509256	0.00581394375	-0.07697484306
10	-0.00034785736	0.00458282763	-0.06065022018
11	-0.00027333930	0.00361145691	-0.04778827947
12	-0.00021517647	0.00284572747	-0.03765409626
13	-0.00016949347	0.00224228829	-0.02966905210
14	-0.00013353651	0.00176679165	-0.02337735208
15	-0.00010521480	0.00139212362	-0.01841989000
16	-0.00008290173	0.00109690695	-0.01451372098
17	-0.00006532112	0.00086429424	-0.01143590436
18	-0.00005146889	0.00068100985	-0.00901077742
19	-0.00004055425	0.00053659318	-0.00709992908
20	-0.00003195421	0.00042280187	-0.00559430009
21	-0.00002517792	0.00033314144	-0.00440795861
22	-0.00001983862	0.00026249462	-0.00347319572
23	-0.00001563160	0.00020682934	-0.00273666102
24	-0.00001231672	0.00016296859	-0.00215631773
25	-0.00000970480	0.00012840906	-0.00169904352

Table 3. (continued)

i	X_i W/m².C	Y_i W/m².C	Z_i W/m².C
26	-0.00000764678	0.00010117830	-0.00133874004
27	-0.00000602518	0.00007972218	-0.00105484343
28	-0.00000474747	0.00006281609	-0.00083115065
29	-0.00000374071	0.00004949515	-0.00065489473
30	-0.00000294744	0.00003899908	-0.00051601609
31	-0.00000232240	0.00003072884	-0.00040658841
32	-0.00000182991	0.00002421240	-0.00032036624
33	-0.00000144185	0.00001907786	-0.00025242856
34	-0.00000113609	0.00001503216	-0.00019889792
35	-0.00000089517	0.00001184440	-0.00015671912
36	-0.00000070534	0.00000933265	-0.00012348487
37	-0.00000055576	0.00000735354	-0.00009729835
38	-0.00000043790	0.00000579413	-0.00007666502
39	-0.00000034504	0.00000456541	-0.00006040724
40	-0.00000027187	0.00000359726	-0.00004759713
41	-0.00000021422	0.00000283442	-0.00003750356
42	-0.00000016879	0.00000223334	-0.00002955046
43	-0.00000013300	0.00000175973	-0.00002328391
44	-0.00000010479	0.00000138656	-0.00001834627
45	-0.00000008257	0.00000109252	-0.00001445571
46	-0.00000006506	0.00000086084	-0.00001139020
47	-0.00000005126	0.00000067829	-0.00000897476
48	-0.00000004039	0.00000053445	-0.00000707155
49	-0.00000003183	0.00000042111	-0.00000557194
50	-0.00000002508	0.00000033181	-0.00000439034

The second characteristic, Eq. 3.88, can be used to determine the validity of the individual response factors. It is argued here that with both characteristics satisfied, keeping in mind that each characteristic was obtained separately using different approaches, it would be extraordinary to have the later portion of response factors correct and the overall sum correct but still have incorrect initial response factors. Before determining if Eq. 3.88 is satisfied in the present example, a new term is introduced.

The "common ratio ($\overline{CR}$)" is the ratio of response factors, discussed earlier in determining Eq. 3.88, for i > M.

$$\overline{CR} = \frac{X_{i+1}}{X_i} = \frac{Y_{i+1}}{Y_i} = \frac{Z_{i+1}}{Z_i} = e^{-\delta\beta_1} \quad , \quad i > M \qquad (3.89)$$

Calculating the common ratio using Tables 2 and 3

$$\frac{X_{40}}{X_{39}} = \frac{-0.00000027187}{-0.000000034504} = 0.7879376$$

$$\frac{Y_{40}}{Y_{39}} = \frac{0.00000359726}{0.000000456541} = 0.7879379$$

$$\frac{Z_{40}}{Z_{39}} = \frac{-0.00004759713}{-0.00006040724} = 0.7879375$$

$$\overline{CR} = e^{-\delta\beta_1} = e^{-(1)(0.238336556)} = 0.7879375$$

It is obvious that the second characteristic is also satisfied. Also, the common ratio ($\overline{CR}$) was calculated using the first root only.

The common factor in all three types of response factors (Eq. 3.86) is $\lambda_k^i = e^{-i\beta_k\delta}$. For large values of i, i = 30

$$e^{-i\delta\beta_1} = e^{-(30)(1)(0.2383365)} = 0.000784789$$

$$e^{-i\delta\beta_2} = e^{-(30)(1)(1.3334891)} = 0.0$$

It is obvious that the effect of the second root and any other roots on the response factors for large values of i is zero. Therefore, taking the ratio of response factors leads, once again to

$$\frac{X_{i+1}}{X_i} = \frac{Y_{i+1}}{Y_i} = \frac{Z_{i+1}}{Z_i} = \frac{e^{-(i+1)\delta\beta_1}}{e^{-i\delta\beta_1}} = e^{-\delta\beta_1} \quad , \; i > M \tag{3.90}$$

The advantage of using the TRFM is the efficiency in computer, or computational, time it provides. The main benefit derived from using this method is that once the response factors have been calculated for a specific wall and a fixed time increment (usually one hour is a sufficient time increment), they can be stored and used throughout the analysis. Using Eq. 3.81, the surface fluxes can be calculated knowing the surface temperatures of the slab. Energy balances on the outside and inside surface of the slab can be used to solve for both surface temperatures, simultaneously. The analysis on multilayer walls can be conducted quite similarly to single layer walls. Since once the code that calculates the response factors is established, the heat flux formulas through any multilayer or single layer structure are similar. One of the inefficiencies of this method is the large number of response factors that are sometimes needed for an accurate simulation.

Peavy [13] introduced a new type of response factor which he called "Conduction Transfer Functions." A considerably smaller number of this new type of response factors is needed even for the massive walls which usually require a large number of response factors. Throughout this thesis, there will be no change of nomenclature between the thermal response factors [12] to the conduction transfer functions [13]. The adjustment, however, will be in referring to the response factors as the first-order response factors and to the conduction transfer functions as the higher-order response factors.

HIGHER-ORDER RESPONSE FACTORS

Higher-order response factors decrease sharply in magnitude with every term i. Equation 3.84 is satisfied with a smaller number of terms in the summation. Therefore, the thermal response factor method becomes more efficient in computational time. Rewriting Eq. 3.77 and assuming $T_m = 0$ to simplify the derivation

$$\begin{aligned} q_1(\tau) &= \sum_{i=1}^{N} X_i\, T_1(\tau + 1 - i) - \sum_{i=1}^{N} Y_i\, T_n(\tau + 1 - i) \\ q_n(\tau) &= \sum_{i=1}^{N} Y_i\, T_1(\tau + 1 - i) - \sum_{i=1}^{N} Z_i\, T_n(\tau + 1 - i) \end{aligned} \tag{3.91}$$

The nomenclature $X_{i,\ell}$, where ℓ is the order of response factor, is used for the remainder of the of the analysis. Therefore, response factors already derived are of the first-order. The response factors derived next are of order ℓ. According to this new definition of response factors, Eq. 3.86 can be written in the following form (first-order response factors):

$$\begin{aligned} X_{i,1} &= \sum_{k=1}^{N} g_{k,1}\ \lambda_k^i \\ Y_{i,1} &= \sum_{k=1}^{N} g_{k,2}\ \lambda_k^i \\ Z_{i,1} &= \sum_{k=1}^{N} g_{k,3}\ \lambda_k^i \end{aligned} \tag{3.92}$$

Equation 3.91 becomes

$$\begin{aligned} q_1(\tau) &= \sum_{i=1}^{N} X_{i,1}\, T_1(\tau + 1 - i) - \sum_{i=1}^{N} Y_{i,1}\, T_n(\tau + 1 - i) \\ q_n(\tau) &= \sum_{i=1}^{N} Y_{i,1}\, T_1(\tau + 1 - i) - \sum_{i=1}^{N} Z_{i,1}\, T_n(\tau + 1 - i) \end{aligned} \tag{3.93}$$

Expanding the summations for the inside flux

$$q_1(\tau) = X_{1,1}\,T_1(\tau) + X_{2,1}\,T_1(\tau-1) + X_{3,1}\,T_1(\tau-2) + \ldots - Y_{1,1}\,T_n(\tau) - Y_{2,1}\,T_n(\tau-1) - Y_{3,1}\,T_n(\tau-2) - \ldots \tag{3.94}$$

and performing the operation $q_1(\tau) - \lambda_1 q_1(\tau-1)$, where

$$q_1(\tau-1) = X_{1,1}\,T_1(\tau-1) + X_{2,1}\,T_1(\tau-2) + X_{3,1}\,T_1(\tau-3) + \ldots - Y_{1,1}\,T_n(\tau-1) - Y_{2,1}\,T_n(\tau-2) - Y_{3,1}\,T_n(\tau-3) - \ldots \tag{3.95}$$

Eq. 3.94 becomes

$$\begin{aligned} q_1(\tau) - \lambda_1 q_1(\tau-1) = {} & X_{1,1}\,T_1(\tau) + (X_{2,1} - \lambda_1 X_{1,1})\,T_1(\tau-1) \\ & + (X_{3,1} - \lambda_1 X_{2,1})\,T_1(\tau-2) + \ldots \\ & - Y_{1,1}\,T_1(\tau) - (Y_{2,1} - \lambda_1 Y_{1,1})\,T_1(\tau-1) \\ & - (Y_{3,1} - \lambda_1 Y_{2,1})\,T_1(\tau-2) - \ldots \end{aligned} \tag{3.96}$$

Solving for $q_1(\tau)$ and introducing the second-order response factors

$$q_1(\tau) = X_{1,2}\,T_1(\tau) + X_{2,2}\,T_1(\tau-1) + X_{3,2}\,T_1(\tau-2) + \ldots - Y_{1,2}\,T_n(\tau) - Y_{2,2}\,T_n(\tau-1) - Y_{3,2}\,T_n(\tau-2) - \ldots + \lambda_1 q_1(\tau-1) \tag{3.97}$$

where $\lambda_1 = e^{-\delta\beta_1}$ and

$$\begin{aligned} X_{1,2} &= X_{1,1} \\ X_{i,2} &= X_{i,1} - e^{-\delta\beta_1}\,X_{i-1,1}\,, \qquad i \geq 2 \end{aligned} \tag{3.98}$$

$$
\begin{aligned}
Y_{1,2} &= Y_{1,1} \\
Y_{i,2} &= Y_{i,1} - e^{-\delta\beta_1} Y_{i-1,1} \quad , \qquad i \geq 2
\end{aligned}
\tag{3.99}
$$

$$
\begin{aligned}
Z_{1,2} &= Z_{1,1} \\
Z_{i,2} &= Z_{i,1} - e^{-\delta\beta_1} Z_{i-1,1} \quad , \qquad i \geq 2
\end{aligned}
\tag{3.100}
$$

The heat flux on the outside surface of the wall is derived similarly, keeping in mind that $\lambda_1 = \overline{CR}$

$$
\begin{aligned}
q_n(\tau) = {} & Y_{1,2}\, T_1(\tau) + Y_{2,2}\, T_1(\tau - 1) + Y_{3,2}\, T_1(\tau - 2) + \ldots \\
& - Z_{1,2}\, T_n(\tau) - Z_{2,2}\, T_n(\tau - 1) - Z_{3,2}\, T_n(\tau - 2) - \ldots \\
& + \overline{CR}\, q_n(\tau - 1)
\end{aligned}
\tag{3.101}
$$

Therefore, the heat flux equations for the second-order response factors are

$$
\begin{aligned}
q_1(\tau) = {} & \sum_{i=1}^{N} X_{i,2} \left[T_1(\tau + 1 - i) - T_m \right] - \sum_{i=1}^{N} Y_{i,2} \left[T_n(\tau + 1 - i) - T_m \right] \\
& + \overline{CR}\, q_1(\tau - 1) \\
q_n(\tau) = {} & \sum_{i=1}^{N} Y_{i,2} \left[T_1(\tau + 1 - i) - T_m \right] - \sum_{i=1}^{N} Z_{i,2} \left[T_n(\tau + 1 - i) - T_m \right] \\
& + \overline{CR}\, q_n(\tau - 1)
\end{aligned}
\tag{3.102}
$$

Introducing the third-order response factors using a similar manipulation as used in Eq. 3.96, $q_1(\tau) - \lambda_2 q_1(\tau - 1)$, leads similarly to

$$
\begin{aligned}
X_{1,3} &= X_{1,2} = X_{1,1} \\
X_{i,3} &= X_{i,2} - e^{-\delta\beta_2} X_{i-1,2} \ , \qquad i \geq 2 \\
Y_{1,3} &= Y_{1,2} = Y_{1,1} \\
Y_{i,3} &= Y_{i,2} - e^{-\delta\beta_2} Y_{i-1,2} \ , \qquad i \geq 2 \\
Z_{1,3} &= Z_{1,2} = Z_{1,1} \\
Z_{i,3} &= Z_{i,2} - e^{-\delta\beta_2} Z_{i-1,2} \ , \qquad i \geq 2
\end{aligned}
\tag{3.103}
$$

From the manipulation applied to Eq. 3.102, additional terms are obtained for the fluxes at the interior and exterior surfaces

$$
\begin{aligned}
q_1(\tau) &= \sum_{i=1}^{N} X_{i,3} \left[T_1(\tau + 1 - i) - T_m\right] - \sum_{i=1}^{N} Y_{i,3} \left[T_n(\tau + 1 - i) - T_m\right] \\
&+ (\lambda_1 + \lambda_2) q_1(\tau - 1) - \lambda_1 \lambda_2 q_1(\tau - 2) \\
q_n(\tau) &= \sum_{i=1}^{N} Y_{i,3} \left[T_1(\tau + 1 - i) - T_m\right] - \sum_{i=1}^{N} Z_{i,3} \left[T_n(\tau + 1 - i) - T_m\right] \\
&+ (\lambda_1 + \lambda_2) q_n(\tau - 1) - \lambda_1 \lambda_2 q_n(\tau - 2)
\end{aligned}
\tag{3.104}
$$

For ℓ order response factors, the heat flux equations are

$$
\begin{aligned}
q_1(\tau) &= \sum_{i=1_\ell}^{N} X_{i,\ell} \left[T_1(\tau + 1 - i) - T_m\right] - \sum_{i=1}^{N} Y_{i,\ell} \left[T_n(\tau + 1 - i) - T_m\right] \\
&+ \sum_{j=2}^{\ell} (-1)^j C(j-1) q_1(\tau + 1 - j) \\
q_n(\tau) &= \sum_{i=1_\ell}^{N} Y_{i,\ell} \left[T_1(\tau + 1 - i) - T_m\right] - \sum_{i=1}^{N} Z_{i,\ell} \left[T_n(\tau + 1 - i) - T_m\right] \\
&+ \sum_{j=2}^{\ell} (-1)^j C(j-1) q_n(\tau + 1 - j)
\end{aligned}
\tag{3.105}
$$

where

$$
\begin{aligned}
X_{1,\ell} &= X_{1,1} \\
X_{i,\ell} &= X_{i,\ell-1} - e^{-\delta\beta_{\ell-1}} X_{i-1,\ell-1} \quad , \quad i \geq 2 \ \textit{and} \ \ell \geq 2 \\
Y_{1,\ell} &= Y_{1,1} \\
Y_{i,\ell} &= Y_{i,\ell-1} - e^{-\delta\beta_{\ell-1}} Y_{i-1,\ell-1} \quad , \quad i \geq 2 \ \textit{and} \ \ell \geq 2 \\
Z_{1,\ell} &= Z_{1,1} \\
Z_{i,\ell} &= Z_{i,\ell-1} - e^{-\delta\beta_{\ell-1}} Z_{i-1,\ell-1} \quad , \quad i \geq 2 \ \textit{and} \ \ell \geq 2
\end{aligned}
\tag{3.106}
$$

It will be shown later that third- ($\ell=3$) or fourth- ($\ell=4$) order response factors are sufficient to satisfy the characteristics of response factors. Using Eq. 3.105, the temperature and flux histories on both surfaces of the slab are needed. Therefore, provisions in the calculations are needed to maintain the values of fluxes and temperatures as the history needed for the method. As shown in Eq. 3.105, the maximum number of heat fluxes needed is ℓ, which is usually 3 or 4. For the sixth-order response factors, the flux coefficients are

$$
\begin{aligned}
\ell &= 6 \\
C(1) &= \lambda_1 + \lambda_2 + \lambda_3 + \lambda_4 + \lambda_5 \\
C(2) &= \lambda_1[\lambda_2 + \lambda_3 + \lambda_4 + \lambda_5] + \lambda_2[\lambda_3 + \lambda_4 + \lambda_5] \\
&\quad + \lambda_3[\lambda_4 + \lambda_5] + \lambda_4\lambda_5 \\
C(3) &= \lambda_1\lambda_2[\lambda_3 + \lambda_4 + \lambda_5] + \lambda_1\lambda_3[\lambda_4 + \lambda_5] + \lambda_1\lambda_4\lambda_5 \\
&\quad + \lambda_2\lambda_3[\lambda_4 + \lambda_5] + \lambda_4\lambda_5[\lambda_2 + \lambda_3] \\
C(4) &= \lambda_1\lambda_2[\lambda_3\lambda_4 + \lambda_3\lambda_5 + \lambda_4\lambda_5] + \lambda_3\lambda_4\lambda_5[\lambda_1 + \lambda_2] \\
C(5) &= \lambda_1\lambda_2\lambda_3\lambda_4\lambda_5
\end{aligned}
\tag{3.107}
$$

If any lower order, n, response factors is desired, equation 3.107 is simplified by setting $\lambda_j = 0$ *for* $j \geq n$. For example,

$$
\begin{aligned}
&\ell = 1 \\
&C(1) = C(2) = C(3) = C(4) = C(5) = 0 \\
&\ell = 2 \\
&C(1) = \lambda_1 \text{ and } C(2) = C(3) = C(4) = C(5) = 0 \\
&\ell = 3 \\
&C(1) = \lambda_1 + \lambda_2 \text{ and } C(2) = \lambda_1 \lambda_2 \\
&C(3) = C(4) = C(5) = 0
\end{aligned}
\tag{3.108}
$$

CHARACTERISTICS OF THE HIGHER-ORDER RESPONSE FACTORS

The two characteristics derived earlier for the first-order response factors are rederived for the higher-order response factors. For the steady-state condition and assuming $T_m = 0$, $T_n(\tau) = T_n = 0$, *and* $T_1(\tau) = T_1$, the inside surface heat flux of the thermal response factor method (Eq. 3.105) for order ℓ becomes

$$
q_1 = \sum_{i=1}^{N} X_{i,\ell} T_1 + \sum_{j=2}^{\ell} (-1)^j C(j-1)\, q_1 \tag{3.109}
$$

Rearranging the above equation

$$
q_1 \left[1 - \sum_{j=2}^{\ell} (-1)^j C(j-1)\right] = \sum_{i=1}^{N} X_{i,\ell} T_1 \tag{3.110}
$$

The steady-state heat flux equation under the same assumptions is

$$
\begin{aligned}
q_1 &= U T_1 \\
\text{or} \quad U &= \frac{q_1}{T_1}
\end{aligned}
\tag{3.111}
$$

Equating the fluxes and solving for the overall heat transfer coefficient, U

$$U = \frac{\sum_{i=1}^{N} X_{i,\ell}}{1 - \sum_{j=2}^{\ell} (-1)^j C(j-1)} \tag{3.112}$$

For $\ell = 6$

$$U = \frac{\sum_{i=1}^{N} X_{i,6}}{1 - C(1) + C(2) - C(3) + C(4) - C(5)} \tag{3.113}$$

Substituting back for the above coefficients C (j-1) with j = 2, ..., 6 (Eq. 3.107) and rearranging

$$U = \frac{\sum_{i=1}^{N} X_{i,6}}{(1-\lambda_1)(1-\lambda_2)(1-\lambda_3)(1-\lambda_4)(1-\lambda_5)} \tag{3.114}$$

or

$$U = \frac{\sum_{i=1}^{N} X_{i,\ell}}{\prod_{j=2}^{\ell} (1-\lambda_{j-1})} \tag{3.115}$$

For lower-order response factors, n, Eq. 3.114 or 3.115 is simplified by setting $\lambda_j = 0$ *for* $j \geq n$. For example for $\ell = 1$,

$$\text{for } \ell = 1 \qquad U = \sum_{i=1}^{N} X_{i,1}$$

$$\text{for } \ell = 2 \qquad U = \frac{\sum_{i=1}^{N} X_{i,2}}{(1 - \lambda_1)} \tag{3.116}$$

$$\text{for } \ell = 3 \qquad U = \frac{\sum_{i=1}^{N} X_{i,3}}{(1 - \lambda_1)(1 - \lambda_2)}$$

At the steady-state condition, the other response factors are derived similarly

$$U = \frac{\sum_{i=1}^{N} X_{i,\ell}}{\prod_{j=2}^{\ell}(1 - \lambda_{j-1})} = \frac{\sum_{i=1}^{N} Y_{i,\ell}}{\prod_{j=2}^{\ell}(1 - \lambda_{j-1})} = \frac{\sum_{i=1}^{N} Z_{i,\ell}}{\prod_{j=2}^{\ell}(1 - \lambda_{j-1})} \tag{3.117}$$

with

$$\lambda_{j-1} = e^{-\delta\beta_{j-1}} \quad \textit{and}$$
$$\lambda_1 = e^{-\delta\beta_1} = \overline{CR} \tag{3.118}$$

As shown in Eq. 3.106, the higher-order response factor is the corresponding lower-order less a number (smaller numerically). Obviously, the resulting value is smaller. Therefore, the new response factors become smaller and smaller in magnitude. Tables 4 through 6 show this reduction in magnitude of higher-order response factors for the typical roof shown earlier in Tables 1 through 3. For the above example of a typical roof, the first-order response factors required about 50 terms to obtain accurate calculations. The temperatures for the last 50 time increments were needed and kept in memory in order to be used in the analysis and heat flux equations. Using the second-order response factors required only 16 terms of temperatures and one term of heat flux to maintain the same accuracy. Furthermore, using the third-order

response factors requires only 7 temperature and two flux histories. An extensive reduction of the computational steps and computer storage is therefore obtained using the higher-order response factors. Tables 4 - 6 also show that the fourth-, fifth-, and sixth-order response factors did not present any further reduction in magnitude of response factors. Third-order response factors are usually used for typical walls.

The first characteristic, derived and implemented earlier, is also used to check the higher-order response factors. For the above example (typical roof), the overall heat transfer coefficient is calculated using

$$U = \frac{1}{R_{total}} = \frac{1}{R_1 + \frac{\Delta x_2}{k_2} + \cdots + \frac{\Delta x_4}{k_5}} \qquad (3.119)$$

therefore

$$U = \frac{1}{0.36 + \frac{0.051}{0.0433} + \frac{0.102}{1.7307} + \frac{0.02}{0.191} + \frac{0.013}{1.436}} = 0.6050088\ W/m^2C$$

λ_j is calculated for j = 1, ..., 5

$$\lambda_1 = 0.78793746128$$
$$\lambda_2 = 0.26355607774$$
$$\lambda_3 = 0.03020739532$$
$$\lambda_4 = 0.00238418404$$
$$\lambda_5 = 0.00000740502$$

The overall heat transfer coefficient was calculated from the response factors and is presented in Table 7. The agreement between all calculated U values is remarkably close, con-

Table 4. Response Factors $X_{i,\ell}$ with $\ell = 1, 2, \ldots, 6$

i	$X_{i,1}$	$X_{i,2}$	$X_{i,3}$	$X_{i,4}$	$X_{i,5}$	$X_{i,6}$
1	0.219334329	0.219334329	0.219334329	0.219334329	0.219334329	0.219334329
2	-0.082028048	-0.254849783	-0.312656678	-0.319282197	-0.319805130	-0.319806755
3	-0.018130650	0.046502322	0.113669531	0.123114075	0.123875303	0.123877671
4	-0.005720159	0.008565659	-0.003690310	-0.007123971	-0.007417497	-0.007418415
5	-0.002266247	0.002240880	-0.000016651	0.000094824	0.000111808	0.000111863
6	-0.001195405	0.000590256	-0.000000342	0.000000161	-0.000000065	-0.000000065
7	-0.000786349	0.000155556	-0.000000010	0.000000000	-0.000000000	0.000000000
8	-0.000578596	0.000040997	-0.000000000	0.000000000	-0.000000000	0.000000000
9	-0.000445093	0.000010805	-0.000000000	0.000000000	-0.000000000	-0.000000000
10	-0.000347857	0.000002848	-0.000000000	0.000000000	0.000000000	0.000000000
11	-0.000273339	0.000000751	-0.000000000	0.000000000	-0.000000000	-0.000000000
12	-0.000215176	0.000000198	-0.000000000	-0.000000000	-0.000000000	-0.000000000
13	-0.000169493	0.000000052	-0.000000000	0.000000000	0.000000000	0.000000000
14	-0.000133537	0.000000014	-0.000000000	-0.000000000	-0.000000000	-0.000000000
15	-0.000105215	0.000000004	0.000000000	0.000000000	0.000000000	0.000000000
16	-0.000082902	0.000000001	-0.000000000	-0.000000000	-0.000000000	-0.000000000
17	-0.000065321	0.000000000	-0.000000000	-0.000000000	-0.000000000	-0.000000000

Table 5. Response Factors $Y_{i,\ell}$ with $\ell = 1, 2, \ldots, 6$

i	$Y_{i,1}$	$Y_{i,2}$	$Y_{i,3}$	$Y_{i,4}$	$Y_{i,5}$	$Y_{i,6}$
1	0.000110325	0.000110325	0.000110325	0.000110325	0.000110325	0.000110325
2	0.005127317	0.005040388	0.005011311	0.005007979	0.005007716	0.005007715
3	0.014639764	0.010599759	0.009271334	0.009119955	0.009108015	0.009107978
4	0.016468237	0.004933018	0.002139388	0.001859325	0.001837581	0.001837514
5	0.014380205	0.001404264	0.000104137	0.000039511	0.000035078	0.000035065
6	0.011704076	0.000373374	0.000003272	0.000000126	0.000000032	0.000000032
7	0.009320584	0.000098504	0.000000099	0.000000000	0.000000000	0.000000000
8	0.007370002	0.000025964	0.000000003	0.000000000	0.000000000	0.000000000
9	0.005813944	0.000006843	0.000000000	0.000000000	0.000000000	0.000000000
10	0.004582828	0.000001804	0.000000000	0.000000000	0.000000000	0.000000000
11	0.003611457	0.000000475	0.000000000	0.000000000	0.000000000	0.000000000
12	0.002845727	0.000000125	0.000000000	0.000000000	0.000000000	0.000000000
13	0.002242288	0.000000033	0.000000000	0.000000000	0.000000000	0.000000000
14	0.001766792	0.000000009	0.000000000	0.000000000	0.000000000	0.000000000
15	0.001392124	0.000000002	0.000000000	0.000000000	0.000000000	0.000000000
16	0.001096907	0.000000001	0.000000000	0.000000000	0.000000000	0.000000000
17	0.000864294	0.000000000	0.000000000	0.000000000	0.000000000	0.000000000

Table 6. Response Factors $Z_{i,\ell}$ with $\ell = 1, 2, \ldots, 6$

i	$Z_{i,1}$	$Z_{i,2}$	$Z_{i,3}$	$Z_{i,4}$	$Z_{i,5}$	$Z_{i,6}$
1	3.305132124	3.305132124	3.305132124	3.305132124	3.305132124	3.305132124
2	-1.666613554	-4.270850969	-5.141938628	-5.241778061	-5.249658104	-5.249682579
3	-0.334326179	0.978861074	2.104469804	2.259794377	2.272291740	2.272330614
4	-0.255340512	0.008087608	-0.249897177	-0.313467728	-0.318855494	-0.318872320
5	-0.200153153	0.001039202	-0.001092336	0.006456407	0.007203771	0.007206133
6	-0.157467172	0.000240995	-0.000032893	0.000000103	-0.000015290	-0.000015343
7	-0.124011762	0.000062522	-0.000000993	0.000000000	-0.000000000	0.000000000
8	-0.097697065	0.000016448	-0.000000030	0.000000000	-0.000000000	0.000000000
9	-0.076974843	0.000004334	-0.000000001	0.000000000	-0.000000000	-0.000000000
10	-0.060650220	0.000001142	-0.000000000	-0.000000000	-0.000000000	-0.000000000
11	-0.047788279	0.000000301	-0.000000000	0.000000000	0.000000000	0.000000000
12	-0.037654096	0.000000079	-0.000000000	-0.000000000	-0.000000000	-0.000000000
13	-0.029669052	0.000000021	-0.000000000	0.000000000	0.000000000	0.000000000
14	-0.023377352	0.000000006	-0.000000000	-0.000000000	-0.000000000	-0.000000000
15	-0.018419890	0.000000001	0.000000000	0.000000000	0.000000000	0.0000000 00
16	-0.014513721	0.000000000	-0.000000000	-0.000000000	-0.000000000	-0.000000000
17	-0.011435904	0.000000000	-0.000000000	-0.000000000	-0.000000000	-0.000000000

firming the accuracy of the computer code used to calculate the response factors, for this particular wall.

A procedure for determining the most suitable order of response factors is presented next. After calculating the first and second-order response factors, the number N is determined by satisfying Eq. 3.117. If the difference between the two N values is large (5 or more), new higher-order response factors are calculated and another comparison is performed. If the difference is small (4 or less), this higher-order set is used. For example, Tables 4 through 6 contain six sets of response factors for six different orders. If the procedure outlined above is used, third-order response factors would be required.

ROOTS AND RESPONSE FACTORS OF TYPICAL WALLS

The derivation of the TRFM has been presented. Methods of determining the order of response factors were also given. The accuracy, in predicting response factors, of the computer code was checked and found to be satisfactory for a typical roof. More cases are shown in Appendix B. Plots and tables of response factors and their roots are also given. An accurate procedure for determining the roots [15] is also presented.

VALIDATION OF THE TRFM

The TRFM is validated with other established exact and finite difference methods. A validation of the code with published response factors is presented for the multilayer roof examined earlier in this chapter. The validation of the TRFM is presented in Appendix C.

The flow diagram of the calculation procedure employed in the computer code to determine the response factors of multilayer slabs is shown in Fig. 5.

Table 7. Overall Heat Transfer Coefficient For The Typical Roof

$R_{i,k}$	$\sum_{i=1}^{\infty} R_{i,k}$	$\prod_{j=2}^{\ell}(1-\lambda_{j-1})$	U $W/m^2.C$
$X_{i,2}$	0.128299740	0.2120626	0.6050086
$X_{i,3}$	0.094485563	0.1561722	0.6050088
$X_{i,4}$	0.091631401	0.1514443	0.6050502
$X_{i,5}$	0.091412936	0.1510832	0.6050503
$Y_{i,2}$	0.128299740	0.2120626	0.6050086
$Y_{i,3}$	0.094485563	0.1561722	0.6050088
$Y_{i,4}$	0.091631401	0.1514443	0.6050502
$Y_{i,5}$	0.091412936	0.1510832	0.6050503
$Z_{i,2}$	0.128299740	0.2120626	0.6050086
$Z_{i,3}$	0.094485563	0.1561722	0.6050088
$Z_{i,4}$	0.091631401	0.1514443	0.6050502
$Z_{i,5}$	0.091412936	0.1510832	0.6050503

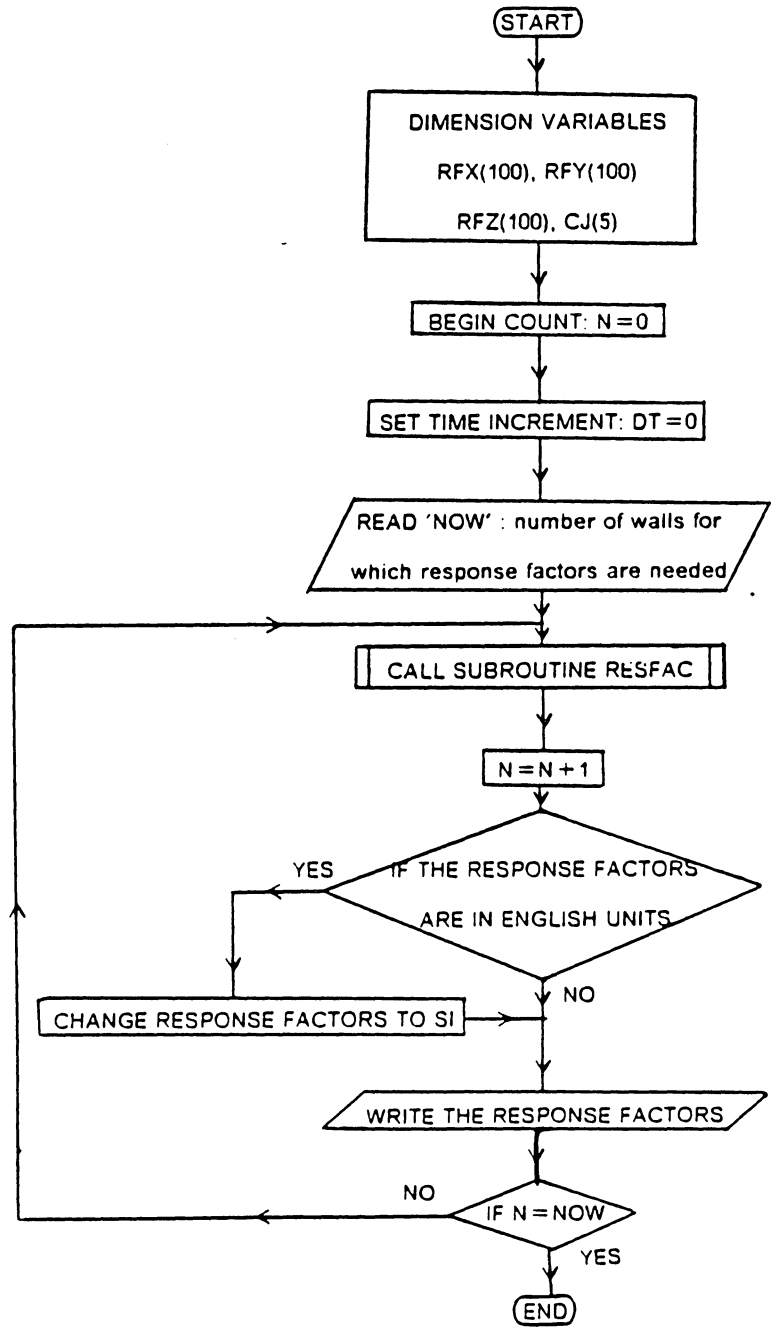

Figure 5. Flow Diagram of the Response Factors Computer Code.

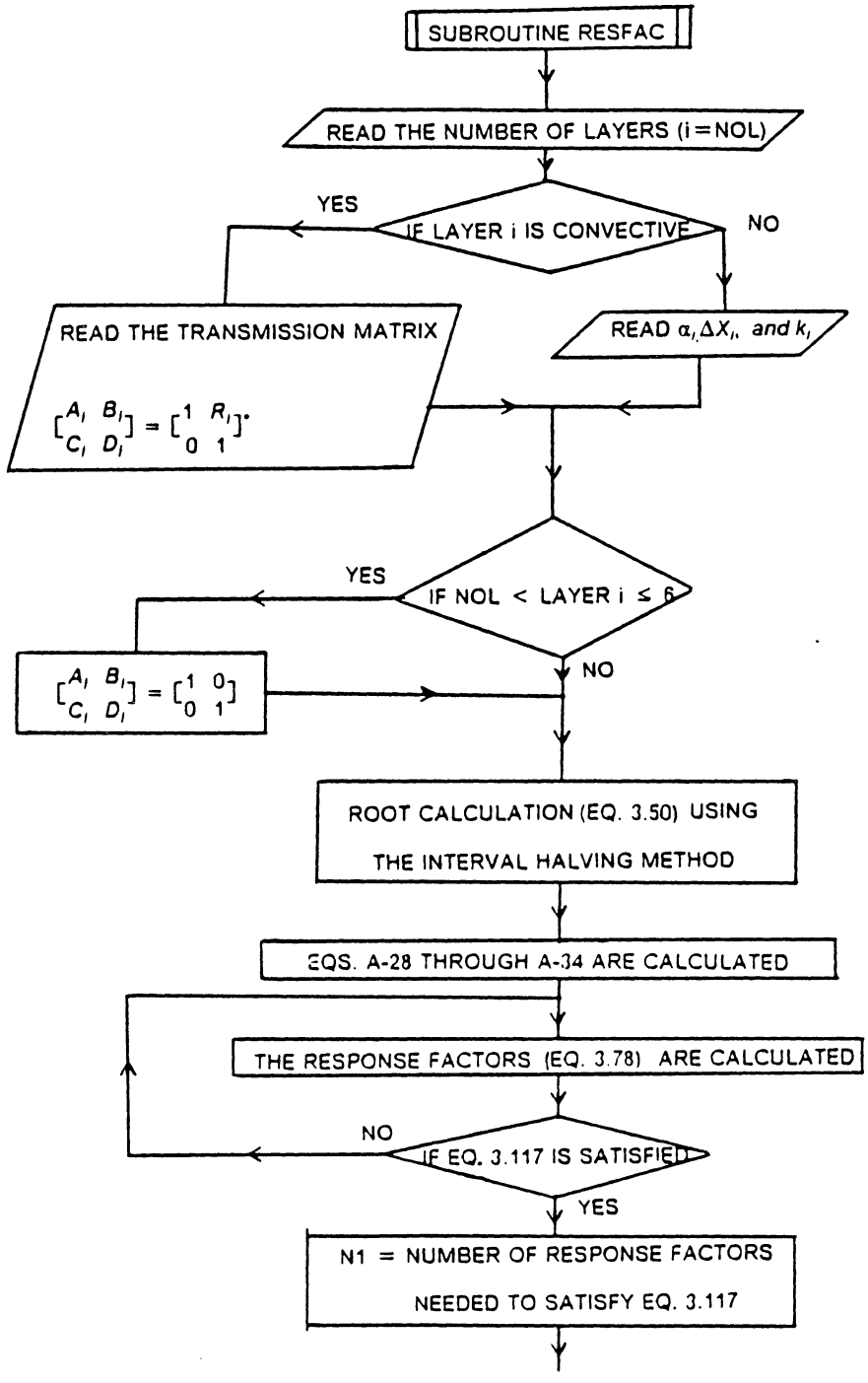

Figure 5. (continued)

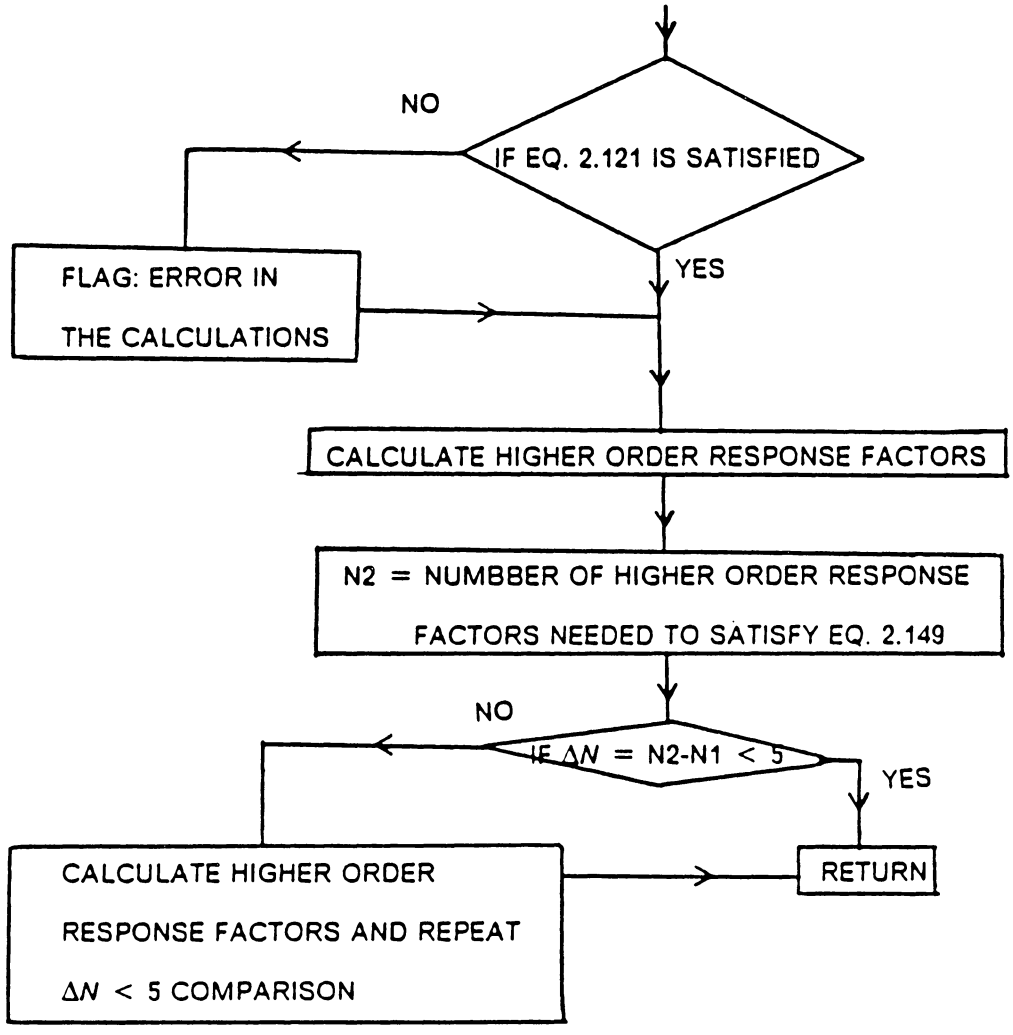

Figure 5. (continued)

4. SINGLE ZONE MODEL

The Thermal Response Factor Method (TRFM) has been developed and validated with other well-known numerical and exact solution methods. In this chapter, the focus is on other mechanisms that significantly affect the energy balance and temperature in rooms. These mechanisms are conduction through the floor slab, infiltration through cracks in the structure, convection, and emission of infrared radiation by the exterior surfaces to the surroundings. After examining these mechanisms, an energy balance on the room air is performed. The resulting equations are solved for either the interior temperature or the heating/cooling load of the room. Finally, the model is validated with experimental data obtained from the National Bureau of Standards (NBS) for several single room houses in Gaithersburg, Maryland.

HEAT TRANSFER THROUGH SLAB-ON-GRADE FLOORS

Conduction through floor slabs has been analyzed widely with solutions ranging from simple to highly tedious. While numerous methods are presented in technical papers and reports, a general model covering all types and shapes of slabs has not yet been introduced. The primary difficulty lies in determining the temperature distribution beneath the slab. The variation of the ground temperature and soil type and moisture level beneath the slab is in-

consistent from one structure to another. This inconsistency presents a problem when determining a general model for the heat loss through the slab. The primary difficulty results from the heat loss at the edges of the slab where the heat path is no longer simple and one-dimensional as it is at the center. That dimensionality is dependent on the geographical presence of the slab. The slab temperature distribution is quite different when the ground drops suddenly at its edge, as is the case when the structure is on a hill. Once the ground temperature is known, any pure conduction model can be used to determine the heat flux through the floor slab.

Kusuda and Bean [32] presented a generalized solution of the temperature distribution below a structure using the Green's function approach. It is widely recognized that at about 8 m or more below the ground surface, the temperature is constant throughout the year. The intermediate layer below the slab, however, affects the interior temperature of the structure. To account for that effect, the analysis from reference 32 has been used to obtain the ground temperature beneath the slab. After determining the ground temperature, the TRFM is used to calculate the slab heat flux.

The generalized solution for January and July months obtained from reference 32 is shown in Fig. 6. The temperature is expressed in non dimensional form $\frac{T - T_a}{T_r - T_a}$, where T (C) is the ground temperature, T_a (C) is the annual average outdoor air temperature, and T_r (C) is the annual average indoor room temperature. The solutions presented in Fig. 6 are for a ground thermal diffusivity of 0.056 m^2/day and a 1.5 slab width-to-length ratio.

The slab on grade is divided into two sections as shown in Fig. 7. Section 1 is located in the center and section 2 includes the perimeter. These two sections (center and perimeter) are introduced to account for the large temperature gradient between the two locations. Values of the ground temperatures, for both sections, are taken from Fig.6, where typical ground temperatures at a depth of 1 m are given next for January and July months.

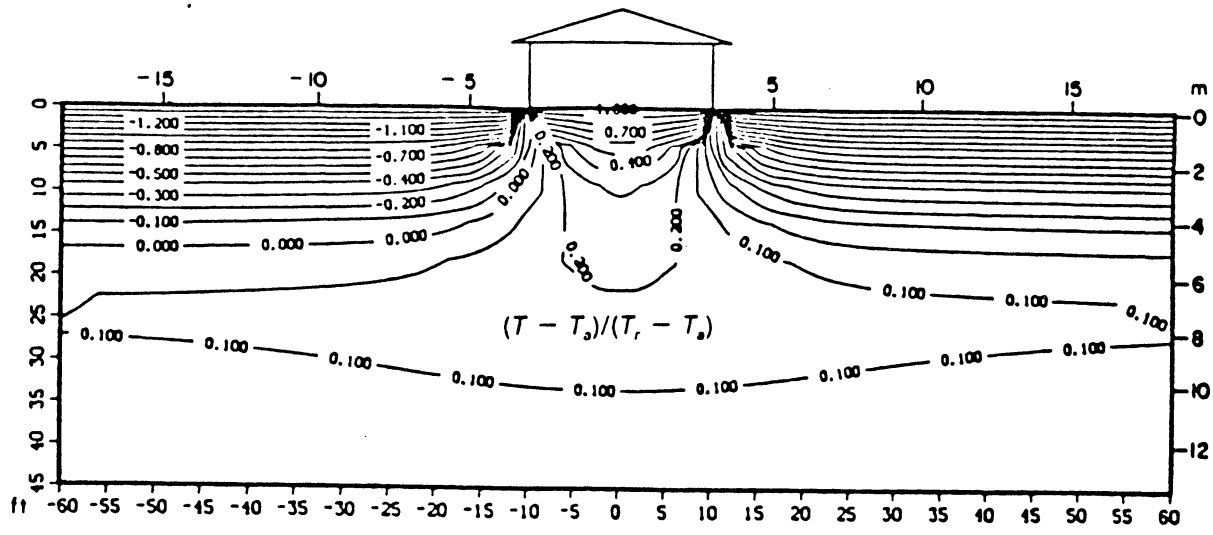

(a) January

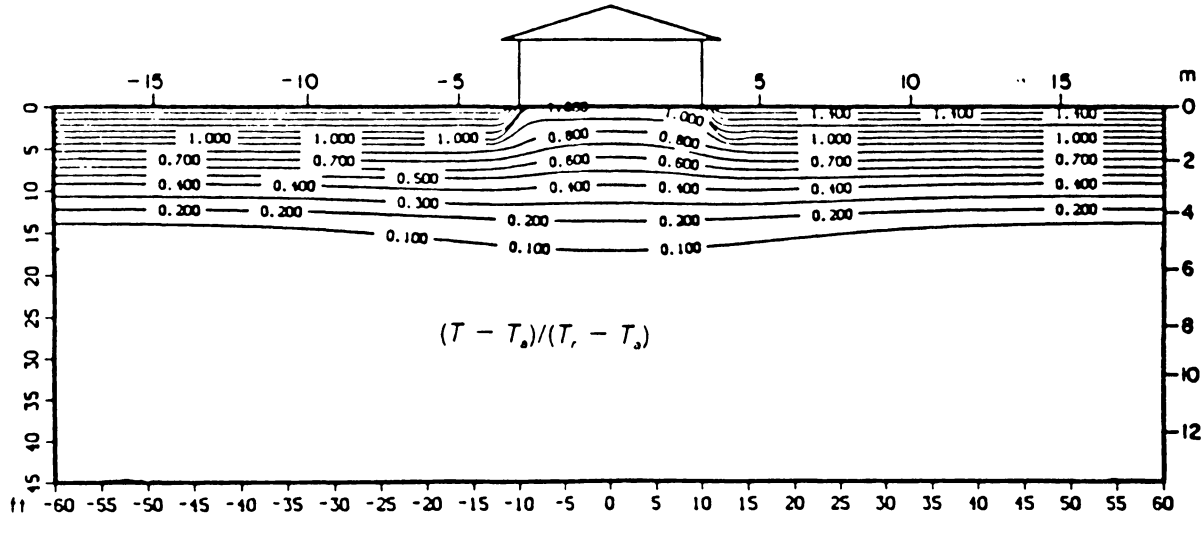

(b) July

Figure 6. Ground Temperature Distribution Below a House on a Flat Terrain For (a) January and (b) July Months.

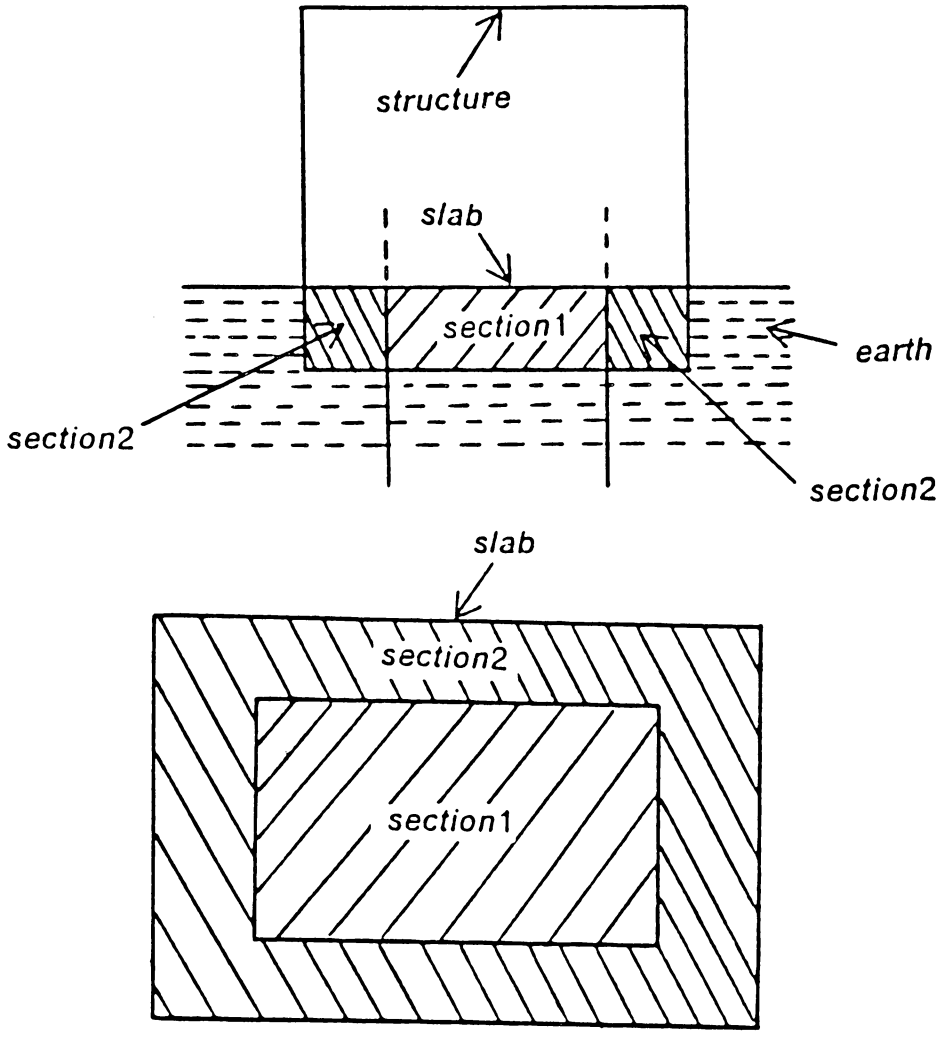

Figure 7. Side and Top View of the Slab

$$
\begin{aligned}
&\textit{JANUARY} && T_g = 0.7T_r + 0.3T_a && \textit{section1}\\
& && T_g = 0.2T_r + 0.8T_a && \textit{section2}\\
&\textit{JULY} && T_g = 0.8T_r + 0.2T_a && \textit{section1}\\
& && T_g = 0.95T_r + 0.05T_a && \textit{section2}
\end{aligned}
\qquad (4.1)
$$

Values of T_a for various locations in the U.S. [32] are given in Table 8.

After determining the temperature at 1 m below the slab, the TRFM is used to calculate the heat flux through it. The inside surface heat flux equation for a multilayer slab, derived in Chapter 3, using the second-order response factors is

$$
q_s(\tau) = \sum_{i=1}^{N} X_{s,2}(i)\,[T_s(\tau + 1 - i) - T_m] - \sum_{i=1}^{N} Y_{s,2}(i)\,[T_g(\tau + 1 - i) - T_m] + \overline{CR}\; q_s(\tau - 1) \qquad (4.2)
$$

where $q_s(\tau)$ is the heat flux at the inside surface of the slab with second-order response factors and time τ, T_s is the inside surface temperature of the slab, T_g is the ground temperature 1 m below the slab, $X_{s,2}(i)$ *and* $Y_{s,2}(i)$ (W/m^2K) are the second-order response factors of the slab, and $\overline{CR} = e^{-\delta\beta_1}$ is the common ratio.

The ground temperature at 1 m depth is assumed to remain constant for the duration of the simulation. The first characteristic of the second-order response factors, derived in Chapter 3, is

$$
\sum_{i=1}^{N} X_{s,2}(i) = \sum_{i=1}^{N} Y_{s,2}(i) = \sum_{i=1}^{N} Z_{s,2}(i) = U_g(1 - \overline{CR}) \qquad (4.3)
$$

Since $T_g(\tau) = T_g$, Eq. 4.3 becomes

Table 8. Average Outside Air Temperatures [32]

STATION	STATE	T_a (C)
Auburn	Alabama	18.33
Decatur	Alabama	13.33
Tempe	Arizona	21.11
Tucson	Arizona	23.89
Brawley	California	26.11
Davis	California	18.89
Fort Collins	Colorado	10.00
Gainesville	Florida	23.33
Athens	Georgia	19.44
Tifton	Georgia	21.67
Moscow	Idaho	8.33
Argonne	Illinois	10.56
Lemont	Illinois	11.11
Urbana	Illinois	11.67
West Lafayette	Indiana	11.11
Burlington	Iowa	12.22
Manhattan	Kansas	12.78
Lexington	Kentucky	12.78
Upper Marlboro	Maryland	13.33
East Lansing	Michigan	10.00
St. Paul	Minnesota	8.89
State Univ.	Mississipi	19.44
Faucett	Missouri	12.22
Kansas City	Missouri	12.22
Sikeston	Missouri	13.89
Bozeman	Montana	6.67
Huntley	Montana	10.00

Table 8. (continued)

STATION	STATE	T_a (C)
Lincoln	Nebrasca	12.22
Norfolk	Nebrasca	12.22
New Brunswick	New Jersey	11.67
Ithaca	New York	9.44
Raleigh	North Carolina	16.67
Columbus	Ohio	11.67
Coshocton	Ohio	11.11
Barndsall	Oklahoma	18.33
Hominy	Oklahoma	17.22
Lake Hefner	Oklahoma	17.78
Pawhuska	Oklahoma	16.67
Ottawa	Ontario	8.33
Corvallis	Oregon	13.33
Pendleton	Oregon	11.67
Calhoun	South Carolina	17.78
Union	South Carolina	15.00
Madison	South Dakota	8.33
Jackson	Tennessee	15.56
Temple	Texas	21.11
Salt Lake City	Utah	10.56
Burlington	Vermont	9.44
Pullman	Washington	8.89
Seattle	Washington	11.67

$$q_s(\tau) = \sum_{i=1}^{N} X_s(i)\,[T_s(\tau + 1 - i) - T_m] - U_g\,(1 - \overline{CR})\,(T_g - T_m) + \overline{CR}\;q_s(\tau - 1) \tag{4.4}$$

where U_g is the overall heat transfer conductance for the slab.

Since the slab is divided into two sections, requiring two average ground temperatures as shown in Fig. 8, the total heat flow through the slab is the sum of the flows through both sections.

$$Q_s(\tau) = A_{s,1}\,q_{s,1}(\tau) + A_{s,2}\,q_{s,2}(\tau) \tag{4.5}$$

INFILTRATION

The infiltration model used for the single zone analysis is presented next. The Air Infiltration Center sponsored a project [37] in which many infiltration models, organized from several countries, were given and compared. From the models, with the assumption of constant interior pressure, the Lawrence Berkeley Laboratory (LBL) model was judged to predict the infiltration better when compared with experimental data. Grimsrud, Modera, and Sherman [36] introduced this model which is summerized below.

$$Q_{infl} = \sqrt{Q_{stack}^2 + Q_{wind}^2} \tag{4.6}$$

where

$$\begin{aligned} Q_{stack} &= L\,f_s\sqrt{\Delta T} \\ Q_{wind} &= L\,f_w\,V \end{aligned} \tag{4.7}$$

or

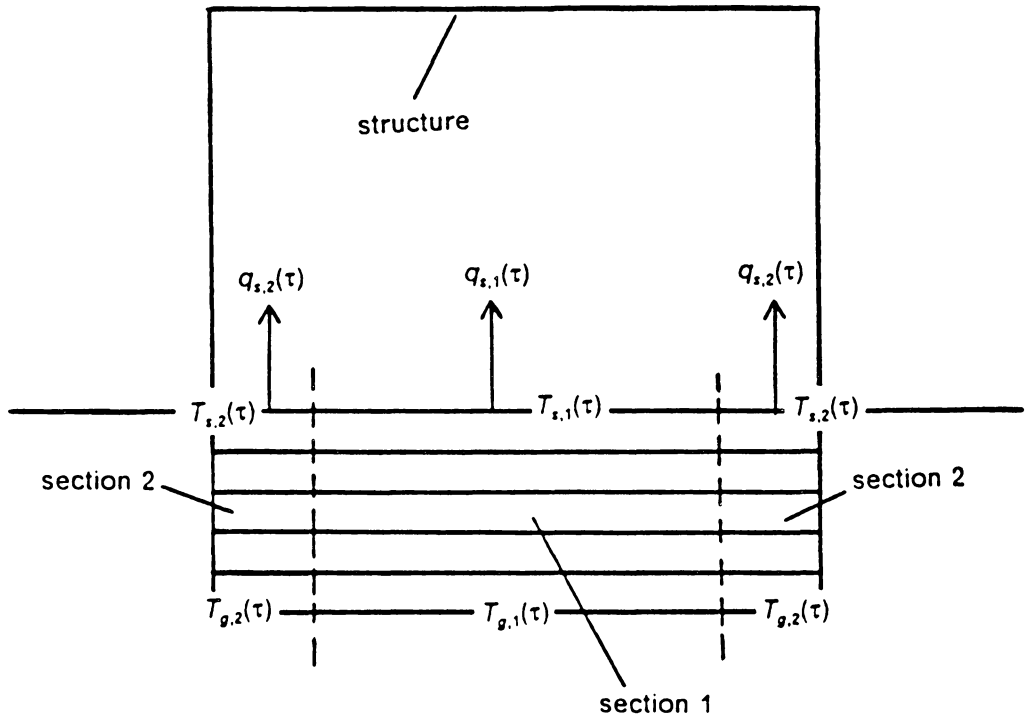

Figure 8. Temperature and Heat Flux Nomenclature of the slab

$$Q_{infl} = L\sqrt{f_s^2 \Delta T + f_w^2 V^2} \tag{4.8}$$

and

Q_{infl} = infiltration rate (m^3/s)

L = effective leakage area (m^2)

ΔT = indoor-outdoor temperature difference (K)

f_s = stack parameter ($m/s/\sqrt{K}$)

V = outside air/wind speed (m/s)

f_s = wind parameter (dimensionless)

and

$$\begin{aligned} f_w &= \frac{C'D'}{D'}[1 - R]^{1/3}\left[\frac{H}{10}^{E'}\right]\left[\frac{10}{H'}^{E'}\right] \\ f_s &= \frac{1 + R/2}{3}\left[1 - \frac{X^2}{[2 - R]^2}\right]^{3/2}\sqrt{\frac{gH}{T_r}} \\ X &= \frac{L_{ceiling} - L_{floor}}{L} \\ R &= \frac{L_{ceiling} + L_{floor}}{L} \end{aligned} \tag{4.9}$$

where

$L_{ceiling}$ = leakage area of the ceiling (m^2)

L_{floor} = leakage area of the floor (m^2)

H = height of the structure (m)

H' = height of the wind measurements (m)

D' and E' = terrain parameters (Table 9)

C' = generalized shielding coefficient (Table 9)

R = fraction of leakage on horizontal surfaces, i.e., the fraction of leakage in the floor and ceiling

Table 9. Coefficients Used in the LBL Infiltration Model [36]

CLASS	E′	D′	DESCRIPTION
1	0.10	1.30	Ocean or other body of water at least 5 km of unrestricted expanse
2	0.15	1.00	Flat terrain with some isolated obstacles (e.g., buildings well sep rated from each other
3	0.20	0.85	Rural areas with low buildings, trees, etc...
4	0.25	0.67	Urban, industrial, or forest areas
5	0.35	0.47	Center of large city

SHIELDING CLASS	C′	DESCRIPTION
1	0.32	No obstructions (trees, fences, nearby houses)
2	0.28	Light local shielding with few obstructions
3	0.24	Some obstructions within two house heights
4	0.18	Obstructions around most of perimeter
5	0.10	Large obstructions surrounding perimeter within two house heights

g = gravitational acceleration (9.8 m/s^2)

T_r = inside room temperature (K)

The effects of the wind measurements relative to the actual location of the structure are taken into consideration in the LBL model. The effects of the surroundings and terrain on the infiltration are also included. It should be noted that this model would not be useful for large structures where the constant pressure assumption inside the envelope is no longer valid. Therefore, a more detailed model is needed and will be introduced later for the multizone analysis.

Infiltration due to openings between rooms and zones constitutes a large portion of the energy transfer within buildings. Balcomb and Yamaguchi [52] introduced a parametric equation to calculate the heat transfer from interconnected rooms due to convection and air movement. The convective heat transfer through a large opening (door, window, or a hallway) between two rooms can be estimated by

$$Q_E = 15.7\, w \sqrt{h^3 \Delta T^3} \qquad (4.10)$$

where Q_E (W) is the convection heat flow, w is the door or hallway width (m), h is the door or hallway height (m), and ΔT (C) is the room-to-room temperature difference.

GENERATED LOADS

The three major sources of generated loads in structures are lights, people, and equipments. The methods for estimating these loads are obtained from the ASHRAE Handbook of Fundamentals [26, 27, and 28]. Generated heat due to people is usually divided into sensible and latent components. Average generated loads by people are given in Table 10 based on 25.56 C room dry-bulb temperature. The adjusted total heat gain column in Table 10 will be

used in this analysis. This adjusted total heat gain is based on normal percentage of men, women, and children for the applications listed. The heat gain from an adult female is 85 percent of that for an adult male. Also, the heat gain from a child is 75 percent of that for an adult male.

The heat gain from lighting is often a major component of the total load in buildings. The instantaneous heat gain from lights is

$$Q_{lights} = 3.412\, W\, F_u\, F_s \qquad (4.11)$$

where Q_{lights} (W) is the instantaneous heat gain due to lights, W (Btu/h) is the summation of all installed light wattage, and F_u (dimensionless) is the use factor ratio of wattage in use to that installed. For example, if the lights were turned off 15 percent of the time, $F_u = 0.85$. F_s is a special allowance factor for lights requiring more power than their rated wattage. For typical 40 W fluorescent lamps, $F_s = 1.20$.

The heat gain from equipment and appliances will be approximated. If the equipment is totally inclosed in the space, the heat gain equals their energy input. However, if a portion of the appliance is set outside the space, only the corresponding percentage is used as the heat gained by the room.

SURFACE ENERGY BALANCES

Having presented most of the significant affecting parameters in the energy balance of a single space or zone, the model is introduced. The single room house or structure is basically composed of four walls, a roof, a slab, some windows, doors, lights, people, and equipment. The outside walls and the roof have similar surface boundary conditions. On the outside surface of these walls, a solar load, convection to the outside air, and emission of infrared

Table 10. Heat Generated by People [26]

DEGREE OF ACTIVITY	TYPICAL APPLICATION	TOTAL HEAT ADULTS, MALE (WATTS)	TOTAL HEAT ADJUSTED (WATTS)	SENSIBLE HEAT (WATTS)	LATENT HEAT (WATTS)
Seated at rest	Theater, movie	115	100	60	40
Seated,very light work, writing	Offices, hotels apartments	140	120	65	55
Seated, eating	Restaurant	150	170	75	95
Seated, light work, typing	Offices, hotels apartments	185	150	75	75
Standing, light work or walking slowly	Retail store, Bank	235	185	90	95
Light bench work	Factory	255	230	100	130
Walking, 3 mph, light machine work	Factory	305	305	100	205
Bowling	Bowling alley	350	280	100	180
Moderate dancy	Dance hall	400	375	120	255
Heavy work, heavy machine work,lifting	Factory	470	470	165	300
Heavy work, athletics	Gymnasium	585	525	185	340

radiation to the surroundings are present. For the inside surfaces, only convection to the inside room air is considered for the single zone model. Radiation between the interior walls of rooms is considered later in multizone structures. The windows have similar boundary conditions on their exterior surfaces. However, part of the solar load is transmitted to the room. A second portion is reflected back to the surroundings and the remaining load is absorbed by the window. In walls, only reflected and absorbed solar loads are present.

The following assumptions apply to the single zone model:

. Radiation from the inside walls, ceiling, and floor surfaces to each other is neglected.

. The solar load transmitted through the windows to the corresponding room is absorbed by the room air and is accounted for in the room air energy balance. There is no provision for solar radiation absorbed directly on the inside surface of walls and floors.

. None of the solar radiation transmitted through each window is reflected back out.

. The solar load on and emission of infrared radiation to the surroundings by the exterior surface of doors are neglected. The mechanisms taken into considerations for doors are convection to the outside and inside air and conduction.

The inside surface conduction heat flux for a multilayer wall k, derived in Chapter 3, is

$$q_{1,k}(\tau) = \sum_{i=1}^{N} X_{k,\ell}(i)\,[T_{1,k}(\tau + 1 - i) - T_m] - \sum_{i=1}^{N} Y_{k,\ell}(i)\,[T_{n,k}(\tau + 1 - i) - T_m] + \sum_{j=2}^{\ell} (-1)^j C_k(j-1) q_{1,k}(\tau + 1 - j) \tag{4.12}$$

The heat flux on the outside surface of a wall k is

$$q_{n,k}(\tau) = \sum_{i=1}^{N} Y_{k,\ell}(i)\,[T_{1,k}(\tau + 1 - i) - T_m] - \sum_{i=1}^{N} Z_{k,\ell}(i)\,[T_{n,k}(\tau + 1 - i) - T_m] + \sum_{j=2}^{\ell} (-1)^j C_k(j-1) q_{n,k}(\tau + 1 - j) \tag{4.13}$$

The positive direction of flux $q_{1,k}(\tau)$ is away from the wall as shown in Fig. 9. The positive direction of flux $q_{n,k}(\tau)$ is toward the wall (Fig. 9). The order of response factors employed is ℓ and, T_m is the initial temperature in the slab. Performing the energy balance on the outside surface of the wall

$$q_{solar}(\tau) + q_{convection}(\tau) + q_{emission}(\tau) + q_{conduction} = 0 \qquad (4.14)$$

where

$$\begin{aligned} q_{solar}(\tau) &= q_{s,k}(\tau) = \alpha_w\, q_{s,n,k}(\tau) \\ q_{convection}(\tau) &= h_{o,v}(\tau)\,[T_o(\tau) - T_{n,k}(\tau)] \\ q_{emission}(\tau) &= \varepsilon\,\sigma\,[T_s^4(\tau) - T_{n,k}^4(\tau)] \\ q_{conduction}(\tau) &= q_{n,k}(\tau) \end{aligned} \qquad (4.15)$$

and

$q_{solar}(\tau)$ = absorbed solar flux by the outside surface of the wall (W/m^2)

$q_{convection}$ = convective heat flux by the outside surface of the wall to the ambient air. (W/m^2)

$q_{emission}(\tau)$ = emitted solar flux by the wall to the surroundings (W/m^2)

$q_{n,k}(\tau)$ = outside surface heat flux of wall k (W/m^2)

$q_{s,n,k}(\tau)$ = total solar flux normal to the outside surface of wall k (W/m^2)

α_w = solar absorption coefficient of the outside surface of the wall (dimensionless)

$h_{o,v}(\tau)$ = convective heat transfer coefficient of the outside surface of a vertical wall (W/m^2K)

$T_o(\tau)$ = outside air temperature (K)

$T_{n,k}(\tau)$ = outside surface temperature of wall k (K)

ε = emissivity of the outside surface of the wall (dimensionless)

σ = Stefan-Boltzmann constant, 5.669×10^{-8} ($W/m^2.K^4$)

$T_s(\tau)$ = effective sky temperature (K)

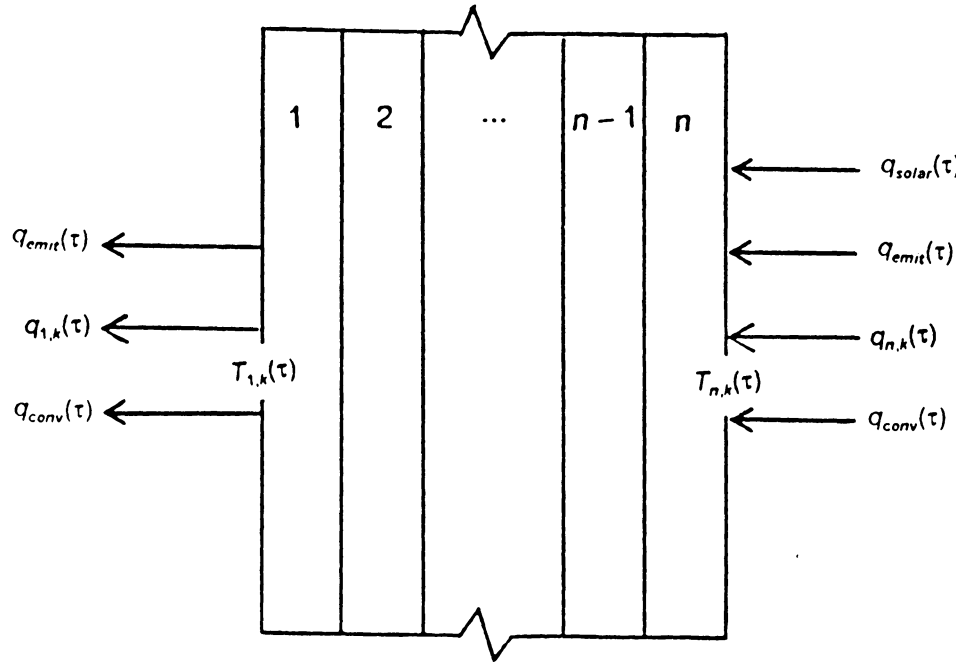

Figure 9. Typical Multilayer Wall: the positive direction of heat fluxes are also shown

Rewriting the emission flux in a form similar to the convective flux.

$$\begin{aligned} q_{emission}(\tau) &= \varepsilon\sigma[T_s^4(\tau) - T_{n,k}^4(\tau)] \\ &= \varepsilon\sigma[T_s^2(\tau) + T_{n,k}^2(\tau)][T_s^2(\tau) - T_{n,k}^2(\tau)] \\ &= \varepsilon\sigma[T_s^2(\tau) + T_{n,k}^2(\tau)][T_s(\tau) + T_{n,k}(\tau)][T_s(\tau) - T_{n,k}(\tau)] \\ &= h_{k,r}(\tau)[T_s(\tau) - T_{n,k}(\tau)] \end{aligned} \tag{4.16}$$

where

$$h_{k,r}(\tau) = \varepsilon\sigma[T_s^2(\tau) + T_{n,k}^2(\tau)][T_s(\tau) + T_{n,k}(\tau)] \tag{4.17}$$

Substituting Eqs. 4.13, 4.15, and 4.16 into Eq. 4.14

$$\begin{aligned} &q_{s,k}(\tau) + h_{o,v}(\tau)[T_o(\tau) - T_{n,k}(\tau)] + h_{k,r}(\tau)[T_s(\tau) - T_{n,k}(\tau)] \\ &+ \sum_{i=1}^{N} Y_{k,\ell}(i)[T_{1,k}(\tau + 1 - i) - T_m] - \sum_{i=1}^{N} Z_{k,\ell}(i)[T_{n,k}(\tau + 1 - i) - T_m] \\ &+ \sum_{j=2}^{\ell} (-1)^j C(j-1) q_{n,k}(\tau + 1 - j) = 0 \end{aligned} \tag{4.18}$$

Expanding further for i = 1 in the summations

$$\begin{aligned} &q_{s,k}(\tau) + h_{o,v}(\tau)T_o(\tau) - h_{o,v}(\tau)Tn,k(\tau) + h_{k,r}(\tau)T_s(\tau) - h_{k,r}(\tau)Tn,k(\tau) \\ &+ Y_{k,\ell}(1)[T_{1,k}(\tau) - T_m] - Z_{k,\ell}(1)[T_{n,k}(\tau) - T_m] \\ &+ \sum_{i=2}^{N} Y_{k,\ell}(i)[T_{1,k}(\tau + 1 - i) - T_m] - \sum_{i=2}^{N} Z_{k,\ell}(i)[T_{n,k}(\tau + 1 - i) - T_m] \\ &+ \sum_{j=2}^{\ell} (-1)^j C_k(j-1) q_{n,k}(\tau + 1 - j) = 0 \end{aligned} \tag{4.19}$$

Defining the coefficients which are calculated at the start of each time step

$$S_{to} = \sum_{i=2}^{N} Y_{k,\ell}(i)[T_{1,k}(\tau + 1 - i) - T_m] - \sum_{i=2}^{N} Z_{k,\ell}(i)[T_{n,k}(\tau + 1 - i) - T_m]$$
$$S_{fo} = \sum_{j=2}^{\ell} (-1)^j C_k(j - 1) q_{n,k}(\tau + 1 - j) \qquad (4.20)$$

Substituting into Eq. 4.19 and expanding further

$$q_{s,k}(\tau) + h_{o,v}(\tau)T_o(\tau) - h_{o,v}(\tau)T_{n,k}(\tau) + h_{k,r}(\tau)T_s(\tau) - h_{k,r}(\tau)T_{n,k}(\tau)$$
$$+ Y_{k,\ell}(1)\, T_{1,k}(\tau) - Y_{k,\ell}(1)\, T_m - Z_{k,\ell}(1)\, T_{n,k}(\tau) + Z_{k,\ell}(1)T_m \qquad (4.21)$$
$$+ S_{to} + S_{fo} = 0$$

Solving for $T_{n,k}(\tau)$

$$T_{n,k}(\tau) = \frac{\left\{ \begin{matrix} q_{s,k}(\tau) + h_{o,v}(\tau)T_o(\tau) + h_{k,r}(\tau)T_s(\tau) + S_{to} \\ + Y_{k,\ell}(1)[T_{1,k}(\tau) - T_m] + Z_{k,\ell}(1)T_m + S_{fo} \end{matrix} \right\}}{h_{o,v}(\tau) + h_{k,r}(\tau) + Z_{k,\ell}(1)} \qquad (4.22)$$

In Eq. 4.22, the response factors are calculated with layer 1 adjacent to the room and layer n to the outside. The above equation is nonlinear since $h_{k,r}$ depends on $T_{n,k}(\tau)$. Therefore, an iterative procedure is used when solving for $T_{n,k}(\tau)$. A value for $T_{n,k}(\tau)$ is assumed, $h_{r,k}(\tau)$ is calculated from Eq. 4.17, and Eq. 4.22 is used to calculate $T_{n,k}(\tau)$. The procedure is repeated until convergence is obtained.

Equation 4.22 contains other unknowns such as $T_{1,k}(\tau)$ which in turns is dependent on the inside room temperature. Next, equations resulting from other energy balances will be used to solve for the interior wall surface and room temperatures at every time step τ.

Performing an energy balance at the inner surface of the exterior wall,

$$q_{convection}(\tau) + q_{1,k}(\tau) = 0 \tag{4.23}$$

where

$$\begin{aligned} q_{convection}(\tau) &= h_{i,v}(\tau)[T_{1,k}(\tau) - T_r(\tau)] \\ q_{1,k}(\tau) &= \sum_{i=1}^{N} X_{k,\ell}(i)[T_{1,k}(\tau + 1 - i) - T_m] - \sum_{i=1}^{N} Y_{k,\ell}(i)[T_{n,k}(\tau + 1 - i) - T_m] \\ &\quad + \sum_{j=2}^{\ell} (-1)^j C_k(j-1) q_{1,k}(\tau + 1 - j) \end{aligned} \tag{4.24}$$

The inside surface temperature of the wall is $T_{1,k}(\tau)$ and $T_r(\tau)$ is the inside room air temperature. Defining the coefficients calculated at the start of each time step

$$\begin{aligned} S_{ti} &= \sum_{i=2}^{N} X_{k,\ell}(i)[T_{1,k}(\tau + 1 - i) - T_m] - \sum_{i=2}^{N} Y_{k,\ell}(i)[T_{n,k}(\tau + 1 - i) - T_m] \\ S_{fi} &= \sum_{j=2}^{\ell} (-1)^j C_k(j-1) q_{1,k}(\tau + 1 - j) \end{aligned} \tag{4.25}$$

Expanding the summations in Eq. 4.24 around i = 1 and substituting the above coefficients

$$\begin{aligned} &X_{k,\ell}(1)T_{1,k}(\tau) + h_{i,v}(\tau)T_{1,k}(\tau) - X_{k,\ell}(1)T_m - Y_{k,\ell}(1)[T_{n,k}(\tau) - T_m) \\ &- h_{i,v}(\tau)T_s(\tau) + S_{ti} + S_{fi} = 0 \end{aligned} \tag{4.26}$$

Solving for $T_{1,k}(\tau)$

$$T_{1,k}(\tau) = \frac{X_{k,\ell}(1)T_m + Y_{k,\ell}(1)[T_{n,k}(\tau) - T_m] + h_{i,v}(\tau)T_r(\tau) - S_{ti} - S_{fi}}{X_{k,\ell}(1)T_m + h_{i,v}(\tau)} \tag{4.27}$$

Equations 4.22 and 4.27 are used to calculate the outside and inside surface temperatures of all four walls of the single room structure. Equations 4.22 and 4.27 are also used to calculate the outside and inside surface temperatures of the roof. In these equations, the corresponding convective coefficients and response factors of the ceiling are used.

Performing an energy balance on the inside surface of section 1 of the slab

$$q_{convection}(\tau) + q_{s,1}(\tau) = 0 \tag{4.28}$$

where

$$\begin{aligned} q_{convection}(\tau) &= h_{i,h}(\tau)[T_{1,k}(\tau) - T_r(\tau)] \\ q_{s,1}(\tau) &= \sum_{i=1}^{N} X_{s,2}[T_{s,1}(\tau + 1 - i) - T_m] - U_g(1 - \overline{CR})[T_{g,1} - T_m] \\ &\quad + \overline{CR}\, q_{s,1}(\tau - 1) \end{aligned} \tag{4.29}$$

Assigning for section 1 of the slab

$$\begin{aligned} S_{ts1} &= \sum_{i=2}^{N} X_{s,2}(i)\,[T_{s,1}(\tau + 1 - i) - T_m] - U_g(1 - \overline{CR})[T_{g,1} - T_m] \\ S_{fs1} &= \overline{CR}\; q_{s,1}(\tau - 1) \end{aligned} \tag{4.30}$$

Solving for the surface temperature of section 1 of the slab

$$T_{s,1}(\tau) = \frac{X_{s,2}(1)T_m + h_{i,h}(\tau)T_r(\tau) - S_{ts1} - S_{fs1}}{X_{s,1}(1)T_m + h_{i,h}(\tau)} \tag{4.31}$$

The surface temperature of section two of the slab is obtained similarly

$$T_{s,2}(\tau) = \frac{X_{s,2}(1)T_m + h_{i,h}(\tau)T_r(\tau) - S_{ts2} - S_{fs2}}{X_{s,2}(1)T_m + h_{i,h}(\tau)} \tag{4.32}$$

where

$$\begin{aligned} S_{ts2} &= \sum_{i=2}^{N} X_{s,2}(i)\,[T_{s,2}(\tau + 1 - i) - T_m] - U_g\,[1 - \overline{CR}]\,[T_{g,2} - T_m] \\ S_{fs2} &= \overline{CR}\; q_{s,2}(\tau - 1) \end{aligned} \tag{4.33}$$

and

$$\begin{aligned} q_{s,2}(\tau) = \sum_{i=1}^{N} X_{s,2}[T_{s,2}(\tau + 1 - i) - T_m] &- U_g\,(1 - \overline{CR})[T_{g,2} - T_m] \\ &+ \overline{CR}\; q_{s,2}(\tau - 1) \end{aligned} \tag{4.34}$$

SURFACE ENERGY BALANCES OF WINDOWS AND DOORS

Common loads are present on the exterior surfaces of walls and windows. The difference is that windows have a portion of the solar load transmitted to the room as shown in Fig. 10. An expression for the exterior surface temperature is deduced similarly to Eq. 4.22. However, since windows do not have large thermal mass, the TRFM is not applied. The well-known quasisteady-state equation is used.

$$q = U\,\Delta T \tag{4.35}$$

The heat flux on the outside surface of window k is

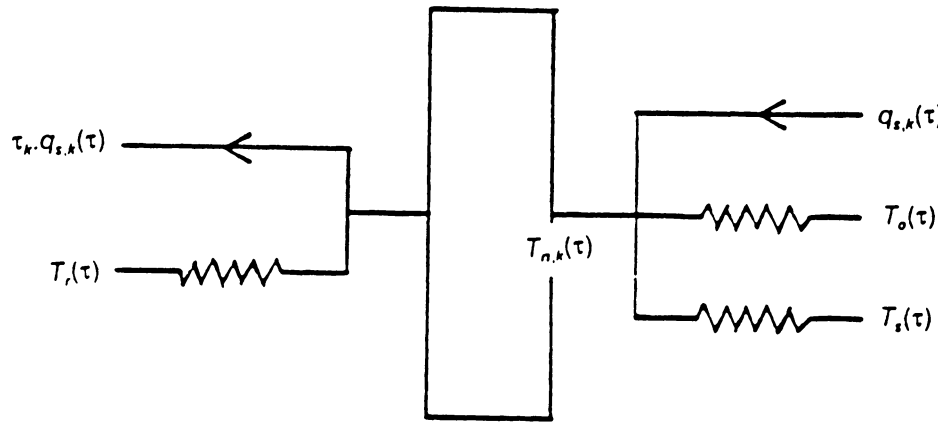

Figure 10. **Typical Window with Energy Loads on Both Surfaces:** the nomenclature is used throughout the surface energy balances

$$q_{w,k}(\tau) = U_w [\, T_{w,k}(\tau) - T_r(\tau) \,] \tag{4.36}$$

where

$$U_w = \frac{1}{R_{total}} = \frac{1}{\frac{1}{h_{i,v}} + \frac{\Delta x_{w,1}}{k_{w,1}} + \cdots + \frac{\Delta x_{w,n}}{k_{w,n}}} \tag{4.37}$$

The overall heat transfer coefficient of most typical windows is given in the ASHRAE Handbook of Fundamentals [29, 30, and 31].

Similar to equation 4.22, the outside surface temperature of the window is determined by performing an energy balance on its outside surface and solving for that temperature

$$T_{w,k}(\tau) = \frac{\alpha_w q_{s,n}(\tau) + h_{o,v}(\tau) T_o(\tau) + h_{w,r}(\tau) T_s(\tau) + U_w T_r(\tau)}{U_w + h_{o,v}(\tau) + h_{w,r}(\tau)} \tag{4.38}$$

where

$$h_{w,r}(\tau) = \varepsilon_w \sigma [\, T_s^2(\tau) + T_{w,k}^2(\tau) \,] [\, T_s(\tau) + T_{w,k}(\tau) \,] \tag{4.39}$$

Solar and infrared radiation heat transfer are neglected for outside door surfaces since the area is a small portion of the overall area of the building envelope. The quasisteady-state heat flux equation on the outside surface of the door is then

$$q_{d,k}(\tau) = U_d [\, T_{d,k}(\tau) - T_r(\tau) \,] \tag{4.40}$$

For an n-layer door

$$U_d = \frac{1}{R_{dtotal}} = \frac{1}{\frac{1}{h_{i,v}} + \frac{\Delta x_{d,1}}{k_{d,1}} + \cdots + \frac{\Delta x_{d,n}}{k_{d,n}}} \tag{4.41}$$

Similarly to Eqs. 4.22 and 4.36, the outside surface temperature of a door k is determined by performing an energy balance on its outside surface and solving for that temperature giving

$$T_{d,k}(\tau) = \frac{h_{o,v}(\tau)T_o(\tau) + U_d T_r(\tau)}{U_d + h_{o,v}(\tau)} \tag{4.42}$$

ROOM ENERGY BALANCE

Expressions for the surface temperatures of various walls, windows, doors, slab, and roof have been developed. An infiltration model as well as the generated loads reflecting the presence of specific number of people and some types of equipment have been selected. A single-room or -zone building with no internal partitioning is modeled next. In the energy balance on the room air, the various areas of walls, doors, and windows are obviously needed. Figure 11 shows the principal parameters in the single room structure which will be used in developing the desired model. For the single room model, the interior furnishings and other internal mass are not included. The moisture load is also not included in the analysis. Also, the thermal capacitance of the room air is neglected. Performing an energy balance on the room air gives

$$\begin{aligned} &\sum_{k=1}^{5} A_k\, q_{1,k}(\tau) + \sum_{k=1}^{n} A_{w,k}\, q_{w,k}(\tau) + \sum_{k=1}^{m} A_{d,k}\, q_{d,k}(\tau) + Q_i(\tau) + Q_h(\tau) \\ &+ A_{s,1}\, q_{s,1}(\tau) + A_{s,2}\, q_{s,2}(\tau) + \Sigma Q_g(\tau) + \sum_{k=1}^{n} \tau_{w,k}(\tau)\, q_{s,k}(\tau) = 0 \end{aligned} \tag{4.43}$$

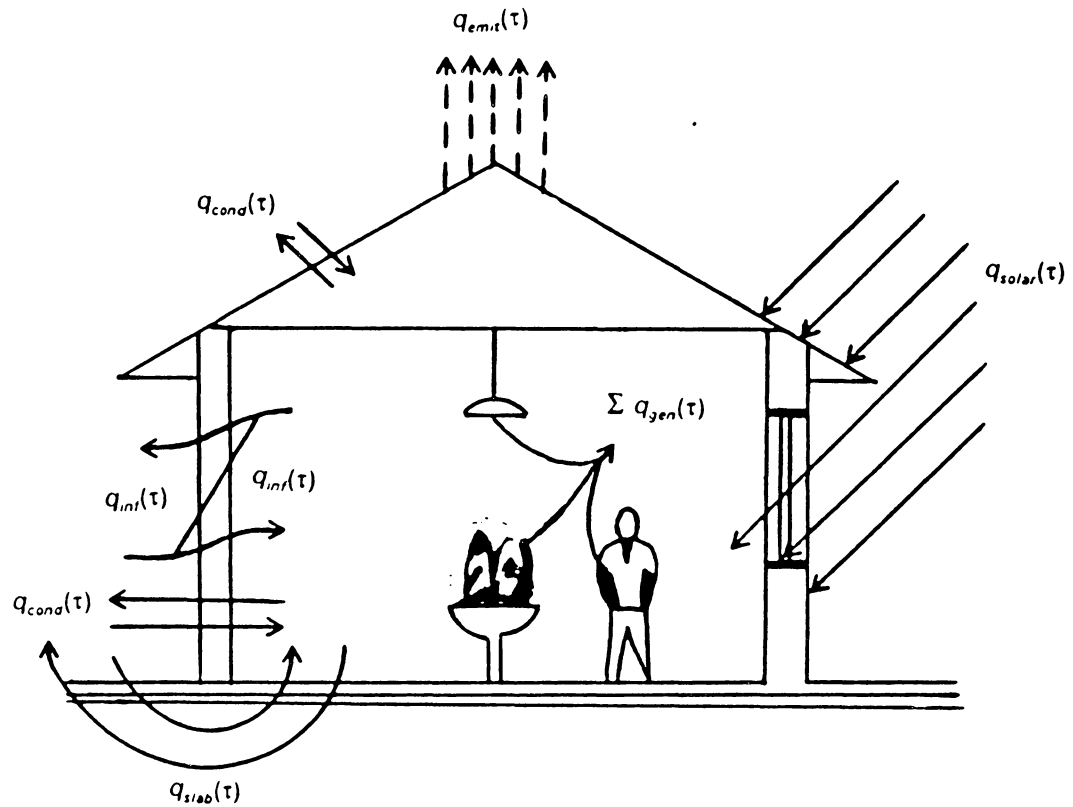

Figure 11. Typical Single Room Structure

Table 11 contains the nomenclature used in the single room model. Rewriting Eq. 4.43 with the new nomenclature and substituting the corresponding heat flux equations

$$\begin{aligned}
&\sum_{k=1}^{4} h_{i,v}(\tau)\, A_k \left[T_{1,k}(\tau) - T_r(\tau)\right] + h_{i,h}(\tau)\, A_5 \left[T_{1,5}(\tau) - T_r(\tau)\right] \\
&+ \sum_{k=1}^{n} U_w\, A_{w,k} \left[T_{w,k}(\tau) - T_r(\tau)\right] + \sum_{k=1}^{m} U_d\, A_{d,k} \left[T_{d,k}(\tau) - T_r(\tau)\right] \\
&+ h_{i,h}(\tau)\, A_{s,1} \left[T_{g,1}(\tau) - T_r(\tau)\right] + h_{i,h}(\tau)\, A_{s,2} \left[T_{g,2}(\tau) - T_r(\tau)\right] \\
&+ Q_i(\tau) + Q_g(\tau) + Q_h(\tau) + \sum_{k=1}^{n} \tau_{w,k}(\tau)\, q_{s,k}(\tau) = 0
\end{aligned} \tag{4.44}$$

Expanding around the room temperature

$$\begin{aligned}
&- \sum_{k=1}^{4} h_{i,v}(\tau)\, A_k\, T_r(\tau) - h_{i,h}(\tau)\, A_5\, T_r(\tau) - \sum_{k=1}^{n} U_w\, A_{w,k}\, T_r(\tau) \\
&- \sum_{k=1}^{m} U_d\, A_{d,k}\, T_r(\tau) - h_{i,h}(\tau)\, A_{s,1}\, T_r(\tau) - h_{i,h}(\tau)\, A_{s,2}\, T_r(\tau) \\
&+ \sum_{k=1}^{4} h_{i,v}(\tau)\, A_k\, T_{1,k}(\tau) + h_{i,h}(\tau)\, A_5\, T_{1,5}(\tau) + \sum_{k=1}^{n} U_w\, A_{w,k}\, T_{w,k}(\tau) \\
&+ \sum_{k=1}^{m} U_d\, A_{d,k}\, T_{d,k}(\tau) + h_{i,h}(\tau)\, A_{s,1}\, T_{s,1}(\tau) + h_{i,h}(\tau)\, A_{s,2}\, T_{s,2}(\tau) \\
&+ Q_i(\tau) + Q_g(\tau) + \sum_{k=1}^{n} \tau_{w,k}(\tau)\, q_{s,k}(\tau) + Q_h(\tau) = 0
\end{aligned} \tag{4.45}$$

Solving for the room temperature

Table 11. Nomenclature Used In The Single Room Model

PARAMETER		DESCRIPTION
$T_{n,k}(\tau)$	=	outside surface temperature of wall k at time τ (k = 1, 2, 3, 4 and 5, represent north, south, east, west and the roof, respectively)
$T_{1,k}(\tau)$	=	inside surface temperature of wall k at time τ (k = 1, 2, 3, 4 and 5)
$T_{d,k}(\tau)$	=	outside door surface temperature of side k at time τ (k = 1, 2, 3 and 4, represent door location on the north, south, east and the west side, respectively)
$T_{w,k}(\tau)$	=	outside window surface temperature of side k at time τ (k = 1, 2, 3 and 4)
$T_o(\tau)$	=	outside air temperature at time τ
$T_s(\tau)$	=	effective sky temperature at time τ
$T_r(\tau)$	=	room air temperature at time τ
$T_{s,1}(\tau)$	=	surface temperature of slab, section 1
$T_{s,2}(\tau)$	=	surface temperature of slab, section 2
$T_{g,1}$	=	ground temperature, below section 1 of the slab
$T_{g,2}$	=	ground temperature, below section 2 of the slab
T_m	=	initial or mean temperature of the room

Table 11. (continued)

PARAMETER		DESCRIPTION
$h_{i,v}(\tau)$	=	inside convective heat transfer coefficient for a vertical surface at time τ
$h_{i,h}(\tau)$	=	inside convective heat transfer coefficient for a horizontal surface at time τ
$h_{o,v}(\tau)$	=	outside convective heat transfer coefficient for a vertical surface at time τ
$h_{o,h}(\tau)$	=	outside convective heat transfer coefficient for a horizontal surface at time τ
$h_{k,r}(\tau)$	=	non-linear radiation coefficient for the outside surface of wall k at time τ
$h_{w,r}(\tau)$	=	non-linear radiation coefficient for the outside surface of window k at time τ
$\varepsilon_k(\tau)$	=	outside surface emissivity of wall k at time τ (k = 1, 2, 3, 4 and 5, represent north, south, east, west and the roof, respectively)
$\varepsilon_{w,k}(\tau)$	=	outside surface emissivity of window k at time τ (k = 1, 2, 3, and 4 represent north, south, east and the west side, respectively)
$\alpha_{w,k}(\tau)$	=	solar absorptivity of window k at time τ (k = 1, 2, 3, and 4)

Table 11. (continued)

PARAMETER		DESCRIPTION
$q_{s,k}(\tau)$	=	normal solar load on wall k at time τ (k = 1, 2, 3, 4, 5, and 6 represent north, south, east, west and the roof, respectively)
$Q_h(\tau)$	=	heating load to the room
$Q_g(\tau)$	=	generated load to the room
$Q_i(\tau)$	=	infiltration load to the room
$q_{n,k}(\tau)$	=	outside flux of wall k (k = 1, 2, 3, 4 and 5) at time τ
$q_{1,k}(\tau)$	=	inside flux of wall k (k = 1, 2, 3, 4 and 5) at time τ
$q_{s,1}(\tau)$	=	inside flux of the slab at time τ, section 1
$q_{s,2}(\tau)$	=	inside flux of the slab at time τ, section 2
$q_{d,k}(\tau)$	=	outside flux of the door on wall k at time τ
$q_{w,k}(\tau)$	=	outside flux of the window on wall k at time τ
U_g	=	slab's overall heat transfer conductance
$U_{w,k}$	=	overall heat transfer conductance, windows on side k of the walls.
$U_{d,k}$	=	overall heat transfer conductance, doors on side k of the walls.

Table 11. (continued)

PARAMETER		DESCRIPTION
A_k	=	area of wall k (k = 1, 2, 3, 4 and 5)
$A_{d,k}$	=	door area on wall k (k = 1, 2, 3 and 4)
$A_{w,k}$	=	window area on wall k (k = 1, 2, 3 and 4)
$A_{s,1}$	=	slab area of section 1
$A_{s,2}$	=	slab area of section 2
$X_{k,l}(i)$	=	response factor X of wall k and order l i = 1,n
$Y_{k,l}(i)$	=	response factor Y of wall k and order l i = 1,n
$Z_{k,l}(i)$	=	response factor Z of wall k and order l i = 1,n
$C_k(i)$	=	flux coefficient of wall k with i = 1 to l
$\overline{CR}$	=	slab common ratio
$\tau_{w,k}(\tau)$	=	solar transmittance of a window on wall k

$$T_r(\tau) = \frac{\begin{aligned}&\sum_{k=1}^{4} h_{i,v}(\tau)\, A_k\, T_{1,k}(\tau) + h_{i,h}(\tau)\, A_5\, T_{1,5}(\tau) + \sum_{k=1}^{n} U_w\, A_{w,k}\, T_{w,k}(\tau)\\ &+ \sum_{k=1}^{m} U_d\, A_{d,k}\, T_{d,k}(\tau) + h_{i,h}(\tau)\, A_{s,1}\, T_{s,1}(\tau) + h_{i,h}(\tau)\, A_{s,2}\, T_{s,2}(\tau)\\ &+ Q_i(\tau) + Q_g(\tau) + Q_h(\tau) + \sum_{k=1}^{n} \tau_{w,k}(\tau)\, q_{s,k}(\tau)\end{aligned}}{\begin{aligned}&\sum_{k=1}^{4} h_{i,v}(\tau)\, A_k + h_{i,h}(\tau)\, A_5 + \sum_{k=1}^{n} U_w\, A_{w,k}\\ &+ \sum_{k=1}^{m} U_d\, A_{d,k} + h_{i,h}(\tau)\, A_{s,1} + h_{i,h}(\tau)\, A_{s,2}\end{aligned}} \qquad (4.46)$$

Most of the parameters in Eq. 4.46 are known at the start of the analysis. The surface temperatures of the walls, doors, and windows are determined iteratively along with the room temperature. The infiltration, heating, and the generated loads are also calculated initially. The above equation is applicable for single room or zone structures.

Equation 4.46 is used to calculate the room temperature at every time step. An iterative procedure is needed to obtain the solution. The following parameters, fixed throughout the iteration, are calculated or specified initially:

1. The response factors of the walls, roof, and slab ($X_{k,\ell}(i)$, $Y_{k,\ell}(i)$, $Z_{k,\ell}(i)$, $C_k(j)$ with k=1, 2, 3, 4, and 5, ℓ=3, i=15, j = 1, 2, ..., ℓ ; $X_{s,2}(i)$, $Y_{s,2}(i)$, $Z_{s,2}(i)$, *and* $\overline{CR}$)

The representation employed is

k = 1 North wall

k = 2 South wall

k = 3 East wall

k = 4 West wall

k = 5 Roof or top wall

2. The overall heat transfer coefficients of the slab, windows, and doors (U_g, $U_{w,k}$, $U_{d,k}$)

3. The inside and outside convective heat transfer coefficients for the walls. ($h_{i,v}(\tau)$, $h_{i,h}(\tau)$, $h_{o,v}(\tau)$, *and* $h_{o,h}(\tau)$)

4. The outside effective emissivities and solar absorptivities of the outside surfaces of the walls, roof, windows, and the transmittance of the windows ($\varepsilon_k(\tau)$, $\varepsilon_{d,k}(\tau)$, $\varepsilon_{w,k}(\tau)$, $\alpha_k(\tau)$, $\alpha_{w,k}(\tau)$, *and* $\tau_{w,k}(\tau)$)

5. The surface areas of the walls, roof, doors, windows, and both sections of the slab. (A_k, $A_{d,k}$, $A_{w,k}$, $A_{s,1}$, *and* $A_{s,2}$)

6. The normal solar load on the outside envelope of the structure and the heating, generation, and infiltration, using the LBL model, loads to the room. ($q_{s,k}(\tau)$, $Q_h(\tau)$, $Q_g(\tau)$, *and* $Q_i(\tau)$)

7. The outside ambient, sky, initial, and ground temperature below both sections of the slab. ($T_o(\tau)$, $T_s(\tau)$, T_m, $T_{g,1}(\tau)$, *and* $T_{g,2}(\tau)$)

The iteration procedure for the room air temperature is as follows:

A. Since usually $\ell = 3$ and $i = 15$, i.e., using 15 third-order response factors, the temperature histories are required for the previous 14 time steps and the flux histories are required for the last two time steps. At the start of the analysis, however, no temperature or flux histories are known. The temperatures for the last 14 time steps are assigned a constant value, higher than the initial temperature. The flux histories are set to zero. The error resulting from this assumption is eliminated by starting the analysis about 50 time steps before the desired start of the analysis. Therefore, the history needed in the TRFM is obtained.

B. At the first iterative step, the room temperature ($T_r(\tau)$) and the inside surface temperatures of the walls ($T_{1,k}(\tau)$ with k = 1, 2, 3, 4, and 5) are given the previous time step values, at $\tau - 1$. The newly obtained temperatures after each iteration are used in the calculations.

C. Equations 4.31 and 4.32 are used to calculate the inside surface temperature of both sections of the floor slab, $T_{s,1}(\tau)$ and $T_{s,2}(\tau)$, respectively.

D. Equation 4.22 is used to calculate the outside surface temperature of the walls and roof, i.e., k = 1, 2, 3, 4, and 4. Since Eq. 4.17 is nonlinear ($h_{k,r}(\tau)$ is dependent on $T_{n,k}(\tau)$), the iterative

procedure explained earlier is employed. Usually five iterations are needed to obtain a 0.1 percent convergence.

E. Equations 4.38 and 4.42 are used to calculate the outside surface temperature of windows and doors, respectively.

F. Using Eq. 4.27, the inside surface temperature of the walls and ceiling are calculated, i.e., k = 1, 2, 3, 4 and 5.

G. Equation 4.46 is used to calculate an inside room temperature, $T_r(\tau)$

H. $T_r(\tau)$ is compared with its old value from the previous iteration. If convergence is obtained within 0.05 C, the iteration is stopped. If not, steps C through H are repeated. Usually, three to four overall iterations were needed to meet the desired convergence criterion.

The above procedure is repeated at every time step. The fluxes $q_{n,k}(\tau)$ (Eq. 4.13), $q_{1,k}(\tau)$ (Eq. 4.12), $q_{s,1}(\tau)$ (Eq. 4.29), and $q_{s,2}(\tau)$ (Eq. 4.34) are used as part of the history for the next time step. Therefore, these fluxes are calculated after convergence of all temperatures at each time step.

Recapping the steps in the above analysis, two iteration procedures are used, one overall and several internal iterations. The overall iteration affects the room and all of the inside and outside surface temperatures in the envelope. The internal iterations are used to determine the outside surface temperatures of the envelope. Initially, the room and inside wall surface temperatures are given arbitrary values. After the inside and outside surface temperatures of the envelope are calculated, the room temperature is determined and compared with the value from the previous iteration. If the convergence criterion is met, the iteration is stopped. The outside and inside heat fluxes of all walls are then determined using the final temperatures. These fluxes are used as histories in the next time step calculations. The same procedure is repeated at every time step until the desired total number of time increments is reached.

The heating and cooling loads are the usual result in most HVAC calculations. Based on a set interior temperature, known as the interior design temperature, the heating or cooling loads are calculated. An expression for the energy supplied or extracted from the room is determined similarly to the method employed when determining the interior temperature. An energy balance on the room air is performed and the heating or cooling load is determined instead of the room temperature (Eq. 4.44). Rewriting Eq. 4.44

$$\begin{aligned}
&\sum_{k=1}^{4} h_{i,v}(\tau)\, A_k \left[T_{1,k}(\tau) - T_r(\tau)\right] + h_{i,h}(\tau)\, A_5 \left[T_{1,5}(\tau) - T_r(\tau)\right] \\
&+ \sum_{k=1}^{n} U_w\, A_{w,k} \left[T_{w,k}(\tau) - T_r(\tau)\right] + \sum_{k=1}^{m} U_d\, A_{d,k} \left[T_{d,k}(\tau) - T_r(\tau)\right] \\
&+ h_{i,h}(\tau)\, A_{s,1} \left[T_{g,1}(\tau) - T_r(\tau)\right] + h_{i,h}(\tau)\, A_{s,2} \left[T_{g,2}(\tau) - T_r(\tau)\right] \\
&+ Q_i(\tau) + Q_g(\tau) + Q_h(\tau) + \sum_{k=1}^{n} \tau_{w,k}(\tau)\, q_{s,k}(\tau) = 0
\end{aligned} \tag{4.44}$$

Solving for the heating or cooling load

$$\begin{aligned}
Q_h(\tau) = &- Q_i(\tau) - Q_g(\tau) - \sum_{k=1}^{n} \tau_{w,k}(\tau)\, q_{s,k}(\tau) \\
&- \sum_{k=1}^{4} h_{i,v}(\tau)\, A_k \left[T_{1,k}(\tau) - T_r(\tau)\right] - h_{i,h}(\tau)\, A_5 \left[T_{1,5}(\tau) - T_r(\tau)\right] \\
&- \sum_{k=1}^{n} U_w\, A_{w,k} \left[T_{w,k}(\tau) - T_r(\tau)\right] - \sum_{k=1}^{m} U_d\, A_{d,k} \left[T_{d,k}(\tau) - T_r(\tau)\right] \\
&- h_{i,h}(\tau)\, A_{s,1} \left[T_{g,1}(\tau) - T_r(\tau)\right] - h_{i,h}(\tau)\, A_{s,2} \left[T_{g,2}(\tau) - T_r(\tau)\right]
\end{aligned} \tag{4.47}$$

or

$$\begin{aligned}
Q_h(\tau) = &- Q_i(\tau) - Q_g(\tau) - \sum_{k=1}^{n} \tau_{w,k}(\tau)\, q_{s,k}(\tau) \\
&+ \sum_{k=1}^{4} h_{i,v}(\tau)\, A_k \left[T_r(\tau) - T_{1,k}(\tau)\right] + h_{i,h}(\tau)\, A_5 \left[T_r(\tau) - T_{1,5}(\tau)\right] \\
&+ \sum_{k=1}^{n} U_w\, A_{w,k} \left[T_r(\tau) - T_{w,k}(\tau)\right] + \sum_{k=1}^{m} U_d\, A_{d,k} \left[T_r(\tau) - T_{d,k}(\tau)\right] \\
&+ h_{i,h}(\tau)\, A_{s,1} \left[T_r(\tau) - T_{g,1}(\tau)\right] + h_{i,h}(\tau)\, A_{s,2} \left[T_r(\tau) - T_{g,2}(\tau)\right]
\end{aligned} \tag{4.48}$$

Equation 4.48 is the desired heating or cooling load expression. The energy balances used in determining the inside and outside surface temperatures of the walls, roof, doors, windows, and inside surface temperatures of the slab are still valid. The solution is simpler since no overall iterations are needed. The exterior surface temperatures of the walls are determined using the localized iterations. Since the room temperature is known, the inside and outside surface temperatures are calculated at the start of each time step. The LBL infiltration model and the methodology presented earlier for determining the generation loads are also used. Since the temperature and flux histories are not known at the start of the analysis, the analysis is started 50 time steps before the desired start of calculations. Initially, the flux histories are assumed zero and the temperature histories are assumed constant, equal to the given inside room temperature. Equation 4.48 is used for determining the cooling as well as the heating loads. In Eq. 4.48, the heating loads have positive values and the cooling loads have negative values.

NBS TEST HOUSES

The single room model can be used to analyze any single zone structure including a warehouse. A validation of the model is necessary to determine the accuracy and the validity of the calculation procedure. The National Bureau of Standards built six test buildings in Gaithersburg, Maryland, to study the effect of wall mass on the heating and cooling loads required in a structure.

Six-single room test buildings were instrumented for measuring heating and cooling loads, wall heat transmission, and indoor temperatures. All six buildings were tested during a winter heating season, an intermediate heating season (spring season), and a summer cooling season. The description of the experimental set-up and test buildings, as presented in references 22 through 25, is given next.

Each test building is 6.1 m wide, 6.1 m long, and 2.3 m high. All six buildings had the same floor plan, orientation, and all other parameters except for the four exterior wall properties (Table 12). The walls notation and description are:

No. 1. Insulated lightweight wood frame

No. 2. Uninsulated lightweight wood frame

No. 3. Insulated masonry (outside mass)

No. 4. Uninsulated masonry

No. 4. Log

No. 6. Insulated masonry (inside mass)

Two double-hung insulating glass windows were located on the south-facing walls and two on the north-facing walls. The total window area of each house was 4.07 m^2 and the wall area A_k = 2.035 m^2 with k = 1 (north wall), k = 2 (south wall), etc. Each window's overall heat transfer coefficient and solar transmittance were assumed to remain constant throughout the analysis, $U_{w,k} = U_w = 2.04\ W/m^2K$ and $\tau_{w,k}(\tau) = \tau_w = 0.61$. Each test building had an 1.81 m^2 door with an overall heat transfer coefficient of 0.818 W/m^2K ($U_{d,k} = U_d = 0.818\ W/m^2K$) and door area $A_{d,k} = A_d = 1.81\ m^2$. The slab and roof, which were common for all six test buildings, are described in Table 12. Each test building was equipped with a centrally located 4.1 kW electric forced air heating plant and a 3800 W split-unit vapor-compression air-conditioning system. The evaporator coil was installed above the electric heating element. The compressor and condenser were located in an outdoor unit located at the center of the north wall of each test building.

The wind speed and direction were measured with a rotating-cup anemometer and a potentiometer-type, wind-direction vane mounted on a 7.6 m high mast located near the test buildings. The outdoor temperature and humidity were measured with a thermocouple and Dunmore-type relative humidity transducer mounted 0.305 m from the center of the north-facing wall of the instrumentation building. The hemispherical radiation incident on a south-facing vertical surface was measured with a pyranometer mounted 0.305 m above the ground

Table 12. Description of the NBS Test Houses

PROPERTIES OF TEST BUILDINGS	ΔX (m)	k (W/m.C)	ρ (kg/m^3)	C_p (kJ/kg.C)	$\alpha.10^5$ (m^2/s)
WALL PROPERTIES					
NO. 1. Insulated Lightweight Wood Frame:					
Gypsum Board 7	0.0127	0.16	801	4.165	4.8
2 x 4 studs placed 0.4 m o.c.	0.092	0.11538	513	1.382	16.27
R-2.0 Blanket Insu. Between Studs	0.092	0.0476	32.04	0.837	177.5
Exterior Plywood	0.016	0.1154	720.8	1.214	13.185
NO. 2. Uninsulated Lightweight Wood Frame					
Gypsum Board 7	0.0127	0.16	801	4.165	4.8
2 x 4 studs placed 0.4 m o.c.	0.092	0.11538	513	1.382	16.27
R-0.17 Air Space: h = 5.678 (W/m^2C)	0.092	--	--	--	--
Exterior Plywood	0.016	0.1154	720.8	1.214	13.185
NO. 3. Insulated Masonry (Outside Mass)					
Gypsum Board 7	0.0127	0.16	801	4.165	4.8
Polystyrene Insulation	0.051	0.026	43.24	1.214	40.78
Furring Strips Placed 0.61 m o.c.	0.051	0.115	512.6	1.381	16.24
R-0.12 Air Space: h = 8.229 (W/m^2C)	0.0063	--	--	--	--
Concrete Block	0.102	0.52	977.0	0.837	63.56
Face Brick	0.089	0.63	2002.2	0.921	34.16

Table 12. (continued)

PROPERTIES OF TEST BUILDINGS	ΔX (m)	k (W/m.C)	ρ (kg/m^3)	C_p (kJ/kg.C)	$\alpha.10^5$ (m^2/s)
WALL PROPERTIES					
NO. 4. Uninsulated Masonry					
Gypsum Board	0.0127	0.16	801	4.165	4.8
R-0.16 Air Space: h = 6.042 (W/m^2C)	0.019	--	--	--	--
Furring Strips Placed 0.41 m o.c.	0.019	0.115	512.6	1.381	16.24
Concrete Block	0.204	0.72	977.0	0.837	88.05
NO. 5. Log					
Square Lodge-pole Pine Log	0.178	0.11538	414.8	1.632	17.04
NO. 6. Insulated Masonry (Inside Mass)					
Plaster	0.0127	0.225	720.8	0.837	37.27
Concrete Block	0.204	0.725	977.0	0.837	88.65
Perlite Insulation	0.089	0.053	136.2	1.088	35.75
Face Brick	0.089	0.63	2002.2	0.921	34.16

Table 12. (continued)

PROPERTIES OF TEST BUILDINGS	ΔX (m)	k (W/m.C)	ρ (kg/m^3)	C_p (kJ/kg.C)	$\alpha_d 10^5$ (m^2/s)
CEILING PROPERTIES					
Gypsum Board	0.0127	0.16	801	4.165	4.8
2 X 4 Stud	0.092	0.11538	513	1.382	16.27
Glass-fiber Insulation	0.280	0.0476	32.04	0.837	177.42
FLOOR PROPERTIES					
Polystyrene Insulation	0.051	0.026	43.24	1.214	40.78
Concrete Slab	0.102	1.385	2402.7	0.837	68.84
Gravel	0.102	0.865	1922.2	0.837	53.74
Earth	0.305	0.865	1922.2	0.837	53.74

and centered on the south-facing wall of building No. 1. Signals from the wind speed sensor and solar vertical pyranometer were integrated using analog integrators to obtain average hourly values. The instantaneous signals from the other weather transducers were fed to a data acquisition system which recorded the signals at hourly intervals.

The total electrical energy used by each test building was measured using a watt-hour meter equipped with a demand metering device which generated a contact closure for each 3.60 Wh consumed. The watt-hour meters were also read manually at 10 hours each work day. The heating load for each test building was determined by subtracting the constant internal load from the total electric energy consumption. For the summer cooling energy measurements, the cumulative cooling load (Q_c) was determined from the relation

$$Q_c = \dot{m}\ C_p \int_0^P \Delta T\, dt + W\ h_{fg} \qquad (4.49)$$

where $\dot{m}$ (kg/s) is the mass flow rate of air through cooling plant, ΔT (C) is the temperature drop of air upon passing through cooling plant, t (h) is the time, W (kg) is the mass of condensate collected during period P, h_{fg} (kJ/kg) is the latent heat of vaporization for water, and P (h) is the time period over which the blower of the cooling plant operates. The first and second terms represent the sensible and latent portions of the cooling load, respectively. The temperature drop (ΔT) was measured with a 32-junction copper-constantan thermopile. The mass flow rate of air (m) through the cooling plant was measured using an air-flow measuring device mounted in a long, straight return air duct.

The electric power to each heating plant was measured using the watt-hour meters. The electric power (P_e) delivered to the heating plant was also determined from the relation

$$P_e = \dot{m}\ C_p\ \Delta T \qquad (4.50)$$

where $\dot{m}$ (kg/s) is the mass flow rate of air through the heating plant measured by the air flow measuring device, C_p (kJ/kg.C) is the specific heat of the air, and ΔT (C) is the temperature drop of air passing through the heating plant, measured with the thermopile. The agreement between the measured and calculated electric power was within 6 percent and, therefore, the uncertainty in the sensible load measuring system was $\pm$ 6 percent. Condensate from the evaporator coil of each air conditioner was collected in a 19 cm diameter, 0.86-m-high cylinder. Installed in the bottom of each cylinder was a pressure transducer which produced a D.C. signal proportional to the weight of water in the cylinder.

The indoor air temperature was measured with thermocouples mounted along two thermocouple strings installed 1.5 m levels from the center of the north- and south-facing walls of each test building. Air temperature thermocouples were located along each string at 5.1 cm, 0.31 m, 0.61 m, and 1.5 m levels above the floor and 5.1 cm below the ceiling. The earth temperature under each floor slab was measured with a copper-constantan thermocouple installed at the center of the slab and 0.51 m below the floor surface.

VALIDATION OF THE PROPOSED MODEL

The measured parameters, including the inside room air temperatures and the corresponding heating or cooling loads, were of a great interest to the present research. Since all of the parameters were known, it was possible to use the experimental data and calculate the room temperature. These data provided a test for establishing the validity of the model.

During the winter season (February), the solar loads on horizontal and vertical surfaces and the outside air temperatures were measured for 200 hours. The heating loads and the indoor temperatures were measured for the last 63 hours. Because of the needed history of temperatures and fluxes required in the TRFM, It was necessary to run the computer code and simulate the test building for several hours before the real analysis started. Unless a large

number of time increments (50 time increments) are used, a large error would be present during the initial calculations. Therefore, the simulations were started, using a time increment of one hour and a fixed room temperature, under the assumption of constant initial room temperature and up to time step 137. For the remaining 63 hours, the room temperature is calculated.

The inside room air temperature was calculated using the measured heating or cooling loads, outside air and ground temperatures, and the transmittance of windows. The measured outside air speed and direction were used in the LBL infiltration model. Buildings 1, 4, and 5 (insulated lightweight wood frame, uninsulated masonry, and the insulated masonry-inside mass, respectively) were used for the winter (February) calculations. The insulated masonry-outside mass (No. 3), was used for the spring (April) calculations. Because of the availability of data and numerical results of a multiroom house, presented in Chapter 5, only four simulations were conducted.

In Figs. 12, 13, and 14, the measured and calculated inside room temperatures are plotted along with the normal solar load on the south facing wall for 63 hours during the winter (February) season. Good agreement between the measured and calculated room temperatures is obtained. In Fig. 15, the measured and calculated inside room temperatures are plotted along with the normal solar load on the south-facing wall for 100 hours during the spring (April) season. Again, good agreement between the calculated and the measured room temperatures is obtained.

Numerous test runs were made to examine the stability of the single room model by keeping the outside temperature constant and calculating the room temperature until steady-state is reached. After reaching steady-state, the calculations were continued for many hours at the steady-state condition in order to check for stability. No problems were observed. Other test runs were performed to examine the stability of the iterations by running large solar loads (almost 5 times the normal solar load) and maintaining these loads until reaching

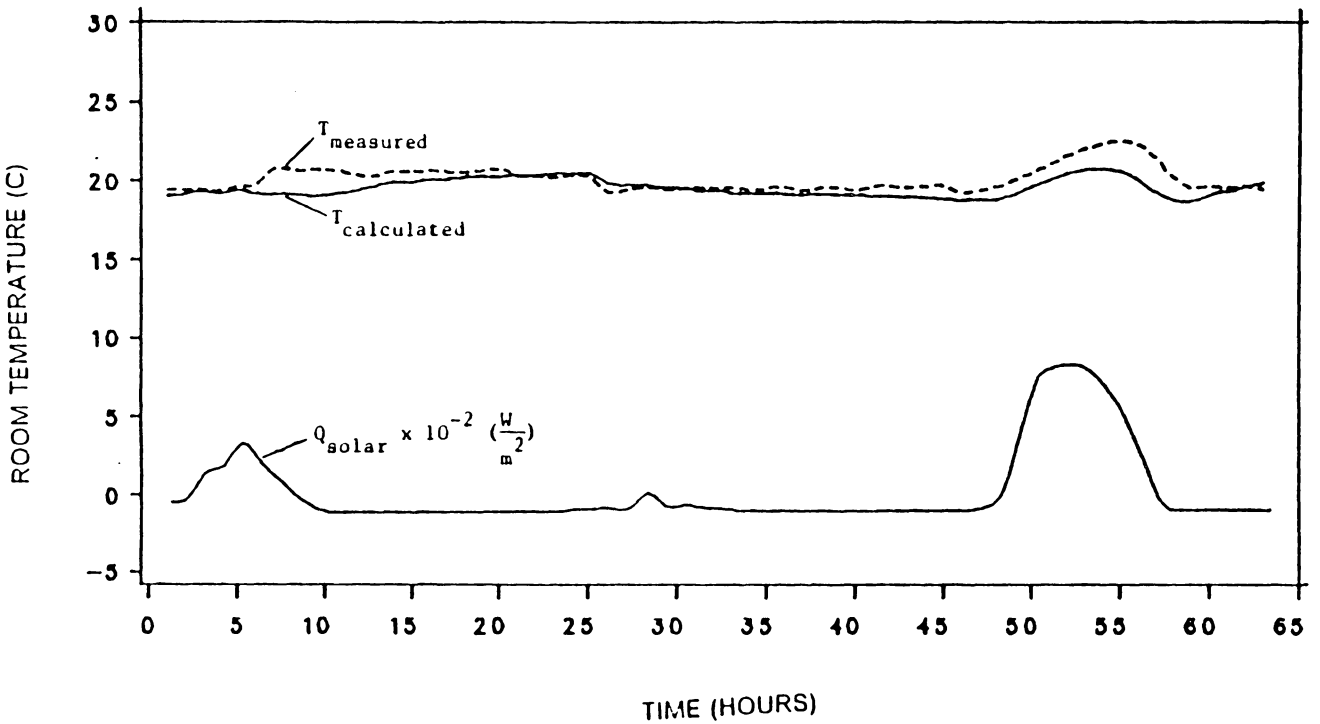

Figure 12. Calculated and Measured Room Temperatures of the Insulated Lightweight Wood Frame House During the Winter (February) season

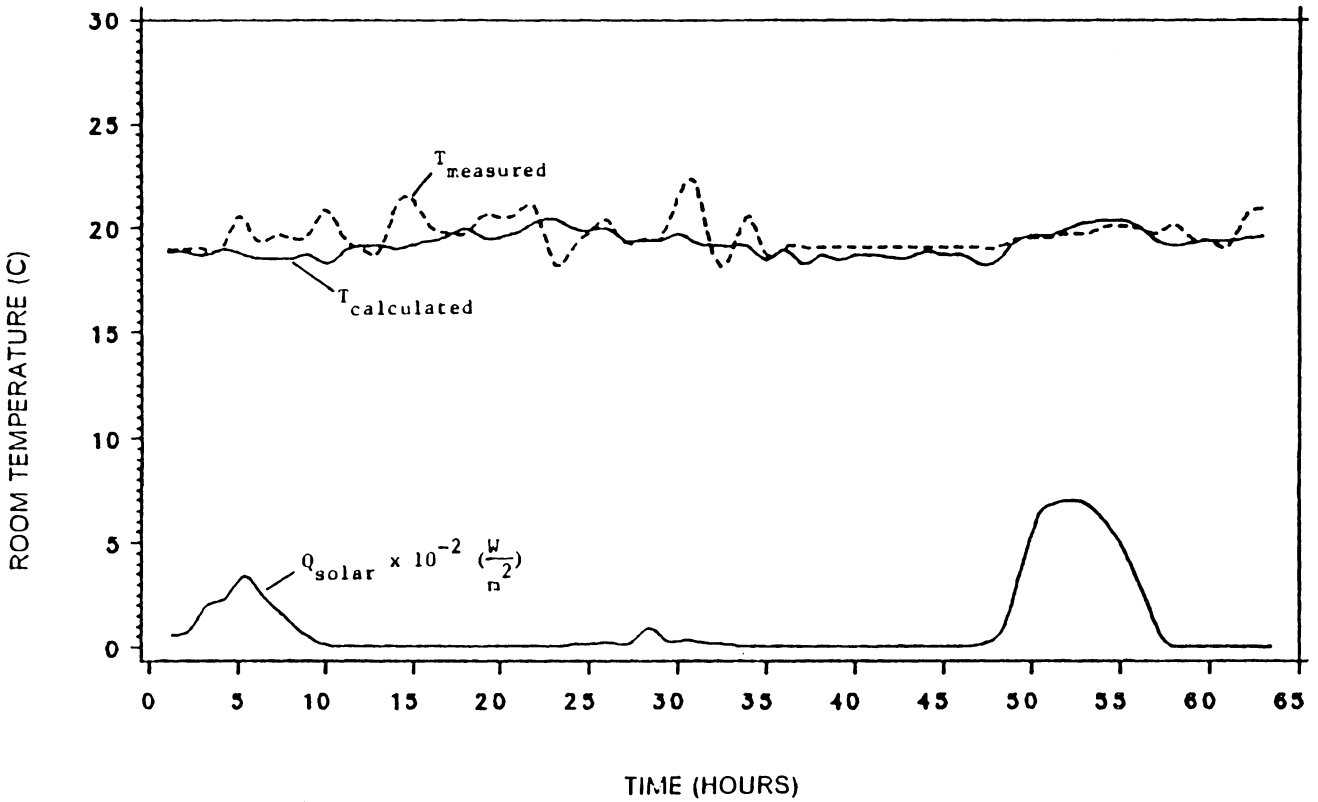

Figure 13. Calculated and Measured Room Temperatures of the Uninsulated Masonry House During the Winter (February) season

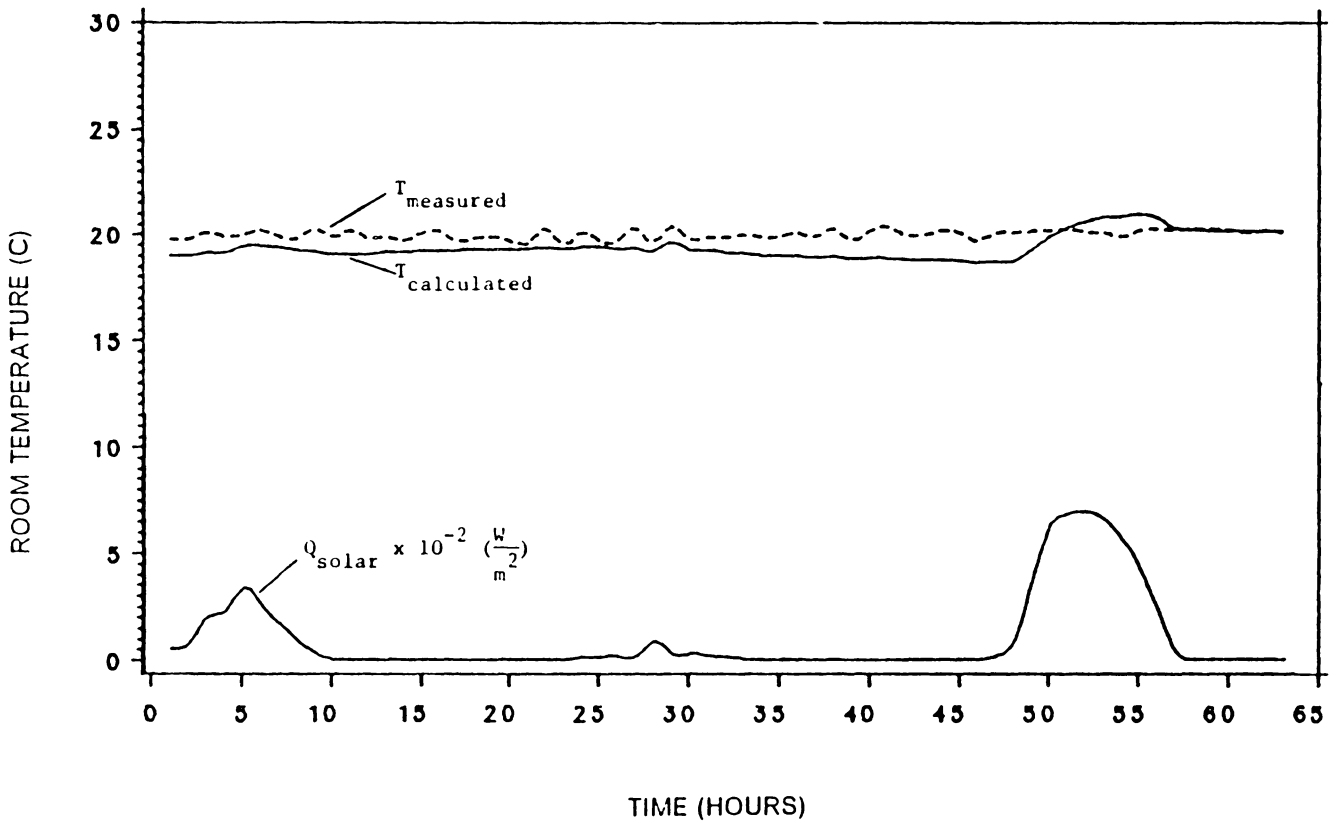

Figure 14. Calculated and Measured Room Temperatures of the Log House During the Winter (February) season

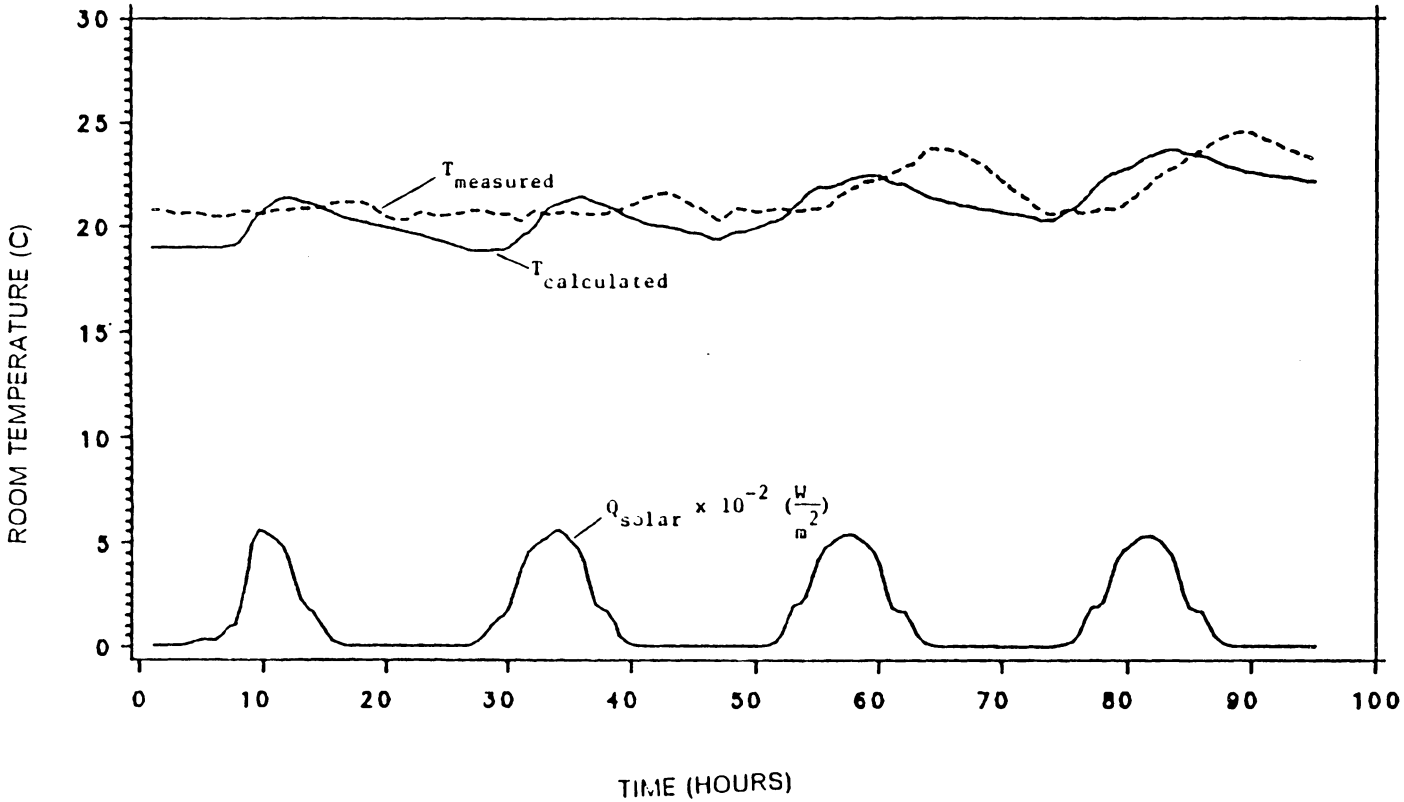

Figure 15. Calculated and Measured Room Temperatures of the Insulated Masonry (outside mass) House During the Spring (April) season

steady-state. Again no instability was present even though the temperature reached upwards of 80 C. Other test runs were performed by increasing the values or setting to zero the solar loads, emissivities, convective coefficients, and internal generation and checking for any irregularities in the temperatures. No irregularities were observed.

In the next chapter, the multi-zone and -floor model is introduced along with validations using experimental data and numerical results for a multiroom house.

5. MULTIZONE MODEL

In Chapter 4, the single zone model was presented and validated with data for single room houses in Gaithersburg, Maryland. In the present chapter, a further expansion of the single room model to multi-rooms and -floors is presented. Validation with experimental data and numerical results from NBSLD, BLAST, and DOE-2 programs for a house in Houston, TX. is also given.

SOLAR LOAD

The American Society of Heating, Refrigerating, and Air-Conditioning Engineers introduced a procedure [49] for calculating the solar load on a given wall along with the solar transmittance, absorptance, and reflectance of windows. This procedure is used in the current analysis and is presented in Appendix D.

INFILTRATION LOAD

The infiltration to each room of the building is required in the current analysis at each time step (τ). The LBL model presented in Chapter 4 is not used for large buildings since the assumption of constant pressure inside the structure is not valid. In large buildings, more involved modelling is required where the pressure in each room or at least in each floor is calculated. The infiltration is then determined from the pressure difference across openings.

Infiltration in buildings is heavily dependent on aperture ("crack") areas and pressure coefficients. These coefficients vary significantly from one building to another. Infiltration models are characterized as approximate methods based on combined empirical data and mathematical formulation. Cracks in walls and window frames are tedious to determine without measurements. The ASHRAE task group on energy calculations in buildings [49] present a procedure for calculating the infiltration based on the pressure difference. The ASHRAE procedure is used in this research and is presented in Appendix E.

EXTERIOR WALLS AND ROOF

The procedure employed for solving exterior surface temperatures of buildings is introduced next. The nomenclature is slightly different from what has been used in Chapter 4. One obvious difference is the addition of one degree of freedom representing the floor location.

In formulating the analysis, it was important to match common characteristics or boundary conditions in the energy balances to determine a general model. The exterior and interior surface energy balances are similar for all walls. Also, the room walls on the same exterior side of a building (north, south, east, west, and roof or top wall) have the same solar load, convective flux to the outside, and emission of infrared radiation to the surroundings. Also,

all surfaces have similar boundary conditions on the interior side, i.e., convective flux to the room temperature. A radiative flux between interior walls is added to the analysis later.

The expressions for outside and inside surface temperatures of exterior walls were derived in Chapter 4. The analysis is similar and does not require modification. The conduction heat flux on the inside surface of a multilayer wall k, in room j, and floor f obtained using the TRFM is

$$q_{1,k,j,f}(\tau) = \sum_{i=1}^{N} X_{k,j,f}(i)\,[T_{1,k,j,f}(\tau + 1 - i) - T_m] - \sum_{i=1}^{N} Y_{k,j,f}(i)\,[T_{n,k,j,f}(\tau + 1 - i) - T_m] + \sum_{j=2}^{\ell} (-1)^j C_{k,j,f}(j-1)\,q_{1,k,j,f}(\tau + 1 - j) \tag{5.1}$$

The heat flux on the outside surface of wall k, room j, and floor f obtained from the TRFM is

$$q_{n,k,j,f}(\tau) = \sum_{i=1}^{N} Y_{k,j,f}(i)\,[T_{1,k,j,f}(\tau + 1 - i) - T_m] - \sum_{i=1}^{N} Z_{k,j,f}(i)\,[T_{n,k,j,f}(\tau + 1 - i) - T_m] + \sum_{j=2}^{\ell} (-1)^j C_{k,j,f}(j-1)\,q_{n,k,j,f}(\tau + 1 - j) \tag{5.2}$$

where $q_{1,k,j,f}(\tau)$ is positive when the flux is pointing away from wall k and $q_{n,k,j,f}(\tau)$ is positive when the flux is pointing toward wall k of room j and floor f. Later, k is replaced by "n" for the north wall, "s" for the south wall, "e" for the east wall and "w" for the west wall of room j and floor f. It is shown later that using this nomenclature, a pattern in the formulation is noted, allowing for an easier model to be developed.

Performing an energy balance on the outside surface of wall k,

$$q_{solar,k}(\tau) + q_{conv,k}(\tau) + q_{emis,k}(\tau) + q_{cond,k} = 0 \tag{5.3}$$

where

$$
\begin{aligned}
q_{solar,k}(\tau) &= \alpha_{w,k}\, q_{s,k}(\tau) \\
q_{conv,k}(\tau) &= h_{o,v}(\tau)\,[T_o(\tau) - T_{n,k,j,f}(\tau)] \\
q_{emis,k}(\tau) &= \varepsilon_k\, \sigma\,[T_s^4(\tau) - T_{n,k,j,f}^4(\tau)] \\
q_{cond,k}(\tau) &= q_{n,k,j,f}(\tau)
\end{aligned}
\tag{5.4}
$$

Substituting the heat fluxes and solving for $T_{n,k,j,f}(\tau)$ gives

$$
T_{n,k,j,f}(\tau) = \frac{\begin{array}{c} q_{s,k,j,f}(\tau) + h_{o,v}(\tau)T_o(\tau) + h_{k,j,f}(\tau)T_s(\tau) + S_T \\ + Y_{k,j,f}(1)[T_{1,k,j,f}(\tau) - T_m] + Z_{k,j,f}(1)T_m + S_q \end{array}}{h_{o,v}(\tau) + h_{k,j,f}(\tau) + Z_{k,j,f}(1)} \tag{5.5}
$$

where

$$
\begin{aligned}
S_T &= \sum_{i=2}^{N} Y_{k,j,f}(i)[T_{1,k,j,f}(\tau + 1 - i) - T_m] - Z_{k,j,f}(i)[T_{n,k,j,f}(\tau + 1 - i) - T_m] \\
S_q &= \sum_{j=2}^{\ell} (-1)^j C_{k,j,f}(j - 1)\, q_{n,k,j,f}(\tau + 1 - j)
\end{aligned}
\tag{5.6}
$$

Equation 5.5 is subject to two important conditions. First, the response factors are calculated with layer 1 of the multilayer wall adjacent to the room air and layer n adjacent to the outside. Second, Eq. 5.5 is nonlinear and is solved iteratively. $T_{n,k,j,f}(\tau)$ is given an arbitrary value, $h_{k,j,f}$ is calculated, and Eq. 5.5 is used to calculate a new $T_{n,k,j,f}(\tau)$. The iteration is continued until convergence.

Performing an energy balance at the inner surface of wall k,

$$
q_{conv,k}(\tau) + q_{1,k,j,f}(\tau) = 0 \tag{5.7}
$$

where

$$q_{conv,k}(\tau) = h_{i,v}(\tau)[T_{1,k,j,f}(\tau) - T_{r,j,f}(\tau)]$$

$$q_{1,k,j,f}(\tau) = \sum_{i=1}^{N} X_{k,j,f}(i)[T_{1,k,j,f}(\tau + 1 - i) - T_m] - Y_{k,j,f}(i)[T_{n,k,j,f}(\tau + 1 - i) - T_m] + \sum_{j=2}^{\ell} C_{k,j,f}(j - 1)\, q_{1,k,j,f}(\tau + 1 - j) \quad (5.8)$$

Similar to the analysis in Chapter 4, solving for $T_{1,k,j,f}(\tau)$

$$T_{1,k,j,f}(\tau) = \frac{X_{k,j,f}(1)T_m + Y_{k,j,f}(1)[T_{n,k,j,f}(\tau) - T_m] - S_{T,k} - S_{q,k} + h_{i,v}(\tau)T_{r,j,f}(\tau)}{X_{k,j,f}(1)T_m + h_{i,v}(\tau)} \quad (5.9)$$

where

$$S_{T,k} = \sum_{i=2}^{N} X_{k,j,f}(i)[T_{1,k,j,f}(\tau + 1 - i) - T_m] - Y_{k,j,f}(i)[T_{n,k,j,f}(\tau + 1 - i) - T_m] \quad (5.10)$$

$$S_{q,k} = \sum_{j=2}^{\ell} (-1)^j C_{k,j,f}(j - 1) q_{1,k,j,f}(\tau + 1 - j)$$

SLAB-ON-GRADE SURFACE TEMPERATURES

The ground temperature beneath the slab was analyzed in the previous chapter. The two ground temperatures calculated are beneath the center section of the slab (section 1) and beneath the perimeter (section 2). The area of section 1 is usually assigned 80 percent of the total slab area. The remainder 20 percent of the slab area (perimeter) is assigned section 2.

The inside surface temperature of section 1 of the slab is

$$T_{s,1,j}(\tau) = \frac{X_{s,2}(1)T_m + h_{i,h}(\tau)T_{r,j}(\tau) - S_{T,s,1} - S_{q,s,1}}{X_{s,1}(1)T_m + h_{i,h}(\tau)} \qquad (5.11)$$

where

$$\begin{aligned} S_{T,s,1} &= \sum_{i=2}^{N} X_{s,2}(i)\,[T_{s,1,j}(\tau + 1 - i) - T_m] - U_g\,(1 - \overline{CR})[T_{g,1} - T_m] \\ S_{q,s,1} &= \overline{CR}\; q_{s,1,j}(\tau - 1) \end{aligned} \qquad (5.12)$$

The inside surface temperature of section 2 is

$$T_{s,2,j}(\tau) = \frac{X_{s,2}(1)T_m + h_{i,h}(\tau)T_{r,j}(\tau) - S_{T,s,2} - S_{q,s,2}}{X_{s,2}(1)T_m + h_{i,h}(\tau)} \qquad (5.13)$$

where

$$\begin{aligned} S_{T,s,2} &= \sum_{i=2}^{N} X_{s,2}(i)\,[T_{s,2,j}(\tau + 1 - i) - T_m] - U_g\,[1 - \overline{CR}\,]\,[T_{g,2} - T_m] \\ S_{q,s,2} &= \overline{CR}\; q_{s,2,j}(\tau - 1) \end{aligned} \qquad (5.14)$$

and

$$\begin{aligned} q_{s,2,j}(\tau) = \sum_{i=1}^{N} X_{s,2}[T_{s,2,j}(\tau + 1 - i) - T_m] &- U_g\,(1 - \overline{CR})[T_{g,2} - T_m] \\ &+ \overline{CR}\; q_{s,2,j}(\tau - 1) \end{aligned} \qquad (5.15)$$

As in Chapter 4, each room is allowed two slab surface areas and ground temperatures. If the slab is enclosed in one section, the area of the other section is set to zero in the calculations.

OUTSIDE WINDOWS AND DOORS

Energy balances on windows are made next. On a given exterior side of a building, all windows have identical boundary conditions on their exterior and interior surfaces. The exterior surface temperature is deduced using an expression similar to Eq. 5.5. The well known quasisteady-state equation is used for the heat flux through the window in terms of its outside surface temperature and the inside room temperature. Similar to the analysis in the previous chapter, the outside surface temperature of the window is determined by performing an energy balance on its outside surface and solving for that surface temperature.

$$T_{w,j,f}(\tau) = \frac{\alpha_w q_{s,k}(\tau) + h_{o,v}(\tau)T_o(\tau) + h_{w,j,k}(\tau)T_s(\tau) + U_w T_{r,j,f}(\tau)}{U_w + h_{o,v}(\tau) + h_{w,j,f}(\tau)} \quad (5.16)$$

where

$$h_{w,j,f}(\tau) = \varepsilon_{w,k}\sigma[T_s^2(\tau) + T_{w,j,f}^2(\tau)][T_s(\tau) + T_{w,j,f}(\tau)] \quad (5.17)$$

Only convection is considered on the outside and inside surfaces of doors. The inside convective thermal resistance is included in the overall heat transfer coefficient. No reference to the floor location of doors exposed to the outside is given. They are assumed on the first floor.

Similarly to Eqs. 5.5 and 5.14, the outside surface temperature of the door is determined by performing an energy balance on its outside surface and solving for that temperature.

$$T_{d,j}(\tau) = \frac{h_{o,v}(\tau)T_o(\tau) + U_d T_{r,j}(\tau)}{U_d + h_{o,v}(\tau)} \qquad (5.18)$$

INTERIOR ROOMS

Rooms and floors are assigned variables as shown in Fig. 16 in order to present a general model. It is assumed that each floor contains N rooms in the x direction and P rooms in the y direction. The maximum total number of rooms per floor is N x P. Also, each floor is composed of the same number of rooms. With the present convention, room j at floor f is right under room j of floor f+1. Having the same number of rooms per floor stacked above each other is not a significant limitation of the model but a convenient way to keep track of the rooms. Later, modification to include different size rooms on different floors is discussed under the subheading "Imaginary Walls." Large rooms are subdivided into smaller rooms, to fit the model's requirements, using imaginary walls.

The numbering scheme employed throughout the analysis, as shown in Fig. 17, is as follows:

On the south side of the building and from west to east of the first row (M=1), the rooms are numbered consecutively from 1 to N (these rooms face the south side).

The next row (M = 2) constitutes the adjacent rooms of the first row. Rooms in row 2 are numbered by adding 10 to the room numbers of row 1, i.e., 11 to N+10.

For the third row (M = 3), rooms are numbered by adding 10 to room numbers in row 2, i.e., 21 to N+20.

At M = 4, room numbers are from 31 to N+30, etc.

For the final row, M = P, the rooms are numbered from "1+10(P-1)" to "N+10(P-1)."

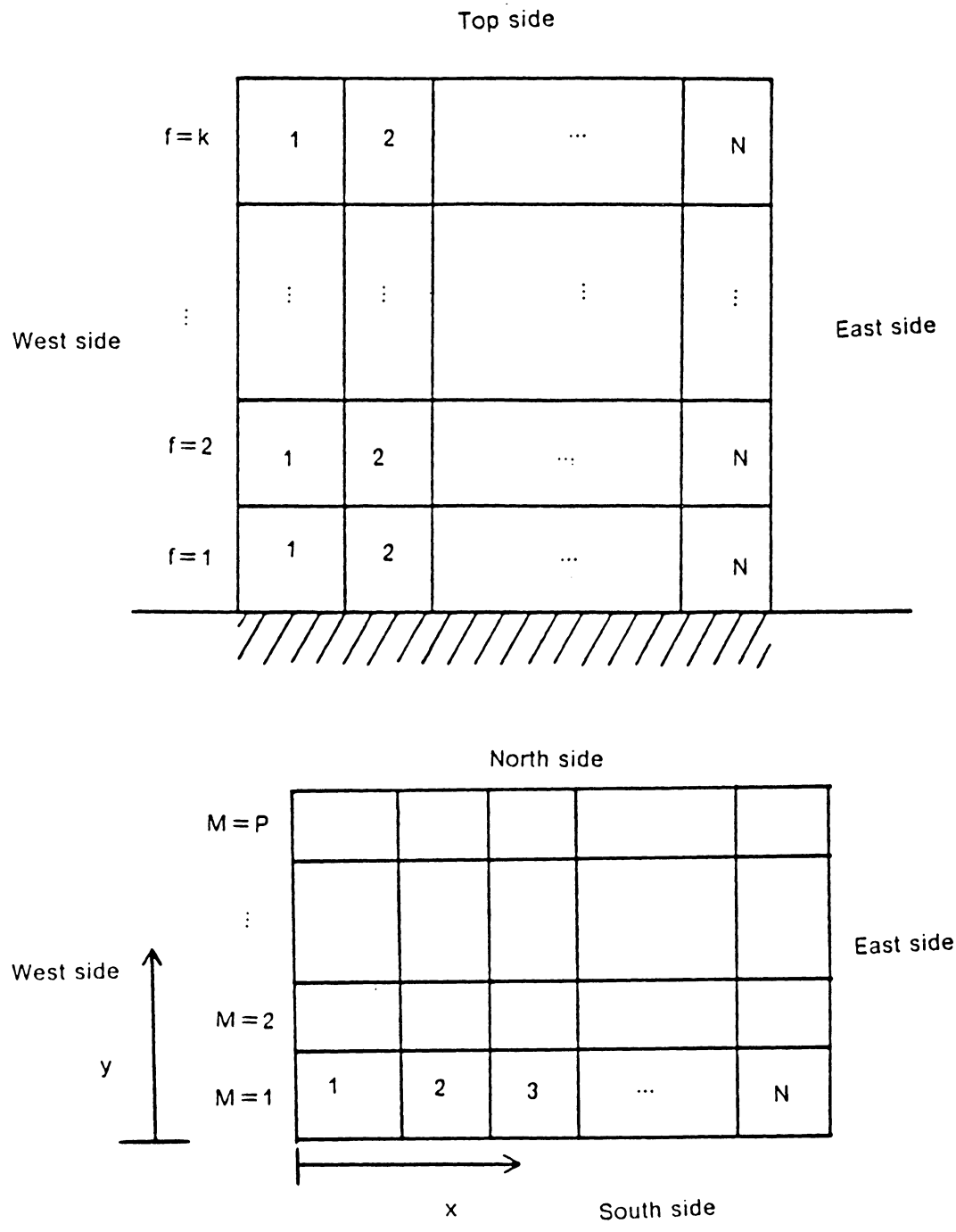

Figure 16. Numbering Scheme for the Rooms on Each Floor, N and M rooms in the x and y direction, respectively

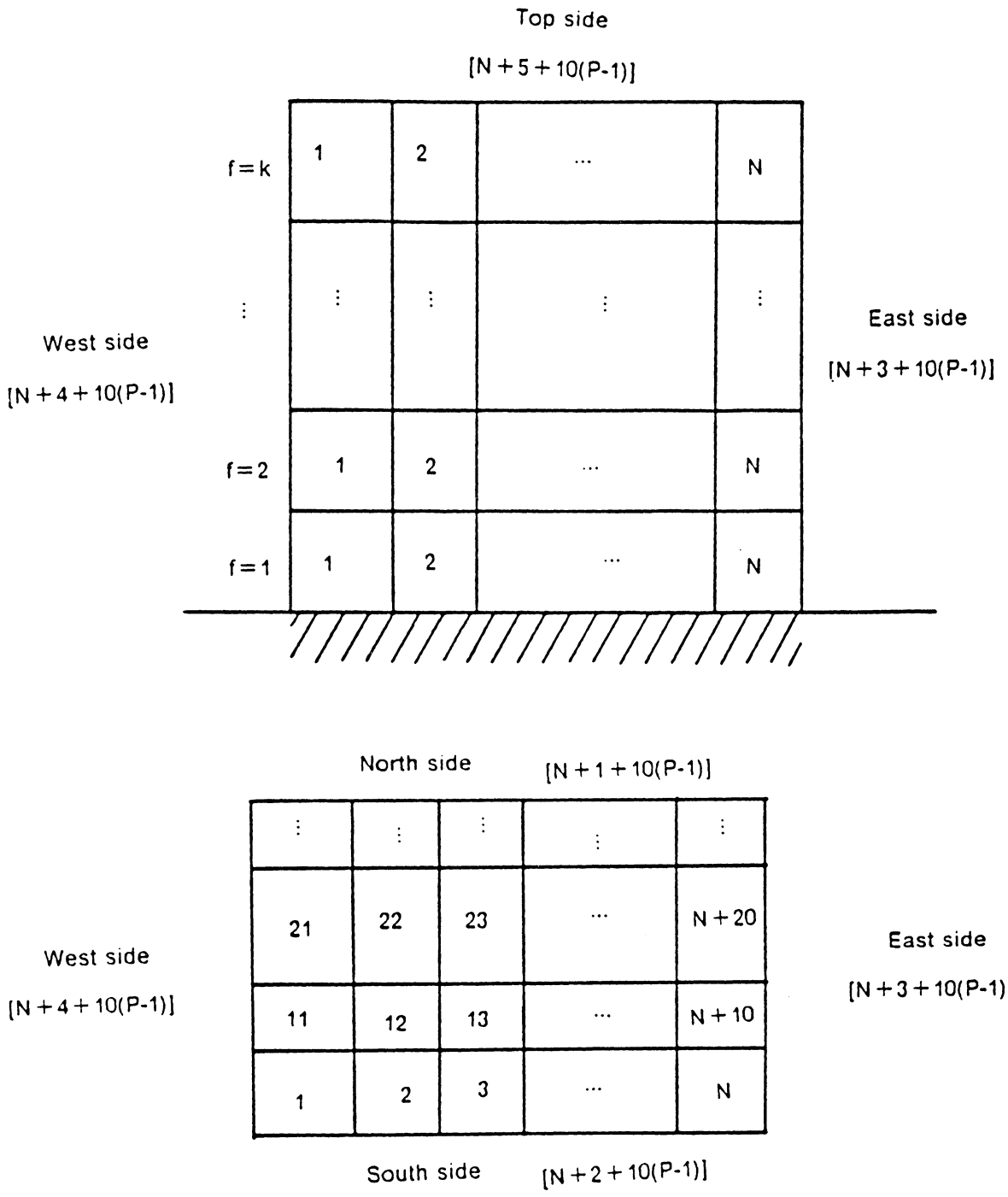

Figure 17. Numbering Scheme for the Rooms and Floors, N and M rooms in the x and y direction, respectively

A building with 40 rectangularly shaped rooms on each floor and 6 floors is used as an example. On each floor, 5 rooms in the x-direction and 8 in the y-direction are present. For the building example, N = 5 and M = 8. In row 1, the rooms are numbered from 1 to 5. In row 2, the rooms are numbered from 11 to 15. In row 3, the rooms are numbered from 21 to 25, etc. In row 8, the rooms are numbered from 71 to 78.

The north, south, east, west, and top sides of the building are assigned the following numbers:

The north side of the building is assigned "N + 10(P-1) + 1"

The south side of the building is assigned "N + 10(P-1) + 2"

The east side of the building is assigned "N + 10(P-1) + 3"

The west side of the building is assigned "N + 10(P-1) + 4"

The top side of the building is assigned "N + 10(P-1) + 5"

For the given building example, the number for the north side is 49 (8 + 10(5-1) + 1), the south side is 50 (8 + 10(5-1) + 2), the east side is 51 (8 + 10(5-1) + 3), the west side is 52 (8 + 10(5-1) + 4), and the top side is 53 (8 + 10(5-1) + 5).

The restriction on the number of rooms in the x direction is 10. The model has no limitation on to the number of rooms in the y direction. The number of rooms in the x direction could be increased by modifying the numbering scheme. For example, in order to modify the numbering scheme to account for 20 rooms in the x direction, the room numbering "1 + 10(P-1)" is increased to "1 + 20(P-1)" and "N + 10(P-1)" to "N + 20(P-1)" for each row. In essence, the analysis has no limitation to the number of rooms in the x or y direction on each floor.

Next, a fully enclosed room is analyzed and a pattern, as shown in Fig. 18, for simplifying the overall analysis is introduced. The room is assigned j and f to indicate its number and floor location, respectively. The following nomenclature is used:

$T_{r,j,f}(\tau)$ = Air temperature of room j at floor f and time τ (K)

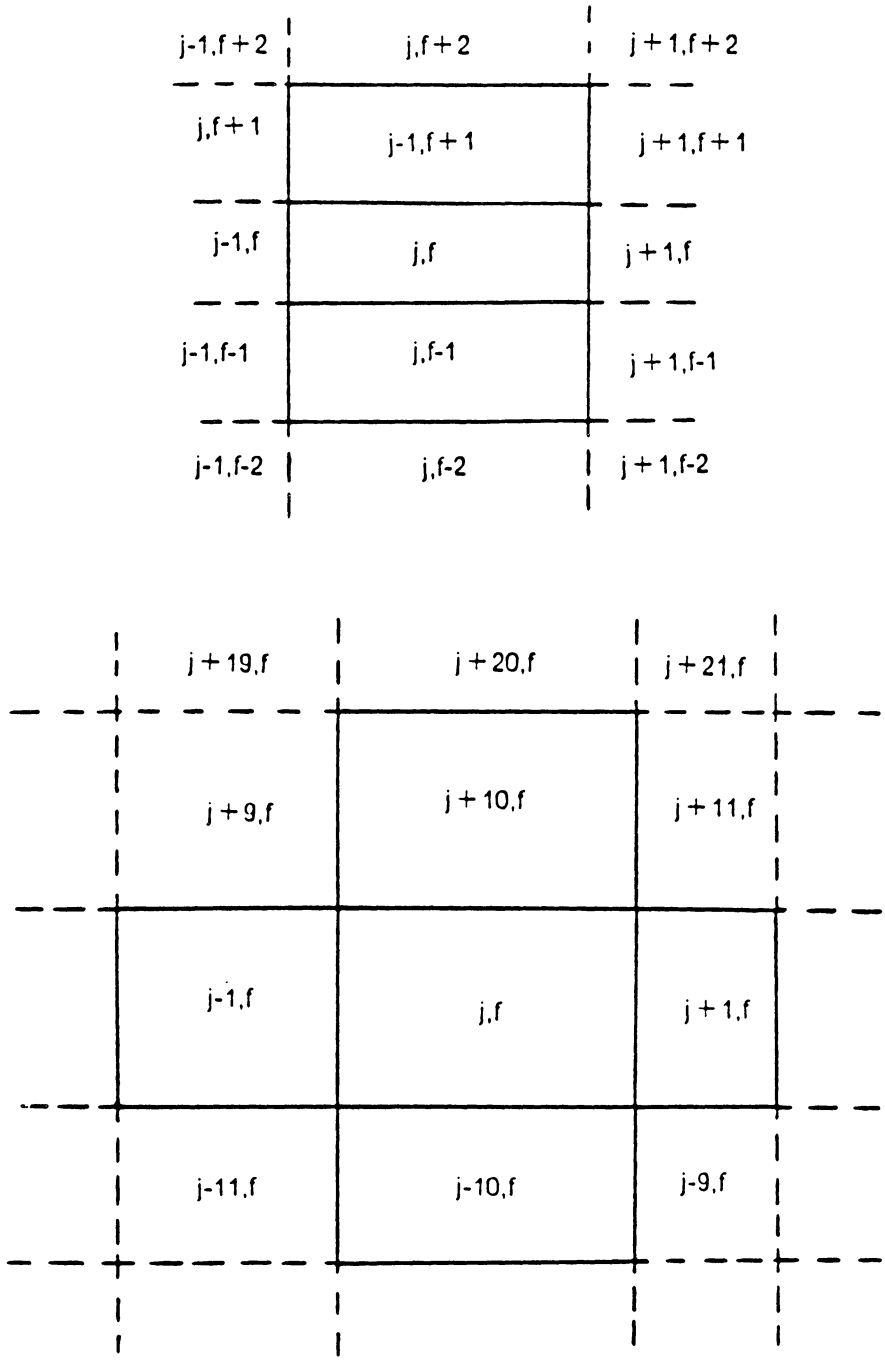

Figure 18. Interior Room Numbering

$T_{n,j,f}(\tau)$ = inside surface temperature of the north wall of room j at floor f and time τ (K)

$T_{s,j,f}(\tau)$ = inside surface temperature of the south wall of room j at floor f and time τ (K)

$T_{e,j,f}(\tau)$ = inside surface temperature of the east wall of room j at floor f and time τ (K)

$T_{w,j,f}(\tau)$ = inside surface temperature of the west wall of room j at floor f and time τ (K)

$T_{c,j,f}(\tau)$ = inside surface temperature of the ceiling of room j at floor f and time τ (K)

$T_{f,j,f}(\tau)$ = inside surface temperature of the floor of room j at floor f and time τ (K)

$q_{n,j,f}(\tau)$ = inside surface flux of the north wall of room j at floor f and time τ (W/m^2)

$q_{s,j,f}(\tau)$ = inside surface flux of the south wall of room j at floor f and time τ (W/m^2)

$q_{e,j,f}(\tau)$ = inside surface flux of the east wall of room j at floor f and time τ (W/m^2)

$q_{w,j,f}(\tau)$ = inside surface flux of the west wall of room j at floor f and time τ (W/m^2)

$q_{c,j,f}(\tau)$ = inside surface flux of the ceiling of room j at floor f and time τ (W/m^2)

$q_{f,j,f}(\tau)$ = inside surface flux of the floor of room j at floor f and time τ (W/m^2)

The numbering of layers in walls determines the inside and outside surfaces. The surface of layer 1 facing the room is the inside surface and the surface of layer n facing the opposing room is the outside surface of the wall. From the numbering scheme introduced earlier, the following pattern for a fully enclosed room is observed:

The outside surface of the north wall of room j is the inside surface of the south wall of room j+10 at the same floor level f.

The outside surface of the south wall of room j is the inside surface of the north wall of room j-10 at the same floor level f.

The outside surface of the east wall of room j is the inside surface of the west wall of room j+1 at the same floor level f.

The outside surface of the west wall of room j is the inside surface of the east wall of room j-1 at the same floor level f.

The outside surface of the ceiling of room j at floor f is the inside surface of the floor of room j at floor f+1.

The outside surface of the floor of room j at floor f is the inside surface of the ceiling of room j at floor f-1.

Obviously, there are some special cases where the room is not totally enclosed by other rooms. For the case where rooms have some walls facing the outside, the numbers issued earlier for north, south, east, west, and top side are used. Continuing the assignment of nomenclature,

$Q_{i,j,f}(\tau)$ = infiltrated load to room j at floor f and time τ, W

$Q_{h,j,f}(\tau)$ = heating load to room j at floor f and time τ, W (the sign convention is positive for the heating load and negative for the cooling load)

$Q_{g,j,f}(\tau)$ = generated load to room j at floor f and time τ, W, from lights, equipment, and/or people.

$A_{j,i,f}$ = area of the wall between room j and i at floor f (m^2)

$A_{c,j,f}$ = ceiling area of room j at floor f (m^2)

$A_{f,j,f}$ = floor area of room j at floor f (m^2)

$X_{e,j,f}(i)$, $Y_{e,j,f}(i)$, & $Z_{e,j,f}(i)$ = response factors of the east wall of room j at floor f (W/m^2K)

$C_{e,j,f}(i)$ = flux coefficient of the east wall of room j at floor f (dimensionless)

$X_{s,j,f}(i)$, $Y_{s,j,f}(i)$, & $Z_{s,j,f}(i)$ = response factors of the south wall of room j at floor f (W/m^2K)

$C_{s,j,f}(i)$ = flux coefficient of the south wall of room j at floor f (dimensionless)

Next, a general room is presented along with energy balances on the interior wall surfaces and the room air. As noted in Chapter 4, the inside and outside wall heat fluxes are calculated in terms of the surface temperatures. The inside flux is positive when pointing away from the inside wall surface and the outside heat flux is positive when pointing into the outside wall surface. For a given room j on floor f, the room on the north side is assigned j + 10, on the south side j-10, on the east side j + 1, and on the west side j-1. Also, the rooms above and below room j at floor f are j at floor f + 1 and j at floor f-1, respectively. Throughout

the analysis, the direction of interior fluxes is chosen east to west and south to north as shown in Fig. 19. The positive interior wall flux directions of room j are pointing toward the wall on the north and west side, and toward the room and away from the wall on the south and east sides. The fluxes pointing into the ceiling and toward the room from the floor are the positive directions.

The general equations for the interior wall surface temperatures are presented without detailed derivation since this analysis has been performed earlier. Since the west wall of room j is the east wall of room j-1 and the north wall of room j is the south wall of room j+10, no assignment of response factors for the north and west walls are needed. Therefore, the south and east walls of each room are assigned response factors. Performing an energy balance on the inside surface of the east wall of room j

$$q_{conv,e}(\tau) + q_{e,j,f}(\tau) = 0 \tag{5.19}$$

Similar to Eq. 5.9, the surface temperature of the east wall is

$$T_{e,j,f}(\tau) = \frac{X_{e,j,f}(1)T_m + Y_{e,j,f}(1)[T_{w,j+1,f}(\tau) - T_m] - S_{T,e} - S_{q,e} + h_{i,v}(\tau)T_{r,j,f}(\tau)}{X_{e,j,f}(1)T_m + h_{i,v}(\tau)} \tag{5.20}$$

where

$$S_{T,e} = \sum_{i=2}^{N} X_{e,j,f}(i)[T_{e,j,f}(\tau + 1 - i) - T_m] - Y_{e,j,f}(i)[T_{w,j+1,f}(\tau + 1 - i) - T_m]$$
$$S_{q,e} = \sum_{j=2}^{\ell} (-1)^j C_{e,j,f}(j - 1)q_{e,j,f}(\tau + 1 - j) \tag{5.21}$$

From an energy balance on the inside surface of the west wall of room j,

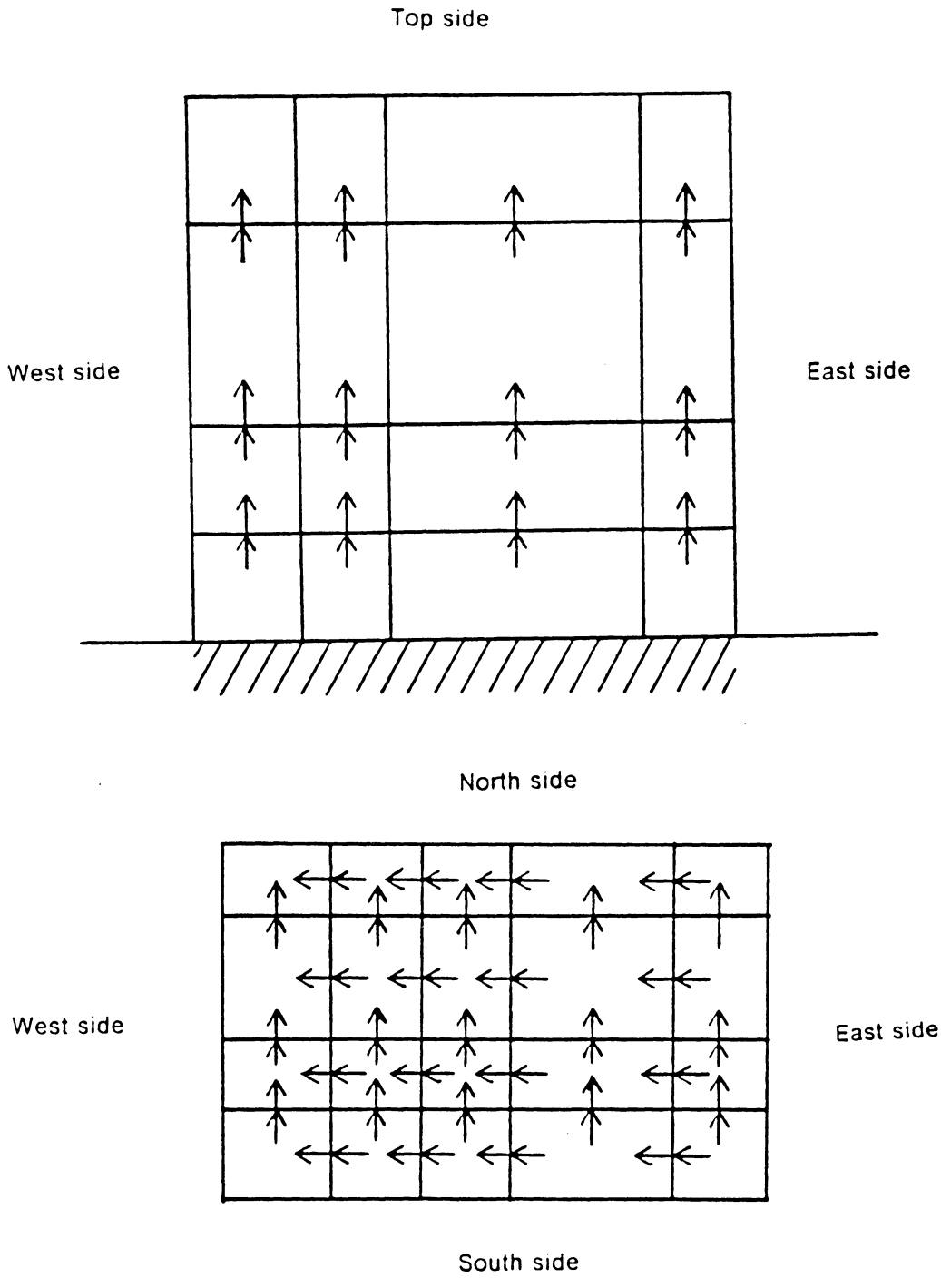

Figure 19. Interior Flux Directions Employed in the Analysis

$$q_{conv,w}(\tau) - q_{wj,f}(\tau) = 0 \tag{5.22}$$

Similarly

$$T_{wj,f}(\tau) = \frac{X_{ej-1,f}(1)T_m + Y_{ej-1,f}(1)[T_{ej-1,f}(\tau) - T_m] + S_{T,w} + S_{q,w} + h_{i,v}(\tau)T_{rj,f}(\tau)}{X_{ej-1,f}(1)T_m + h_{i,v}(\tau)} \tag{5.23}$$

where

$$S_{T,w} = \sum_{i=2}^{N} X_{ej-1,f}(i)[T_{ej-1,f}(\tau + 1 - i) - T_m] - Y_{ej-1,f}(i)[T_{wj,f}(\tau + 1 - i) - T_m] \tag{5.24}$$

$$S_{q,w} = \sum_{j=2}^{\ell} (-1)^j C_{ej-1,f}(j-1)q_{wj,f}(\tau + 1 - j)$$

Repeating the same steps for the north wall of room j

$$T_{nj,f}(\tau) = \frac{X_{sj+10,f}(1)T_m + Y_{sj+10,f}(1)[T_{sj+10,f}(\tau) - T_m] + S_{T,n} + S_{q,n} + h_{i,v}(\tau)T_{rj,f}(\tau)}{X_{sj+10,f}(1)T_m + h_{i,v}(\tau)} \tag{5.25}$$

where

$$S_{T,n} = \sum_{i=2}^{N} X_{sj+10,f}(i)[T_{sj+10,f}(\tau + 1 - i) - T_m] - Y_{sj+10,f}(i)[T_{nj,f}(\tau + 1 - i) - T_m] \tag{5.26}$$

$$S_{q,n} = \sum_{j=2}^{\ell} (-1)^j C_{sj+10,f}(j-1)q_{nj,f}(\tau + 1 - j)$$

The inside surface temperature of the south wall of room j is

$$T_{s,j,f}(\tau) = \frac{X_{s,j,f}(1)T_m + Y_{s,j,f}(1)[T_{n,j-10,f}(\tau) - T_m] - S_{T,s} - S_{q,s} + h_{i,v}(\tau)T_{r,j,f}(\tau)}{X_{s,j,f}(1)T_m + h_{i,v}(\tau)} \quad (5.27)$$

where

$$S_{T,s} = \sum_{i=2}^{N} X_{s,j,f}(i)[T_{s,j,f}(\tau + 1 - i) - T_m] - Y_{s,j,f}(i)[T_{nj-10,f}(\tau + 1 - i) - T_m] \quad (5.28)$$

$$S_{q,s} = \sum_{j=2}^{\ell} (-1)^j C_{s,j,f}(j - 1)q_{s,j,f}(\tau + 1 - j)$$

The inside surface temperature of the ceiling is treated similarly, solving for $T_{c,j,f}(\tau)$

$$T_{c,j,f}(\tau) = \frac{X_{f,j,f+1}(1)T_m + Y_{f,j,f+1}(1)[T_{f,j,f+1}(\tau) - T_m] + S_{T,c} + S_{q,c} + h_{i,h}(\tau)T_{r,j,f}(\tau)}{X_{f,j,f+1}(1)T_m + h_{i,h}(\tau)} \quad (5.29)$$

where

$$S_{T,c} = \sum_{i=2}^{N} X_{f,j,f+1}(i)[T_{f,j,f+1}(\tau + 1 - i) - T_m] - Y_{f,j,f+1}(i)[T_{cj,f}(\tau + 1 - i) - T_m] \quad (5.30)$$

$$S_{q,c} = \sum_{j=2}^{\ell} (-1)^j C_{f,j,f+1}(j - 1)q_{c,j,f}(\tau + 1 - j)$$

And the inside surface temperature of the floor of room j

$$T_{f,j,f}(\tau) = \frac{X_{f,j,f}(1)T_m + Y_{f,j,f}(1)[T_{c,j,f-1}(\tau) - T_m] - S_{T,f} - S_{q,f} + h_{i,h}(\tau)T_{r,j,f}(\tau)}{X_{f,j,f}(1)T_m + h_{i,h}(\tau)} \tag{5.31}$$

where

$$S_{T,f} = \sum_{i=2}^{N} X_{f,j,f}(i)[T_{f,j,f}(\tau + 1 - i) - T_m] - Y_{f,j,f}(i)[T_{c,j,f-1}(\tau + 1 - i) - T_m]$$

$$S_{q,f} = \sum_{j=2}^{\ell} (-1)^j C_{f,j,f}(j - 1)q_{f,j,f}(\tau + 1 - j) \tag{5.32}$$

The inside surface temperature of all walls (north, south, east, west, ceiling, and floor) has been formulated for a room j and floor f. The above formulation is used on all internal surfaces of rooms. For exterior walls or a floor slab, the equations derived earlier for these cases are used.

Interior rooms do not have direct infiltration from the outside. The rooms adjacent to the outside have exterior infiltration and, in turn, convect to the interior rooms. The infiltration model is given in Appendix E.

Convective heat transfer between rooms through large openings is calculated using an empirical equation [52]. The convective heat transfer from room $j + m$ to room j through a large opening (door, window or hallway) of width w and height h is

$$Q_{i,j+m,j,f} = 4.2\, w_{j+m} [h_{j+m} (T_{r,j,f} - T_{r,j+m,f})]^{3/2} \tag{5.33}$$

where j + m could be j + 10, j-10, j + 1, and j-1. Equation 5.33 is repeated for every interior large opening to room j. Therefore, the overall convective load to room j from the surrounding rooms through N openings is

$$Q_{i,j,f}(\tau) = \sum_{k=1}^{N} Q_{i,j+m,j,f}(\tau) \tag{5.34}$$

where, N and m are determined from the physical characteristics of the building. Equations 5.33 and 5.34 are applicable for open interior doors and windows. For closed doors and windows, a conduction heat transfer rate is calculated. The pressure distribution model is used to calculate the infiltration. For closed interior doors and windows, the overall heat transfer coefficient includes the convective heat transfer coefficient of both surfaces. Therefore, no surface temperatures of interior doors or windows are used in the analysis. The heat flux through a closed door or window between rooms j and j + m is

$$q_{k,j,f}(\tau) = U_{k,j,f} \left[T_{r,j+m,f}(\tau) - T_{r,j,f}(\tau)\right] \tag{5.35}$$

where

for k = n (north side of room j), m = 10

for k = s (south side of room j), m = -10

for k = e (east side of room j), m = 1, and

for k = w (west side of room j), m = -1

Since for a given side of room j, multiple doors or windows could be present,

$$Q_{d,w,j,f}(\tau) = \sum_{k=1}^{M} \left[q_{d,j,f}(\tau)\, A_{d,j,j+m} + q_{w,j,f}(\tau)\, A_{w,j,j+m}\right] \tag{5.36}$$

ROOM ENERGY BALANCE

After determining most of the parameters affecting the interior room temperature, an energy balance on the air is used to solve for the room temperature (Fig. 20). (Internal mass and radiation in the room are considered later.) The moisture load is not included in the analysis.

$$\begin{aligned} &q_{conv,n}(\tau)\, A_{n,j,f} + q_{conv,s}(\tau)\, A_{s,j,f} + q_{conv,e}(\tau)\, A_{e,j,f} \\ &+ q_{conv,w}(\tau)\, A_{w,j,f} + q_{conv,c}(\tau)\, A_{c,j,f} + q_{conv,f}(\tau)\, A_{f,j,f} \\ &+ Q_{d,w,j,f}(\tau) + Q_{h,j,f}(\tau) + Q_{g,j,f}(\tau) + Q_{i,j,f}(\tau) = 0 \end{aligned} \tag{5.37}$$

Substituting for the four vertical walls in the room

$$\begin{aligned} q_{conv,n}(\tau) &= h_{i,v}(\tau)\,[T_{n,j,f}(\tau) - T_{r,j,f}(\tau)] \\ q_{conv,s}(\tau) &= h_{i,v}(\tau)\,[T_{s,j,f}(\tau) - T_{r,j,f}(\tau)] \\ q_{conv,e}(\tau) &= h_{i,v}(\tau)\,[T_{e,j,f}(\tau) - T_{r,j,f}(\tau)] \\ q_{conv,w}(\tau) &= h_{i,v}(\tau)\,[T_{w,j,f}(\tau) - T_{r,j,f}(\tau)] \end{aligned} \tag{5.38}$$

and for the two horizontal walls

$$\begin{aligned} q_{conv,c}(\tau) &= h_{i,h}(\tau)\,[T_{c,j,f}(\tau) - T_{r,j,f}(\tau)] \\ q_{conv,f}(\tau) &= h_{i,h}(\tau)\,[T_{f,j,f}(\tau) - T_{r,j,f}(\tau)] \end{aligned} \tag{5.39}$$

Substituting Eqs. 5.38 and 5.39 into Eq. 5.37

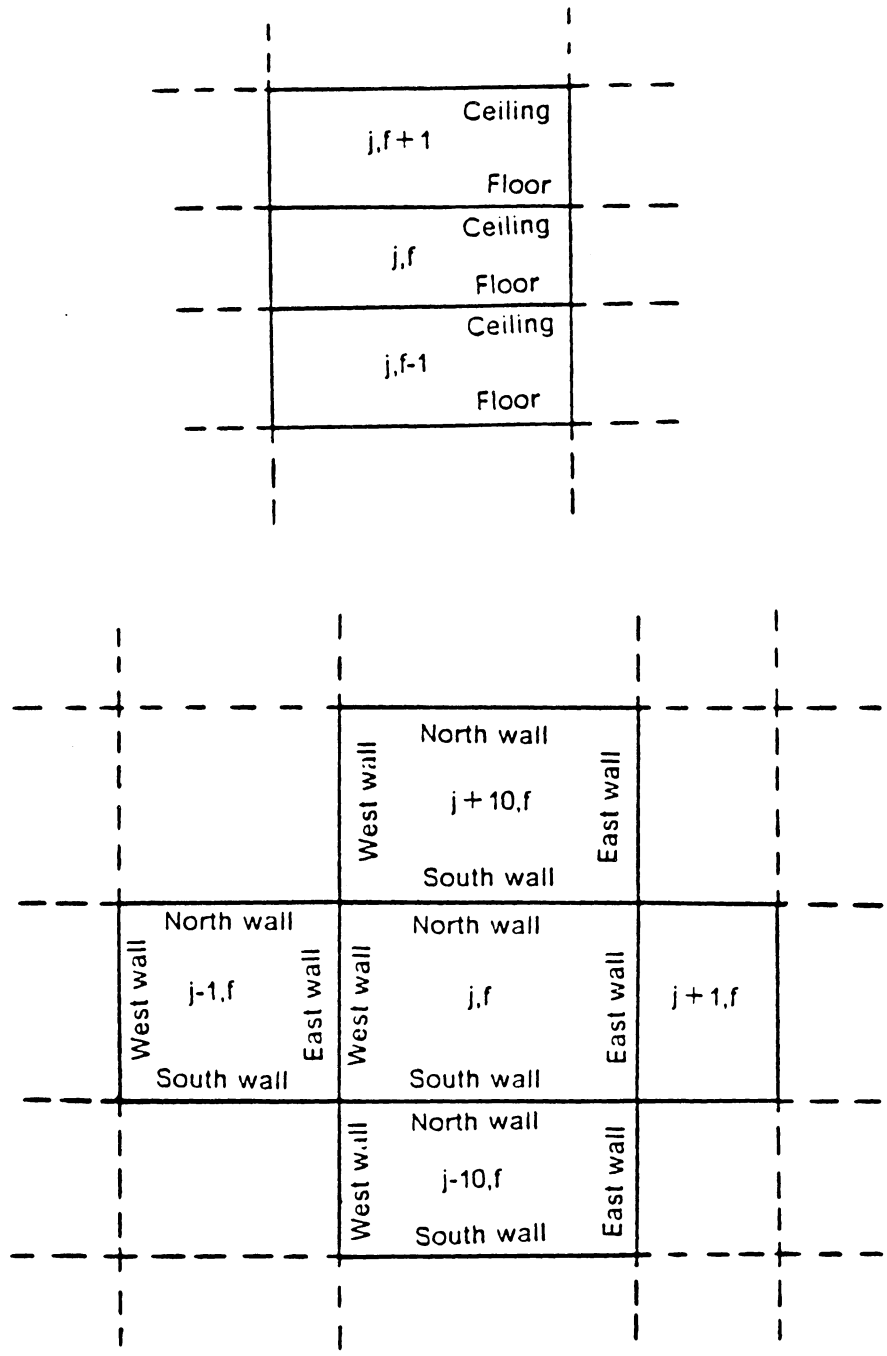

Figure 20. Nomenclature Employed in the Multizone Model

$$
\begin{aligned}
&h_{i,v}(\tau)\,[T_{n,j,f}(\tau) - T_{r,j,f}(\tau)]\,A_{n,j,f} + h_{i,v}(\tau)\,[T_{s,j,f}(\tau) - T_{r,j,f}(\tau)]\,A_{s,j,f} \\
&h_{i,v}(\tau)\,[T_{e,j,f}(\tau) - T_{r,j,f}(\tau)]\,A_{e,j,f} + h_{i,v}(\tau)\,[T_{w,j,f}(\tau) - T_{r,j,f}(\tau)]\,A_{w,j,f} \\
&h_{i,h}(\tau)\,[T_{c,j,f}(\tau) - T_{r,j,f}(\tau)]\,A_{c,j,f} + h_{i,h}(\tau)\,[T_{f,j,f}(\tau) - T_{r,j,f}(\tau)]\,A_{f,j,f} \\
&+ Q_{d,w,j,f}(\tau) + Q_{h,j,f}(\tau) + Q_{g,j,f}(\tau) + Q_{i,j,f}(\tau) = 0
\end{aligned}
\tag{5.40}
$$

Solving for the room temperature

$$
\dot{T}_{r,j,f}(\tau) = \frac{\begin{aligned}
&h_{i,v}(\tau)\,T_{n,j,f}(\tau)\,A_{n,j,f} + h_{i,v}(\tau)\,T_{s,j,f}(\tau)\,A_{s,j,f} \\
&+ h_{i,v}(\tau)\,T_{e,j,f}(\tau)\,A_{e,j,f} + h_{i,h}(\tau)\,T_{f,j,f}(\tau)\,A_{f,j,f} \\
&+ h_{i,v}(\tau)\,T_{w,j,f}(\tau)\,A_{w,j,f} + h_{i,h}(\tau)\,T_{c,j,f}(\tau)\,A_{c,j,f} \\
&+ Q_{d,w,j,f}(\tau) + Q_{h,j,f}(\tau) + Q_{g,j,f}(\tau) + Q_{i,j,f}(\tau)
\end{aligned}}{\begin{aligned}
&h_{i,v}(\tau)\,A_{n,j,f} + h_{i,v}(\tau)\,A_{s,j,f}\,h_{i,v}(\tau)\,A_{e,j,f} \\
&+ h_{i,v}(\tau)\,A_{w,j,f} + h_{i,h}(\tau)\,A_{c,j,f} + h_{i,h}(\tau)\,A_{f,j,f}
\end{aligned}}
\tag{5.41}
$$

or

$$
T_{r,j,f}(\tau) = \frac{S_{h,T,A}(\tau) + Q_{d,w,j,f}(\tau) + Q_{h,j,f}(\tau) + Q_{g,j,f}(\tau) + Q_{i,j,f}(\tau)}{S_{h,A}(\tau)}
\tag{5.42}
$$

where

$$
S_{h,T,A}(\tau) = \begin{aligned}
&h_{i,v}(\tau)\,T_{n,j,f}(\tau)\,A_{n,j,f} + h_{i,v}(\tau)\,T_{s,j,f}(\tau)\,A_{s,j,f} \\
&h_{i,v}(\tau)\,T_{w,j,f}(\tau)\,A_{w,j,f} + h_{i,h}(\tau)\,T_{c,j,f}(\tau)\,A_{c,j,f} \\
&+ h_{i,h}(\tau)\,T_{f,j,f}(\tau)\,A_{f,j,f} + h_{i,v}(\tau)\,T_{e,j,f}(\tau)\,A_{e,j,f}
\end{aligned}
\tag{5.43}
$$

and

$$S_{h,A}(\tau) = \begin{matrix} h_{i,v}(\tau)\, A_{n,j,f} + h_{i,v}(\tau)\, A_{s,j,f} + h_{i,v}(\tau)\, A_{e,j,f} \\ + h_{i,v}(\tau)\, A_{w,j,f} + h_{i,h}(\tau)\, A_{c,j,f} + h_{i,h}(\tau)\, A_{f,j,f} \end{matrix} \quad (5.44)$$

Recapping, the solar load on all four walls and roof (flat or pitched) is calculated in terms of the location, time, surface position, and tilt angles. The transmittance and absorptance of single- and double-pane windows are determined for various extinction coefficients. The infiltration is formulated to calculate the individual room heat loss or gain to or from the surroundings. Also, the surface temperature of walls, floor slab, roof, windows, and doors was formulated. Finally, a general model for the inside room air temperature was presented.

The interior surface temperature equations are in terms of the wall response factors and other parameters. In rooms with walls exposed to the outside or a floor slab, the corresponding response factors are used in these equations. Even though walls may be different along with their response factors, the energy balances performed earlier still hold and are therefore used. Next, the calculation methodology is presented.

MULTIZONE ANALYSIS IN BUILDINGS

The iterative procedure employed to solve for the room temperatures is as follows:

1. At the first calculation for each time step, step A is used. For the iterations, at the same time step, step B is used.

A - A value for all the unknown temperatures is assumed. For $\tau > 0$, the previous values are assumed. For $\tau = 0$, all temperatures are set constant. Step B is skipped.

B - All the unknown temperatures are assumed equal to their corresponding values from the previous iteration.

2. The outside surface temperature of walls, windows, doors, and the roof of the building are calculated. Localized iterations are used to solve the nonlinear temperature equations.

3. The inside surface temperature of walls, ceilings, and floors in the building are calculated. Iteration is not required.

4. The inside air temperature of all rooms in the building is determined.

5. Values from step 4 are compared to step 1.B. If the agreement is within a 0.05 C convergence criterion, the iteration is stopped. If the difference is large, convergence has not been attained and steps 1.B through 5 are repeated.

Two distinct iterations, an overall and several internal (localized) iterations, are applied in every time step. The overall iteration covers steps 1 through 5. The internal iterations are used to determine the outside surface temperatures of walls and windows discussed in step 2.

IMAGINARY WALLS

The assumption of having the same number of rooms with the same dimensions located above each other was introduced earlier in order to facilitate the analysis. The limitation resulting from this restriction is that very few buildings could be modelled correctly. By introducing so-called "imaginary walls," large rooms are partitioned to increase the flexibility of the simulation.

In the computer code, needed imaginary walls are specified along with their locations. Each imaginary wall is designated "i, j, and f" where the wall is between rooms i and j and f is the floor location. Therefore, rooms i and j are actually one room. With this modification, different shaped zones can exist on different floors. As long as these large rooms are partitioned to have the same size and location on different floors, the requirements of the model are met. As long as these walls are not included in the calculations and the rooms separated by these walls are considered in the analysis as one room, the physical characteristics of the building have not been compromised. An important advantage is obtained. The effect of

small rooms on larger adjacent rooms can be readily studied. By partitioning large rooms, whether on the same floor or above each other, each side of the room would have surface temperatures equalling the adjacent rooms. The surface temperatures on each side of the room are taken into consideration in the room energy balance.

U-SHAPED BUILDINGS

It is impractical to modify the analysis to account for all existing shapes of buildings. If the need for analyses of a specific building arises, it is possible to modify the current formulations. The modification to analyze U-shaped buildings is presented next. U-shaped structures are rectangular structures less a block of rooms on one side. The rooms needed to be omitted from the rectangular shape in order to obtain the desired U-shape are identified and are not included in the calculations.

A U-shaped building could be facing north, south, east, west, or any other direction. The difference between a U-shaped building toward the north or south is the solar load. All other boundary conditions are the same. By performing the analysis on one side only, the modification is performed once. The south side is chosen as the U-shape side in the current analysis. If the U-shaped building is facing the east side, for example, the solar load on the south side is replaced by the east side solar load and the remaining sides are assigned the new solar loads. The analysis is conducted once and the solar load is rotated to fit the physical characteristics of the building.

For every specified imaginary room, all calculations related to that room are skipped. Rooms adjacent to imaginary rooms are exposed to the outside, i.e., nonlinear boundary conditions are present on their exterior surfaces.

HOUSES

The number of houses exceeds by far the number of buildings present in any surrounding. Detailed energy calculations using transient methods have proven to be beneficial and necessary in large commercial buildings. Houses, on the other hand, are sometimes tedious to simulate. The problem originates from lack of knowledge of the parameters needed in the calculations. In many instances doors and windows are left open and infiltration accounts for large percentage of the total energy loss from the house. Not all houses, however, fit in the category discribed above. Many houses are well controlled and insulated. Transient methods could be useful in the process of determining the energy requirements of these houses.

Infiltration in houses varies greatly from one structure to another. The stack effect is negligible and the interior static pressure does not vary significantly from room to room. Therefore, the LBL infiltration model described in Chapter 4 is implemented. The mathematical formulation of the interior and exterior surface temperatures presented earlier in this chapter are used.

Pitched roof attics in houses are common in the United States. Therefore, a modification of the computer code to handle attics and pitched roofs is needed. The solar load on the pitched roof is calculated using the same procedure presented in Appendix D. The interior floor of the attic is subdivided to equal the number of rooms below. The attic sides exposed to the outside are treated similarly to outside walls and roofs implemented earlier.

The attic floor is subdivided into sections equalling the number of rooms below it. The inside surface temperatures of these sections is obtained by performing energy balances on the surface of each section. Performing an energy balance on section j of the inside surface floor of the attic and solving for that surface temperature

$$T_{a,j}(\tau) = \frac{X_a(1)T_m + Y_a(1)[T_{c,j,k}(\tau) - T_m] - S_{T,a,j} - S_{q,a,j} + h_{i,h}(\tau)T_a(\tau)}{X_a(1)T_m + h_{i,h}(\tau)} \tag{5.45}$$

where

$$\begin{aligned} S_{T,a,j} &= \sum_{i=2}^{N} X_a(i)[T_{a,j}(\tau + 1 - i) - T_m] - Y_a(i)[T_{c,j,k}(\tau + 1 - i) - T_m] \\ S_{q,a,j} &= \sum_{j=2}^{\ell} (-1)^j C_a(j-1) q_{a,j}(\tau + 1 - j) \end{aligned} \tag{5.46}$$

After calculating all interior surface temperatures, an energy balance is performed on the attic air

$$\sum_{k=1}^{4} q_{conv,k}(\tau)\, A_k + \sum_{j=1}^{N} q_{conv,j}(\tau)\, A_j + Q_{i,a}(\tau) = 0 \tag{5.47}$$

The convective fluxes from the walls of the attic are

$$\begin{aligned} q_{conv,k}(\tau) &= h_{i,k}(\tau)\,[T_{1,k}(\tau) - T_a(\tau)] \\ q_{conv,j}(\tau) &= h_{i,h}(\tau)\,[T_{a,j}(\tau) - T_a(\tau)] \end{aligned} \tag{5.48}$$

Substituting Eq. 5.48 into Eq. 5.47 and solving for the attic air temperature

$$T_a(\tau) = \frac{\sum_{k=1}^{4} h_{i,k}\, T_{1,k}(\tau)\, A_k + \sum_{j=1}^{N} h_{i,h}(\tau)\, T_{a,j}(\tau)\, A_j + Q_{i,j,f}(\tau)}{\sum_{k=1}^{4} h_{i,k}\, A_k + \sum_{j=1}^{N} h_{i,h}\, A_j} \tag{5.49}$$

The attic temperature is calculated at every iteration and compared to the previous value for convergence. Infiltration from the outside to the attic is calculated using the LBL model. Infiltration through the attic floor to the rooms is neglected. Radiation between the interior surfaces of the attic is neglected.

HEATING AND COOLING LOADS

Most HVAC calculations are performed to determine the heating and cooling loads for a structure under set interior temperature. The current analysis is modified to determine the heating or cooling load of structures. An energy balance on the room air is performed and the heating or cooling load is solved instead of the room temperature. The equations for the surface temperatures, infiltration, generation, and the numbering scheme introduced earlier are valid. Rewriting the energy balance equation on the room air

$$\begin{aligned} &h_{i,v}(\tau)\left[T_{n,j,f}(\tau) - T_{r,j,f}(\tau)\right] A_{n,j,f} + h_{i,v}(\tau)\left[T_{s,j,f}(\tau) - T_{r,j,f}(\tau)\right] A_{s,j,f} \\ &h_{i,v}(\tau)\left[T_{e,j,f}(\tau) - T_{r,j,f}(\tau)\right] A_{e,j,f} + h_{i,v}(\tau)\left[T_{w,j,f}(\tau) - T_{r,j,f}(\tau)\right] A_{w,j,f} \\ &h_{i,h}(\tau)\left[T_{c,j,f}(\tau) - T_{r,j,f}(\tau)\right] A_{c,j,f} + h_{i,h}(\tau)\left[T_{f,j,f}(\tau) - T_{r,j,f}(\tau)\right] A_{f,j,f} \\ &+ Q_{d,w,j,f}(\tau) + Q_{h,j,f}(\tau) + Q_{g,j,f}(\tau) + Q_{i,j,f}(\tau) = 0 \end{aligned} \tag{5.50}$$

Solving for $Q_{h,j,f}(\tau)$

$$\begin{aligned} Q_{h,j,f}(\tau) = {} & h_{i,v}(\tau)\left[T_{r,j,f}(\tau) - T_{n,j,f}(\tau)\right] A_{n,j,f} + h_{i,v}(\tau)\left[T_{r,j,f}(\tau) - T_{s,j,f}(\tau)\right] A_{s,j,f} \\ & h_{i,v}(\tau)\left[T_{r,j,f}(\tau) - T_{e,j,f}(\tau)\right] A_{e,j,f} + h_{i,v}(\tau)\left[T_{r,j,f}(\tau) - T_{w,j,f}(\tau)\right] A_{w,j,f} \\ & h_{i,h}(\tau)\left[T_{r,j,f}(\tau) - T_{c,j,f}(\tau)\right] A_{c,j,f} + h_{i,h}(\tau)\left[T_{r,j,f}(\tau) - T_{f,j,f}(\tau)\right] A_{f,j,f} \\ & - Q_{d,w,j,f}(\tau) - Q_{g,j,f}(\tau) - Q_{i,j,f}(\tau) \end{aligned} \tag{5.51}$$

The inside and outside surface temperatures are determined as before and the above equation is used to calculate the heating or cooling load. When $Q_{hj,r}(\tau)$ is positive, it is the heating load and when negative, it is the cooling load.

INTERNAL RADIATION IN ROOMS

Equations for the interior room temperature and heating load have been formulated neglecting the effects of furnishings and internal radiation between the walls in the rooms. It could be argued that these two assumptions would alter the result significantly. Indeed, most of the available computer codes (NBSLD, TARP, DOE-2, BLAST-2, TRACE, etc.) consider radiation between interior walls.

The mean radiative temperature (MRT) method is widely used for calculating the configuration (view) factors between interior rooms. Walton [98] introduced the MRT/Balance Method. He calculated configuration factors for interior walls in rooms based on their emissivities and area ratios. Carroll [99 and 100] modified the above method by introducing the MRT/Network method.

The radiation heat transfer between two surfaces i and j enclosed in a room is

$$Q_{ij} = \sigma A_i F_{ij} (T_i^4 - T_j^4) \tag{5.52}$$

where A_i is the surface area of wall i, F_{ij} is the view factor of wall j by wall i, and T_i and T_j are the absolute surface temperatures of wall i and j, respectively. Recalling the reciprocity relations for radiation heat transfer,

$$A_i F_{ij} = A_j F_{ji} \tag{5.53}$$

and for wall surface i enclosed by the other walls in the room

$$\sum_{j=1}^{6} F_{ij} = 1 \tag{5.54}$$

Noting that for a given flat wall i

$$F_{ii} = 0 \tag{5.55}$$

The approximation in the MRT method is in the determination of the view factors F_{ij}. The MRT method is presented in Appendix F. Equation 5.52 is used to determine the radiation heat flux between surfaces i and j. A linearization of that equation is used in order to facilitate the formulation and calculation process. Equation 5.52 is linearized

$$Q_{ij} = 4 \sigma A_i F'_{ij} \bar{T}^3 (T_i - T_j) \tag{5.56}$$

where $\bar{T}$ is the average absolute temperature of surfaces i and j. Carroll [99 and 100] showed that this linearization introduce negligible error into typical HVAC calculations. The overall infrared radiation heat transfer from all surfaces in the room to surface i is

$$Q_r(\tau) = \sum_{j \neq i}^{6} Q_{ij}(\tau) = \sum_{j \neq i}^{6} 4 \sigma A_i F'_{ij} \bar{T}^3 (T_i(\tau) - T_j(\tau)) \tag{5.57}$$

Equations 5.42 and 5.51 apply for determining the room temperature and the heating or cooling loads, respectively. The modifications are to the interior surface energy balances. Rewriting the energy balance equation on the interior surface of the east wall of room j and including radiation between the interior walls

$$Q_{conv,e}(\tau) + Q_{e,j,f}(\tau) + Q_{r,e}(\tau) = 0 \tag{5.58}$$

Solving for the surface temperature of the east wall,

$$T_{e,j,f}(\tau) = \frac{\begin{array}{l} A_e X_{e,j,f}(1) T_m + A_e Y_{e,j,f}(1)[T_{w,j+1,f}(\tau) - T_m] \\ - A_e S_{T,e} - A_e S_{q,e} + A_e h_{i,v}(\tau) T_{r,j,f}(\tau) + \sum_{j \neq e}^{6} 4\sigma A_e F'_{ej} \bar{T}^3 T_j(\tau) \end{array}}{A_e X_{e,j,f}(1) T_m + A_e h_{i,v}(\tau) + \sum_{j \neq e}^{6} 4\sigma A_e F'_{ej} \bar{T}^3} \quad (5.59)$$

where $S_{T,e}$ *and* $S_{q,e}$ are given in Eq. 5.21. Performing an energy balance on the inside surface of the west wall of room j

$$Q_{conv,w}(\tau) - Q_{w,j,f}(\tau) + Q_{r,e}(\tau) = 0 \quad (5.60)$$

Similarly to Eq. 5.23,

$$T_{w,j,f}(\tau) = \frac{\begin{array}{l} A_w X_{e,j-1,f}(1) T_m + A_w Y_{e,j-1,f}(1)[T_{e,j-1,f}(\tau) - T_m] \\ + A_w S_{T,w} + A_w S_{q,w} + A_w h_{i,v}(\tau) T_{r,j,f}(\tau) + \sum_{j \neq w}^{6} 4\sigma A_w F'_{wj} \bar{T}^3 T_j(\tau) \end{array}}{A_w X_{e,j-1,f}(1) T_m + A_w h_{i,v}(\tau) + \sum_{j \neq w}^{6} 4\sigma A_w F'_{wj} \bar{T}^3} \quad (5.61)$$

where $S_{T,w}$ *and* $S_{q,w}$ are given in Eq. 5.24. Performing an energy balance on the inside surface of the north wall of room j and solving for that surface temperature

$$T_{n,j,f}(\tau) = \frac{\begin{array}{l} A_n X_{s,j+10,f}(1) T_m + A_n Y_{s,j+10,f}(1)[T_{s,j+10,f}(\tau) - A_n T_m] \\ + A_n S_{T,n} + A_n S_{q,n} + A_n h_{i,v}(\tau) T_{r,j,f}(\tau) + \sum_{j \neq n}^{6} 4\sigma A_n F'_{nj} \bar{T}^3 T_j(\tau) \end{array}}{A_n X_{s,j+10,f}(1) T_m + A_n h_{i,v}(\tau) + \sum_{j \neq n}^{6} 4\sigma A_n F'_{nj} \bar{T}^3} \quad (5.62)$$

where $S_{T,n}$ *and* $S_{q,n}$ are given in Eq. 5.26. Similarly, the inside surface temperature of the south wall of room j is

$$T_{s,j,f}(\tau) = \frac{\begin{array}{l} A_s X_{s,j,f}(1) T_m + A_s Y_{s,j,f}(1)[T_{n,j-10,f}(\tau) - T_m] \\ - A_s S_{T,s} - A_s S_{q,s} + A_s h_{i,v}(\tau) T_{r,j,f}(\tau) + \sum_{j \neq s}^{6} 4\sigma A_s F'_{sj} \bar{T}^3 T_j(\tau) \end{array}}{A_s X_{s,j,f}(1) T_m + A_s h_{i,v}(\tau) + \sum_{j \neq s}^{6} 4\sigma A_s F'_{sj} \bar{T}^3} \quad (5.63)$$

where $S_{T,s}$ *and* $S_{q,s}$ are given in Eq. 5.28. Performing the energy balance on the interior surface of the ceiling and solving for $T_{c,j,f}(\tau)$

$$T_{c,j,f}(\tau) = \frac{\begin{array}{l} A_c X_{f,j,f+1}(1) T_m + A_c Y_{f,j,f+1}(1)[T_{f,j,f+1}(\tau) - T_m] \\ + A_c S_{T,c} + A_c S_{q,c} + A_c h_{i,h}(\tau) T_{r,j,f}(\tau) + \sum_{j \neq c}^{6} 4\sigma A_c F'_{cj} \bar{T}^3 T_j(\tau) \end{array}}{A_c X_{f,j,f+1}(1) T_m + A_c h_{i,h}(\tau) + \sum_{j \neq c}^{6} 4\sigma A_c F'_{cj} \bar{T}^3} \quad (5.64)$$

where $S_{T,c}$ *and* $S_{q,c}$ are given in Eq. 5.30. Similarly, the inside surface temperature of the floor of room j is

$$T_{f,j,f}(\tau) = \frac{\begin{array}{l} A_f X_{f,j,f}(1) T_m + A_f Y_{f,j,f}(1)[T_{c,j,f-1}(\tau) - T_m] \\ - A_f S_{T,f} - A_f S_{q,f} + A_f h_{i,h}(\tau) T_{r,j,f}(\tau) + \sum_{j \neq f}^{6} 4\sigma A_f F'_{fj} \bar{T}^3 T_j(\tau) \end{array}}{A_f X_{f,j,f}(1) T_m + A_f h_{i,h}(\tau) + \sum_{j \neq f}^{6} 4\sigma A_f F'_{fj} \bar{T}^3} \quad (5.65)$$

where $S_{T,f}$ *and* $S_{q,f}$ are given in Eq. 5.32

INTERNAL MASS (FURNISHINGS) IN THE ROOM

The effect of internal mass in rooms is negligible if the rooms are lightly furnished. Many buildings, however, contain large furnishings inside each room. Examples of such buildings are libraries, institutional and office type buildings, etc. A modification is introduced to account for furnishings in rooms. All internal furnishings are assumed to be at the temperature of the room. Therefore, furnishings can be included in the energy balance on the room air as storage capacity. Performing an energy balance on the room air and including the internal mass,

$$\begin{array}{l} h_{i,v}(\tau)\,[T_{n,j,f}(\tau) - T_{r,j,f}(\tau)]\,A_{n,j,f} + h_{i,v}(\tau)\,[T_{s,j,f}(\tau) - T_{r,j,f}(\tau)]\,A_{s,j,f} \\ h_{i,v}(\tau)\,[T_{e,j,f}(\tau) - T_{r,j,f}(\tau)]\,A_{e,j,f} + h_{i,v}(\tau)\,[T_{w,j,f}(\tau) - T_{r,j,f}(\tau)]\,A_{w,j,f} \\ h_{i,h}(\tau)\,[T_{c,j,f}(\tau) - T_{r,j,f}(\tau)]\,A_{c,j,f} + h_{i,h}(\tau)\,[T_{f,j,f}(\tau) - T_{r,j,f}(\tau)]\,A_{f,j,f} \\ + Q_{d,w,j,f}(\tau) + Q_{h,j,f}(\tau) + Q_{g,j,f}(\tau) + Q_{i,j,f}(\tau) = M\,C_p \dfrac{T_{r,j,f}(\tau) - T_{r,j,f}(\tau - 1)}{60} \end{array} \quad (5.66)$$

Solving for the room temperature

$$T_{r,j,f}(\tau) = \frac{\begin{array}{l} h_{i,v}(\tau)\, T_{n,j,f}(\tau)\, A_{n,j,f} + + Q_{h,j,f}(\tau) h_{i,v}(\tau)\, T_{s,j,f}(\tau)\, A_{s,j,f} \\ + h_{i,v}(\tau)\, T_{e,j,f}(\tau)\, A_{e,j,f} + + Q_{g,j,f}(\tau) h_{i,h}(\tau)\, T_{f,j,f}(\tau)\, A_{f,j,f} \\ + h_{i,v}(\tau)\, T_{w,j,f}(\tau)\, A_{w,j,f} + + Q_{i,j,f}(\tau) h_{i,h}(\tau)\, T_{c,j,f}(\tau)\, A_{c,j,f} \\ + Q_{d,w,j,f}(\tau) + \left(\frac{M\, C_p}{60}\right)_{j,f} T_{r,j,f}(\tau - 1) \end{array}}{\begin{array}{l} h_{i,v}(\tau)\, A_{n,j,f} + h_{i,v}(\tau)\, A_{s,j,f} + h_{i,v}(\tau)\, A_{e,j,f} \\ + h_{i,v}(\tau)\, A_{w,j,f} + \dfrac{(M\, C_p)_{j,f}}{60} + h_{i,h}(\tau)\, A_{c,j,f} + h_{i,h}(\tau)\, A_{f,j,f} \end{array}} \qquad (5.67)$$

Solving for the heating or cooling load

$$\begin{aligned} Q_{h,j,f}(\tau) = {} & h_{i,v}(\tau)\left[T_{r,j,f}(\tau) - T_{n,j,f}(\tau)\right] A_{n,j,f} + h_{i,v}(\tau)\left[T_{r,j,f}(\tau) - T_{s,j,f}(\tau)\right] A_{s,j,f} \\ & h_{i,v}(\tau)\left[T_{r,j,f}(\tau) - T_{e,j,f}(\tau)\right] A_{e,j,f} + h_{i,v}(\tau)\left[T_{r,j,f}(\tau) - T_{w,j,f}(\tau)\right] A_{w,j,f} \\ & h_{i,h}(\tau)\left[T_{r,j,f}(\tau) - T_{c,j,f}(\tau)\right] A_{c,j,f} + h_{i,h}(\tau)\left[T_{r,j,f}(\tau) - T_{f,j,f}(\tau)\right] A_{f,j,f} \\ & - Q_{d,w,j,f}(\tau) - Q_{g,j,f}(\tau) - Q_{i,j,f}(\tau) \\ & - \frac{(MC_p)_{j,f}}{60}\left[T_{r,j,f}(\tau) - T_{r,j,f}(\tau - 1)\right] \end{aligned} \qquad (5.68)$$

VALIDATION OF THE MULTIZONE MODEL

An important stage in the work was to validate the mathematical model and the supporting code. Experimental data and numerical results were presented by Kusuda, et al. [82] for a test house in Houston, TX. Measured interior temperatures, solar loads, cooling loads, and attic temperatures were reported for September 1 through 3. Also, the solar loads, cooling loads, and attic temperatures were calculated using the NBSLD, BLAST-2, and DOE-2 com-

puter codes. This information provided a basis for validating the present work with measured data and calculated results.

The Houston test house experimental study was carried out during the summer of 1977 under the joint sponsorship of the Department of Energy and the National Bureau of Standards to study ventilation in residences and attics as energy conservation measures [82]. A 31.25 MJ (2.1-ton) central air-conditioning system, located in the center of the house, was used.

For the present simulations of the Houston test house, four rooms, a garage space, and an attic were differentiated in the model. The floor plan of the Houston test house is shown in Fig. 21. Two different types of simulations were conducted to compare the present with previous analyses. The first simulation consisted of setting the inside temperature of all rooms to 24.4 C (76 F), given in Kusuda et al. [82] as the inside set temperature, and calculating the cooling load required to maintain this set temperature for three consecutive days. The measured outside air temperature was used in the calculations. During three consecutive days of measurements (Sept. 3-5), the daily solar and outside temperature profiles repeated closely, allowing the use of the same daily profiles in the simulations. The measured outside, inside, and attic temperatures [82] used repetitively for the three days are plotted in Fig. 22.

The solar profile was calculated using the present model and compared with measured and calculated profiles, using the BLAST-2 and DOE-2 programs. The results are shown in Fig. 23. The actual solar profile was predicted well by all three codes. The response factors based on a one-hour time step were calculated and used throughout the analysis. The wall construction materials are listed in Table 13.

Infiltration was calculated using the pressure distribution model discussed in Appendix E. The first two days established the required history of temperatures and heat fluxes, which is essential in the TRFM. The comparisons are based on results from the third (last) day. Only the total sensible cooling load and overall interior temperature are given by Kusuda et

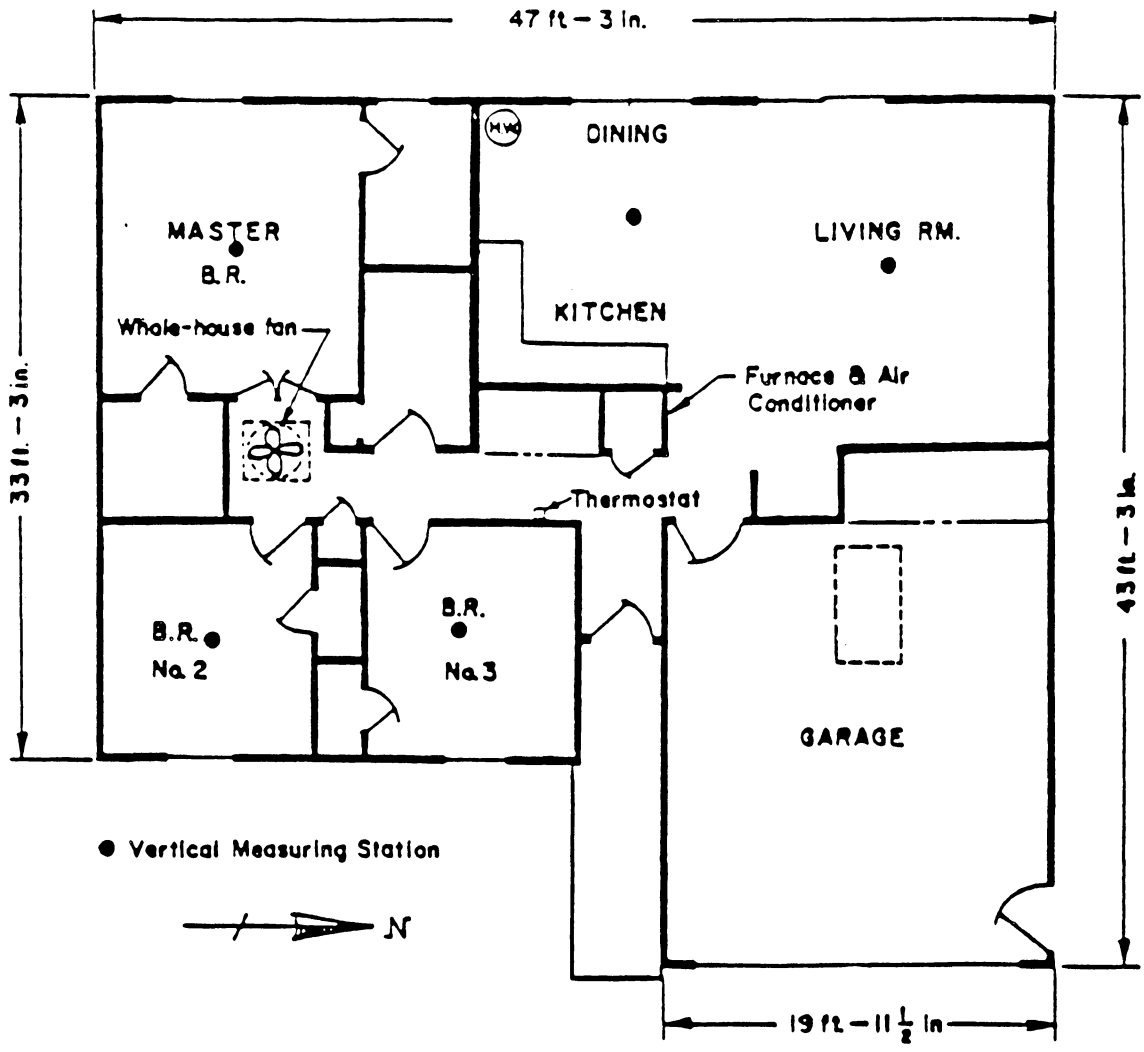

Figure 21. Floor Plan of the Houston Test House

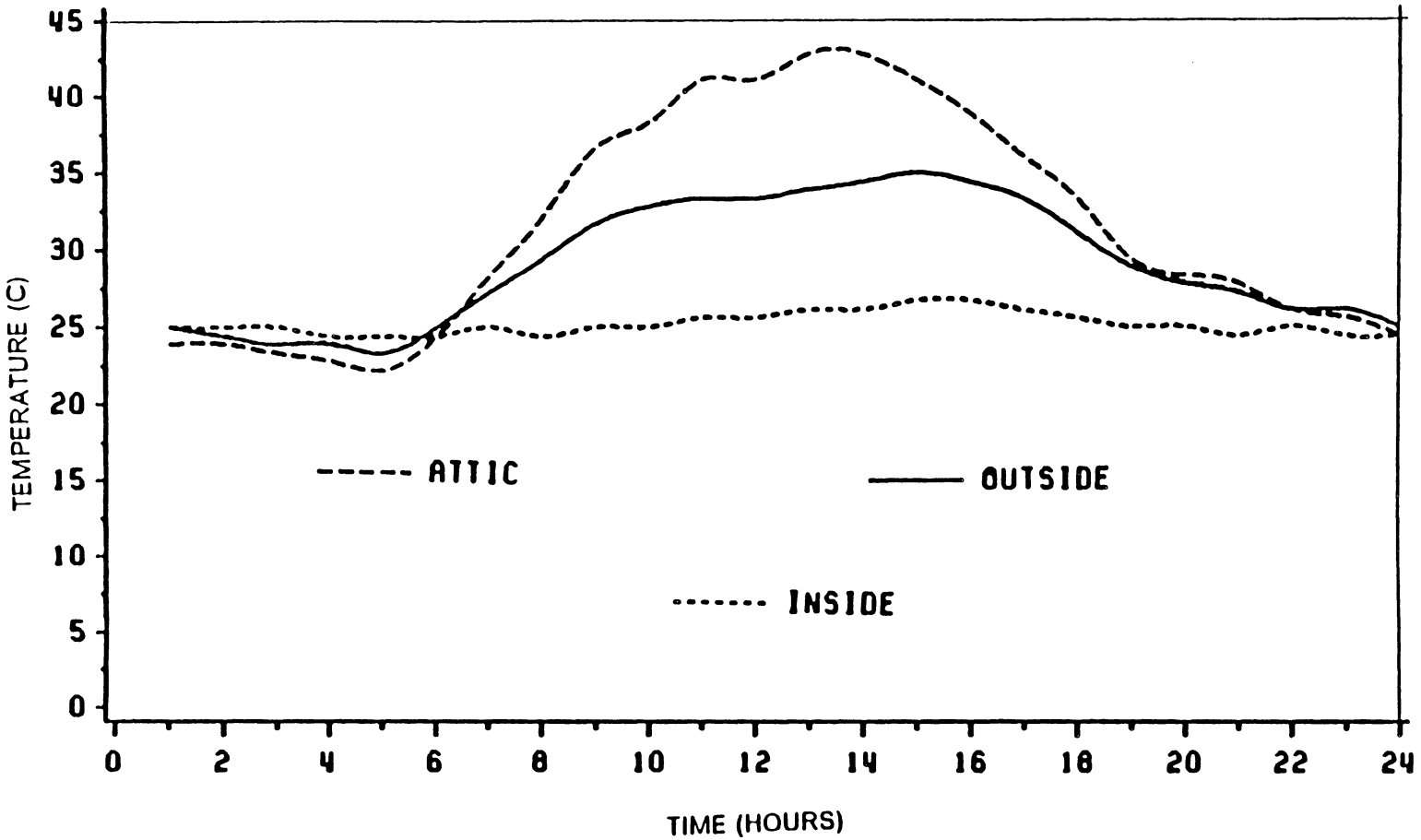

Figure 22. Measured Interior, Outdoor, and Attic Temperature Profiles

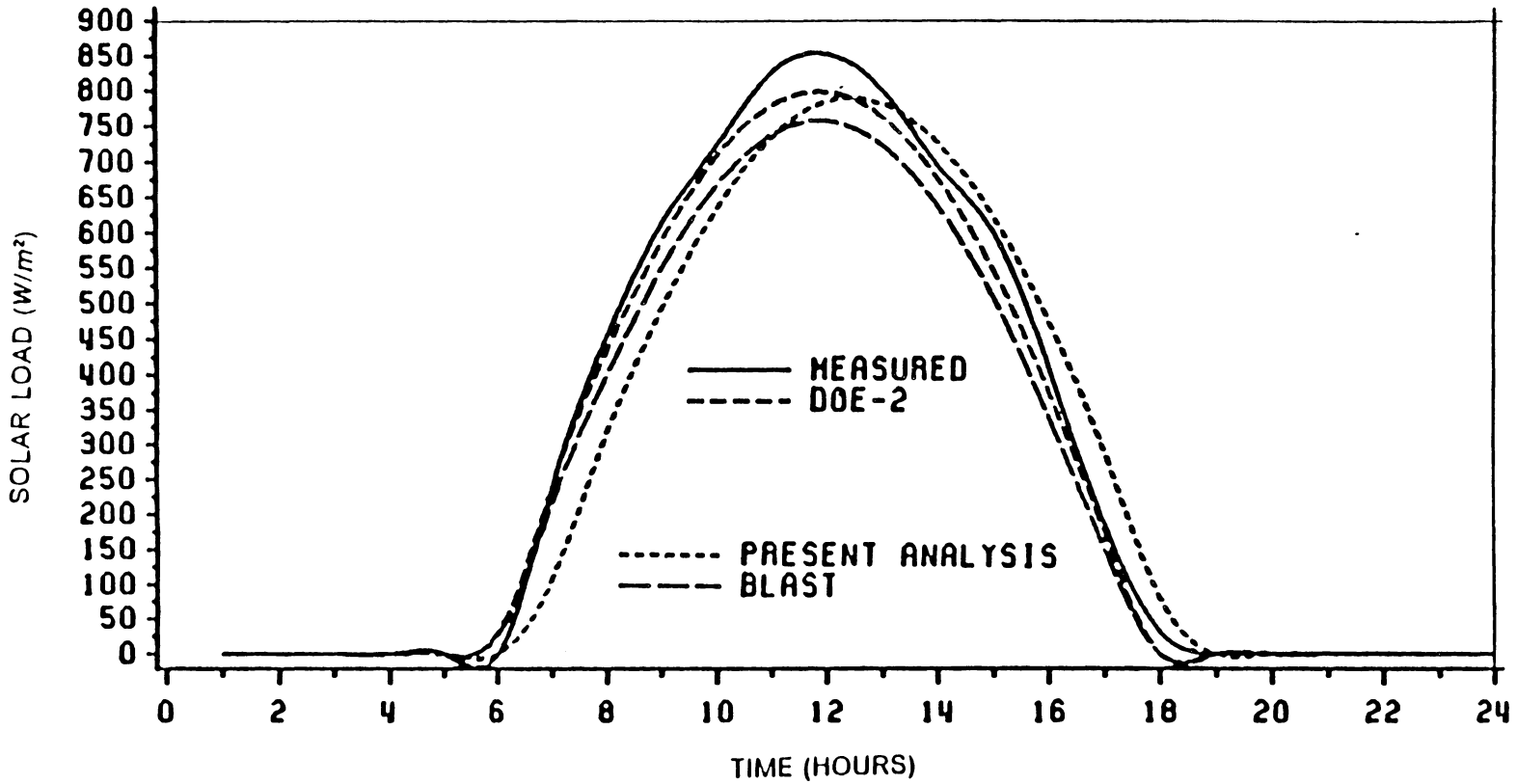

Figure 23. Total Hemispherical Solar Profile (measured and calculated).

Table 13. Description of the Walls of the Houston Test House [82]

	Layer Description		Δx	k	ρ	c	R
1. South wall, west wall, part of east and north walls:	Gypsum board		0.031	0.12	55	0.26	
	Batt insulation		0.302	0.025	2	0.2	
	Air space		--	—	—	—	0.91
	Brick		0.250	0.42	120	0.2	
2. Part of east wall including the garage space:	Gypsum board		0.031	0.12	55	0.26	
	Batt insulation		0.302	0.025	2	0.2	
	Gypsum board		0.031	0.12	55	0.26	
	Air space	garage	--	--	--	—	0.91
	Sheathing (wood)		0.083	0.070	37	0.60	
3. Part of north wall #2 including the garage space:	Gypsum board		0.031	0.12	55	0.26	
	Batt insulation		0.302	0.025	2	0.2	
	Gypsum board		0.031	0.12	55	0.26	
	Air space		--	--	--	--	0.91
	Gypsum board		0.031	0.12	55	0.26	
	Batt insulation		0.302	0.025	2	0.2	
	Air space	garage	--	--	--	--	0.91
	Brick	space	0.330	0.42	120	0.2	
4. Floor:	Carpet and underlay		0.034	0.037	7	0.18	
	Concrete		0.333	1.0	140	0.2	
	Earth		1.000	0.363	125	0.43	
5. Roof:	Plywood		0.031	0.080	34	0.38	
	Shingle		0.021	0.084	73	0.2	
6. Attic floor:	Gypsum board		0.031	0.12	55	0.26	
	Rockwool insulation		0.250	0.025	5.7	0.20	

		(multiplication factor to SI)
Δx:	thickness (ft)	0.3048 to m
k:	thermal conductivity (Btu ft/hr, ft^2, °F)	1.731 to W/(m·K)
ρ:	density (lb/ft^3)	16.01 kg/m^3
c:	specific heat (Btu/lb, F)	4.186 kJ/(kg·K)
R:	thermal resistance (hr, ft^2 F/Btu)	0.176 $(K \cdot m^2)/W$

al. [82] for every hour. Consequently, the cooling loads obtained from the current analysis for each room were added at every time step to obtain an overall cooling load for the house. Similarly, the temperatures predicted for each room were area-averaged at every time step for comparison. In Fig. 24, the measured and calculated sensible cooling load profiles using the present analysis and the DOE-2 program are shown. The current analysis predicted the measured cooling loads moderately well. The DOE-2 program overpredicted the cooling loads during the night time simulations. In Fig. 25, the measured and calculated sensible cooling load profiles using the present analysis and the BLAST-2 program are shown. The BLAST program predicted well the cooling loads during the night time. During the afternoon, the BLAST program overpredicted the cooling load by almost 1.2 KW at 4:00 PM. Figure 26 shows the measured and calculated sensible cooling load profile using the present analysis and NBSLD program. Cooling loads calculated using the NBSLD agreed well with the measured and current results.

The measured and calculated attic temperature using the current analysis and the DOE-2, BLAST-2, and NBSLD programs are examined next. In Fig. 27, the measured and calculated attic temperature profiles using the present analysis and the DOE-2 program are shown. The current analysis simulated the attic temperature well. The DOE-2 program did not predict the attic temperature as accurately. In Fig. 28, the measured and calculated attic temperature profiles using the present analysis and the BLAST-2 program are shown. Both analysis predicted the attic temperature well but the present analysis gives better results. In Fig. 29, the measured and calculated attic temperature profiles using the present analysis and the NBSLD program are shown. The attic temperatures calculated by the current analysis and the NBSLD program compared well with the measured values.

In the second simulation, the measured cooling loads are used to solve for the indoor temperature of each room. The cooling load required for each room was obtained by dividing the overall load by the number of rooms. After solving for the individual room temperature, an area-weighted average was obtained for the overall interior temperature of the house.

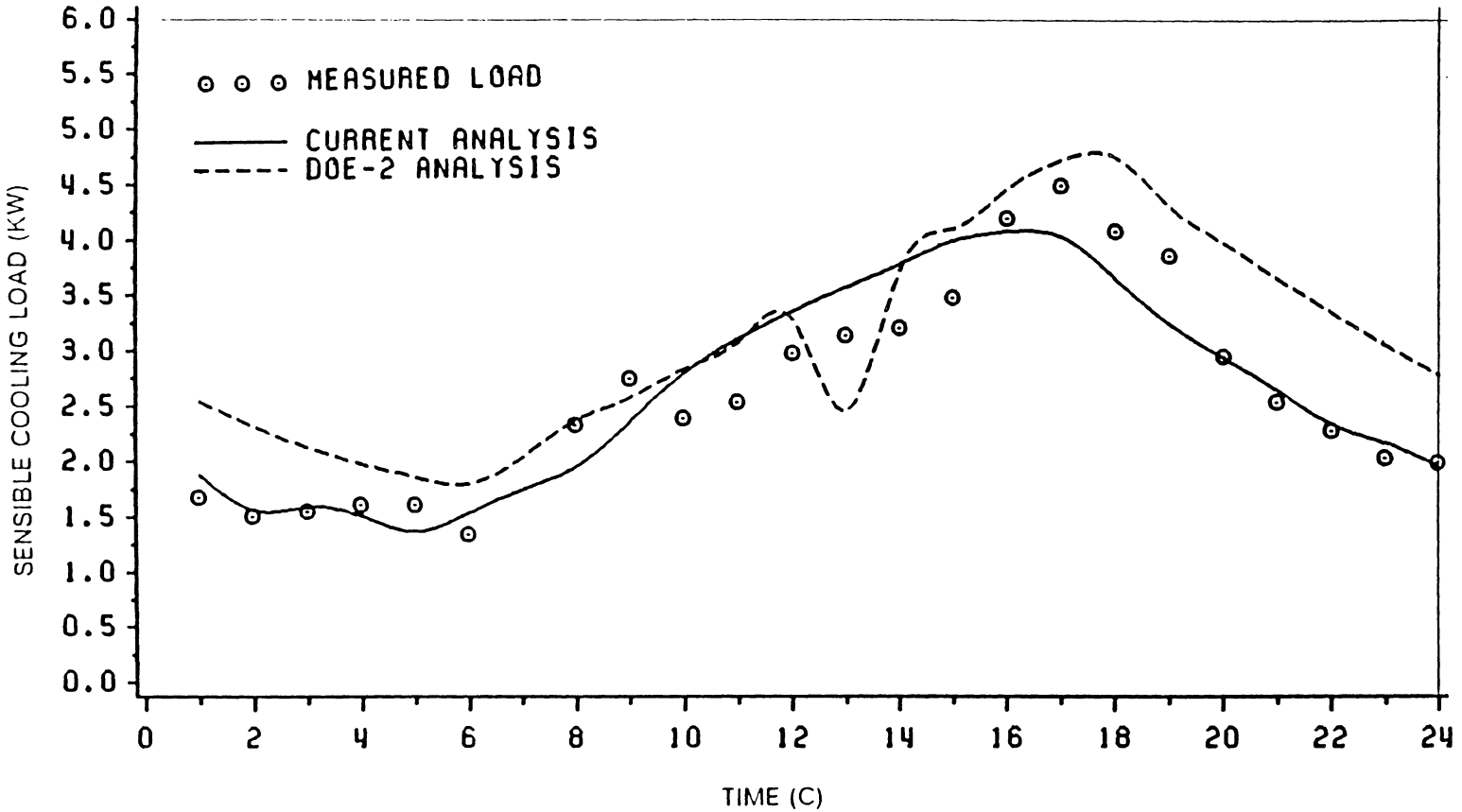

Figure 24. Comparison of the Calculated and Measured Sensible Cooling Loads for the Houston Test House

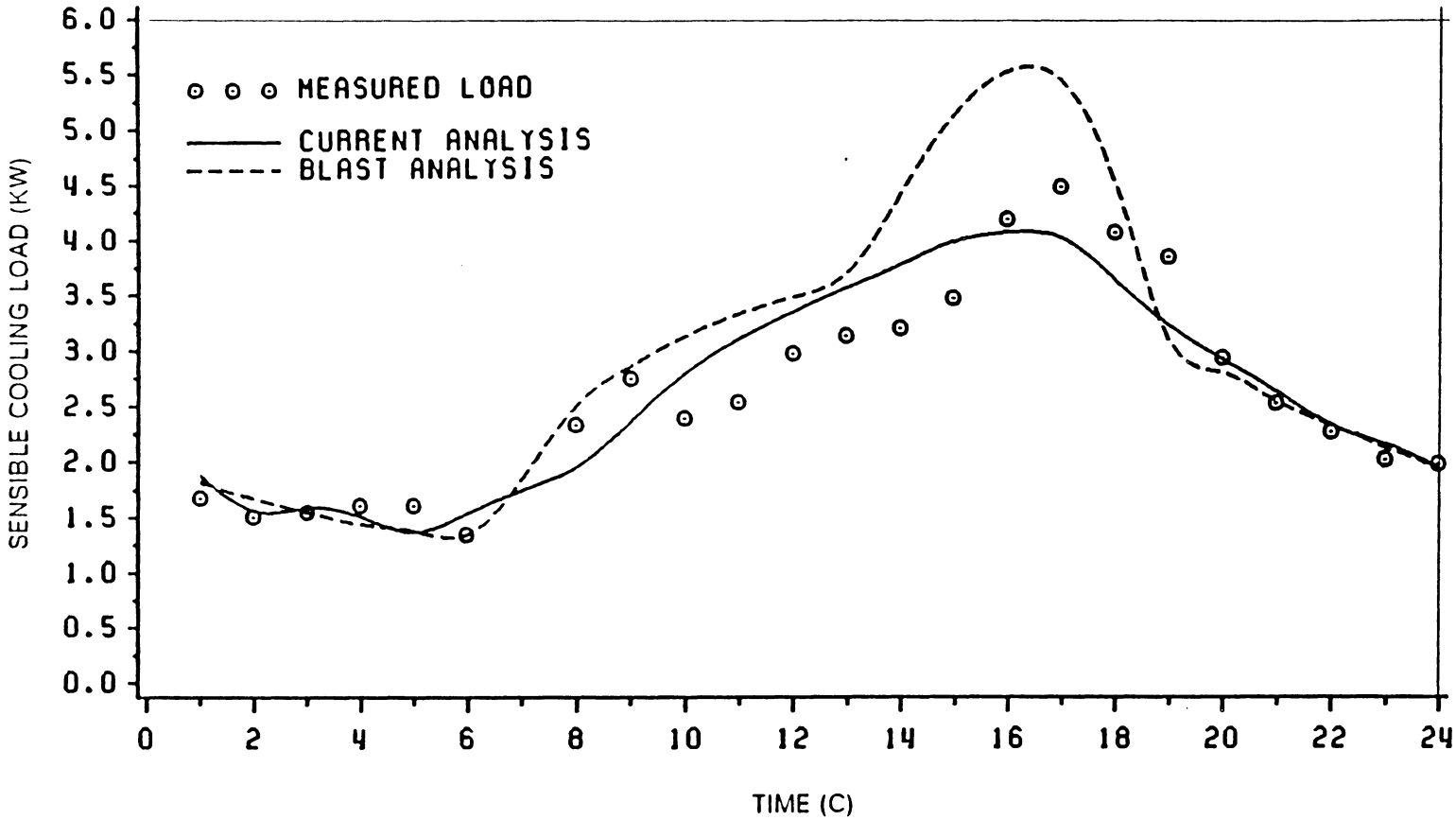

Figure 25. Comparison of the Calculated and Measured Sensible Cooling Loads for the Houston Test House

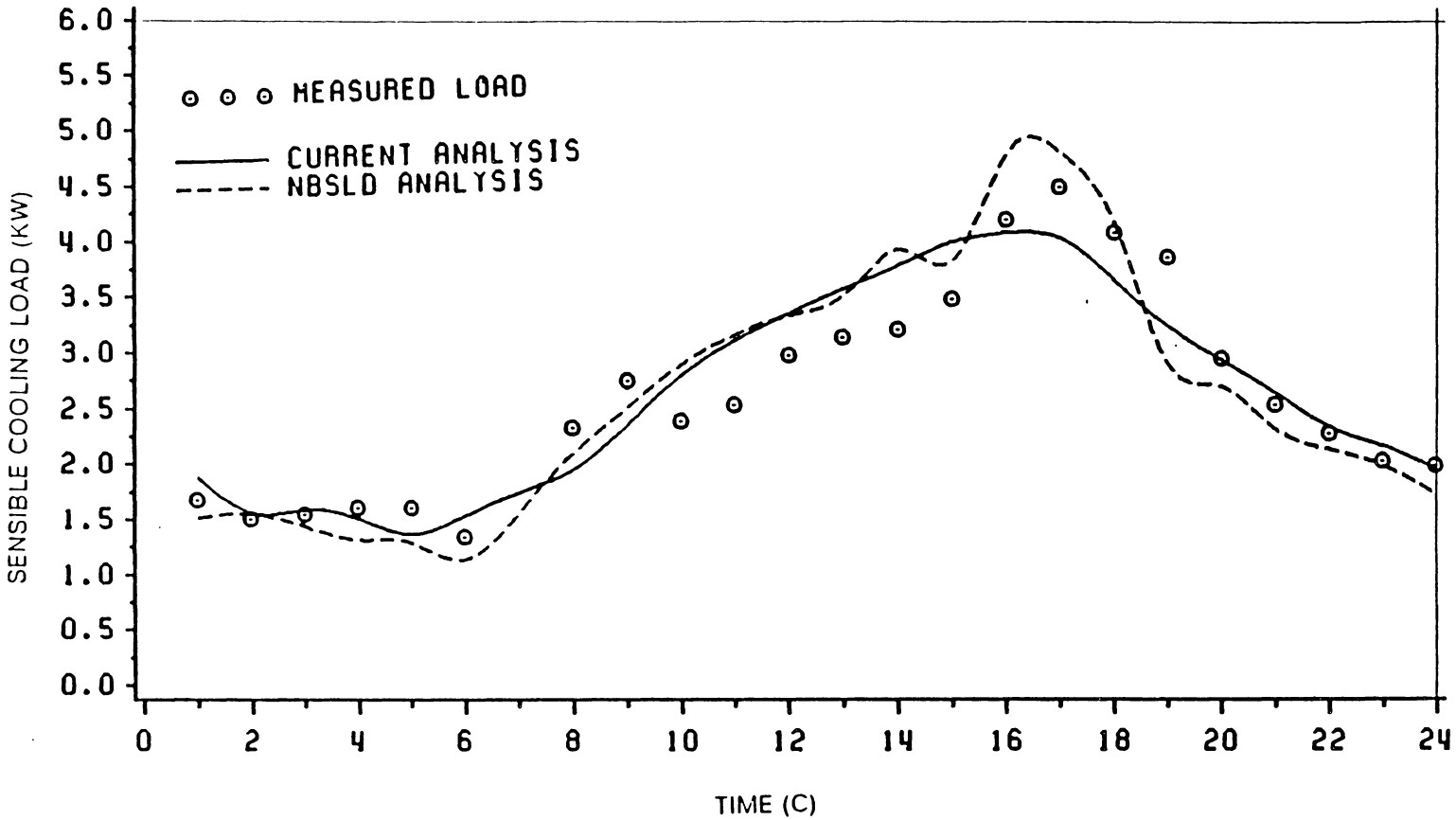

Figure 26. Comparison of the Calculated and Measured Sensible Cooling Loads for the Houston Test House

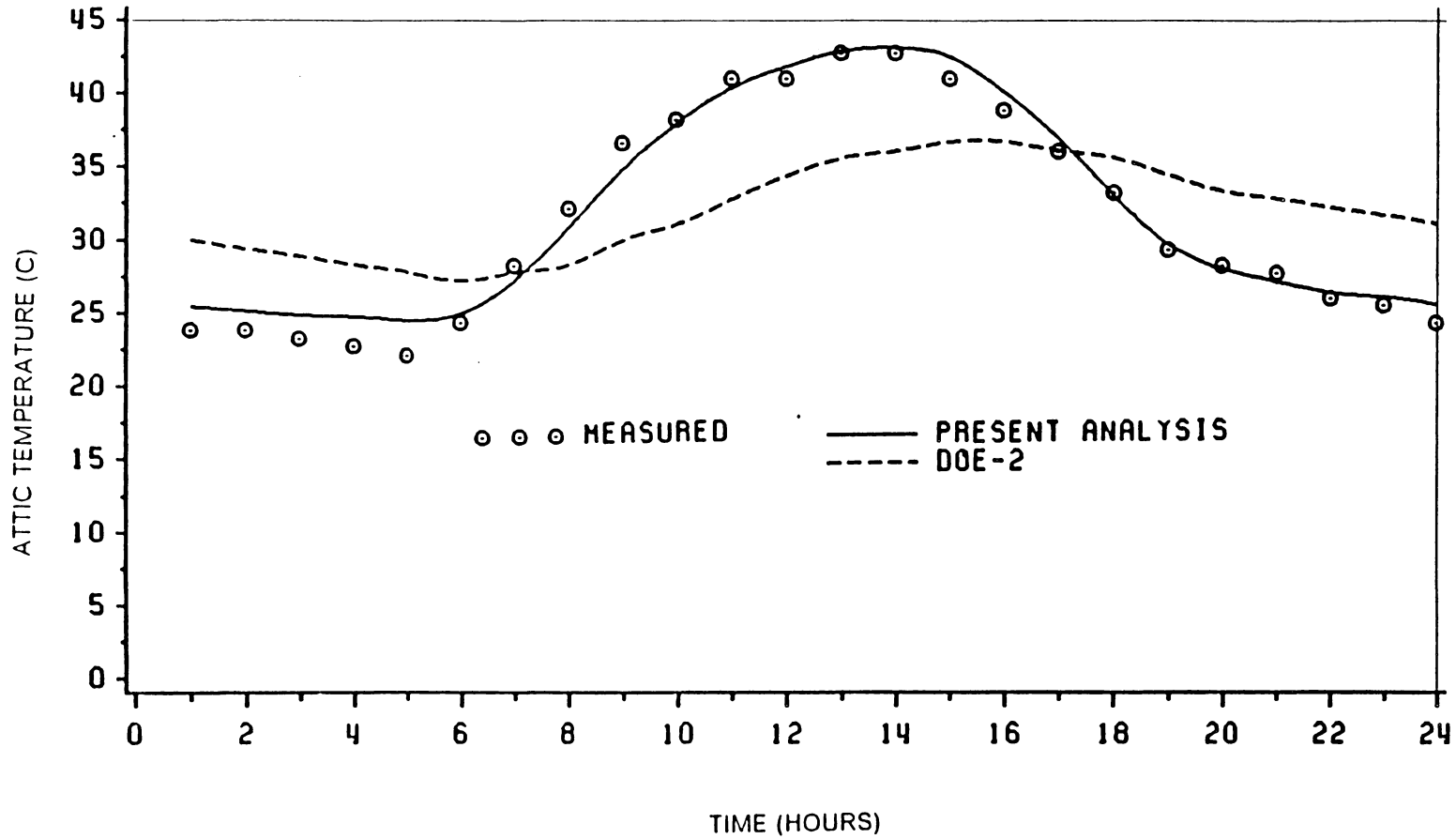

Figure 27. Calculated and Measured Attic Temperature

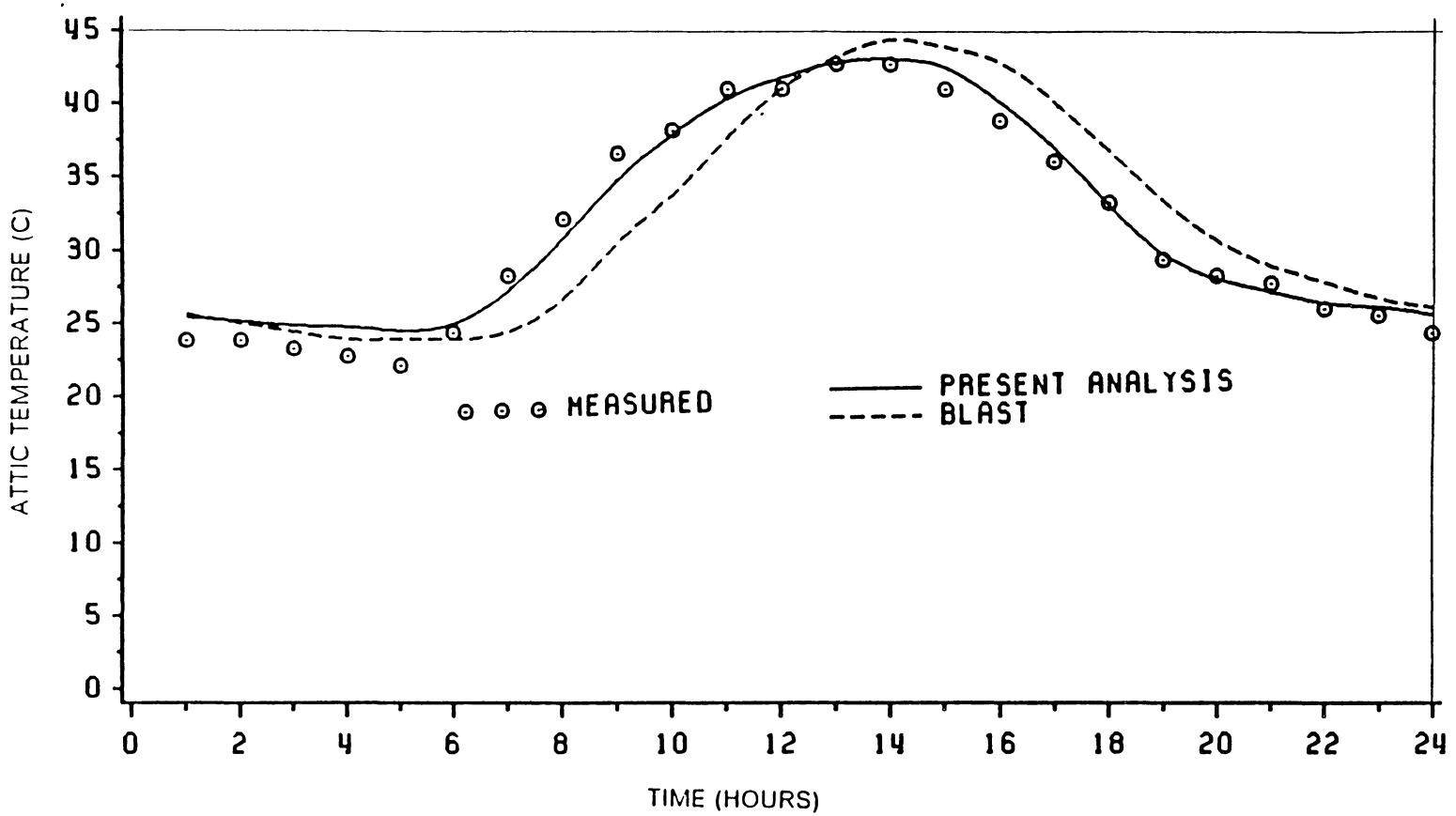

Figure 28. Calculated and Measured Attic Temperature

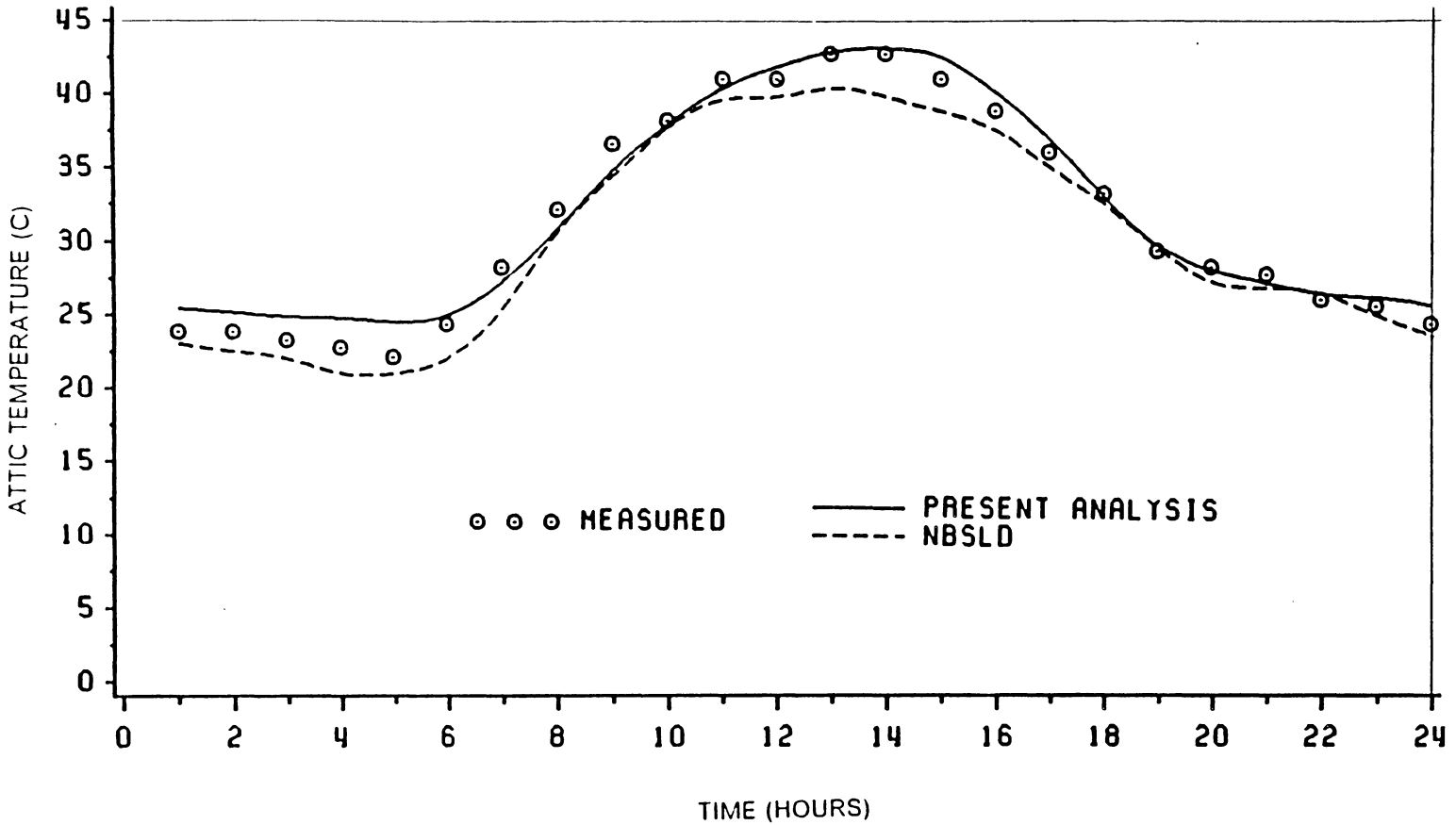

Figure 29. Calculated and Measured Attic Temperature

Overall interior temperatures of the house are plotted in Fig. 30 along with the corresponding measured values. The comparison between measured data and numerical results is judged satisfactory.

In the next chapter, the effect of various parameters on the interior temperature response of the Houston house and a building on the VPI & SU campus is examined during winter and summer power outages.

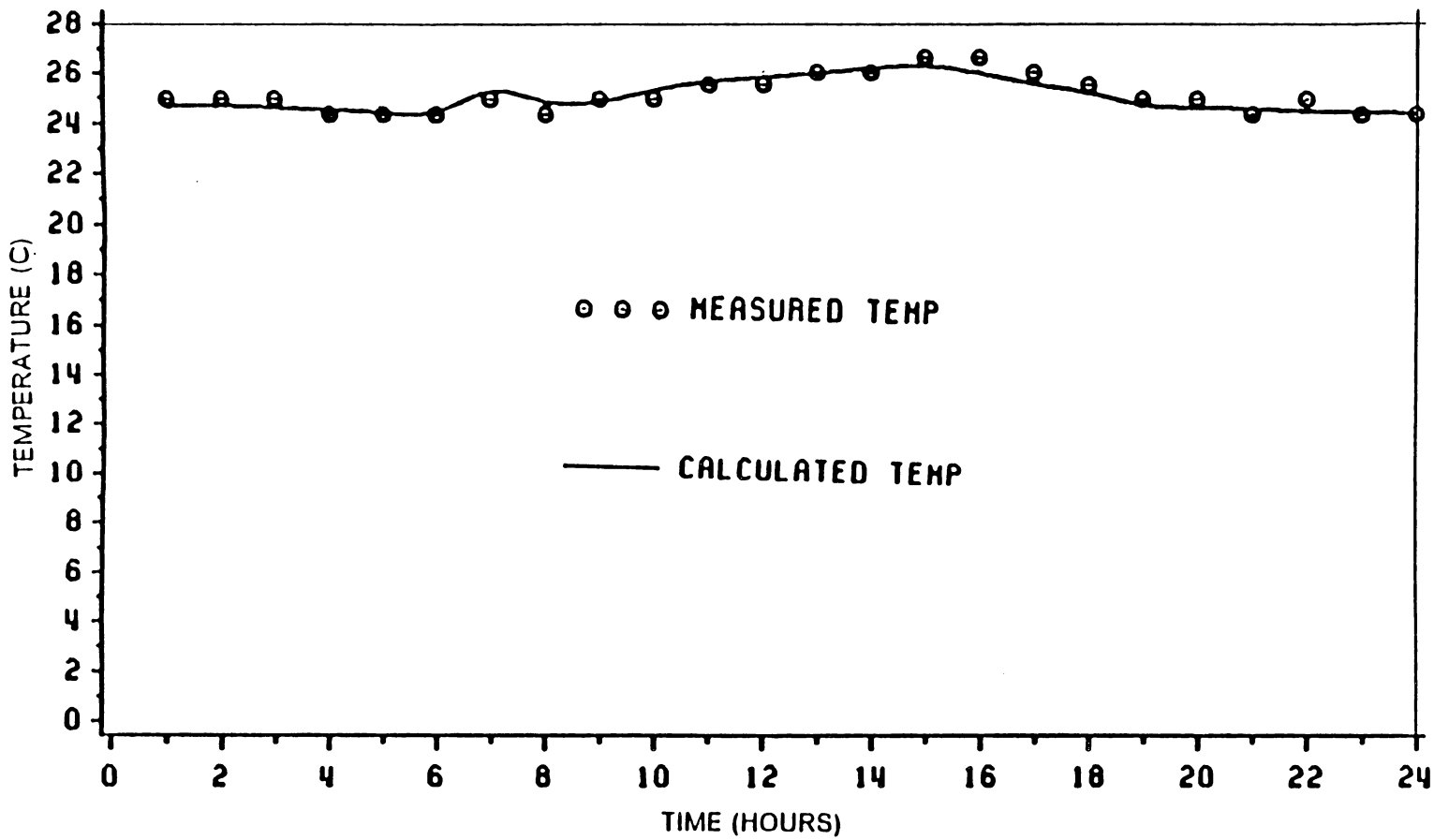

Figure 30. Calculated and Measured Indoor Temperature for the Houston Test House

6. RESULTS AND DISCUSSIONS

The multizone model has been presented and validated with both numerical results and experimental data in Chapter 5. A supporting computer code to determine the dynamic thermal response of structures to controlled and uncontrolled HVAC system shutdowns has also been described. Either interior temperatures for prescribed heating or cooling rates, or heating and cooling loads for specified set temperatures can be calculated for buildings. In this chapter, the effect of various parameters on the transient response of houses and commercial buildings is presented. The reference house used in the simulations is the Houston test house described in the previous chapter. The reference building is Williams Hall on the VPI & SU campus.

The parameters examined in the current research are:

. Infrared radiation

. Wall mass

. Insulation position in exterior walls

. Furnishings inside rooms

. Infiltration load uncertainties

. Exterior wall vertical convective coefficient

. Ground temperature

. The 97.5 per cent design temperature criterion

The temperature response of buildings to startup of its HVAC system after a power outage is also investigated.

HOUSTON HOUSE SIMULATIONS

Winter and summer power outages are simulated for the Houston test house. The effect of various parameters on the interior temperature of the house is presented. The interior temperature of the house is plotted for the duration of the power outages.

As shown in Fig. 21, the Houston house contains two bedrooms, a master bedroom, a living room, a garage space, and an attic. The outside temperature and solar load profiles used in the calculations are described in Chapter 5. The winter exterior temperature profile is obtained by subtracting a constant value (30 C) from the summer temperature profile. The summer and winter exterior temperature profiles are shown in Fig. 31. No solar heating is assumed for winter power outage simulations. The summer power outage is started at noon. The winter power outage is started at midnight. The outside temperature profiles, shown in Fig. 31, are denoted as the "Summer" and "Winter" temperature profiles. For simulations longer than 24 hours, the same temperature and solar profiles are repeated. The initial temperature in the house in both cases is 24.4 C. To satisfy the history needed in using the TRFM, calculations started 48 hours before the actual simulation began. The interior temperature of the structure was constant at 24.4 C during this 48-hour period.

The interior temperature of each room is calculated with the heating or cooling rates set to zero. The volume-weighted average temperature along with the north, east, and south side room temperatures of the house are plotted in Fig. 32 for a summer power outage beginning at noon. The south-side room temperature was about 0.5 C higher than the temperatures of remaining rooms after 4 hours and for the duration of the power outage. The interior tem-

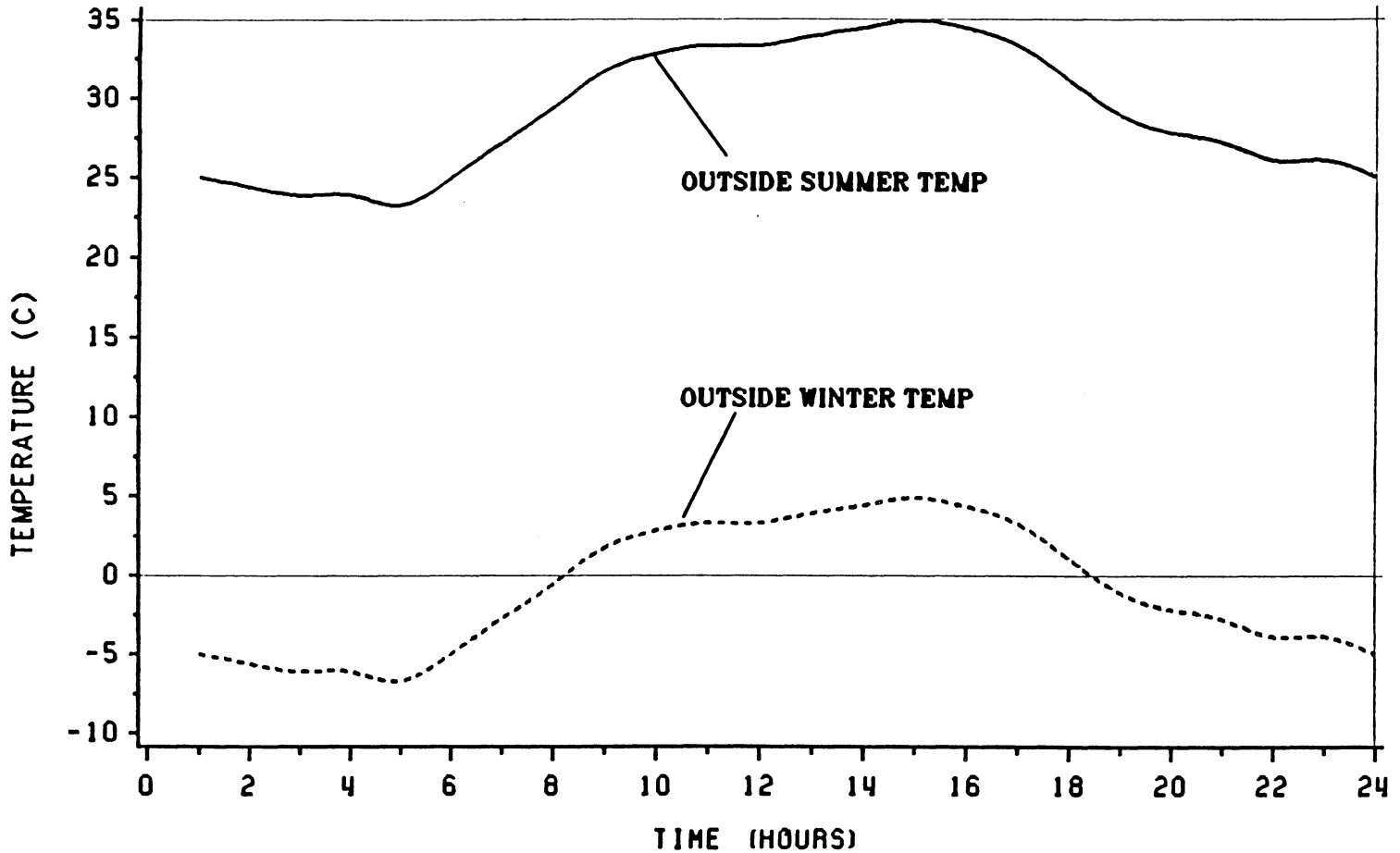

Figure 31. Outside Summer and Winter Temperature Profiles

perature of the house reached 27.5 C after 4 hours of summer power outage simulation. A 32 C maximum interior temperature was reached after 100 hours of simulation.

In Fig. 33, the volume-weighted interior temperature along with the north, east, and west side room temperatures are plotted for a midnight winter power outage. the temperature difference between the north and south side rooms was 1 C after 5 hours and for the duration of the power outage. The interior temperature of the house dropped to 7 C after 90 hours of winter power outage simulation.

WILLIAMS HALL SIMULATIONS

The reference building used in the simulations is Williams Hall. Williams Hall is U-shaped and faces north-west. The building direction was changed to accommodate a more general analysis, the U-shape faces south. Williams Hall has three floors with 36 rooms per floor. The floor plan of Williams Hall is shown in Fig. 34. All three floors were identical in dimensions, i.e., the same plan is used for all three floors. A description of the interior and exterior walls, the slab, and a typical window and door of Williams Hall are given in Table 14. In Fig. 35, the floor plan implemented in the computer code, is shown along with the room numbering used. The imaginary walls and rooms are also shown.

The solar load used in the summer power outage simulations was calculated for Blacksburg, VA. on July 1. The solar load profiles on the north, south, east, and west walls are shown in Fig. 36. Trees and adjacent buildings were located on the south side of the building. Therefore, the solar load on that side was reduced by 60 percent to account for solar radiation blocked by the surrounding structures. The corresponding transmitted solar load profiles through the double pane windows on all four sides of the building are shown in Fig. 37. The exterior summer and winter temperature profiles used in the calculations are those

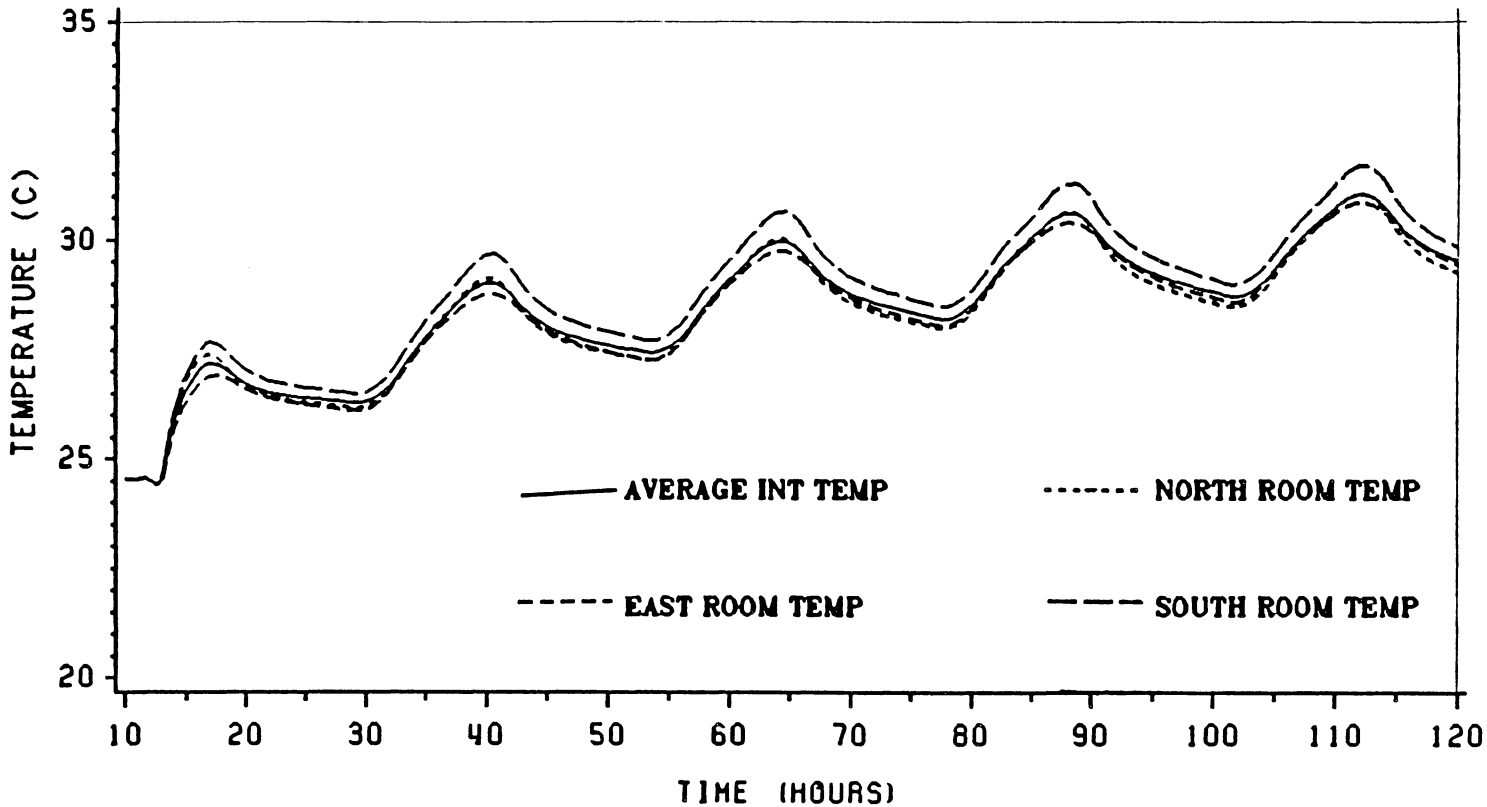

Figure 32. Interior Temperature Profile of the Houston House During a Summer Power Outage

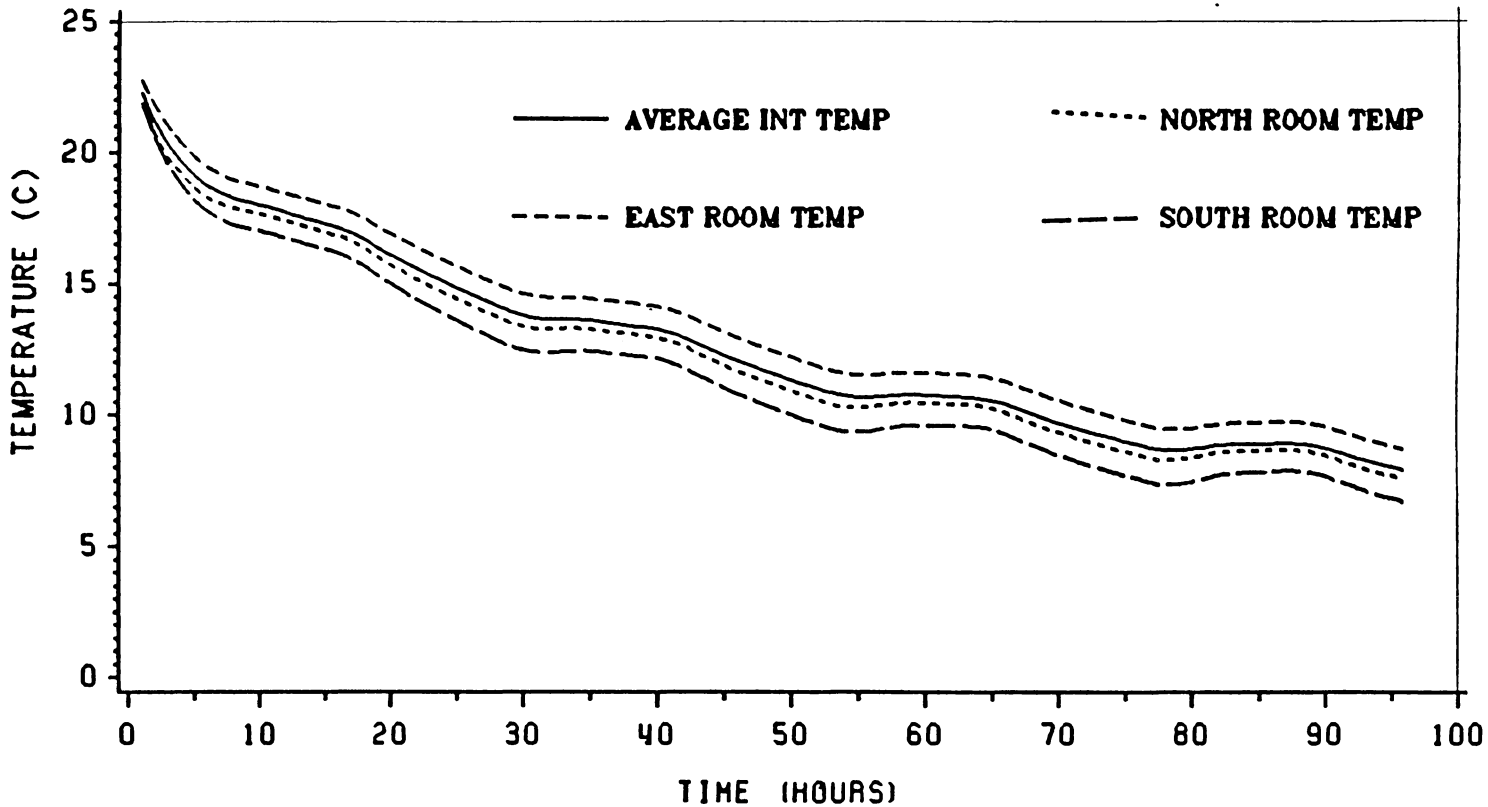

Figure 33. Interior Temperature Profile of the Houston House During a Winter Power Outage

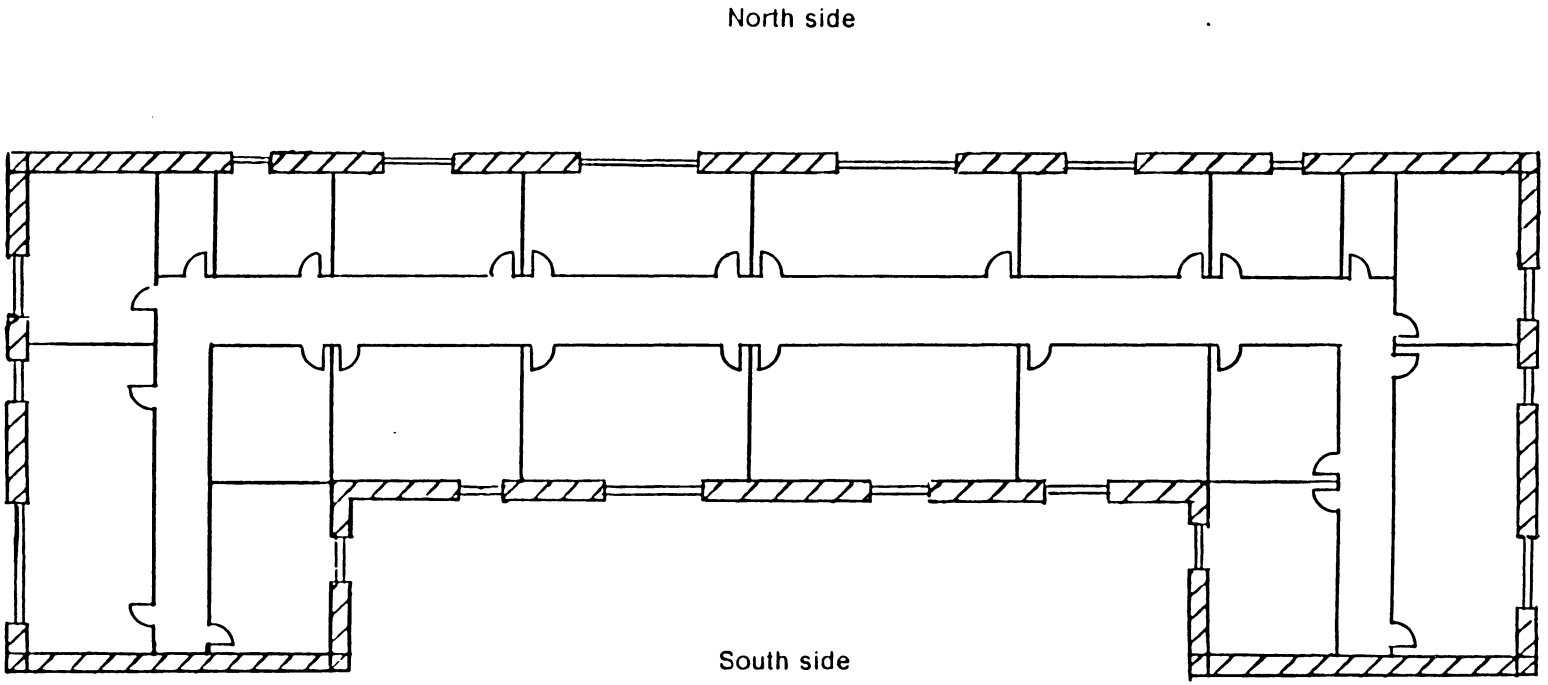

Figure 34. Floor Plan of Williams Hall, All Three Floors Have The Same Floor Plan

Table 14. Description of the Walls, slab, windows, and doors of Williams Hall

PROPERTIES OF TEST BUILDINGS	ΔX (m)	k (W/m.C)	ρ (kg/m³)	C_p (kJ/kg.C)	$\alpha 10^5$ (m^2/s)
EXTERIOR WALLS					
Gypsum Board	0.0127	0.16	801	4.165	4.8
Concrete	0.352	0.52	977	0.837	63.56
Limestone	0.178	0.93	1650	0.9	62.5
INTERIOR WALLS					
Cinder Block	0.152	0.61	861	0.9	78.1
ROOF					
Acoustical Tile	0.0826	0.23	100	2.4	94.7
R-0.16 Air Space: h = 6.106 (W/m^2C)	0.304	--	--	--	--
Limestone	0.0508	0.93	1650	0.9	62.5
Foam Glass in Asphalt	0.0508	0.61	1900	0.9	35.67

Table 14. (Continued)

PROPERTIES OF TEST BUILDINGS	ΔX (m)	k (W/m.C)	ρ (kg/m^3)	C_p (kJ/kg.C)	$\alpha 10^5$ (m^2/s)
CEILINGS/FLOORS					
Acoustical Tile	0.0826	0.23	100	2.4	94.7
R-0.16 Air Space: h = 6.106 (W/m^2C)	0.304	--	--	--	--
Concrete	0.102	0.72	977.0	0.837	88.05
SLAB					
Concrete	0.102	0.72	977.0	0.837	88.05
Gravel	0.152	0.865	1922.2	0.837	53.74
Earth	0.102	0.865	1922.2	0.837	53.74
DOORS	0.0127	0.028	--	--	--
WINDOWS (double pane)	0.044	0.116	--	--	--

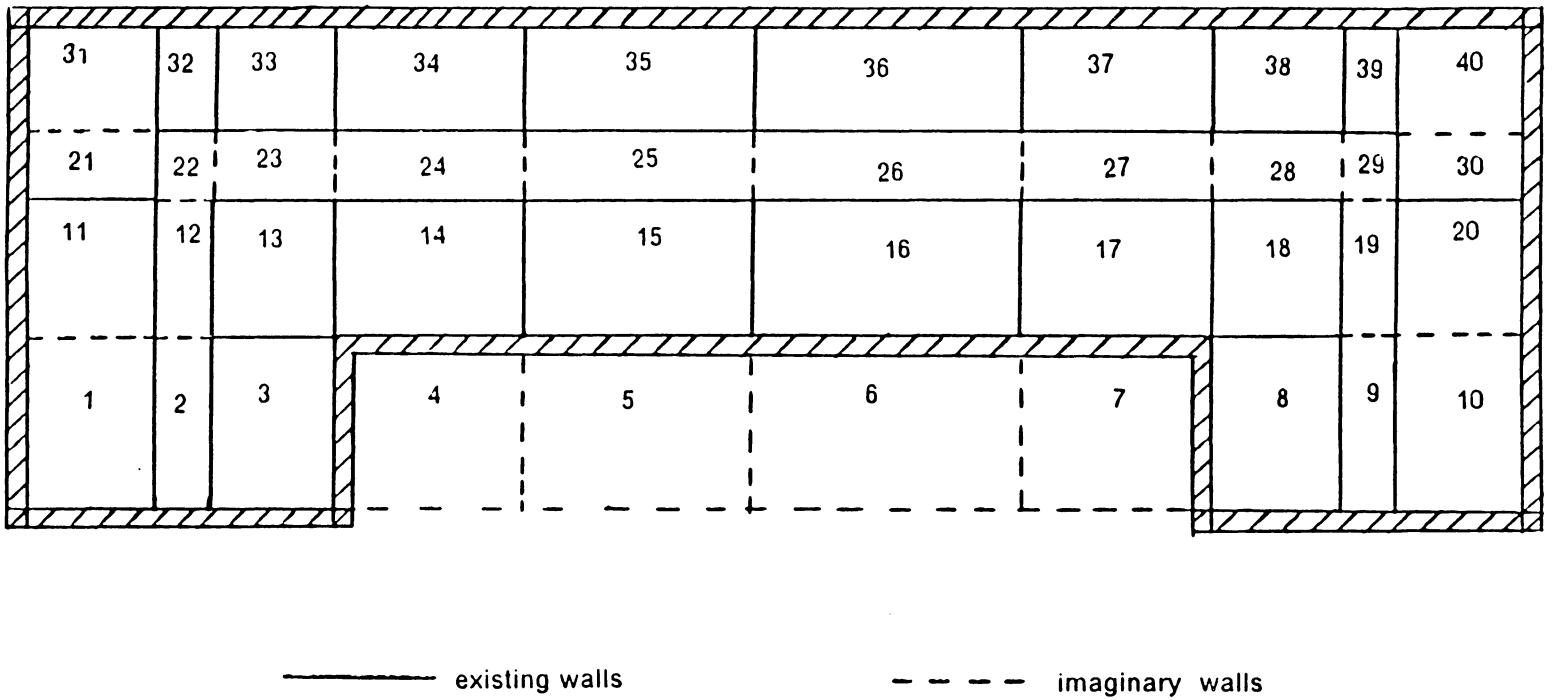

Figure 35. Room Numbering of Williams Hall Employed in the Computer Code

shown in Fig. 31. The summer power outage starts at noon and the winter power outage starts at midnight.

For each floor of Williams Hall, the interior temperature profiles are presented at five locations during a power outage. The locations are on the north, south, east, and west sides and in the center. The corresponding room numbers for these locations are 36 (north side), 16 (south side), 20 (east side), 11 (west side), and 26 (central section). Room 26 is actually part of the hall and not a complete enclosed room. In Fig. 38, the temperature drifts of the five rooms after a midnight winter power outage are presented for the first floor. The north side had the highest temperature drop on each floor because of the large window area present on that side. The south side (room 16) had the least temperature drop of all sides resulting from the small window area present on that side. The temperature profiles of the rooms located on the east, west, and central sides were in between the two limits. The difference between the north and south side room temperatures was approximately 2 C for the first floor, 3.5 C for the second floor, and 1.6 C for the third floor after 5 hours and for the duration of the power outage. As expected, lower temperatures were observed on the higher floors. After 80 hours of simulation, the temperature of room 36 dropped to 8 C on the first floor, 5 C on the second floor, and 1.5 C on the third floor.

In Fig. 39, the temperature drift of the five rooms after a noon-time summer power outage is presented for the first floor. The presence of the solar load changed drastically the temperature response of the rooms. As shown in Fig. 36, the east and west side rooms are exposed to larger solar loads than the south-side rooms because of the trees shading that side. That load affected considerably the temperature response of these rooms after a power outage. The temperature response curve of room 20 on the east side increased by 2.0 C at 10:00 AM. The rooms located on the west and central sides had the highest temperature profiles on each floor. The central room is actually part of the hall. The north and south side rooms had the least temperature increase. The third floor was exposed to solar radiation on all four sides and the roof. During the power outage, rooms 11 (west) and 16 (center) of the first floor

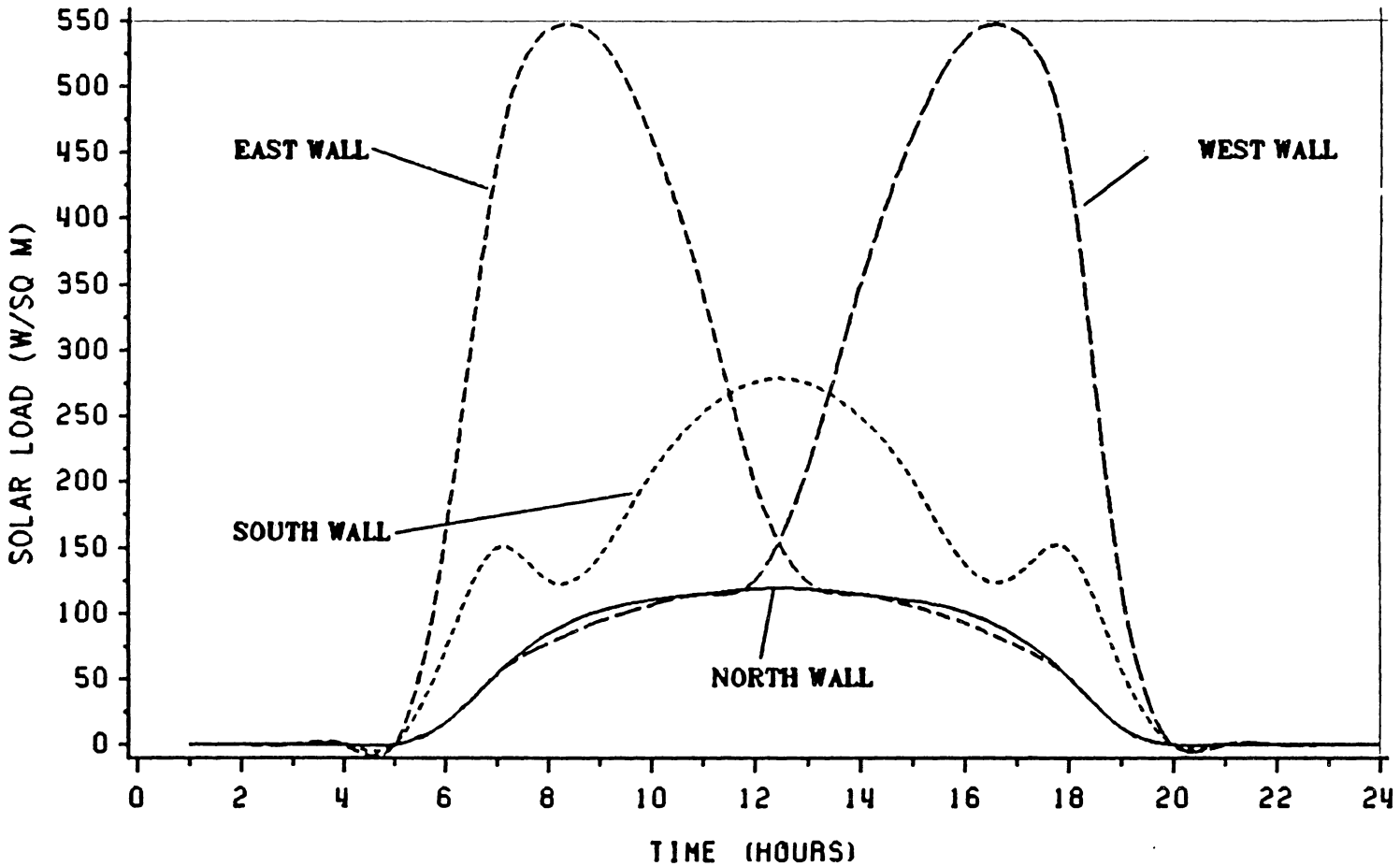

Figure 36. Solar Profiles For July 1, Blacksburg, VA

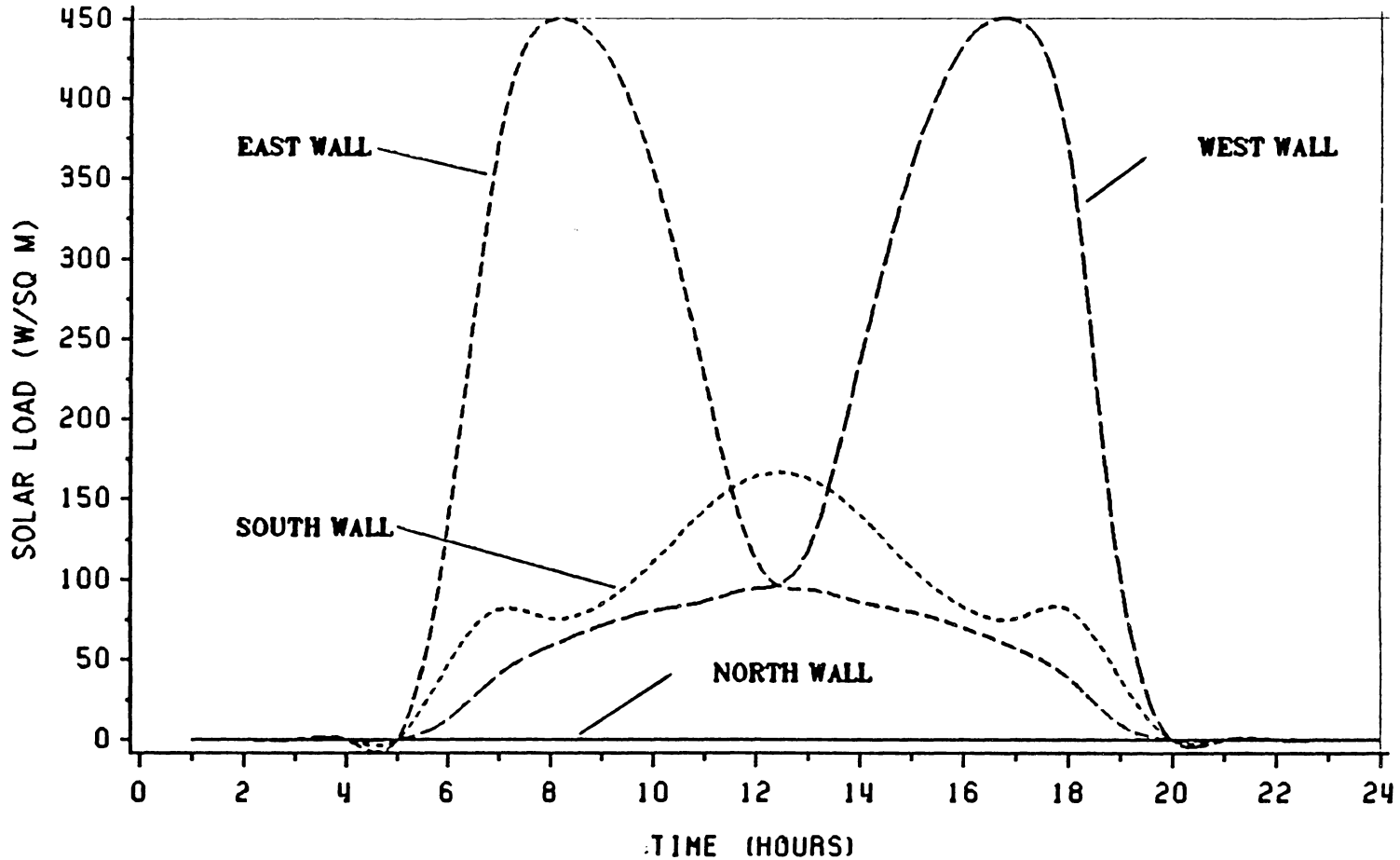

Figure 37. Solar Loads Transmitted Through the Windows (Willlams Hall)

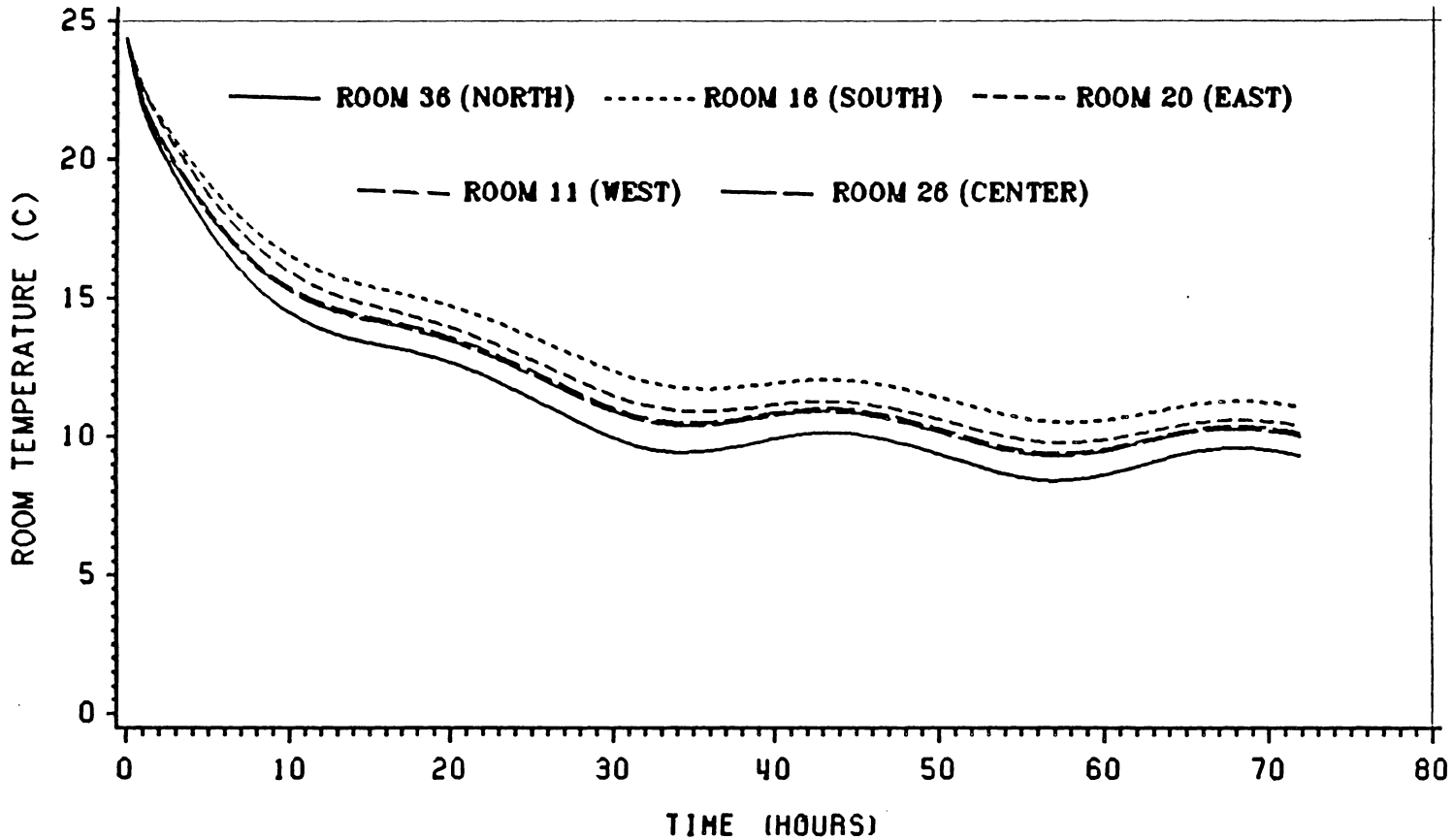

Figure 38. Interior Temperatures of Williams Hall During a Winter Power Outage, First Floor

reached 32 C at 4:00 PM. The temperature of all rooms on the second and third floors increased consistently after each day of power outage. After 80 hours of simulation, the interior temperature of rooms 11 and 16 reached 35 C on the second floor and 37 C on the third floor. The temperature difference between the extreme profiles on each floor was 4 C for the first floor and 4.5 C for the second and third floors after 4 hours and for the duration of the power outage.

EFFECTS OF BUILDING PARAMETERS

The effect of the various parameters listed earlier is investigated individually during summer and winter power outages for the Houston house and Williams Hall. The main reason for considering these parameters is to study their effect on the analysis. The emissivites, sky temperatures, convective coefficients, etc., are usually estimated in HVAC calculations. Their impact on the calculations is not always clear from the literature. Therefore, various test cases are presented next to determine the parameters that more significantly affect the interior temperature of buildings during winter and summer power outages.

For the Houston house, the volume-weighted average interior temperature profile is given for the comparisons. For the academic building, only the extreme temperature profiles of each floor are presented. For winter simulations, the temperature profiles of the north- and south-side rooms are shown. For summer simulations, the temperature profiles of the north- and west-side rooms are shown. In some cases, the calculated results are noted without showing the plots.

Several outside temperature profiles are used in the summer and winter power outage simulations. For each case, the profile is noted by its range. Therefore, the profiles shown in Fig. 31 are labeled as 25 to 35 C and -5 to 5 C temperature profiles. Other exterior tem-

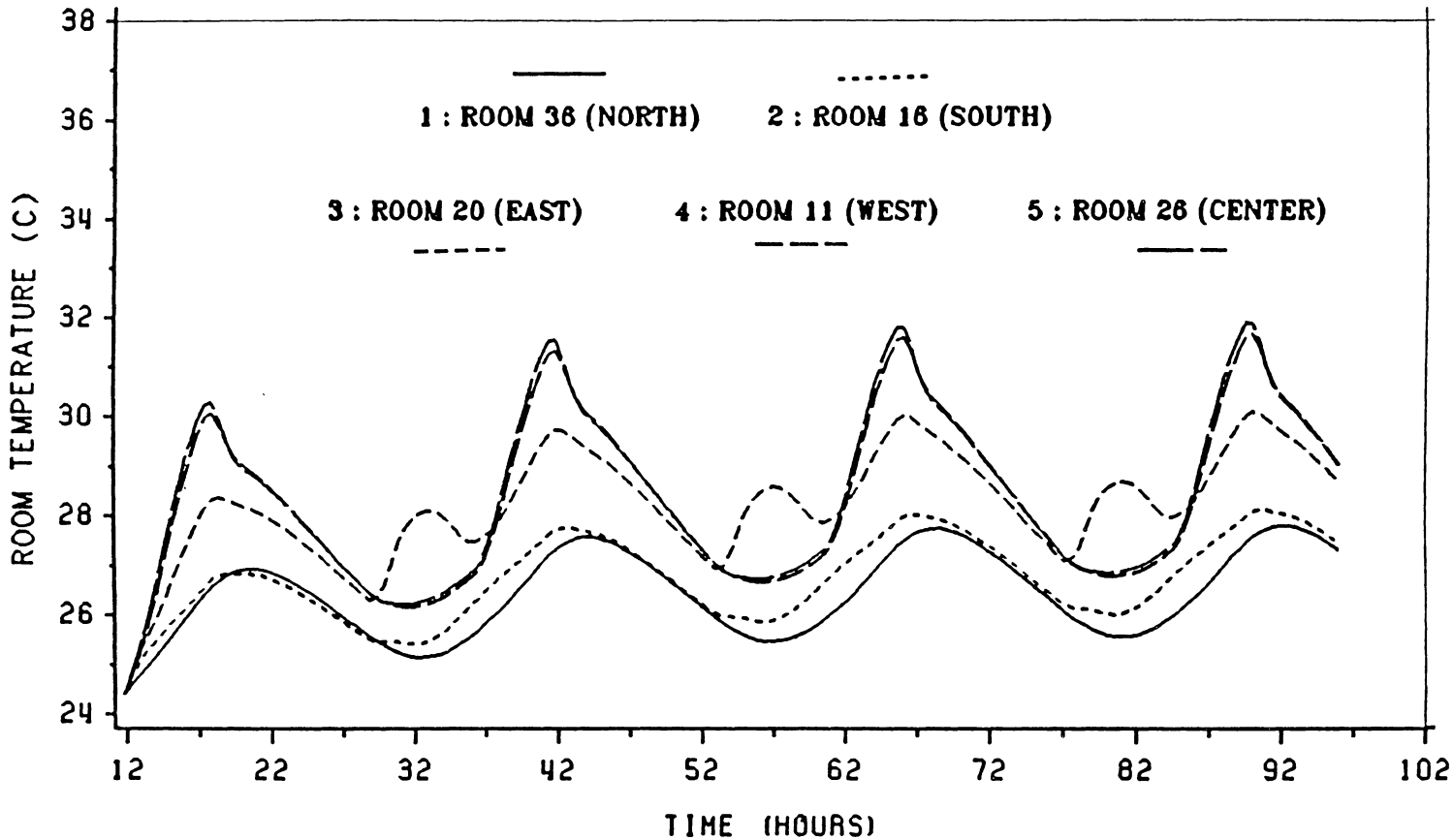

Figure 39. Interior Temperatures of Williams Hall During a Summer Power Outage, First Floor

perature profiles were 5 to 15 C, 28 to 38 C, and -10 to 0 C. These profiles are obtained by subtracting different constants from the 25 to 35 C temperature profile given in Fig. 31.

INFRARED RADIATION

Exterior and interior radiation in structures is accounted for in the current analysis. On the outside walls, long-wave radiation between the surface and an effective sky temperature is included in the model. Inside each room, the MRT method is used to model radiation exchange between surfaces. The effect of the exterior wall emissivities and the sky temperature on the interior temperature response are shown during summer and winter power outages. Interior temperatures of the house and rooms in the academic building are calculated after summer and winter power outages with different exterior wall emissivities and sky temperatures. The effect of including radiation between interior (MRT method) walls is also analyzed.

EXTERIOR WALL EMISSIVITIES

On exterior walls of the structure, convection to the outside, conduction through the wall, solar load, and emission of infrared radiation to an effective sky temperature are taken into account. The effect of several wall emissivities on the interior temperatures in buildings is presented. The effective sky temperature equation used in the current simulations was obtained from Thomas [102],

$$T_s(\tau) = 0.0552 \left[T_o^{1.5}(\tau) \right] \tag{6.1}$$

For the Houston house, exterior wall emissivities of 0.2, 0.5, and 0.9 are used for the winter and summer power outage simulations. The average interior temperature of the house decreased by 0.5 C after 5 hours of the power outage simulation when the exterior wall emissivity is changed from 0.2 to 0.5. A decrease of 1.0 C is noted after 5 hours and for the

duration of the power outage when the emissivity is increased from 0.2 to to 0.9. A 28 to 38 C exterior temperature profile was used. For the winter season power outage, a decrease of 0.5 C is noted after 5 hours of power outage when the emissivity increases from 0.2 to 0.9. A -10 to 0 C exterior temperature profile was used.

For Williams Hall, exterior wall emissivities of 0.2 and 0.9 are used for winter and summer power outage simulations. The outside summer and winter temperature profiles used in the calculations are 25 to 35 C and -5 to 5 C, respectively.

In Fig. 40, the temperature histories of rooms 36 and 26 during a summer power outage are plotted for the third floor. For all floors, the temperature decreased by 0.6 C after 10 hours and for the duration of the power outage when the exterior wall emissivity is changed from 0.2 to 0.9. For the winter season power outage, the interior temperature in all rooms decreased by 0.5 C after 5 hours when the exterior emissivity was changed from 0.2 to 0.9. Increasing the exterior wall emissivity had a positive and negative effect on the interior temperature response of buildings during summer and winter power outages, respectively. The effect of the sky temperature on the interior temperature of buildings is shown next.

SKY TEMPERATURE

In the HVAC literature, several models are available to predict the effective sky temperature based on the ambient temperature and other parameters [102-106]. In this research, three sky temperature approximations are used in the simulations: the sky temperature is taken as ambient temperature, 25 C higher than the ambient temperature, and 25 C lower than the ambient temperature. The two exterior summer temperature profiles used are 15 to 25 C and 28 to 38 C to examine the effect of the sky temperature on the interior temperature. The two exterior properties represent normal and extreme weather conditions.

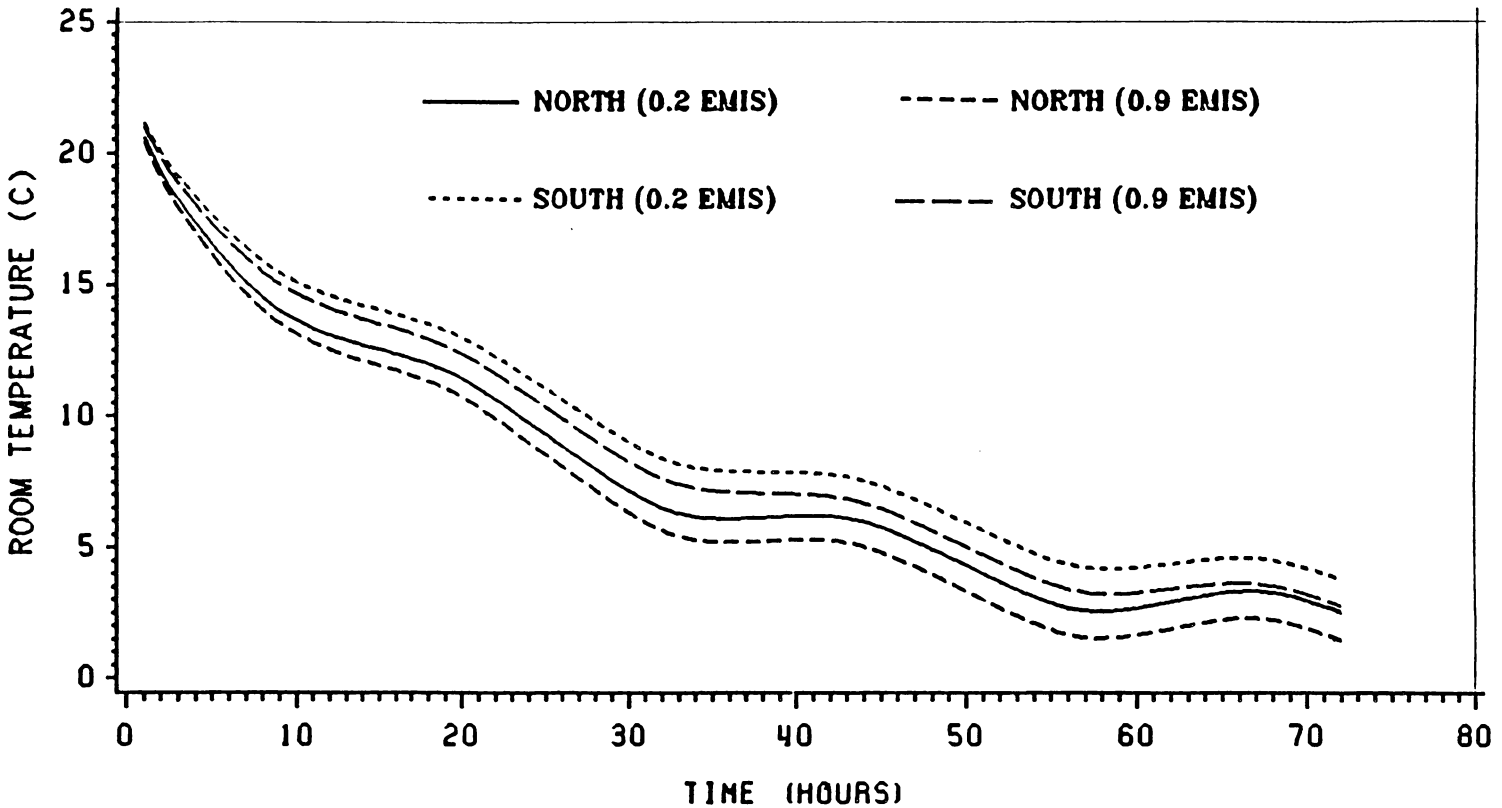

Figure 40. Effect of Exterior Wall Emissivity on the Interior Temperature of the Building During a Winter Power Outage, third floor: the outside temperature range is -5 to 5 C

For 28 to 38 C and 15 to 25 C outside temperature profiles, a 25 C increase in the sky temperature profile above the ambient temperature profile increased the interior temperature of the house by an average of 2 C after 5 hours of power outage. After a 25 C decrease in the sky temperature profile below the ambient temperature profile decreased the house temperature by an average 2 C after 7 hours and for the duration of the power outage.

For the winter season, the outside temperature profiles used were 5 to 15 C and -10 to 0 C. The interior temperature of the house is shown in Fig. 41 for the three sky temperatures with a -10 to 0 C outside temperature profile. In both cases, a 25 C decrease in the sky temperature below the outside temperature profile decreased the interior temperature of the house by 2 C after 7 hours and for the duration of the power outage.

The sky temperature effect on the interior temperature of the building during a summer power outage is studied next. The same sky temperature profiles presented earlier are used for the building power outage simulations. A 25 C decrease in the sky temperature profile below the outside temperature profile decreased the interior temperature of all rooms by 0.9 C for the first floor and 1.2 C for the second and third floors after 8 hours of power outage simulation. The outside temperature profile was 25 to 35 C. The 25 C increase in the sky temperature increased the interior temperature of all rooms in the building by 1.2 C after 8 hours of power outage.

In Fig. 42, the temperature profiles of rooms 36 and 16 are plotted for $T_s(\tau) = T_o(\tau)$ and $T_s(\tau) = T_o(\tau) - 25\,C$ for a winter power outage and for the third floor. The outside temperature profile was -5 to 5 C. A 0.5 C temperature decrease in all rooms after 8 hours of the power outage was obtained for the 25 C lower sky temperature profile. Increasing the sky temperature by 25 C above the ambient temperature profile increased the north and south side temperatures by an average 1 C after 11 hours of the power outage.

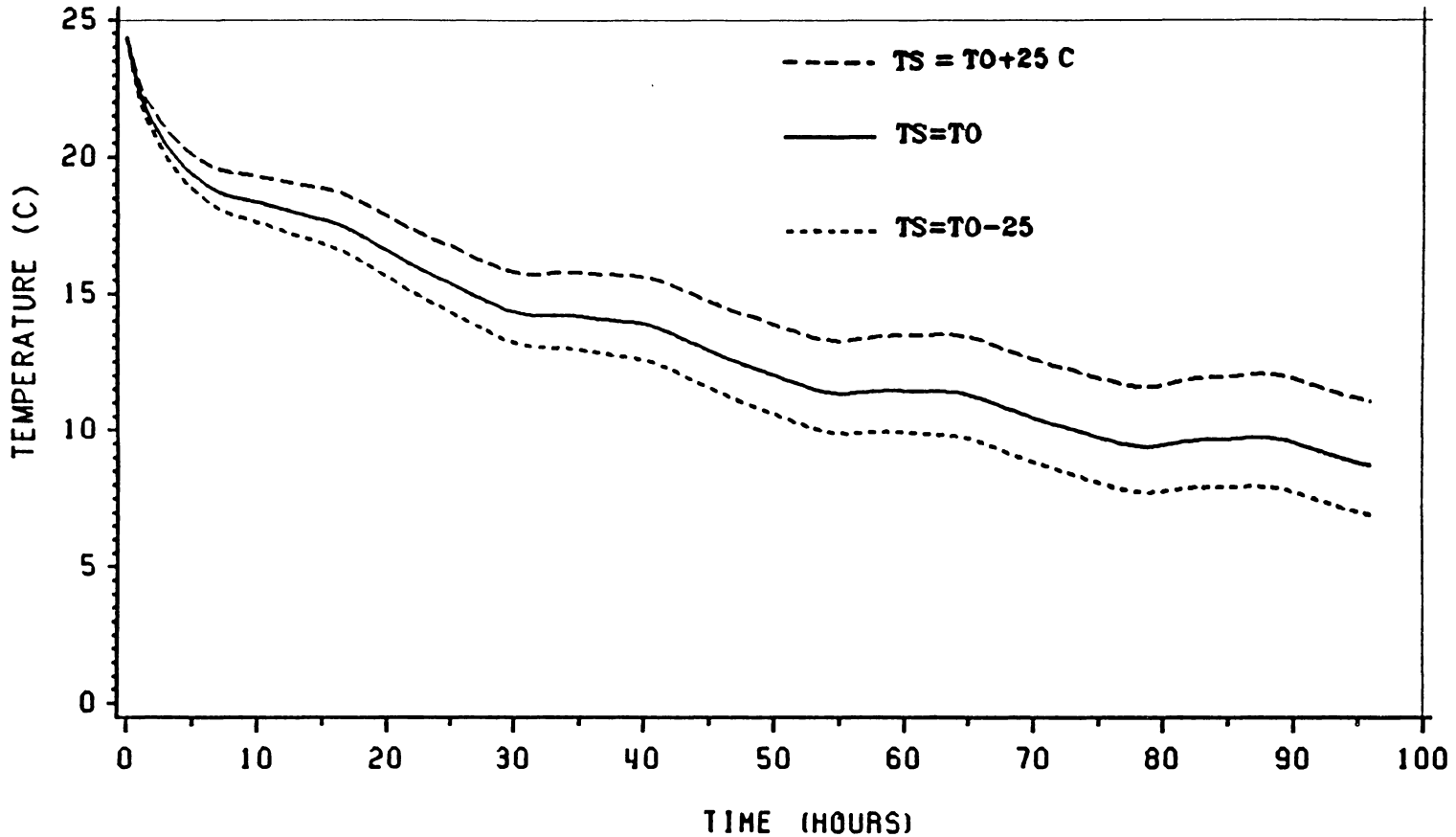

Figure 41. **Effect of Sky Temperature on the Interior Temperature of the House During A Winter Power Outage:** the outside temperature range is -10 to 0 C

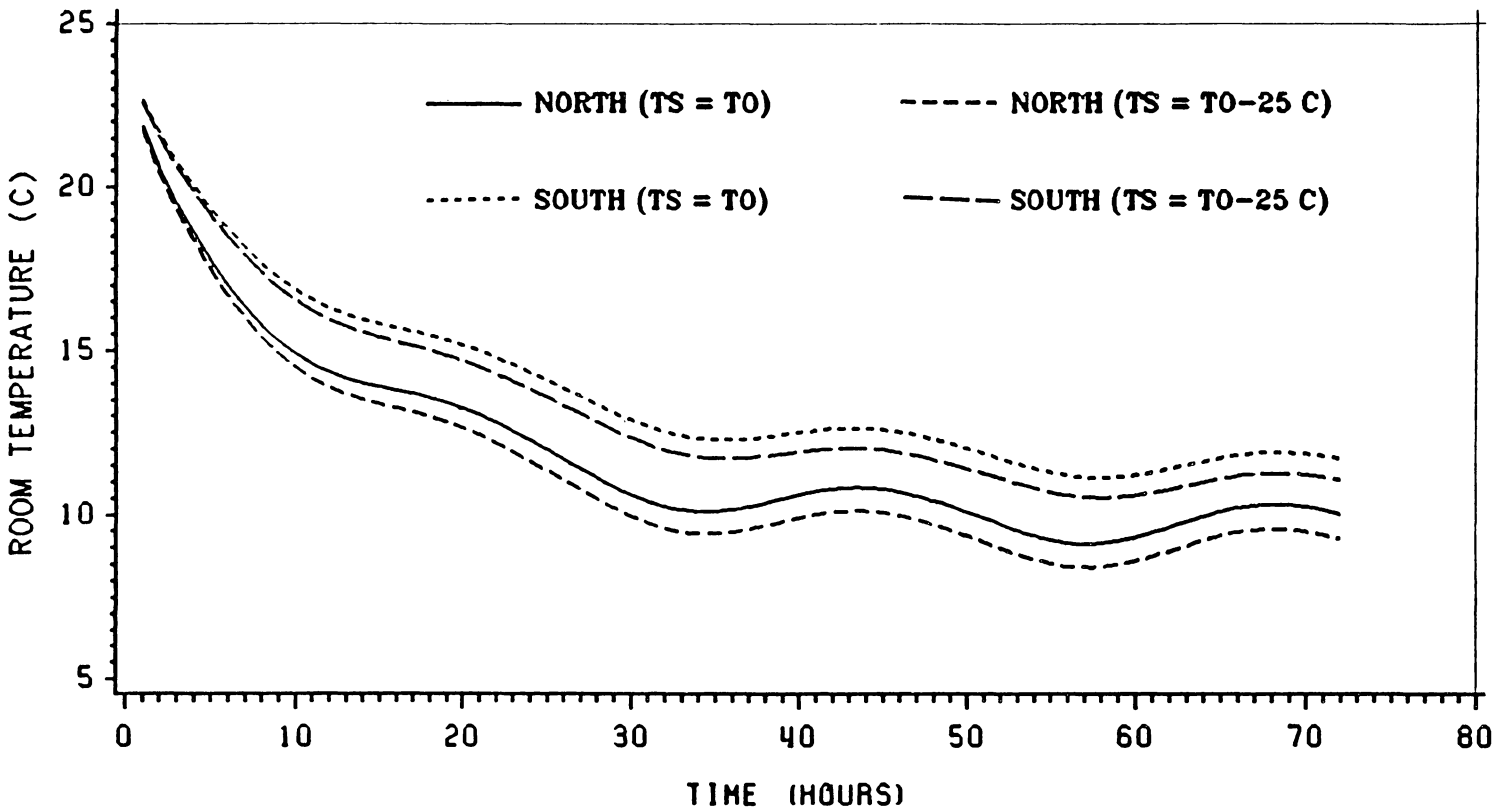

Figure 42. Effect of Sky Temperature on the Interior Temperature of the Building During A Winter Power Outage, Third Floor: the outside temperature range is -5 to 5 C

The effect of the sky temperature and exterior wall emissivity on the interior temperature was small considering the range of values used for these parameters. Next, the effect of radiation between interior walls on the room temperature is presented for both buildings during winter and summer power outages.

MRT RADIATION

The effect of including radiation between interior walls on the interior room temperature response is examined for a typical residential house and a commercial building. In Fig. 43, the interior temperature of the house taking into account and neglecting radiation heat transfer inside each room is plotted during a summer power outage. These results are obtained by setting the heat extraction rate to zero after the required histories are established. This procedure corresponds to letting the inside temperature drift. It is clear that internal radiation has a negligible effect on the temperature response. Internal radiation, also, had a negligible effect on the temperature response for the winter season power outage calculations. Radiation between interior walls was retained in the simulations, even though this graph justifies omitting it.

The effect of radiation between interior walls on the room temperature was investigated for the commercial building. Simulations during summer and winter power outages were conducted considering and neglecting radiation. Both 24.4 and 30 C initial temperatures were used for the summer power outage. The effect of neglecting radiation was negligible in both cases. In Fig. 44, the temperature profiles of the rooms on the north and central sides are given for a summer power outage with and without radiation for the third floor. In this figure, the initial temperature was 30 C. Winter simulations were also conducted and the effect of neglecting radiation between interior walls on the room temperature was negligible.

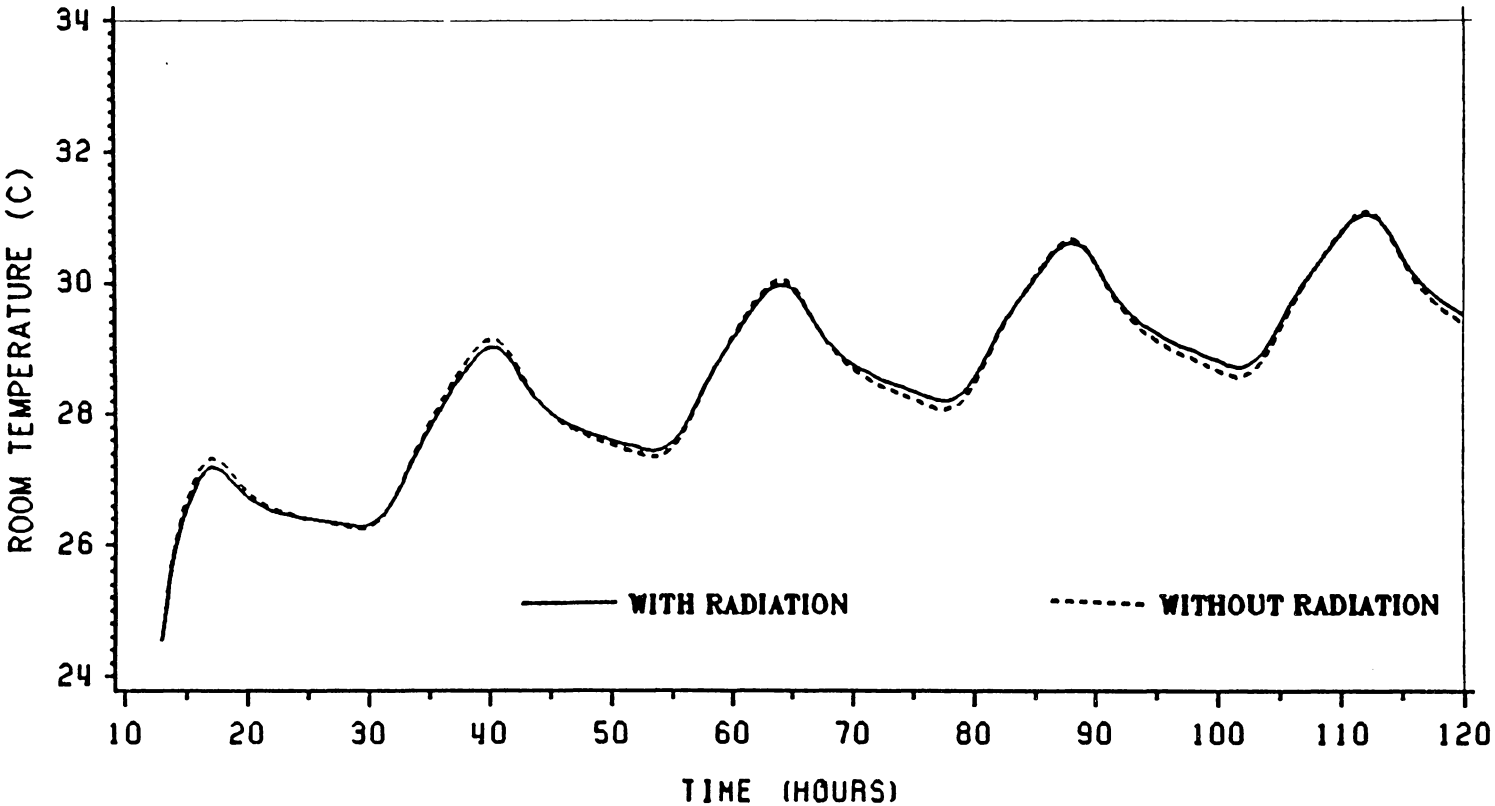

Figure 43. Temperature Response of the House With and Without Interior Radiation; the outside temperature range is 25 to 35 C

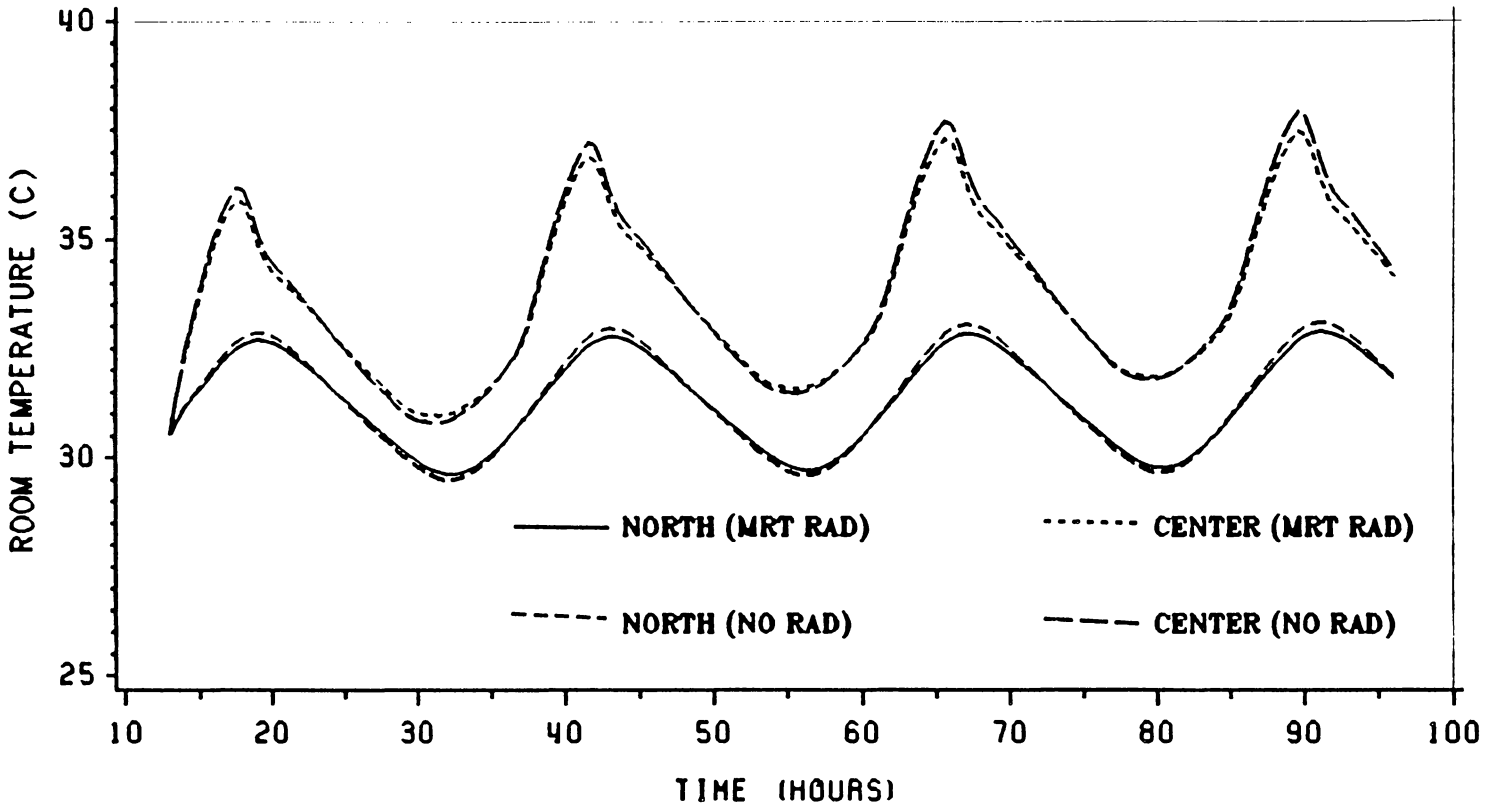

Figure 44. Temperature Response of the Building With and Without Interior Radiation, Third Floor: the outside temperature range is 25 to 35 C

An important parameter in the energy calculations is presented next. The effect of thermal mass in walls is shown for the house and commercial building during winter and summer power outages.

WALL MASS

The effect of wall mass on the heating and cooling loads in buildings has been studied extensively by researchers [1-25]. In this section, the effect of thermal mass in exterior and interior walls on the temperature drift in buildings is examined for summer and winter power outages.

EXTERIOR AND INTERIOR WALL MASS OF THE HOUSE

Two types of exterior and interior walls were considered for the winter and summer simulations. These walls are described in Table 15. The outside wall was changed from the original state (the original outside wall is designated as the "INS OUT" type) to a thermally massive wall (designated as "MASS OUT"). The interior partitioning of the house was changed from the light and insulated ("INS IN") to more thermally massive walls ("MASS IN").

For summer and winter time conditions, the following cases were examined:

. Light and insulated exterior and interior walls
. Thermally massive exterior walls and light and insulated interior walls
. Thermally massive exterior and interior walls
. Light insulated exterior walls and thermally massive interior walls.

Each case was simulated with identical parameters. These parameters are the outside weather, solar load on the house and through windows, infiltration, ground temperature, sky temperature, etc.. The only variation between each case was the wall construction. The

Table 15. Layer Description of the Four Walls Used in the Simulations

WALL	LAYER DESCRIPTION	ΔX	k	α	R	R_{total}
Light Insulated Outside Wall	Gypsum board Batt insulation Air space Brick	0.031 0.302 - 0.25	0.12 0.025 - 0.42	0.00839 0.0625 - 0.0175	0.91	13.8
Thermal Massive Outside Wall	Gypsum board Concrete Block Brick	0.031 0.3 0.25	0.12 1.0 0.42	0.00839 0.0357 0.0175		1.15
Light Insulated Inside Wall	Gypsum board Batt insulation Gypsum board	0.031 0.25 0.031	0.12 0.025 0.12	0.00839 0.0625 0.00839		10.5
Light Massive Inside Wall	Gypsum board Concrete Block Gypsum board	0.031 0.3 0.031	0.12 1.0 0.12	0.00839 0.0357 0.00839		0.76

(multiplication factor to SI)

ΔX : thickness (ft) 0.304 to (m)

k : thermal conductivity (Btu/h.ft.F) 1.731 to (W/m•K)

ρ : specific heat (lb/ft^3) 16.01 to (kg/m^3)

C : specific heat (Btu/lb•F) 4.186 to (W/m•K)

α : thermal diffusivity (ft^2/s) 0.093 to (m^2/s)

R : thermal resistance ($h•ft^2•F/Btu$) 0.176 to ($K•m^2/W$)

simulation was carried out by setting the interior temperature to 24.4 C during the first two days to establish a history. The interior temperature was then calculated for the third day with the heat extraction rate set to zero. Figure 45 shows results for the four cases with a power outage occuring at noon on the third day and lasting 24 hours. The thermal response of the house was improved by a maximum of 1.0 C, at the fifth hour (5:00 PM) of simulation, after changing the light insulated interior walls ($R = 0.85 m^2k/W$) to thermally massive and uninsulated (R=0.13), regardless of the exterior wall type. For the night time simulation (11:00 PM to 6:00 AM), the interior wall mass did not affect the temperature response. The effect of the exterior wall was, as expected, evident when a well-insulated (R=2.44) wall replaced the thermally massive and uninsulated (R=0.21) exterior structure. A summer simulation with a midnight power outage was also performed. The interior wall mass did not affect the temperature response for the first eight hours. This suggests that the temperature response is affected only by the R value of the outside wall during night time summer power outages. The interior wall mass had an effect on the temperature response during the day only. The thermally massive and uninsulated interior walls kept the inside temperature 0.5 to 1.0 C lower than light and insulated interior walls. The same trend is not present during a winter season power outage. In the latter case, the interior wall mass affects the temperature response through the 24 hour analysis, as shown next.

The same four cases are used for the winter season simulation. All other parameters are kept the same for each case in order to show the effect of the type and location of wall material on the temperature response. The outside temperature profile used for the three days of simulations was -5 to 5 C. The solar load on the house was zero. The interior temperature is held at 24.4 C during the first two days. At the start of the third day, the temperature is allowed to drift with no heating energy supplied. These cases simulate power outage with no solar gain during a winter season. Figure 46 shows the results for four cases corresponding to different wall materials. As expected, a larger initial drop in temperature is observed for the thermally massive and uninsulated exterior wall curves compared to the light and insu-

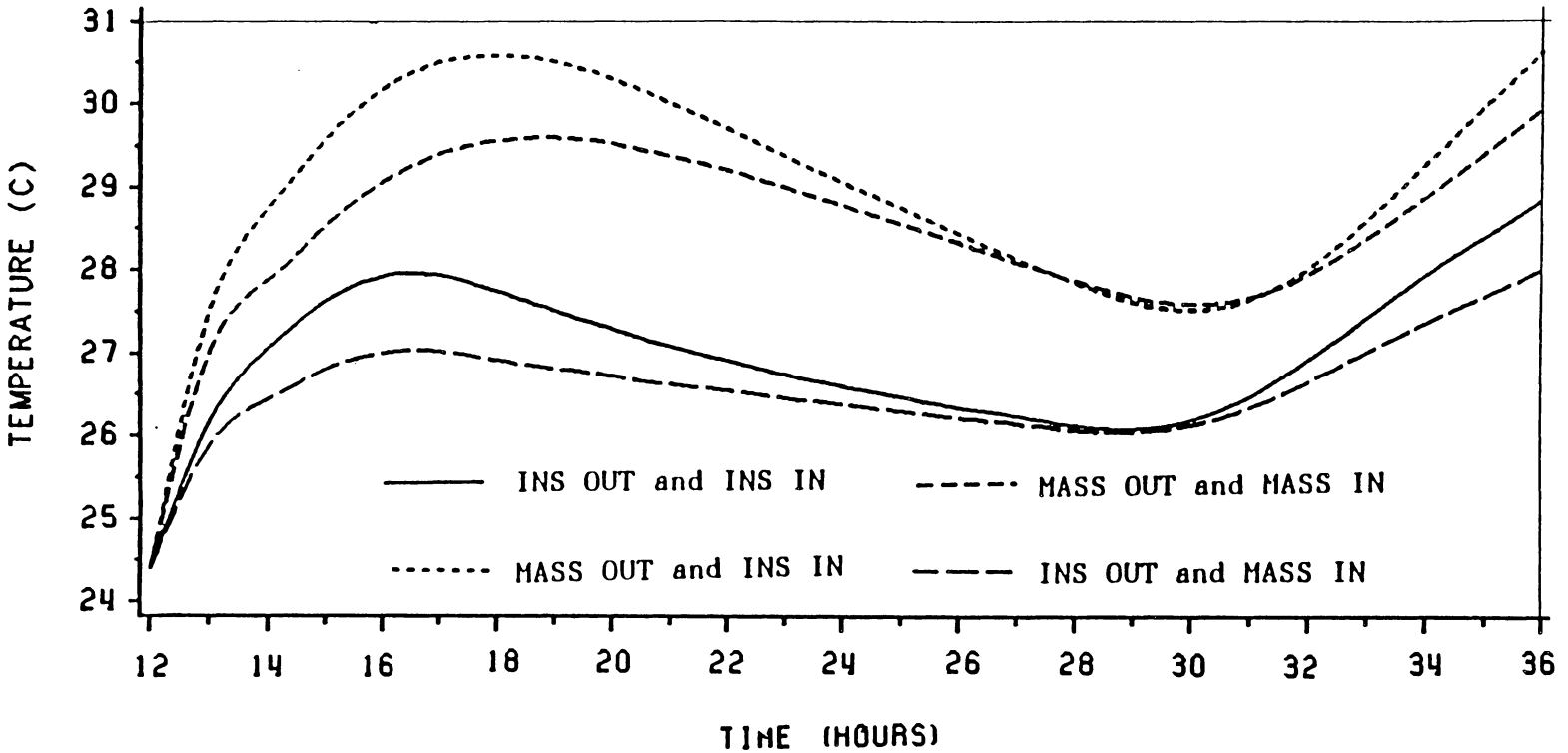

Figure 45. **Effect of Thermal Mass on the Temperature Response of the House During a Summer Power Outage:** the outside temperature range is 25 to 35 C

lated exterior walls cases. The light and well-insulated exterior walls and thermally massive and uninsulated interior partitioning showed the least initial drop of internal temperature (1.0 C) and resulted in maintaining the best overall temperature response. Changing the interior partitioning to light and insulated caused an initial drop of 1.4 C. Cases 2 (MASS OUT and INS IN) and 3 (MASS OUT and MASS IN) showed initial drops of 4.4 and 3.4 C, respectively. During the winter season, changing the interior partitioning from insulated lightweight to uninsulated massive maintained consistently a 2.0 C higher temperature for the remaining 20 hour of simulation for a well-insulated lightweight exterior wall. For a thermally massive exterior wall, changing the interior partitioning from insulated lightweight to uninsulated massive resulted in a 3.0 C higher temperature during the first 10 hours. A 1.0 to 2.0 C higher temperature was observed for the remainder of the simulation.

EXTERIOR WALL MASS OF THE BUILDING

The effect of thermal mass in exterior walls on the temperature response of buildings during winter and summer power outages is presented next. The three R values of the exterior walls used in the simulations are 0.46, 1.4, and 2.46 m^2K/W. For each R value, the wall material was changed from light to thermally massive using concrete instead of insulation layers. The wall descriptions are given in Table 16. Since the building is composed of three floors and 36 rooms per floor, numerous plots would be required for a full presentation of the temperature response of individual rooms. Therefore, the presentation of figures is limited to a small number of rooms and stating the overall temperature response of each floor.

For exterior walls with R-values of 0.459 m^2K/W, the effect of thermal mass on the interior temperature are presented during summer and winter power outages. In Fig. 47, the temperature response of the rooms on the north and central sides of the first floor are presented for massive and light exterior walls. Changing the exterior walls of the building from light to thermally massive, at the same low R value, decreased the interior temperature of all rooms

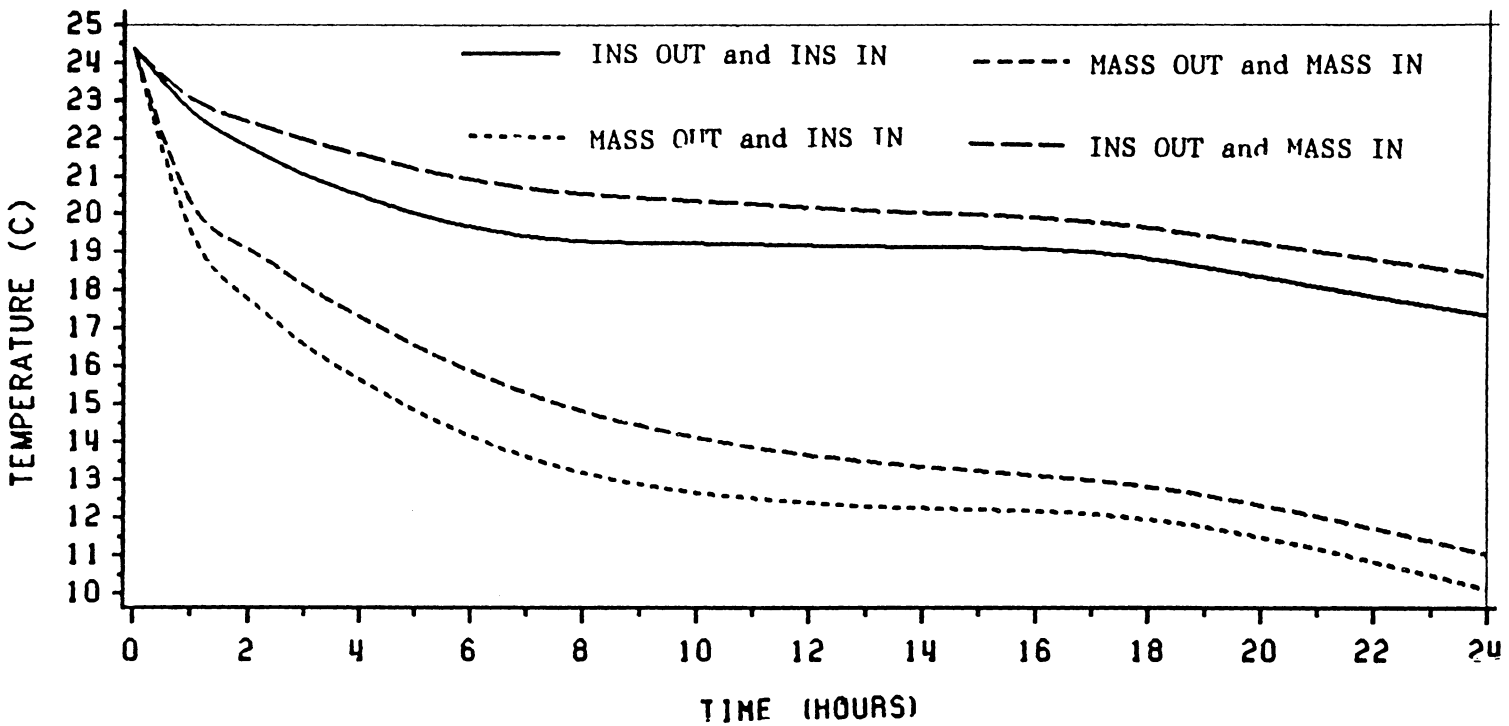

Figure 46. **Effect of Thermal Mass on the Temperature Response of the House During a Winter Power Outage:** the outside temperature range is -5 to 5 C

Table 16. Layer Description of the Three Walls Used in the Simulations

DESCRIPTION OF LAYERS	LAYER No.	ΔX (m)	k (W/m.C)	$\alpha 10^5$ (m^2/s)	R_{total} (m^2C/W)
Wall 1 (massive)					
Gypsum Board	1	0.012	0.16	4.8	
Concrete	2	0.15	0.5	41.5	
Brick	3	0.06	0.72	130.0	
					0.46
Wall 1 (light)					
Gypsum Board	1	0.012	0.16	4.8	
Insulation	2	0.01	0.043	580.6	
Siding Wood	3	0.026	0.17	4.8	
					0.46
Wall 2 (massive)					
Gypsum Board	1	0.012	0.16	4.8	
R-0.88 Air Space	2				
Concrete	3	0.18	0.5	41.5	
Brick	4	0.06	0.72	130.0	
					1.4
Wall 2 (light)					
Gypsum Board	1	0.012	0.16	4.8	
Insulation	2	0.051	0.043	580.6	
Siding Wood	3	0.026	0.17	4.8	
					1.4
Wall 3 (massive)					
Gypsum Board	1	0.012	0.16	4.8	
Insulation	2	0.083	0.043	580.6	
Concrete	3	0.186	0.5	41.5	
Brick	4	0.06	0.72	130.0	
					2.46
Wall 3 (light)					
Gypsum Board	1	0.012	0.16	4.8	
Insulation	2	0.096	0.043	580.6	
Siding Wood	3	0.026	0.17	4.8	
					2.46

and floors by an average 1.0 C during the day and 0.5 C during the night of a summer power outage. For the winter season power outage, and for the same exterior wall R value, the temperature drift after a midnight power outage is plotted in Fig. 48, for the north and south side rooms of the first floor. Changing the exterior wall mass from light to thermally massive, at low R value, increased the temperature of all rooms on all floors by an average of 2.0 C during the night and 0.5 C during the day of the power outage.

Changing the exterior wall mass from light to thermally massive is investigated for walls with R-values of 1.4 and 2.46 m^2K/W . Changing the exterior wall mass from light to thermally massive did not alter the interior temperature response of the building significantly.

EXTERIOR WALL RESISTANCE

From the simulations presented in the preceding section, the temperature difference between rooms at the same floors varied significantly for different exterior wall R-values. For the exterior walls with an R-value of 0.46 m^2K/W, the temperature variation between the rooms was 1.5 C on the first floor, 2.5 C on the second floor, and 1.0 C on the third floor. For the exterior walls with an R-value of 2.46 m^2K/W, the temperature variation between the rooms was 1.0 C on the first floor, 2.0 C on the second floor, and 0.5 C on the third floor. For the summer power outage, the difference between the extremes in the room temperatures on each floor of the building was not affected by the exterior wall thermal resistance. This result is expected since the solar load altered the temperature distribution in the building considerably. The effect of interior wall mass on the temperature response in buildings is presented next.

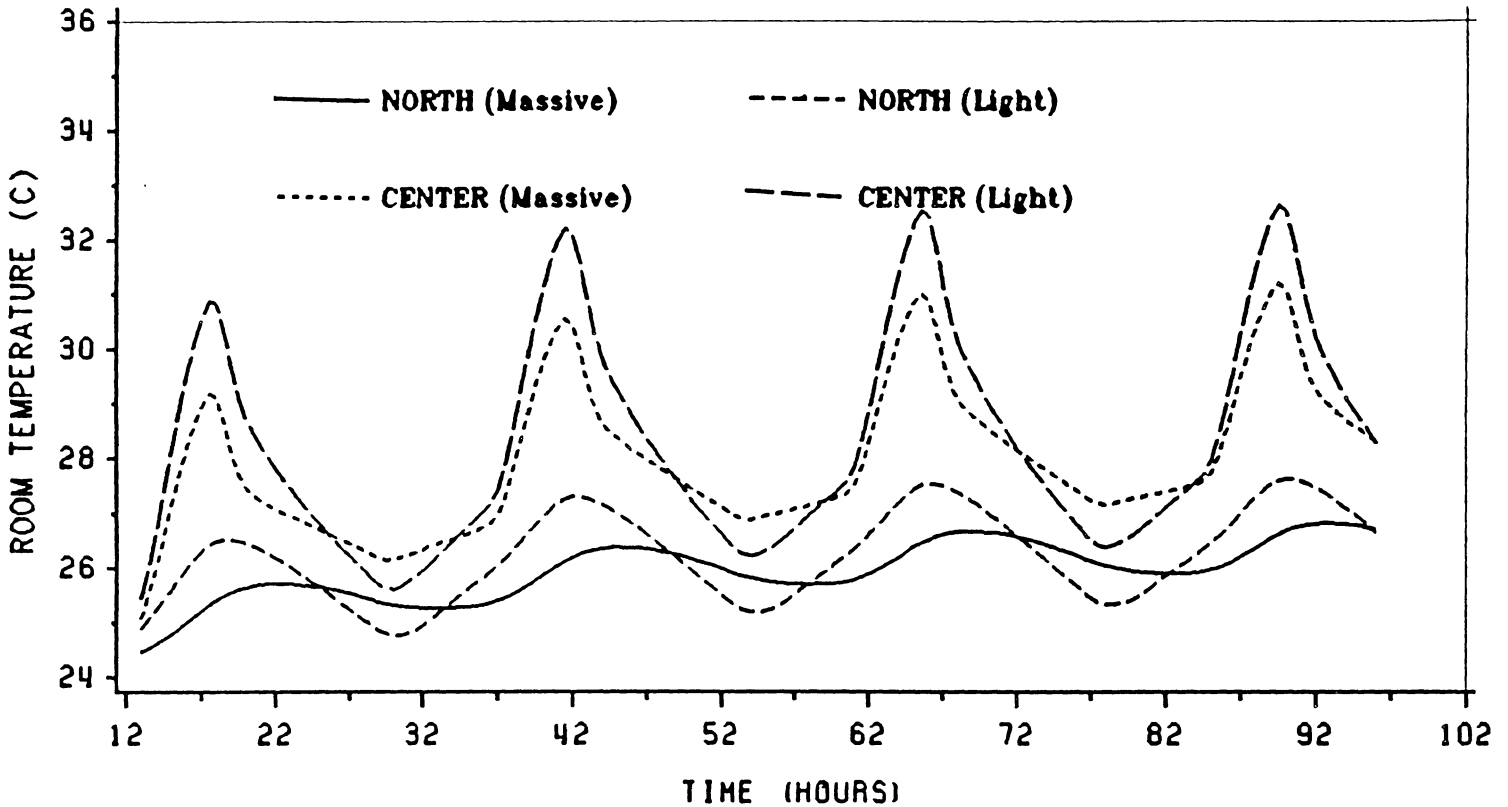

Figure 47. **Effect of The Exterior Wall Mass on the Temperature Response of the Building During a Summer Power Outage, First Floor:** the outside temperature range is 25 to 35 C and R = 0.459 m^2K/W

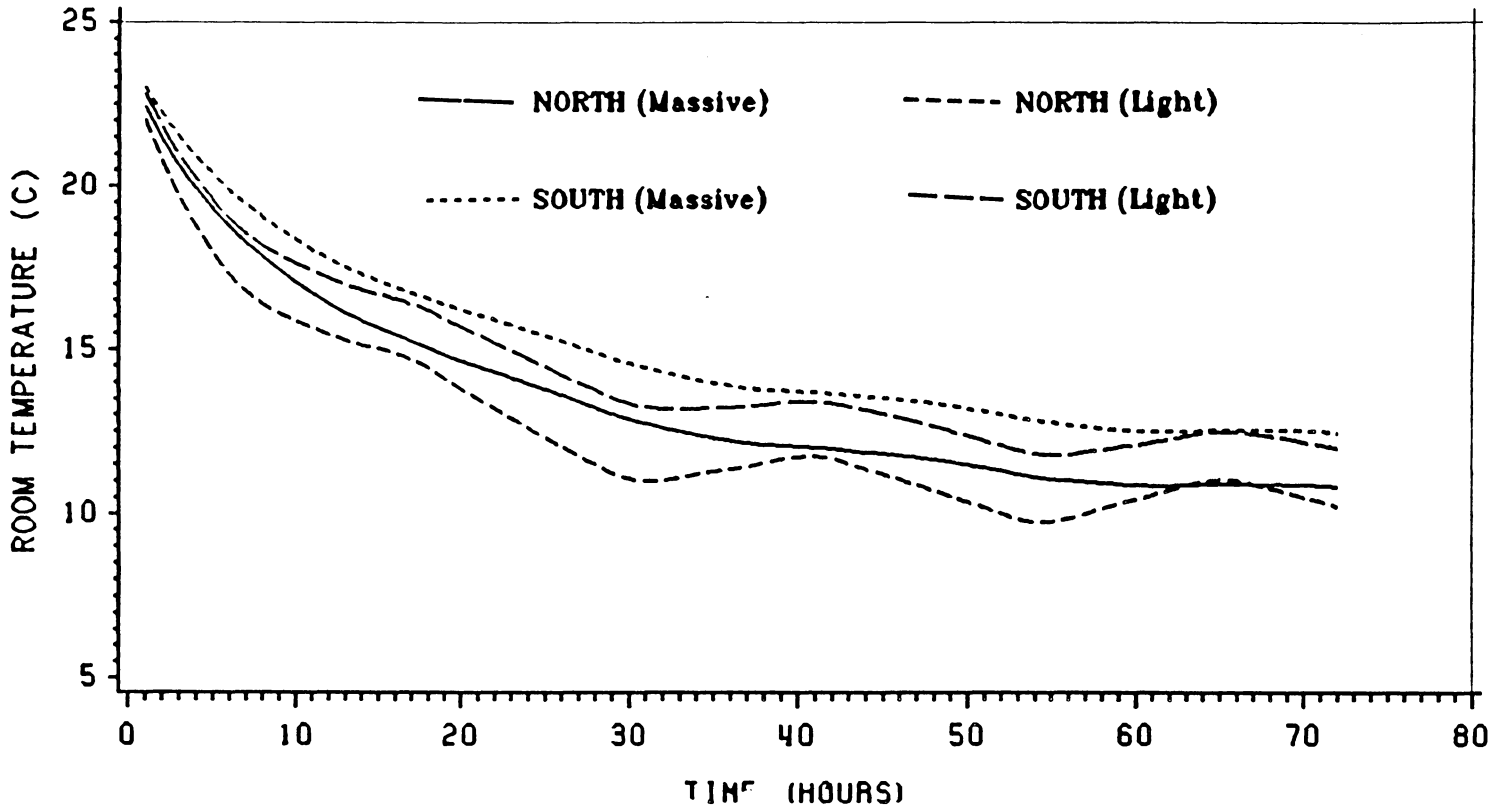

Figure 48. Effect of The Exterior Wall Mass on the Temperature Response of the Building During a Winter Power Outage, First Floor: the outside temperature range is -5 to 5 C and R = 0.459 m^2K/W

INTERIOR WALL MASS OF THE BUILDING

The effect of changing the interior walls from light to thermally massive, at the same R value, is examined for winter and summer power outages. In Fig. 49, the temperature profiles of the rooms on the north and central sides of the third floor are given for light and massive interior walls. For the interior walls with 0.31 m^2K/W R values, changing the wall mass from thermally massive to light (summer power outage) increased the temperature in all rooms by an average 1.0 C for the day time. For the night-time simulations, changing the interior walls from thermally massive to light had a negligible effect on the interior temperatures. For the interior walls with 1.34 m^2K/W R values, changing the wall mass from thermally massive to light increased the temperatures of all rooms by an average 1.0 C after 5 hours and for the duration of the power outage.

For a winter power outage, changing the wall mass from light to thermally massive, at the same R values, affected the temperature response considerably. In Fig. 50, the north and south side room temperature profiles of the third floor are given for 0.31 m^2K/W interior walls. An average 2.0 C lower temperatures after 5 hours and for the duration of the power outage was obtained by changing the interior walls from light to thermally massive. For 1.34 m^2K/W interior walls, the rooms exposed to the outside had 2.0 C lower temperatures after 5 hours and for the duration of the power outage when the interior walls were changed from light to more thermally massive. For internal rooms, changing the interior wall mass from light to thermally massive decreased the temperature profile by 3.5 C consistently after 5 hours of power outage.

INSULATION POSITION IN EXTERIOR WALLS

Two cases are presented here to show the effect of changing the insulation position from the interior to the exterior side of the wall mass. In Table 17, the walls used in the power

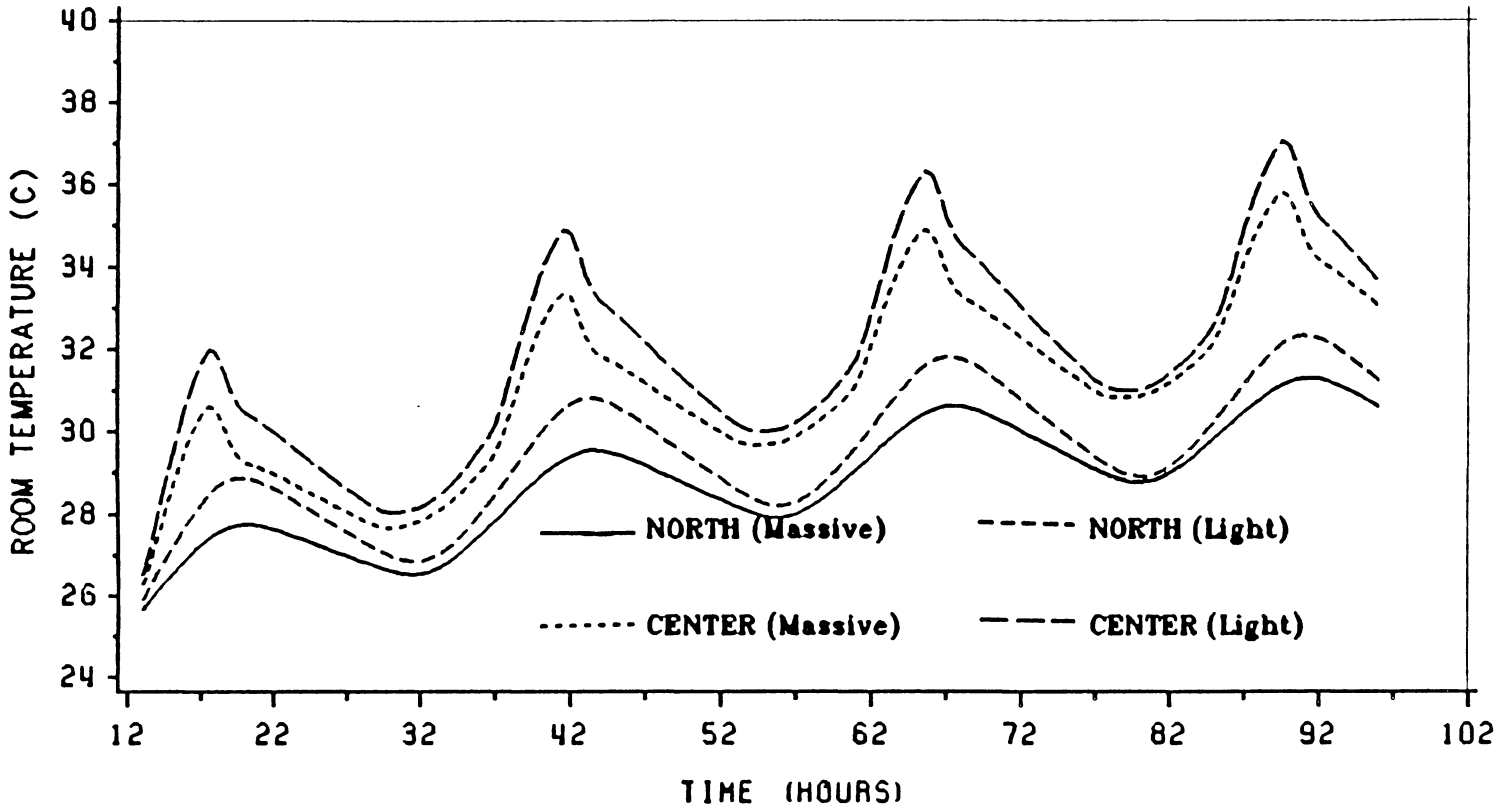

Figure 49. Effect of the Interior Wall mass on the Temperature Response of the Building During a Summer Power Failure, Third Floor: the outside temperature range is 25 to 35 C and R = 0.31 m^2K/W

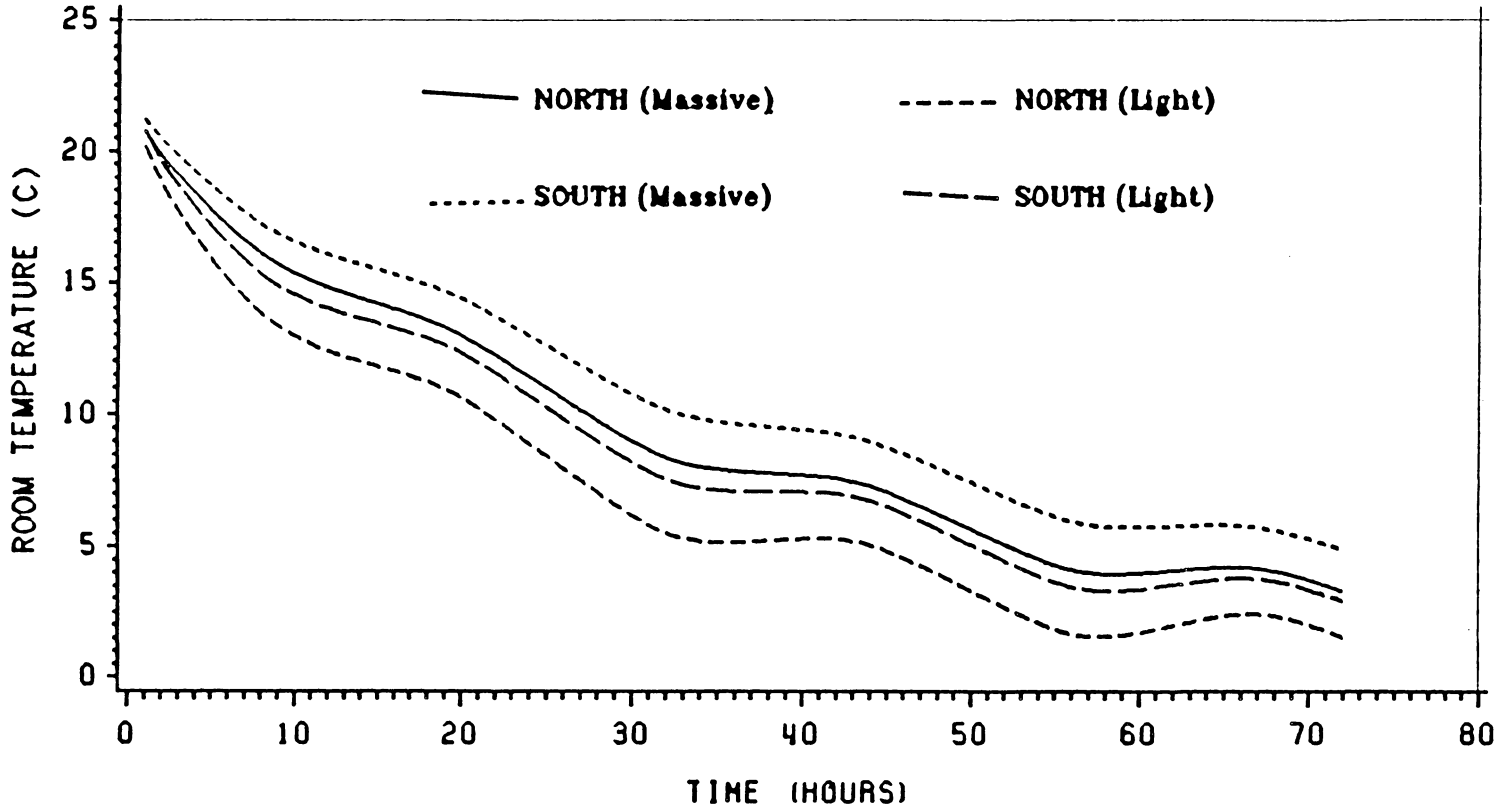

Figure 50. Effect of the Interior Wall mass on the Temperature Response of the Building During a Winter Power Failure, Third Floor: the outside temperature range is -5 to 5 C and R = 0.31 m^2K/W

outage simulations are described. The summer application was based on setting the heat extraction rate to zero and keeping all other parameters constant. The temperature response is plotted for both wall configurations in Fig. 51. Placing the insulation toward the outside rather than the inside of the wall mass reduced the temperature buildup by 0.5 to 1.0 C after three hours and for the remainder of the power outage. As shown in Fig. 52, a consistently better performance was obtained during the winter season by placing the insulation on the outside of the wall mass. The interior temperature of the house was 1.25 C consistently lower when the insulation was placed on the outside instead of the inside of the exterior wall mass.

Next, the effect of the insulation position in the exterior walls is examined for the commercial building during winter and summer power outages. In Fig. 53, the temperature profiles of the north and central side rooms (third floor) are given with the insulation placed on the outside and inside of the exterior wall mass for a summer power outage. Placing the insulation on the outside of the exterior wall mass decreased the temperature of all rooms in the building by 1.0 C after 8 hours of the power outage. For a winter season power outage, the temperature profiles of the north and south side rooms are shown in Fig. 54 for the third floor. Placing the insulation on the outside rather than the inside of the wall mass increased the north and south side room temperatures by 2.0 and 1.5 C, respectively, after 10 hours of the power outage.

FURNISHINGS INSIDE ROOMS

The effect of furnishings on the interior temperature during summer and winter power outages is examined for buildings. In Fig. 55, the average interior temperature response of the house is given for 10, 35, and 60 kg of furnishings ($M_{f,r}$) in each room for a winter power outage. During a winter power outage, the average interior temperature of the house increased by 1 C after 5 hours of the power outage as $M_{f,r}$ is increased from 10 to 35 kg. The interior temperature of the house was further increased by 1 C as $M_{f,r}$ is increased from 35 to

Table 17. Layer Description of Exterior Walls of the House With different Insulation Location

WALL	LAYER DESCRIPTION	ΔX	k	α	R	R_{total}
Insulation on the Outside	Gypsum board	0.031	0.12	0.00839		
	Concrete Block	0.3	1.0	0.0357		
	0.302	0.025	0.0625			
	Brick	0.25	0.42	0.0175		13.2
Insulation on the Inside	Gypsum board	0.031	0.12	0.00839		
	0.302	0.025	0.0625			
	Concrete Block	0.3	1.0	0.0357		
	Brick	0.25	0.42	0.0175		13.2

(multiplication factor to SI)

ΔX : thickness (ft) 0.304 to (m)

k : thermal conductivity (Btu/h.ft^2.F) 1.731 to (W/m•K)

ρ : specific heat (lb/ft^3) 16.01 to (kg/m^3)

C : specific heat (Btu/lb•F) 4.186 to (W/m•K)

α : thermal diffusivity (ft^2/s) 0.093 to (m^2/s)

R : thermal resistance (h•ft^2•F/Btu) 0.176 to (K•m^2/W)

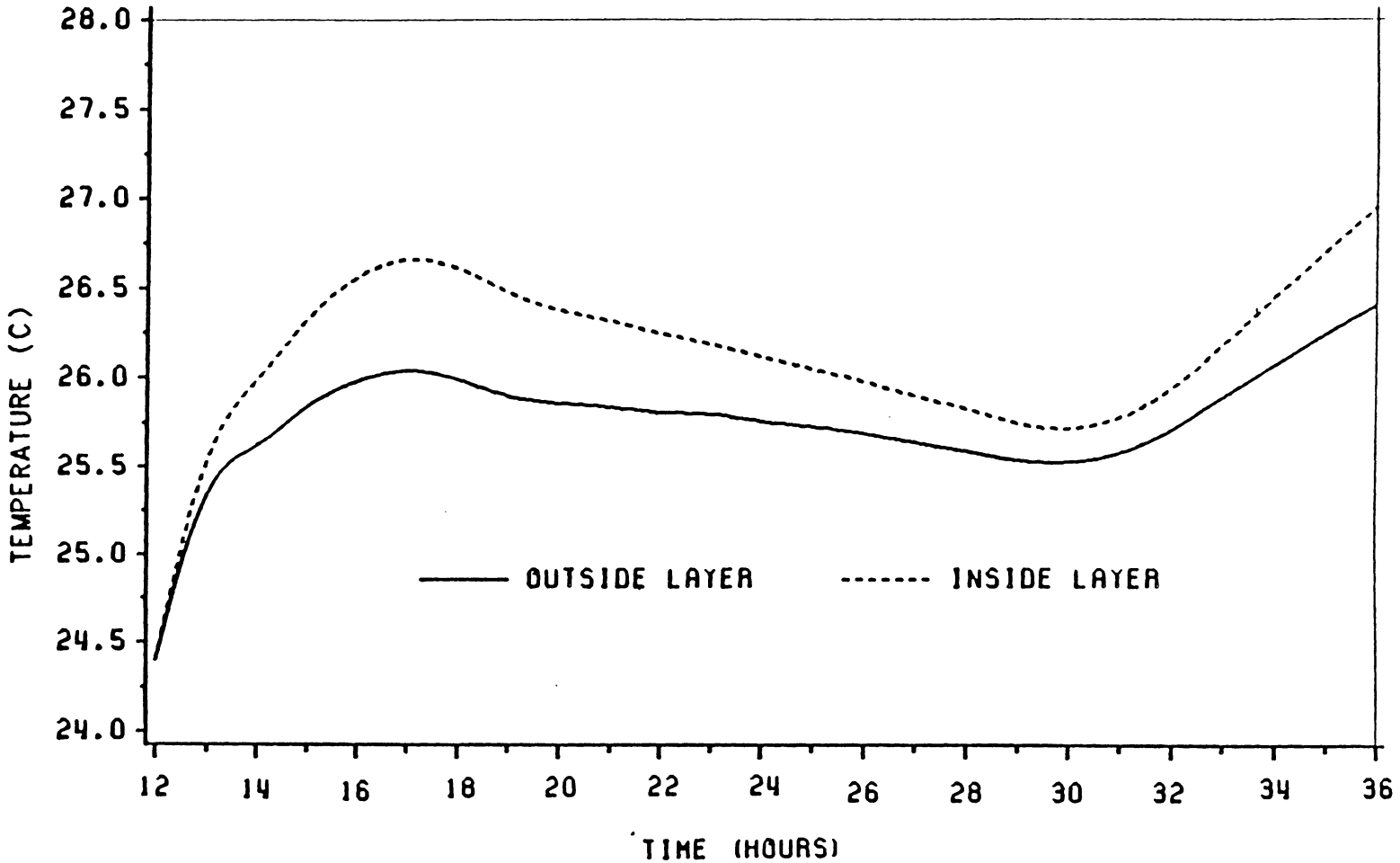

Figure 51. Effect of the Insulation's Location on the Temperature Response of the House During a Summer Power Failure: the outside temperature range is 25 to 35 C

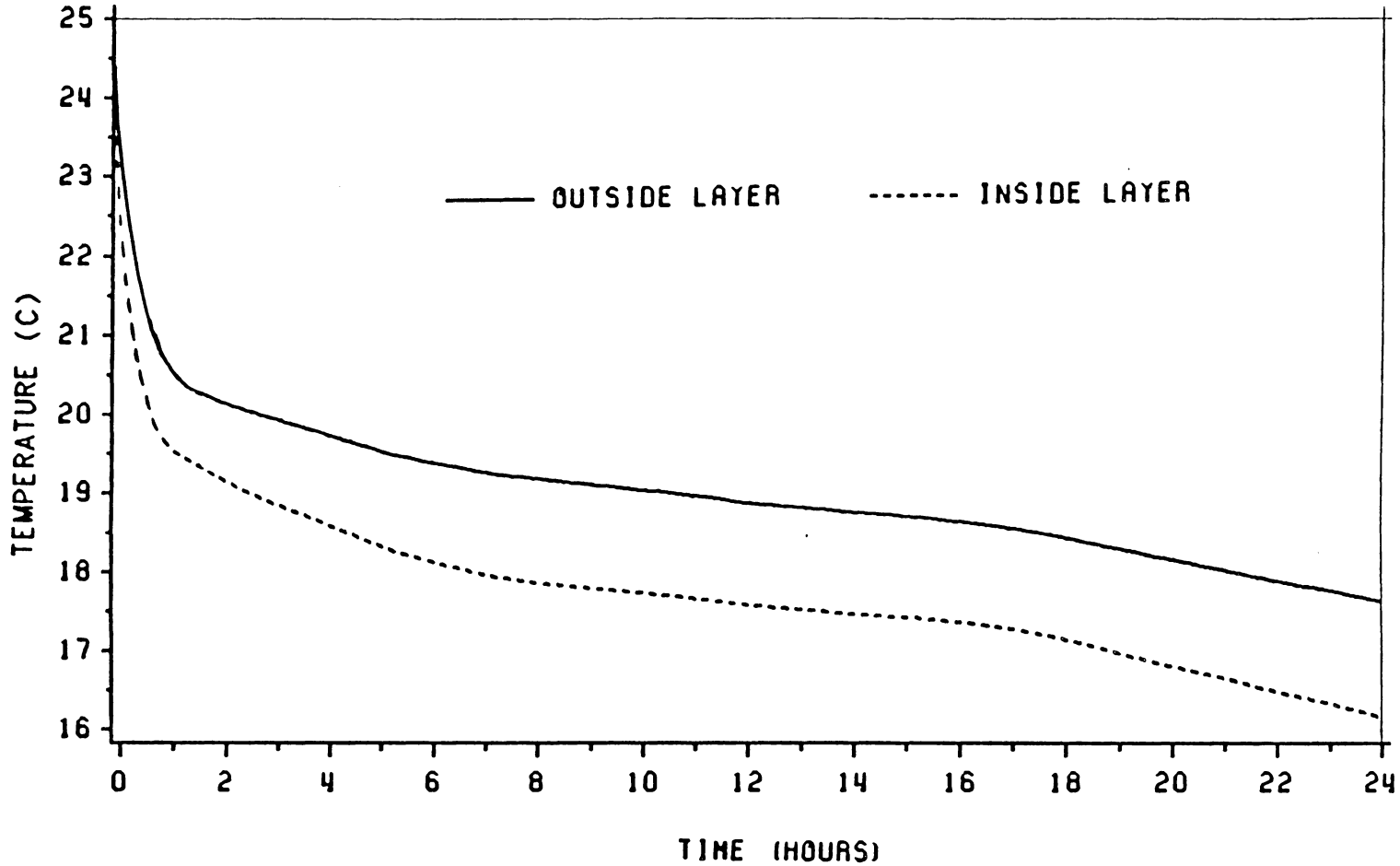

Figure 52. **Effect of the Insulation's Location on the Temperature Response of the House During a Winter Power Failure:** the outside temperature range is -5 to 5 C

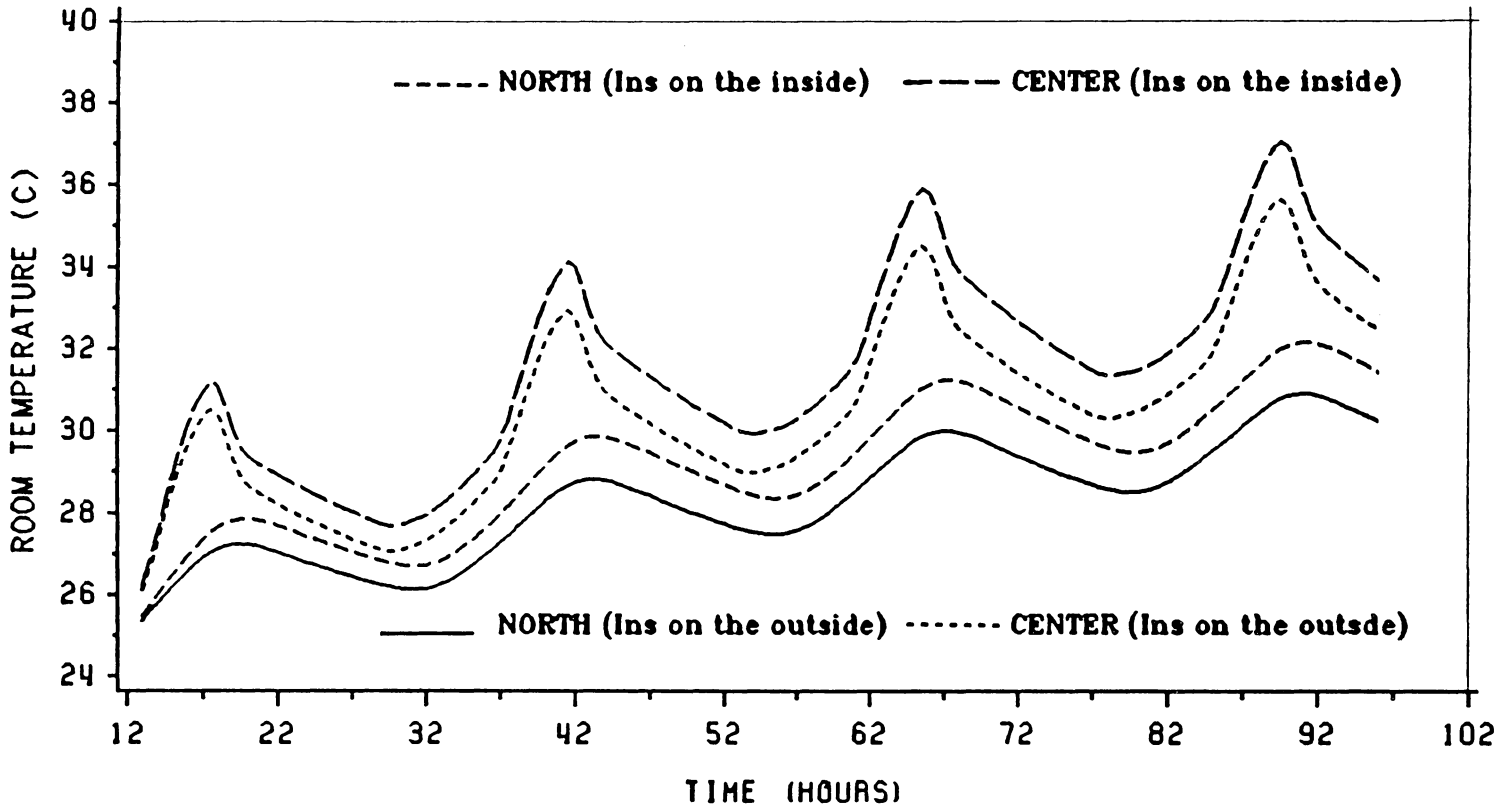

Figure 53. Effect of the Insulation's Location on the Temperature Response of the Building During a Summer Power Failure, Third Floor: the outside temperature range is 25 to 35 C

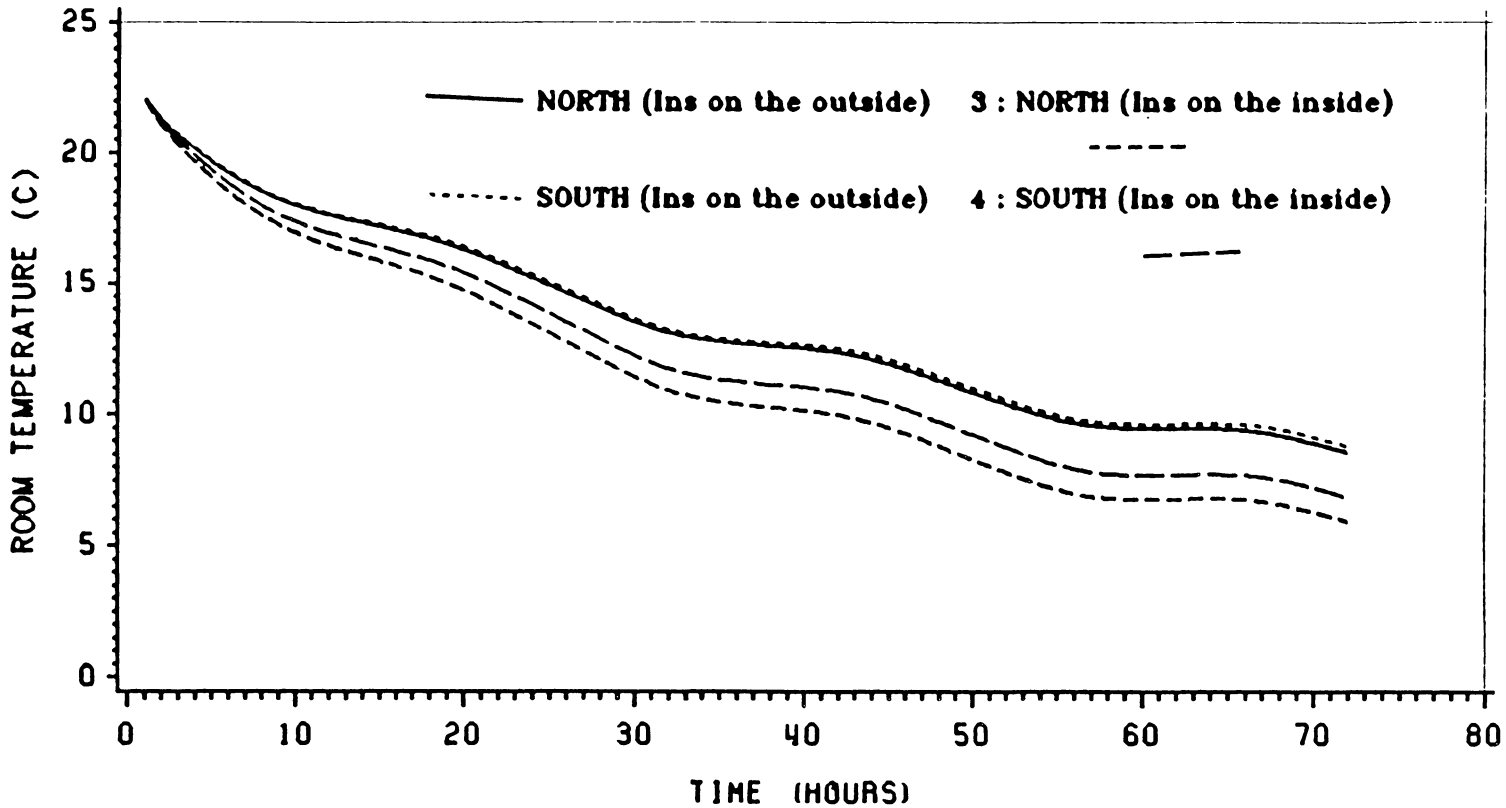

Figure 54. Effect of the Insulation's Location on the Temperature Response of the Building During a Winter Power Failure, Third Floor: the outside temperature range is -5 to 5 C

60 kg. For the summer power outage, increasing the interior furnishing mass from 10 to 35 kg for each room decreased the interior temperature of the house by an average 0.4 C after 3 hours of power outage simulations. A further increase of the furnishing mass from 35 to 60 kg per room decreased the interior temperature curve by an average 0.3 C.

For the building, 0, 10, and 50 kg of furnishings per room were included for each floor. Changing the mass of the furnishings from 0 to 10 kg/room had a negligible effect on the interior temperature response of the building during winter and summer power outages. As expected, changing the mass of the interior furnishings from 0 to 50 kg/room had a significant effect on the room temperatures during summer and winter power outages. A 0.5 C decrease in the room temperature was obtained for all rooms after 5 hours of power outage when the furnishing mass is increased from 0 to 50 kg/room. The exterior temperature profile was 25 to 35 C.

For the winter power outage, the effects of changing the furnishing mass from 0 to 50 kg/room is presented in Fig. 56 for the third floor. The temperature profiles throughout the rooms of the third floor increased by an average 1.0 C and a maximum of 1.5 C for the first ten hours of simulations when the interior furnishing mass was increased from 0 to 50 kg/room. For the first floor and during the first 40 hours of simulations, changing the furnishing mass from 0 to 50 kg/room increased the interior temperature by an average 1.0 C and a maximum of 1.5 C during the first 10 hours of the power outage. After 40 hours, the interior temperature increased by 0.5 C. Next, the infiltration leakage areas are changed to show their effect on the interior temperature of the building during summer and winter power outages.

INFILTRATION UNCERTAINTIES

Infiltration constitutes a large portion of the heat loss (heating season) or gain (cooling season) in buildings and houses. Since infiltration is the dominant mechanism affecting the

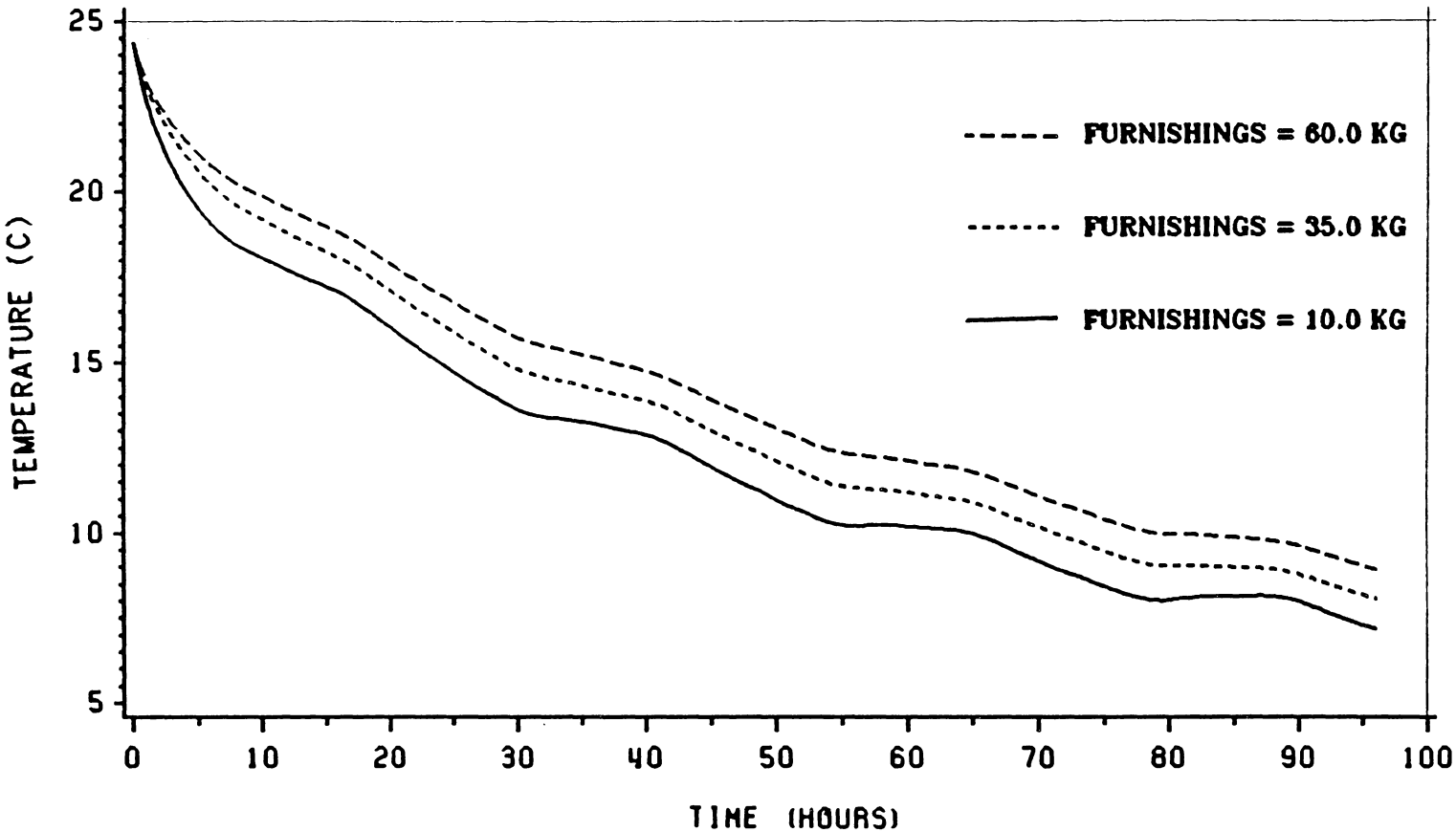

Figure 55. **Effect of the Furnishings on the Interior Temperature of the House During a Winter Power Outage:** the outside temperature range is -10 to 0 C

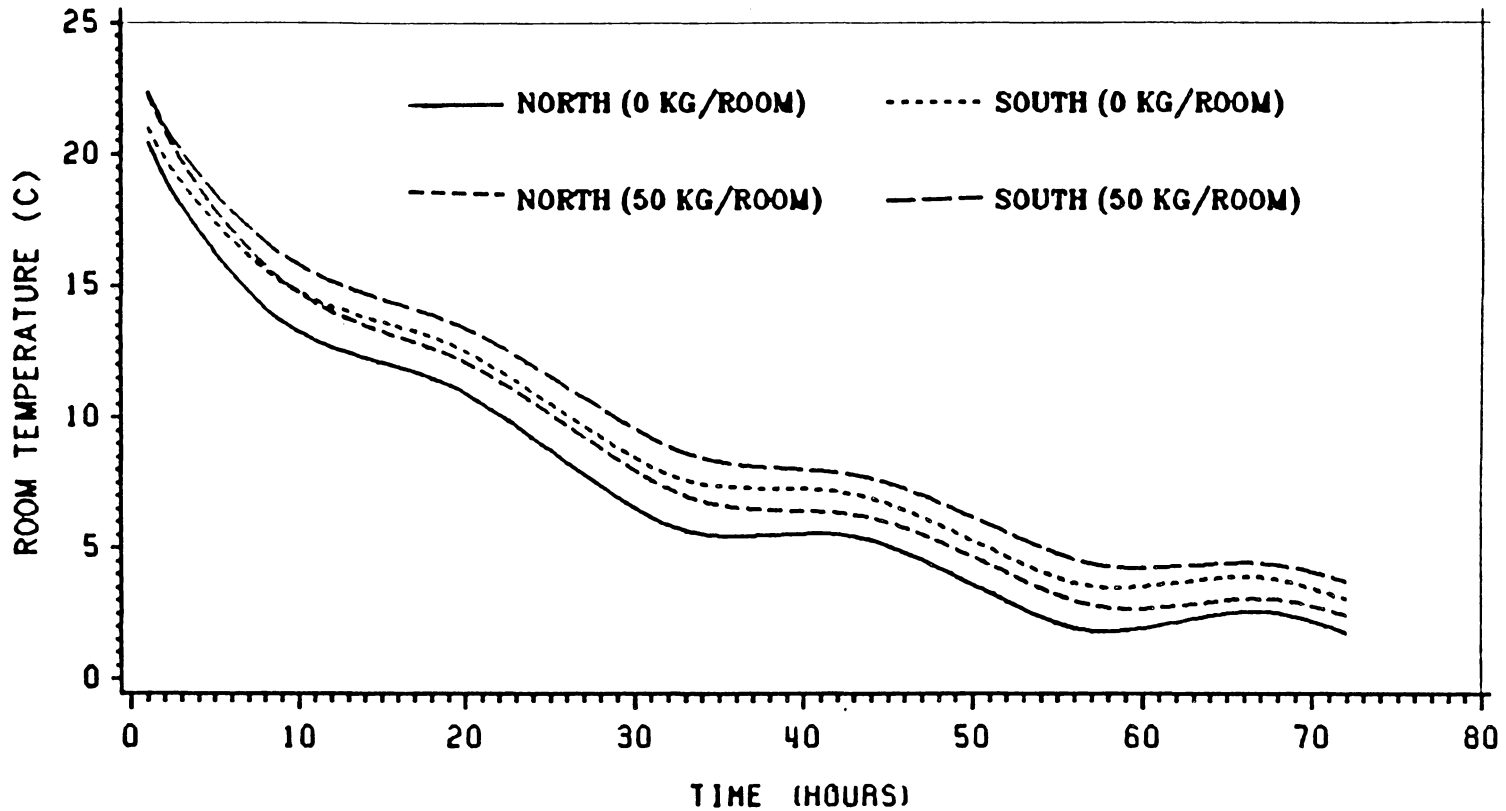

Figure 56. Effect of The Furnishings on the Interior Temperature of the Building During a Winter Power Outage, Third Floor: the outside temperature range is -5 to 5 C

temperature response during power outages, it was not included in the analysis presented earlier. In this section, different infiltration loads are examined for the house and the commercial building by varying the infiltration areas in exterior walls. The effect of the infiltration on the room temperature drift is presented.

In Fig. 57, the average interior temperature of the house is shown for various infiltration areas. These areas are 0.0, 0.132, 0.264, and 0.396 m^2. The leakage areas were distributed equally to each of the five rooms and the garage space. As expected, including infiltration altered the interior temperature response of the house considerably. For the summer power outage, increasing the overall leakage area of the house from 0.0 to 0.132 m^2 increased the interior temperature by 2 C during the day. For the night time, the effect was negligible. Further increase of the infiltration areas from 0.132 to 0.264, and finally to 0.396 m^2, increased the interior temperature of the house in the afternoon by 1.0 and 0.5 C, respectively. The infiltration loads of each room were similar since the room sizes did not differ largely and the infiltration areas were identical. The infiltration loads corresponding to the four infiltration areas are presented in Fig. 58 for the room on the south side of the house. As expected, the infiltration load was maximum during the first hour after the power outage.

For the winter season, the overall interior temperature of the house is plotted with and without infiltration in Fig. 59. The same leakage areas are used for the winter power outage simulations. The interior temperature of the house decreased by a maximum of 9.0 C during the night and 5.0 C during the day when the overall infiltration areas were changed from 0.0 to 0.132 m^2. Further increase of the infiltration areas to 0.264 and 0.396 m^2 decreased the interior temperature of the house by an additional 2.5 and 5.0 C, respectively.

The infiltration effect on the interior temperature in buildings is investigated by increasing the leakage areas in exterior walls. The pressure throughout each floor remained constant during the power outage. Since the pressure distribution in each floor is strongly coupled with the HVAC air supply, the pressure difference between rooms on the same floors was negligi-

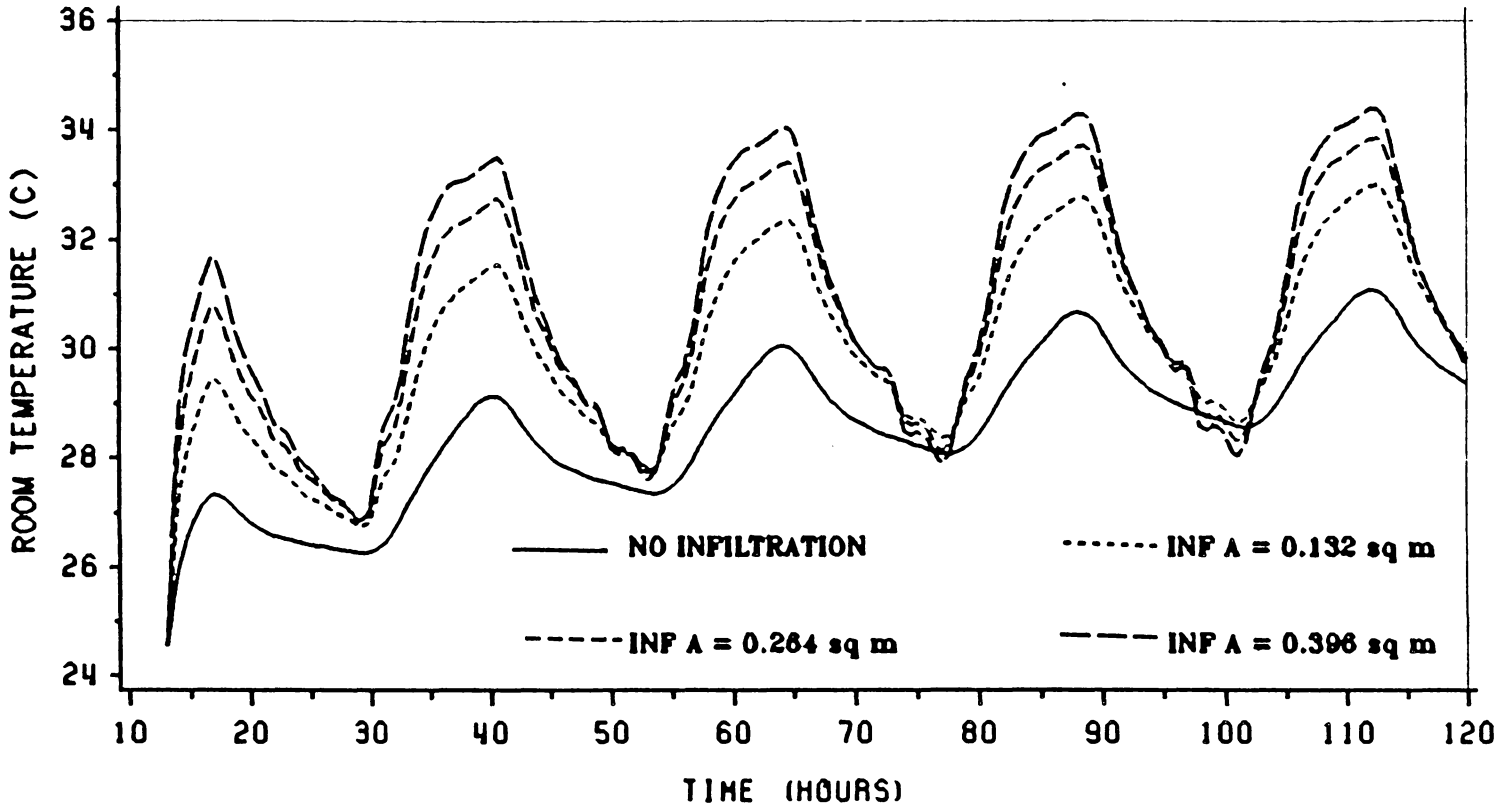

Figure 57. Temperature Response of the House With and Without Infiltration: the outside temperature range is 28 to 38 C

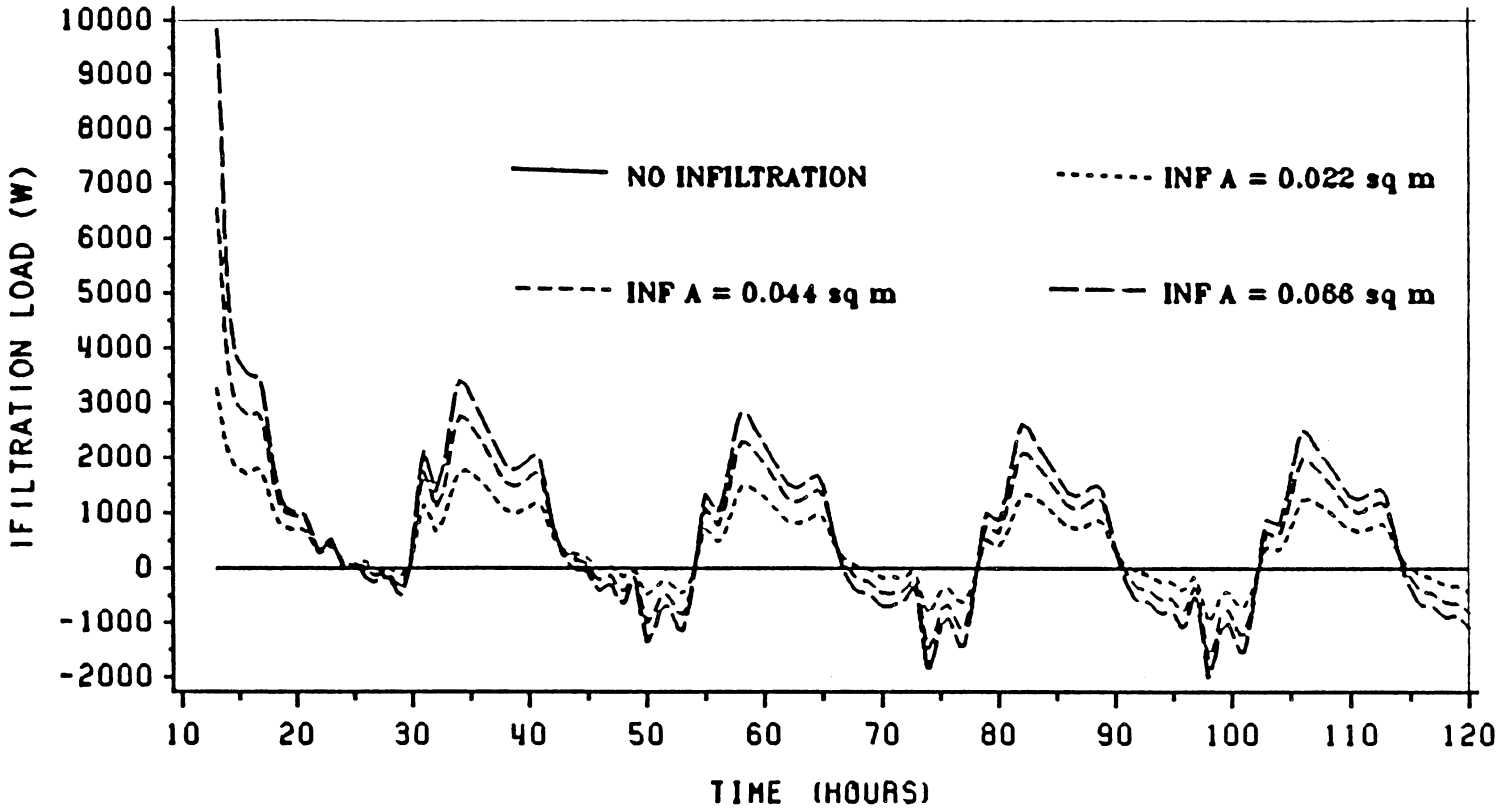

Figure 58. Infiltration Loads of the South Side Room in the House: the outside temperature range is 28 to 38 C

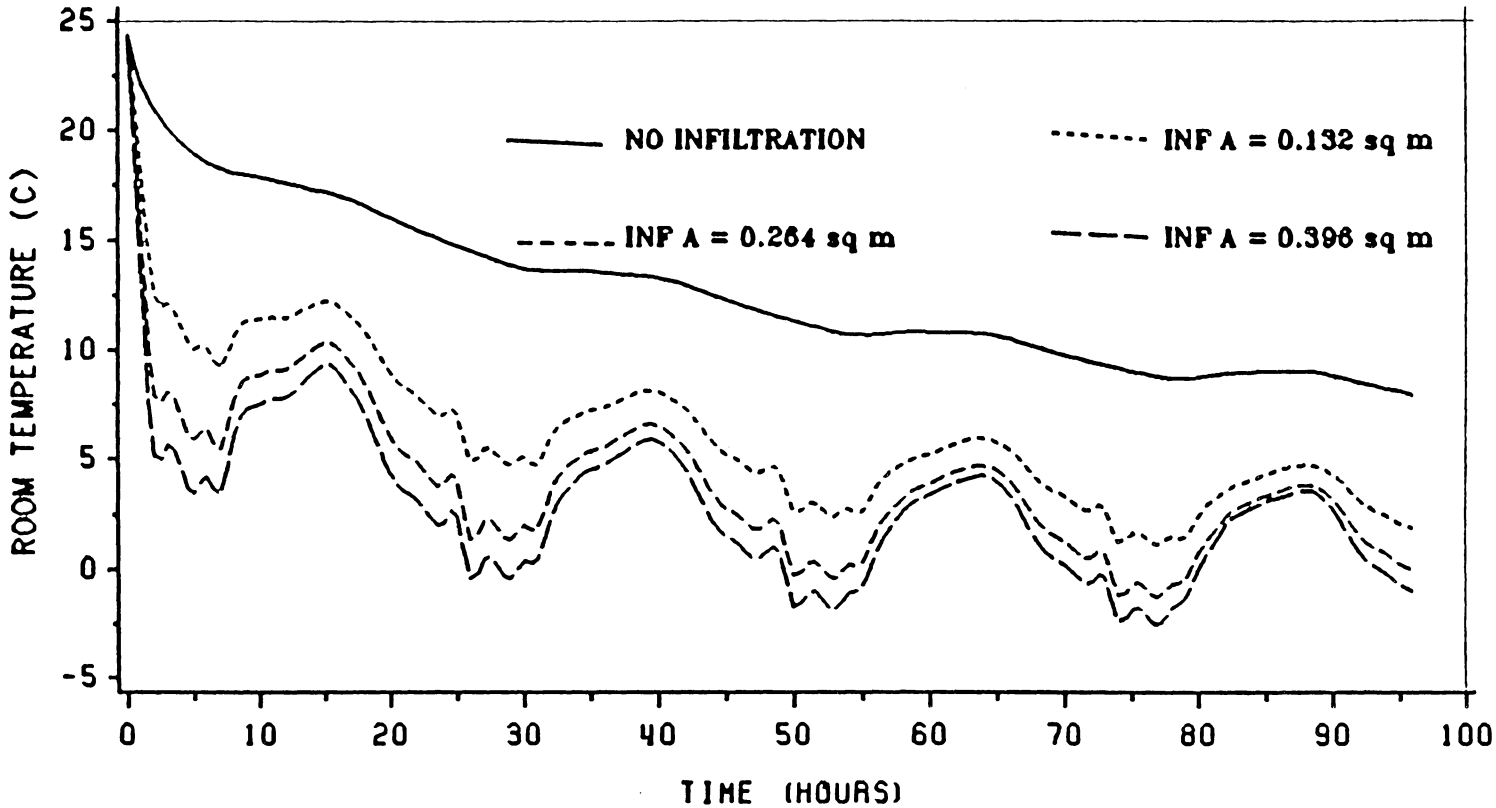

Figure 59. Temperature Response of the House With and Without Infiltration: the outside temperature range is -5 to 5 C

ble. For the rooms adjacent to the outside, infiltration is calculated using the outside and inside pressure difference. For interior rooms, natural convection accounts for the heat transfer between rooms.

The effect of the infiltration areas on the interior temperature is presented for various locations in the building. For the cases presented next, the infiltration areas are given along with the corresponding temperature profiles.

In Fig. 60, the infiltration effect on the temperature response of the building during a summer power outage is shown for room 36 (north side) of the first floor with 0.0, 0.002, 0.004, and 0.012 m^2 leakage areas. Increasing the infiltration areas from 0.0 to 0.002, 0.004, and 0.012 m^2 increased the interior temperature of room 36 during the afternoon by 0.7, 1.3, and 2.8 C, respectively. The effect during the night was negligible. For room 36 (north side) of the third floor, increasing the infiltration area from 0.0 to 0.002, 0.004, and 0.012 m^2 for each room shifted the interior temperature response curve by 4 hours. The largest effect was present during the night with the interior temperature decreasing at midnight of the second day by 0.5, 1.0, and 2.0 C, respectively. In Fig. 61, the temperature response of room 26 (central room) is presented with various infiltration crack areas for the third floor. For the interior temperature of room 26 on the first floor, the infiltration had a large positive effect during the day and negligible effect during the night. For the third floor, the infiltration decreased the temperature of room 26 considerably during the night of the summer power outage.

For a winter power outage, the infiltration effect on the interior temperature is examined for the institutional building. The leakage areas used earlier are used for the winter power outage simulations. The effect of increasing the infiltration is presented for different rooms in the building. In Fig. 62, the temperature response for various infiltration areas is presented for room 36 (north side) of the first floor. A similar temperature response is noted on all floors for the winter season simulations. Increasing the infiltration areas from 0.0 to 0.002, 0.004, and 0.012 m^2 decreased the temperature response curve after 5 hours by an average 2.0, 4.5, and

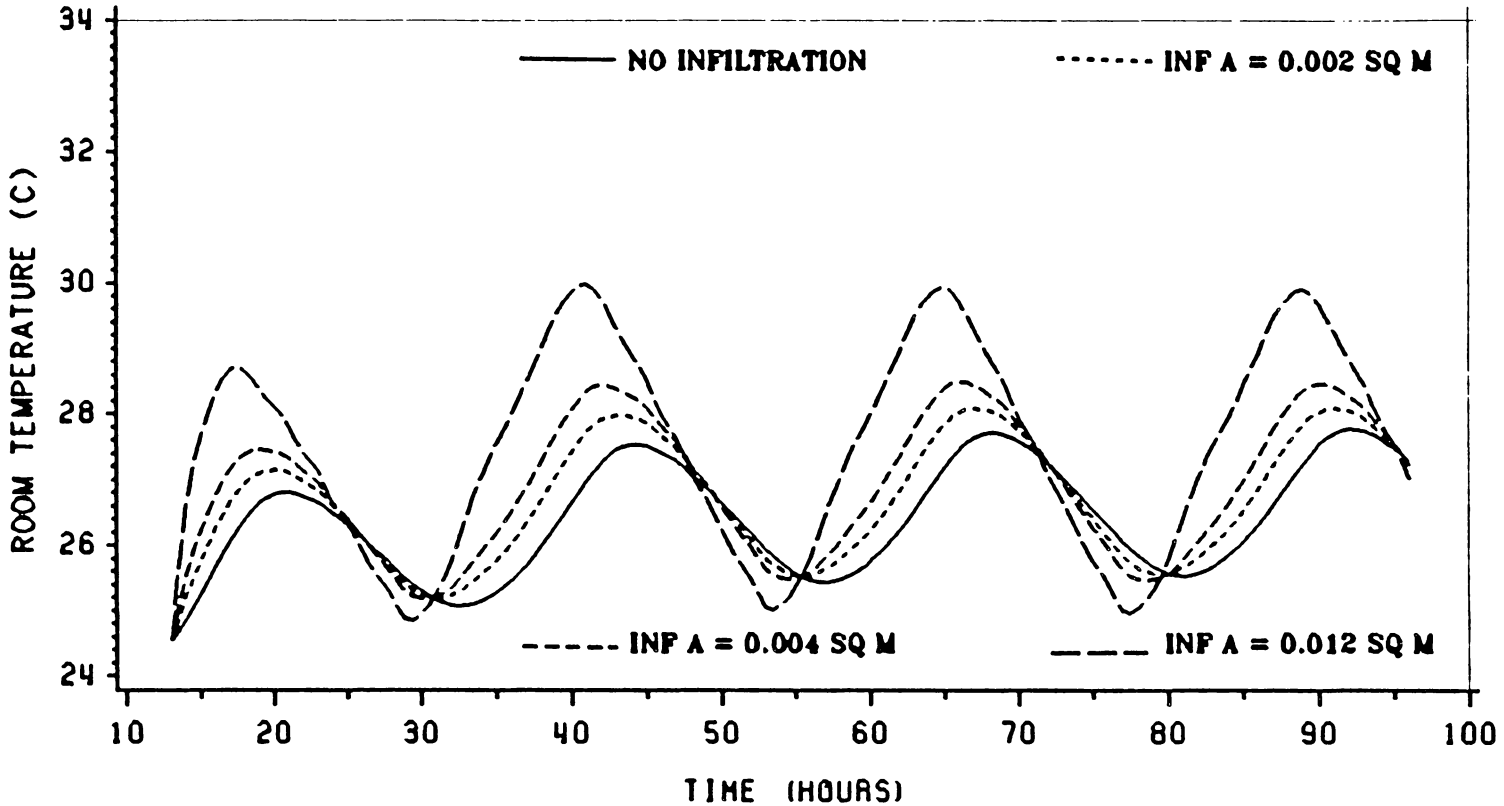

Figure 60. Temperature Response of Room 36 (North Side) With and Without Infiltration, First Floor: the outside temperature range is 25 to 35 C

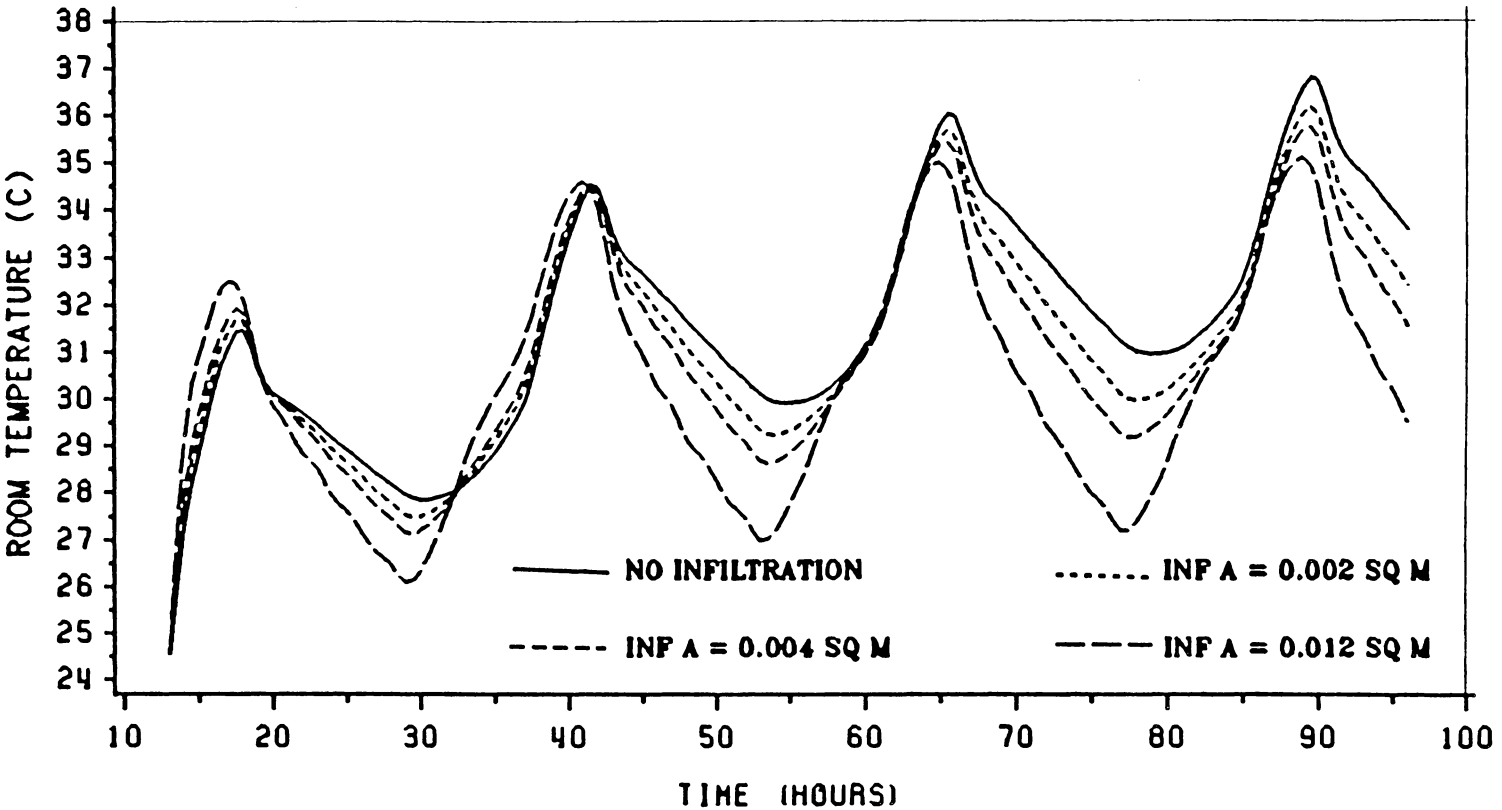

Figure 61. Temperature Response of Room 26 (Central Room) With and Without Infiltration, Third Floor: the outside temperature range is 25 to 35 C

7.5 C, respectively, for all rooms. The convective coefficient on the exterior walls reflects the wind speed outside the building. Next, the wind effect on the interior temperature of the two buildings is shown for winter and summer power outages.

EXTERIOR WALL VERTICAL CONVECTIVE COEFFICIENTS

The effect of the exterior vertical convective coefficient (h_o) on the temperature response of the commercial building and house during summer and winter power outages is investigated next. The three constant exterior wall convective coefficients used are 10, 25, and 40 W/m^2C. For the duration of the power outage, each convective coefficient is held constant at the corresponding value and on all four exterior sides of the structure. For the summer power outage, a 2 C decrease in the interior temperature of the house was obtained after 3 hours of simulation when h_o is increased from 10 to 25 W/m^2C. Further increase of h_o from 25 to 40 W/m^2C did not affect the interior temperature response significantly. In Fig. 63, the interior temperature response of the house for a winter power outage is presented for the three different exterior wall convective coefficients. A decrease of 2 C in the interior temperature of the house was obtained after 4 hours of the power outage when h_o is increased from 10 to 25 W/m^2C. Increasing further h_o from 25 to 40 W/m^2C did not affect the interior temperature response significantly.

The effect of the outside convective coefficient on the temperature drift in the institutional building is also shown. The exterior wall convective coefficients were 10 and 35 W/m^2C . During a summer power outage and for room 36 of the first floor, the temperature decreased by an average 0.5 C, reaching 25 C after 30 hours, when the outside convective coefficient is increased from 10 to 35 W/m^2C. For room 26 of the first floor, the temperature reached 26.5 C after 30 hours when the outside convective coefficient was increased from 10 to 35 W/m^2C. For the second floor, increasing the outside convective coefficient had a negligible effect on the interior temperature response of room 36 during the first 42 hours of simulations. The

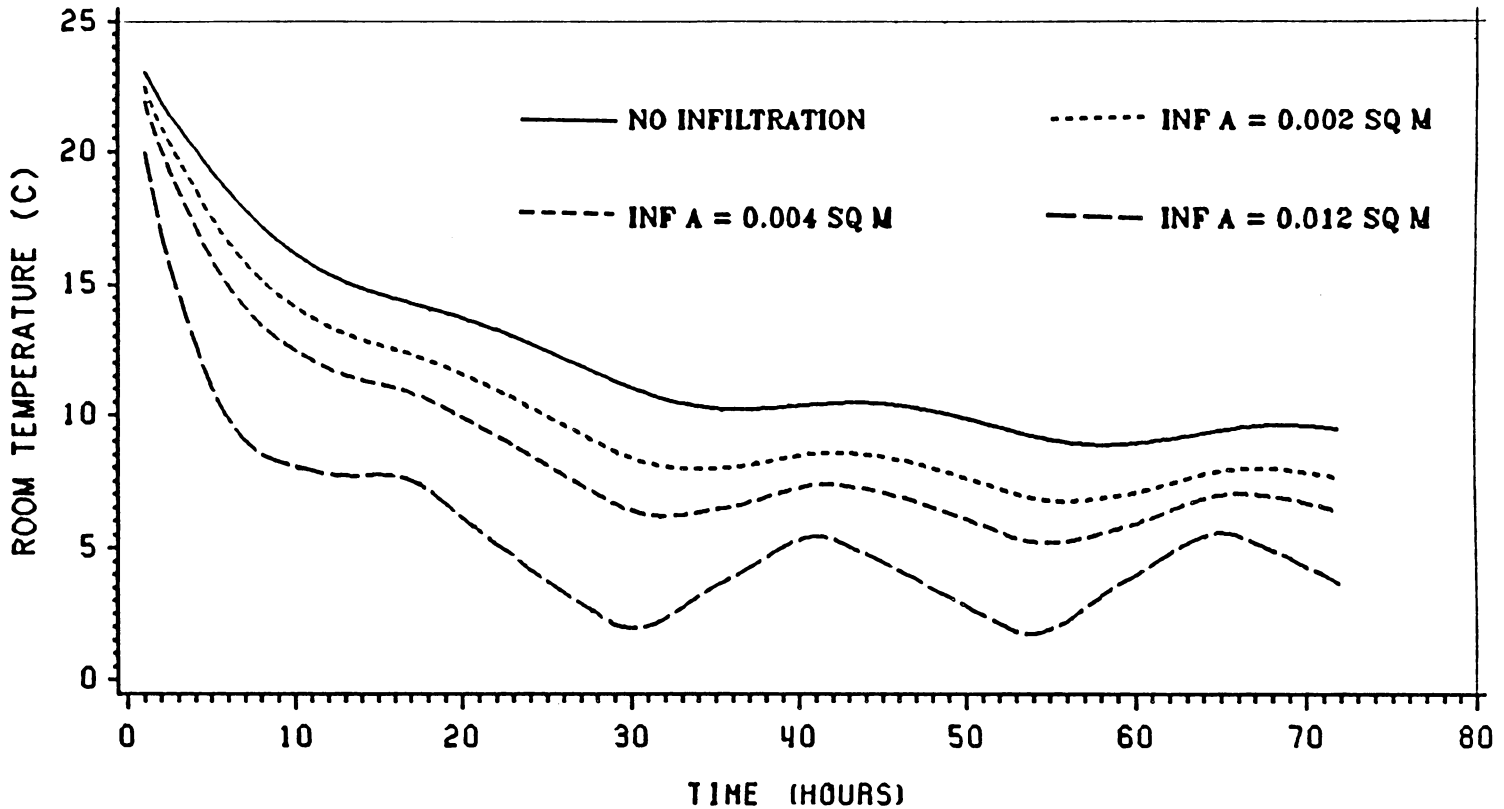

Figure 62. Temperature Response of Room 36 (North Side) With and Without Infiltration, First Floor: the outside temperature range is -5 to 5 C

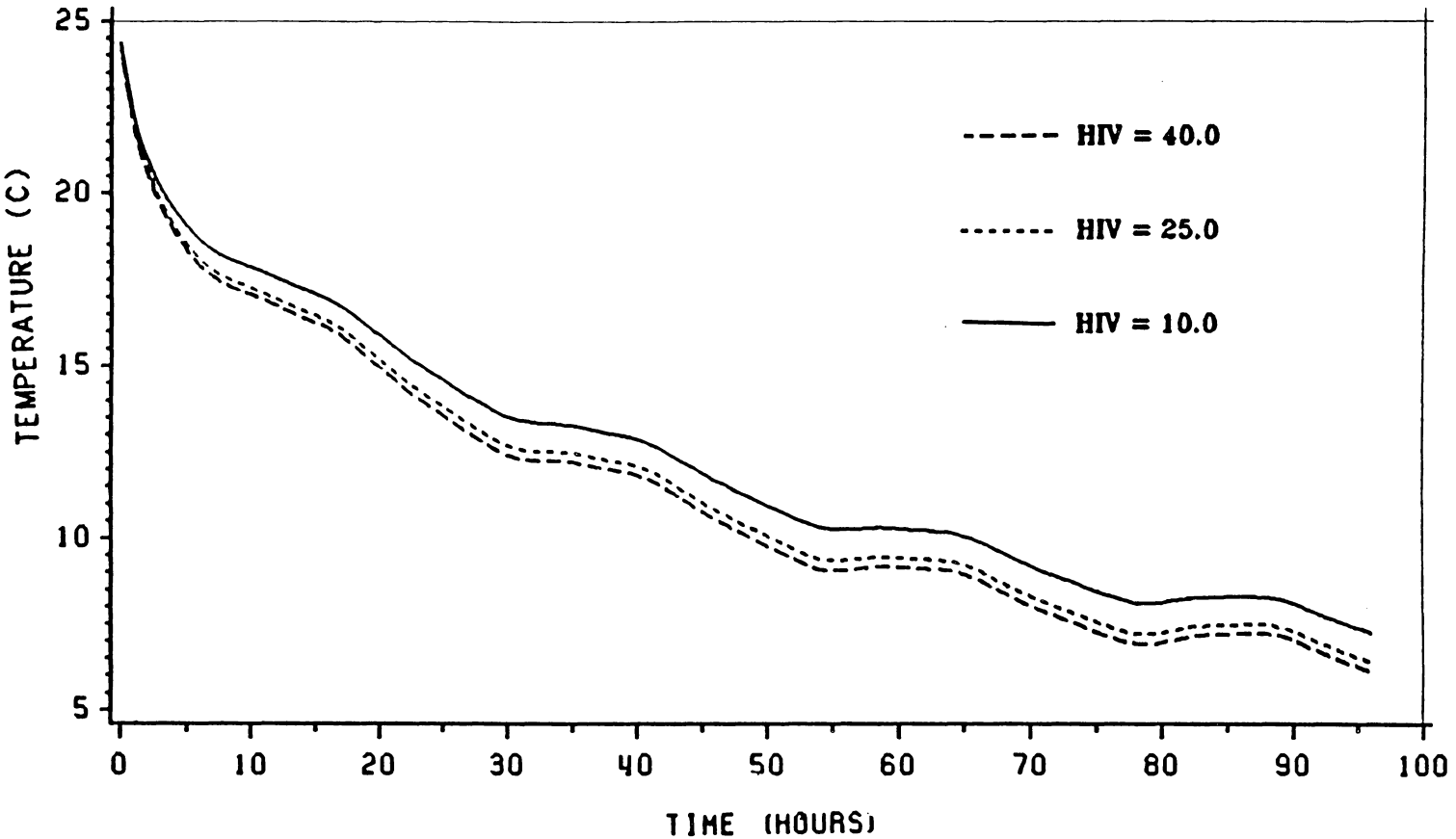

Figure 63. Effect of The Outside Convective Coefficient on the Interior Temperature of the House During a Winter Power Outage: the outside temperature range is -10 to 0 C

temperatures of rooms 36 and 26 decreased by an average of 1.5 C and 3.0 C, respectively after 5 hours of simulations when the exterior convective coefficient is increased from 10 to 35 W/m^2C. The effect of increasing the outside convective coefficient from 10 to 35 W/m^2C on the interior temperature during a winter power outage was examined and found to decrease the interior temperature by an average of 0.5 C in all rooms after 5 hours of simulations.

The effect of closing vs opening all doors inside buildings was examined and found negligible for summer and winter power outages.

GROUND TEMPERATURE

The ground temperature was held constant for the duration of the power outage simulations. The effect of the ground temperature on the interior temperature response is presented next. The ground temperature below the slab is fixed at the given value and the TRFM is used to calculate the conduction heat transfer through the floor slab. In the summer season simulations, 10, 25, and 45 C ground temperatures are used at a reference depth of 1 m. The interior temperature of the house increased by 11.5 C after 100 hours of simulations when the ground temperature was changed from 10 to 25 C. A further increase of 11.5 C was attained after 100 hours of simulations when the ground temperature was increased from 25 to 45 C. For a winter season power outage, changing the ground temperature from 25 to 10 C decreased the interior temperature by 14 C after 90 hours of simulations. Changing the ground temperature from 10 to -5 C decreased the interior temperature by 14 C after 90 hours of simulations.

The effect of the ground temperature on the interior temperature response of the building is shown next. As expected, changing the ground temperature affected the interior temperature response of rooms on the first floor. The effect was negligible on the room temperatures of the second and third floors. The ground temperature used for the summer simulations were

22 and 32 C. For the winter simulations, the ground temperatures were 22 and 5 C. For the summer season power outage, changing the ground temperature from 22 to 32 C increased the temperature of rooms on the first floor by 1.5 C after 10 hours of simulation. In Fig. 64, the temperature response of the north and south side rooms of the first floor during a winter power outage are presented for 22 and 5 C ground temperatures. Changing the ground temperature from 22 to 5 C decreased the temperature of all rooms on the first floor by 1.0 C after 8 hours and for the duration of the power outage.

RESTARTING THE HVAC SYSTEM AFTER A POWER OUTAGE

When the HVAC system is restarted following an extended power outage, the time required for the interior temperature of the house or institutional building to reach 24.4 C is analyzed. In other cases, where only partial HVAC system recovery is attained, it would still be important to determine the temperature response of the structure. For both winter and summer seasons, several constant heating and cooling loads are used in calculating the interior temperature.

For the Houston house, a 28 to 38 C exterior summer temperature profile is used in the simulations. The three cooling loads used in the simulations are: 300, 450, and 700 W/room. Initial temperatures of 29 and 38 C are used in the simulations before the HVAC system is restarted. Starting with an initial temperature of 29 C, the interior temperature of the house reached 24.4 C after 7 hours of 700 W/room, 14 hours of 450 W/room, and 40 hours of 300 W/room cooling loads. In Fig. 65, the average interior temperature curve of the house is presented for the three cooling loads starting with an initial temperature of 38 C. The interior temperature of the house reached 24.4 C after 30 hours of 700 W/room, 60 hours of 450 W/room, and 90 hours of 300 W/room cooling loads.

For the winter season, four heating loads are used for the interior temperature calculations of the house. These loads are: 400, 800, 1000, and 1200 W/room. With an initial tem-

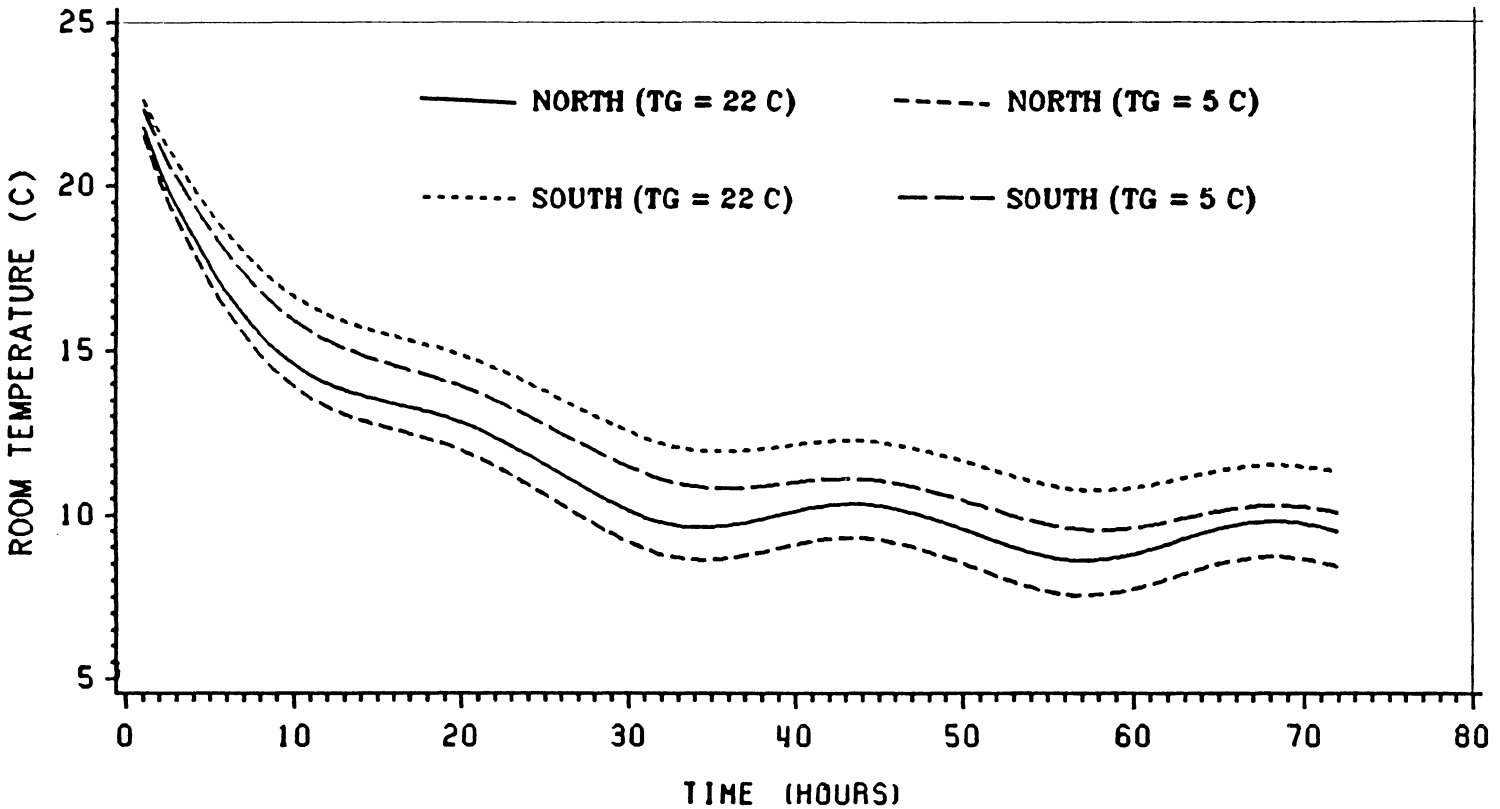

Figure 64. Effect of the Ground Temperature at a depth of 1 m on the Interior Temperature of the Building, First Floor: the outside temperature range is -5 to 5 C

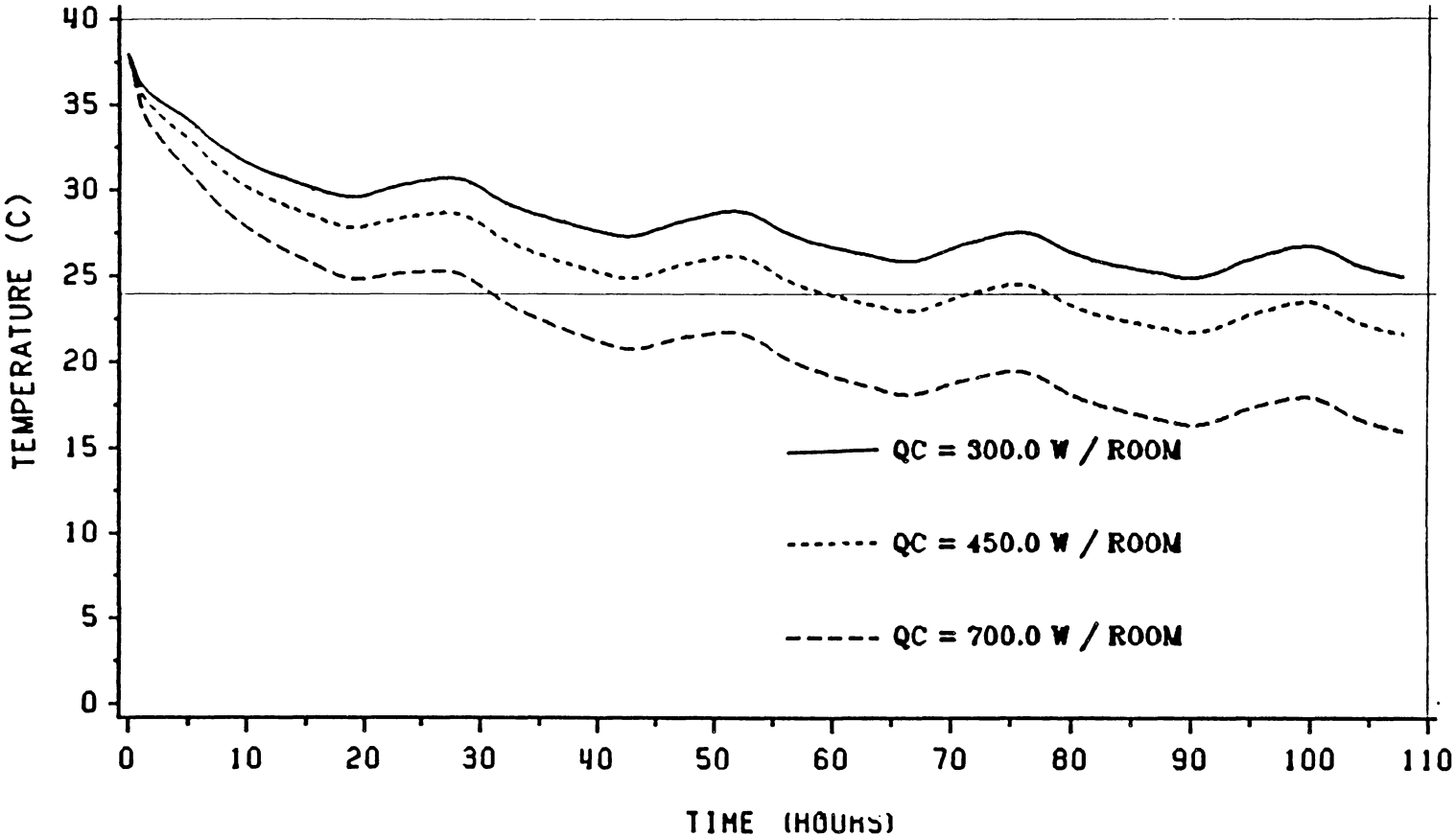

Figure 65. **Restarting the AC With an Initial House Temperature of 88 C :** the outside temperature range is 28 to 38 C

perature of 10 C and a -10 to 0 C outside temperature profile, the interior temperature of the house reached 24.4 C after 25 hours of 1200 W/room and 40 hours of 1000 W/room heating loads. After 90 hours of 400 and 800 W/room heating loads, the interior temperature reached 22 and 15 C, respectively. For an initial temperature of 5 C, the heater is restarted and the interior temperature profiles for the house are shown in Fig. 66 for all four heating loads. The interior temperature of the house reached 24.4 C after 35 hours of 1200 W/room and 60 hours of 1000 W/room heating loads. After 90 hours of 400 and 800 W/room heating loads, the interior temperature reached 18 and 14 C, respectively.

Restarting the HVAC system for the building with partial or limited energy supply was also examined. During the summer simulations, The required cooling load for the third floor was almost three times the load required for the first floor. The second floor required almost twice the heat amount of extraction than the first floor. The same trend was present during winter simulations.

97.5 PERCENT DESIGN TEMPERATURE

In HVAC calculations, an outside design temperature temperature is used in the calculations to determine the heating or cooling loads of the structure in order to maintain the desired interior temperature. ASHRAE has presented a set of outside design temperatures corresponding to numerous locations in the United States and Canada. For every location, two winter and summer exterior design temperatures are given. They are the 97.5 and 99 percent design temperatures. As given in references 26 through 28, there would be a approximately 22 hours at or below the 99 percent winter outdoor design temperature and 54 hours at or below the 97.5 value. In a normal summer, approximately 30 hours would be at or above the 99 percent design value and 150 hours at or above the 97.5 percent design value. The magnitude and duration of extreme temperatures during these hours are not given.

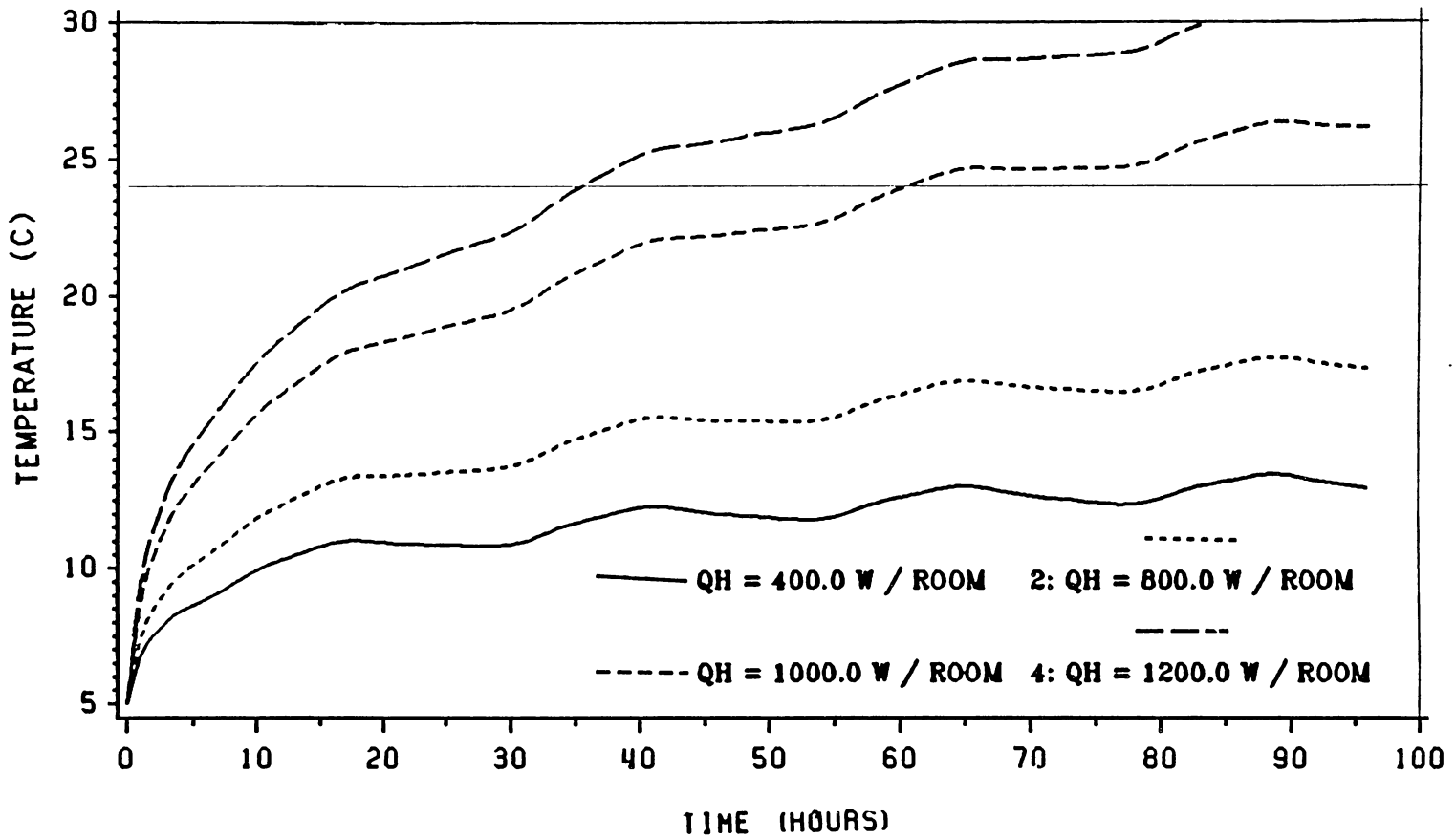

Figure 66. **Restarting the Heater With an Initial House Temperature of 5 C :** the outside temperature range is -10 to 0 C

Therefore, the outside temperature could be above the outdoor design temperature by a large difference for few hours every day or many hours for few days.

In the current analysis, the effect of the outdoor temperature exceeding by a small or large amount the design value on the interior temperature is presented for the house and commercial building. In most HVAC calculations, the 97.5 percent outdoor design temperature is used. Therefore, there are 54 hours in the winter season and 150 hours in the summer season where the temperature will go below and above the outdoor design value, respectively. Several temperature profiles are used to study the effect of internal temperature dropping below a set point of 24 C during extreme weather in the winter and summer seasons. The 97.5 percent outside design temperature for the winter and summer seasons were chosen arbitrarily as -15 and 33 C, respectively. Two outside temperature profiles are used for each season and are presented in Figs. 67 and 68, respectively. The winter temperature profiles are denoted as the -20 to -14 C and -16 to -14 C outside temperature profiles. The summer temperature profiles are denoted as the 34 to 38 C and 34 to 36 C outside temperature profiles. These profiles are used in the HVAC calculations to study the effect of extreme weather on the interior temperature in buildings and houses. Under these conditions, the capacity of the HVAC is exceeded. The interior temperature drops below (winter) or rises above (summer) the set temperature.

The heating and cooling loads are calculated for the institutional building and house. These loads are used with the outside temperature profiles obtained from Figs. 67 and 68 to determine the interior temperature in the structure. In Fig. 69, the interior temperature of the house is shown for the two outside winter temperature profiles. A maximum of 0.8 C drop was present at 5:00 AM when the -21 to -13 C outside temperature profile was used. A small effect on the interior temperature of the house was present when the -21 to -13 C outside temperature profile was used. For the summer season, a maximum increase of 0.8 C was present at 6:00 PM using the 34 to 38 C exterior temperature profile.

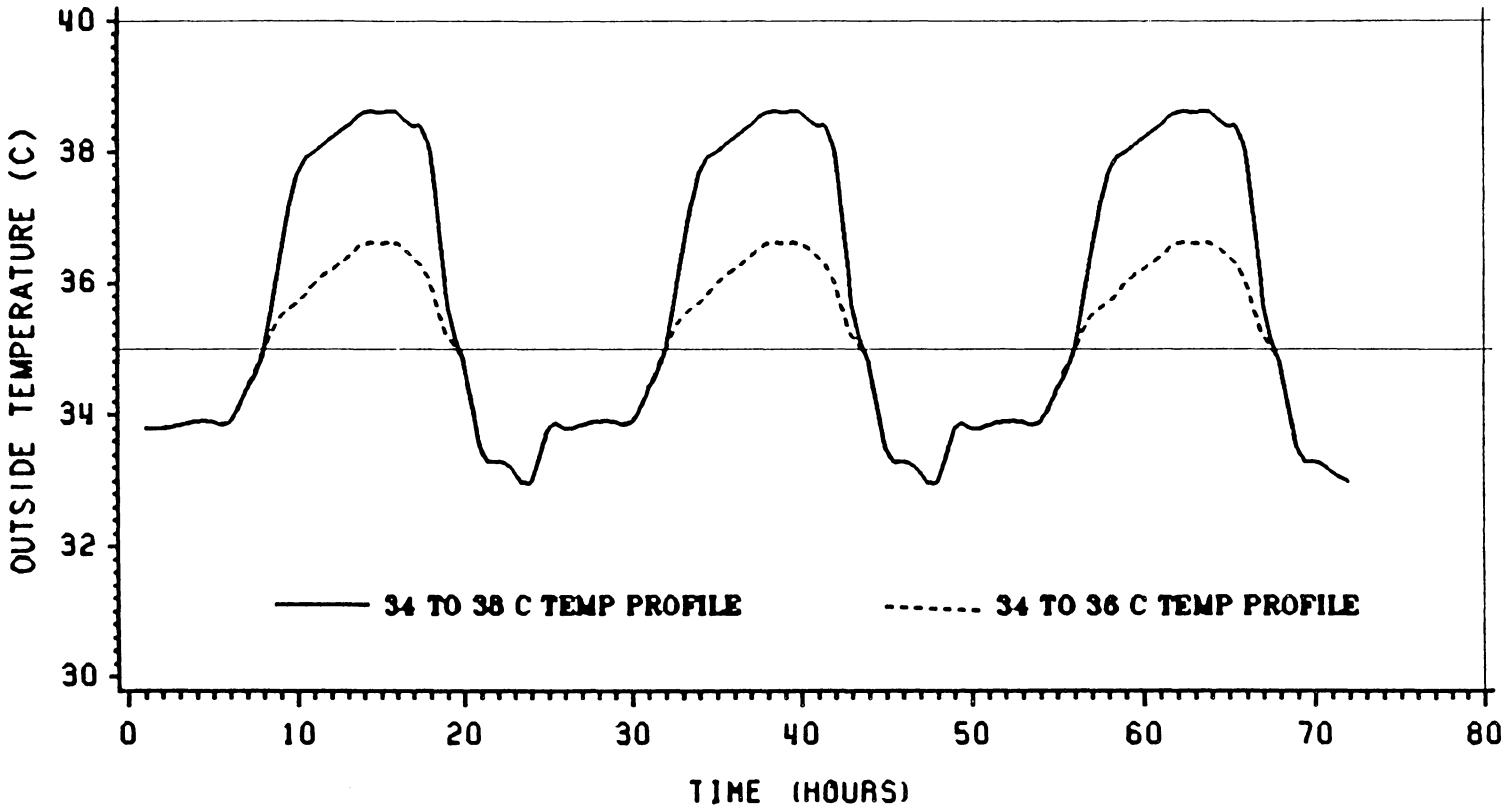

Figure 67. Outside Temperature Profiles for a Summer Season

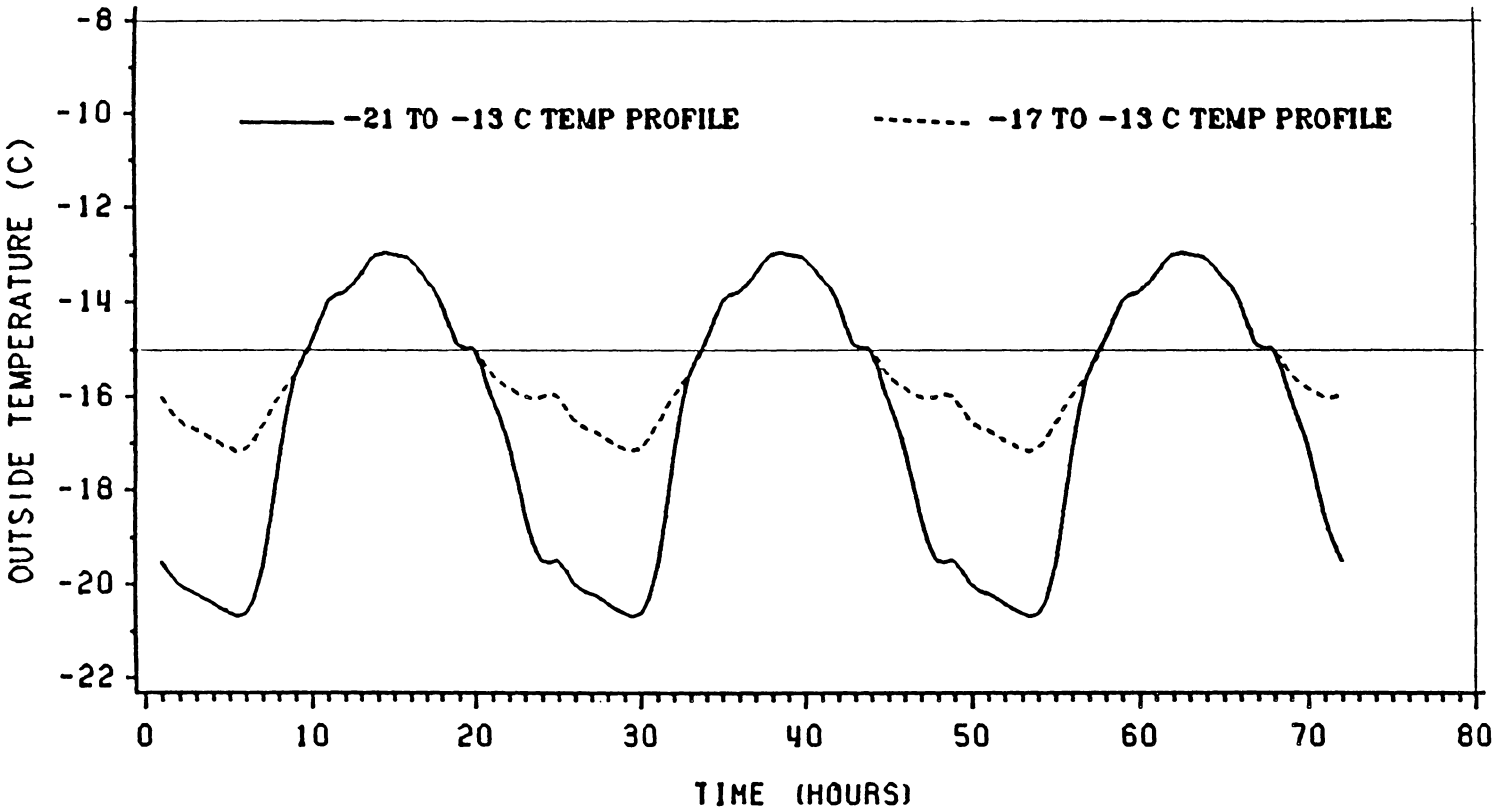

Figure 68. Outside Temperature Profiles for a Winter Season

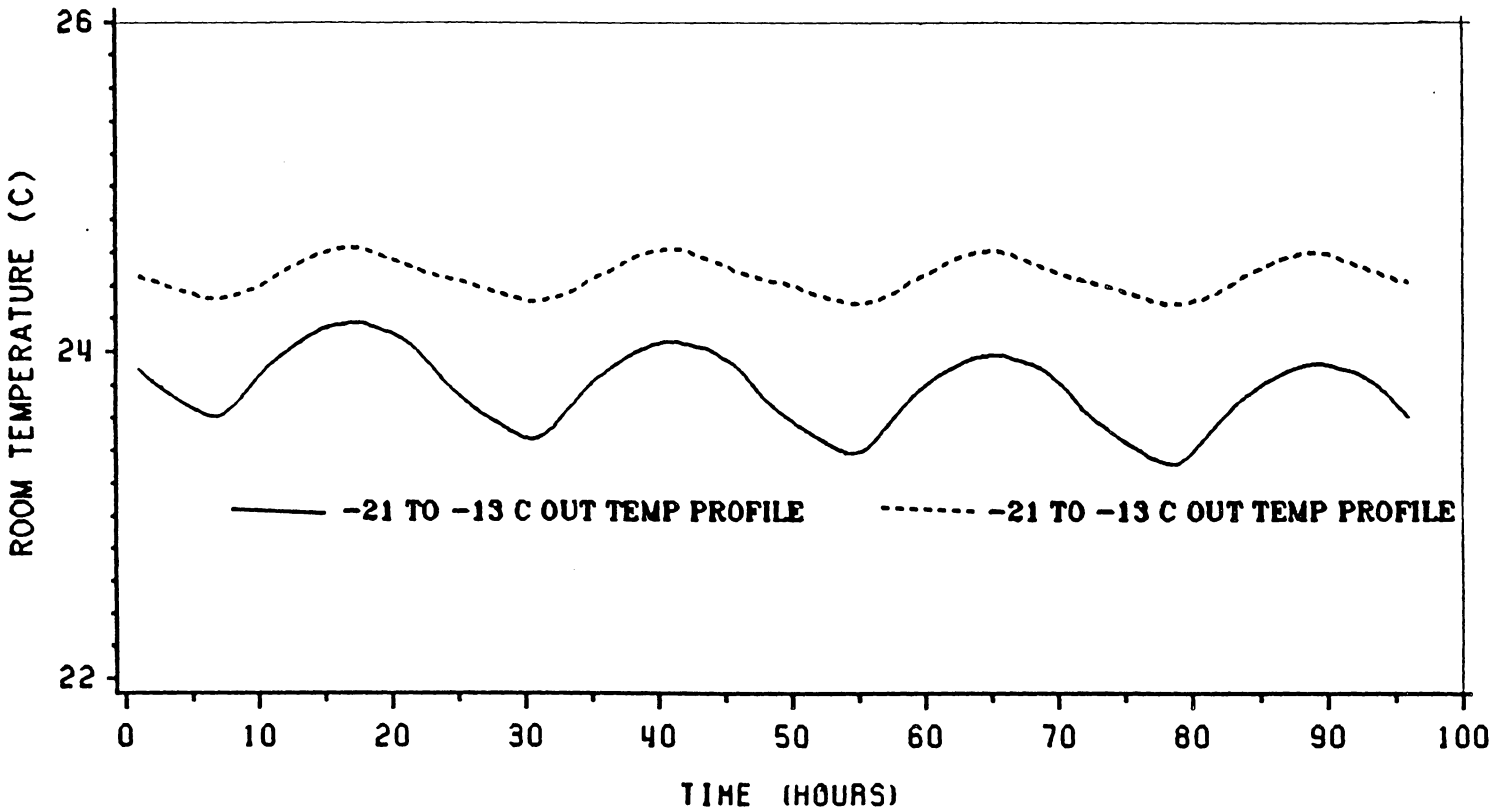

Figure 69. Interior Temperature Profiles of the House During a Winter Season: the outside temperature profiles are -21 to -13 C and -16 to -13 C

For the building, the heating and cooling loads were calculated based on -15 and 35 C exterior outside design temperatures for the winter and summer seasons, respectively. In Fig. 70, the temperature distribution of five rooms on the first floor are presented for the winter season. The outside temperature profile was -21 to -13 C. As expected, the deviation of the room temperatures from 24 C on all floors was significantly large. Temperatures on the first and second floors reached 21.5 C during the night and 25.0 C during the day. Temperatures on the third floor reached 20.5 C during the night and 24.8 C during the day. A 1.0 C temperature difference between the two extreme profiles (north south side rooms) on all floors was present.

The second outside temperature profile (-16 to -13 C) was used for another winter simulation. All three floors showed similar temperature variations, reaching 23.4 C during the night and 25.5 C during the day.

It is obvious that a new criterion for determining the outdoor design temperature is needed. Using the available design temperatures does not provide accurate information and would almost certainly overload the HVAC system during winter or summer extreme weather.

The results of the all simulations presented in this chapter are summarized in Tables 18 through 21.

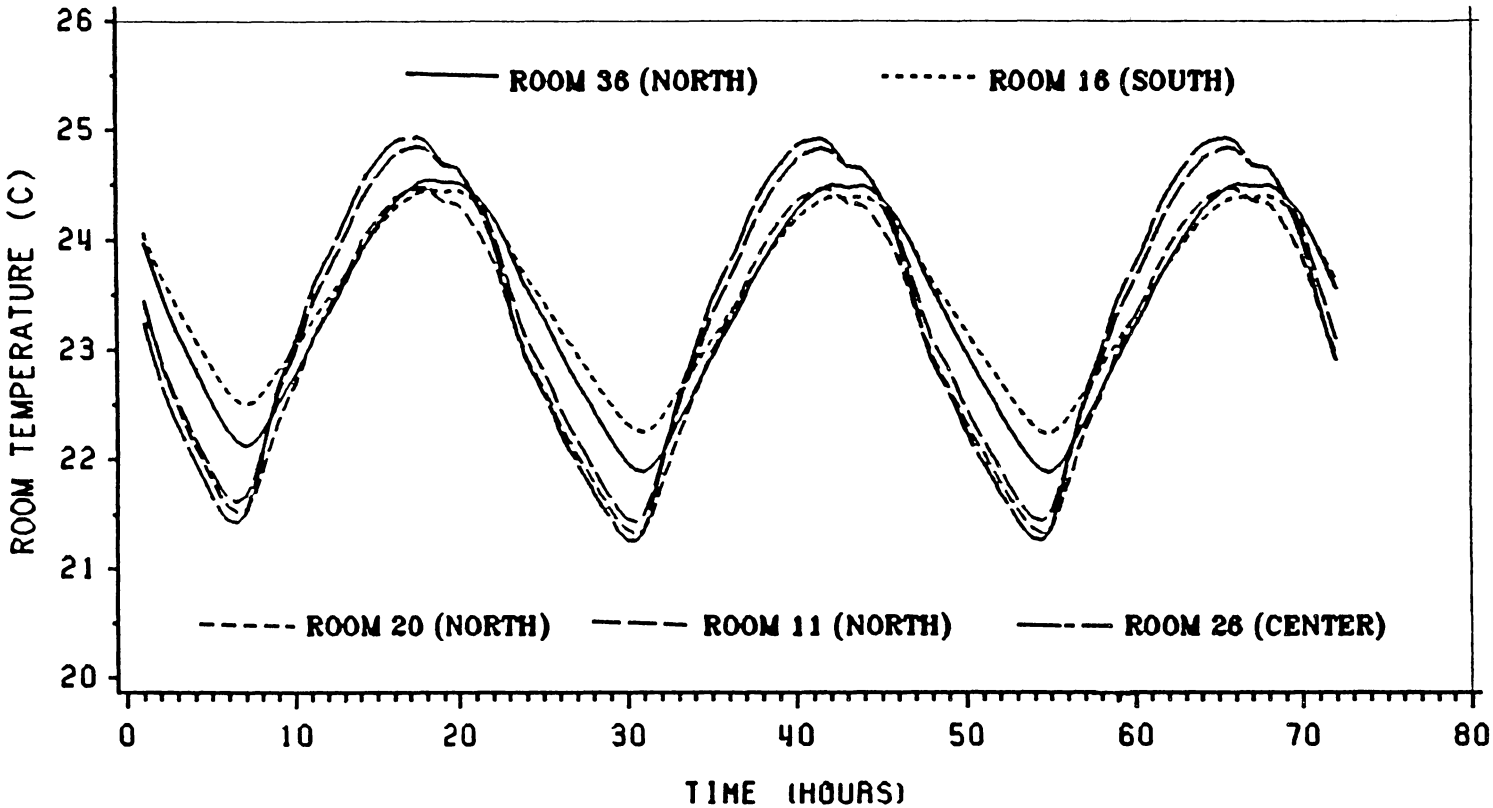

Figure 70. **Interior Temperature Profiles of the Building During a Winter Season, First Floor:** the outside temperature profile is -21 to -13 C

Table 18. Summary of Test Cases for the Houston House, Summer Season

PARAMETER	HOUSTON HOUSE ANALYSES	RESULTS (SUMMER)
Exterior wall emissivity	changing the emissivity from 0.2 to 0.9	1.0 C decrease in the interior temperature after 5 hours of power outage
Sky temp.	from ambient to 25 C higher than the ambient temp.	2.0 C increase in the interior temp. after 7 hours of power outage
MRT radiation	radiation vs. no radiation between interior walls	no effect on the interior temperature response
Interior wall mass	from light to thermally massive	a maximum of 1.0 C lower temp. after 4 hours of power outage
Insulation position	outside vs the inside of wall mass in exterior walls	reduced the temperature build up by 0.5 to 1.0 C after 3 hours of power outage
Furnishings	10 to 60 kg/room	reduced the temperature build up by 0.7 C after 3 hours of power outage
Infiltration	0.0 to 0.132 m^2 per room	increased the interior temp. by 2 C during the day and no effect during the night
	0.132 to 0.264 m^2 per room	increased the interior temp. by 1 C during the afternoon and no effect during the night
Exterior wall vertical conv. coefficient	10 to 25 $W/m^2.C$	decreased the interior temp. by 2 C after 3 hours of power outage
Ground temp.	10 to 25 C	increased the interior temp. by 11.5 C after 100 hours of power outage

Table 19. Summary of Test Cases for the Houston House, Winter Season

PARAMETER	HOUSTON HOUSE ANALYSES	RESULTS (WINTER)
Exterior wall emissivity	changing the emissivity from 0.2 to 0.9	0.5 C decrease in the interior temperature after 5 hours of power outage
Sky temp.	from ambient to 25 C lower than the ambient temp.	2.0 C decrease in the interior temp. after 7 hours of power outage
MRT radiation	radiation vs. no radiation between interior walls	no effect on the interior temperature response
Interior wall mass	from light to thermally massive	a maximum of 3.0 C higher temp. after 4 hours of power outage for low-R exterior walls
	from light to thermally massive	a maximum of 2.0 C higher temp. after 4 hours of power outage for high-R exterior walls
Insulation position	outside vs the inside of wall mass in exterior walls	increased the interior temperature by 1.25 C after 1 hour of power outage
Furnishings	10 to 60 kg/room	increased the interior temperature by 2.0 C after 5 hours of power outage
Infiltration	0.0 to 0.132 m^2 per room	decreased the interior temp. by 9 C during the night and 5 C during the day
	0.132 to 0.264 m^2 per room	increased the interior temp. by 2.5 C after 1 hour of power outage
Exterior wall vertical conv. coefficient	10 to 25 $W/m^2.C$	decreased the interior temp. by 2 C after 3 hours of power outage
Ground temp.	25 to 10 C	decreased the interior temp. by 14 C after 100 hours of power outage

Table 20. Summary of Test Cases for Williams Hall, Summer Season

PARAMETER	WILLIAMS HALL ANALYSES	RESULTS (SUMMER)
Exterior wall emissivity	changing the emissivity from 0.2 to 0.9	0.6 C decrease in the interior temperature after 10 hours of power outage
Sky temp.	from ambient to 25 C higher than the ambient temp.	1.2 C increase in the interior temp. after 8 hours of power outage
MRT radiation	radiation vs. no radiation between interior walls	no effect on the interior temperature response
Exterior wall mass	from light to thermally massive (0.46 $m^2.C/W$)	1.0 C decrease in the interior temp. during the day and 0.5 C during the night
	from light to thermally massive (R = 1.4 & 2.46$m^2.C/W$)	no effect on the interior temperature
Interior wall mass	from light to thermally massive (0.31$m^2.C/W$)	1.0 C decrease in the interior temp. during the day and no effect during the night
	from light to thermally massive (1.34$m^2.C/W$)	1.0 C decrease in the interior temp. after 5 hours of power outage
Insulation position	from outside to inside of the wall mass in exterior walls	reduced the temperature build up by 1.0 after 8 hours of power outage
Furnishings	0 to 50 kg/room	reduced the temperature build up by 0.5 C after 5 hours of power outage
Infiltration	0.0 to 0.002, 0.004, and 0.012 m^2 per room	increased the interior temp. by 0.7, 1.3, and 2.8 C,respectively, during the afternoon and 0.5, 1.0, and 2.0 C, respectively, during the night
Exterior wall vertical conv. coefficient	10 to 35 $W/m^2.C$	decreased the interior temp. of the third floor by 2.5 C after 5 hours of power outage
Ground temp.	22 to 32 C	increased the interior temp. of the first floor by 1.5 C after 10 hours of power outage

Table 21. Summary of Test Cases for Williams Hall, Winter Season

PARAMETER	WILLIAMS HALL ANALYSES	RESULTS (WINTER)
Exterior wall emissivity	changing the emissivity from 0.2 to 0.9	0.5 C decrease in the interior temperature after 10 hours of power outage
Sky temp.	from ambient to 25 C lower than the ambient temp.	0.5 C decrease in the interior temp. after 8 hours of power outage
MRT radiation	radiation vs. no radiation between interior walls	no effect on the interior temperature response
Exterior wall mass	from light to thermally massive (0.46 $m^2.C/W$)	2.0 C increase in the interior temp. during the night and 0.5 C during the day
	from light to thermally massive (R = 1.4 & 2.46$m^2.C/W$)	no effect on the interior temperature
Interior wall mass	from light to thermally massive (0.31$m^2.C/W$)	2.0 C increase in the interior temp. after 5 hours of power outage
	from light to thermally massive (1.34$m^2.C/W$)	increased the interior temp. of rooms exposed to the outside by 2 C and of interior rooms by 3.5 C after 5 hours of power outage
Insulation position	outside vs the inside of wall mass in exterior walls	increased the interior temp. by 1.5 to 2.0 C after 10 hours of power outage
Furnishings	0 to 50 kg/room	increased the interior temperature by a maximum of 1.5 C after 10 hours of power outage
Infiltration	0.0 to 0.002, 0.004, and 0.012 m^2 per room	decreased the interior temp. by 2.0, 4.5, and 7.5 C after one hour of power outage
Exterior wall vertical conv. coefficient	10 to 35 $W/m^2.C$	decreased the interior temp. by 0.5 C after 5 hours of power outage
Ground temp.	changing it from 22 to 5 C	decreased the interior temp. of the first floor by 1.0 C after 8 hours of power outage

7. CONCLUSIONS AND RECOMMENDATIONS

A model and calculation methodology has been developed for buildings experiencing an interruption in heating or cooling system operation. The primary emphasis in the analysis is the simulation of temperature response resulting from arbitrary but specified heat supply or extraction rates. Results predicted by the present method agree well with measurements for single- and multi-room residential buildings.

The method was used to investigate the effects of radiation heat transfer between interior wall surfaces, exterior wall emissivities, and effective sky temperature on the interior temperature response of buildings during winter and summer power outages. The effect of thermal mass in exterior and interior walls and the positioning of insulation in exterior walls on the interior temperature response of buildings was also examined during winter and summer power outages. The effect of other parameters, such as interior furnishings, infiltration, exterior wall convective coefficients, and the ground temperature, on the temperature response was examined for a typical institutional building and a house. Power failure simulations were started at midnight in the winter and noon in the summer seasons.

Infiltration was the most significant influencing parameter on the interior temperature of buildings during winter and summer power outages.

Changing a lightweight insulated interior partitioning of a house to thermally massive and uninsulated had a significant positive effect on the temperature response for a winter season power outage. A similar improvement was observed during the day of a summer season power outage.

Changing the exterior walls of the building from light to thermally massive had a significant positive effect on the interior temperature during winter and summer power outages for low R-values (0.3 m^2K/W). For exterior walls with high R-value (1.4 and 2.46 m^2K/W), the effect was negligible.

Changing the interior wall mass from light to thermally massive in buildings had a significant positive effect on the interior temperatures of rooms exposed to the outside during winter and summer power outages. For fully enclosed rooms, the effect on the interior temperature was positive and almost twice as large as for the outside rooms.

Positioning the insulation on the outside of the wall mass rather than on the inside in exterior walls had a positive effect on the interior temperature of the house during a winter season power outage. Positioning of insulation in the same location had a smaller effect during the first few hours in the summer application. The largest effect was present in the afternoon.

Placing the insulation on the outside of the wall mass rather than on the inside in exterior walls of the building during a summer power outage decreased the interior temperature of all rooms by 1 C. For a winter season power outage, placing the insulation on the outside of the wall mass increased the interior temperature by 1.7 C in all rooms. Also, positioning of insulation in the same location during a winter season power outage, decreased considerably the difference in temperatures between the rooms on each floor of the building.

Furnishings inside rooms had a significant positive effect on the interior temperature of buildings during a winter power outage. During a summer power outage, furnishings had a negligible effect on the interior temperature drift in buildings.

Increasing the outside convective coefficient from 10 to 25 W/m^2C had a significant positive effect on the interior temperature of buildings during a summer power outage. The effect was negligible during a winter power outage.

The ground temperature affected significantly the interior temperature in the house and the first floor of a commercial building during winter and summer power outages. For the second and third floors of the building, the ground temperature had a negligible effect on the interior temperature.

The effect of extreme weather on the interior temperature during full operation of the HVAC system was more significant for the commercial building than the house.

The effect of including infrared radiation heat transfer between interior surfaces on the temperature response in buildings was investigated and found negligible. The effect of the uncertainties in sky temperature and exterior wall emissivity was small during both winter and summer power outages.

8. REFERENCES

1. Mackey, C. O. and Wright, L. T., "Periodic Heat Flow--Homogeneous Walls or Roofs," *ASHVE Transactions*, Vol. 50, 1944, pp. 293-299.

2. Mackey, C. O. and Wright, L. T., "Periodic Heat Flow-Composite Walls or Roofs," *ASHVE Transactions*, Vol. 52, 1946, pp. 283-290.

3. Stewart, J. P., "Solar Heat Gains Through Walls and Roofs for Cooling Load Calculations," *ASHVE Transactions*, Vol. 54, 1948, pp. 283-296.

4. Brisken, W. R. and Reque, S. G., "Heat Load Calculations by Thermal Response," *ASHRAE Transactions*, Vol. 62, 1956, pp. 391-398.

5. Carslow, H. S. and Jaeger, J. C., *Conduction of Heat in Solids*, Oxford at the Clarendon Press, p. 326, 1957.

6. Pipes, L. A., "Matrix Analysis of Heat Transfer Problems," *Franklin Institute Journal*, Vol. 263, 1957,pp. 195-204.

7. Hill, I. R., "A Method for Computing the Transient Temperature of Thick Walls from Arbitrary Variation of Adiabatic Wall Temperature and Heat Transfer Coefficient," *National Advisory Committee for Aeronautics*, Technical Note 4105, 1957.

8. Muncey, R. W., "The Thermal Response of a Building to Sudden Change of Temperature or Heat Flow," *Australian Journal of Applied Science*, Vol. 14, 1963, pp. 123-128.

9. Mitalas, G. P. and Arseneault, J. G., "Fortran 4 Program to Calculate Heat Flux Response Factors for Multi-Layer Slabs," *Division of Building Research, National Research Council of Canada*, DBR Computer Program No. 23, 1967.

10. Stephenson, D. G. and Mitalas, G. P., "Cooling Load Calculations by Thermal Response," *ASHRAE Transactions*, Vol. 73, 1967, pp. 3.1.1-3.1.7.

11. Mitalas, G. P., "Calculation of Transient Heat Flow Through Walls and Roofs," *ASHRAE Transactions*, Vol. 74, part 2, 1968, pp.182-188.

12. Kusuda, T., "Thermal Response Factors for Multi-Layer Structures of Various Heat Conduction Systems," *ASHRAE Transactions*, Vol. 75, 1969, pp. 246-271.

13. Peavy, J. S., "Determination and Verification of Thermal Response Factors for Thermal Conduction Application," *U.S. National Bureau of Standards Intermemo Report* , December, 1977, NBSIR 77-1405.

14. Peavy, B. A., "A Note on Response Factors and Conduction Transfer Functions," *ASHRAE Transactions*, Vol. 84, 1978, pp. 688-690.

15. Hittle, D. C. and Bishop, R., "An Improved Root-Finding Procedure for Use in Calculating Transient Heat Flow Through Multi-layered slabs," *Journal of Heat and Mass Transfer*, Vol. 26, 1984, pp. 1685-1693.

16. Pederson, C. O. and Mouen, E. D., "Application of System Identification Techniques to the Determination of Thermal Response Factors from Experimental Data," *ASHRAE Transactions*, Vol. 79, part 2, 1973, pp.127-136.

17. Stephenson, D. G. and Mitalas, G. P., "Calculation of Heat Conduction Transfer Functions for Multi-Layer Slabs," *ASHRAE Transactions*, Vol. 77, part 2, 1971, pp. 117-126.

18. Mitalas, G. P. and Arseneault, J. G., "Fortran 4 Program to Calculate Z-Transfer Function for the calculation of Transient Heat Transfer Through Walls and Roofs," *U.S. National Bureau of Standards, Building Science Series*,, Vol. 39, 1971, pp.633-668.

19. Mitalas, G. P., "Comments on the Z-transfer Function Method for Calculating Heat Transfer in Buildings," *ASHRAE Transactions*, Vol. 84, part 1, 1978, pp. 667-674.

20. Sherman, M. H., Sonderegger, R. G. and Adams, J. W., "The Determination of the Dynamic Performance of Walls," *ASHRAE Transactions*, Vol. 88, part 1, 1982, pp. 689-712.

21. Condon, P.E., Carroll, W.L. and Sonderegger, R.C., "A New Measurement Strategy for insitu Testing of Wall Thermal Performance," *Proceedings of the ASHRAE/ORNL DOE Conference on Thermal Performance of the Exterior Envelopes of Buildings*, ASHRAE, New York, 1981; Lawrence Berkeley Laboratory Report, LBL-8822, June 80.

22. Burch, D. M., Remmert, W. E., Krintz, D. F. and Barnes, C. S., "A Field Study of the Wall Mass on the Heating and Cooling Loads of Residential Buildings," *Proceedings of the Building Thermal Mass Seminar*, Knoxville, TN., June 2-3, 1982.

23. Burch, D. M., Walton, G. N., Cavanaugh, K., "The Effect of Wall Mass on Annual Heating and Cooling Loads of Single-Family Residences For Five Selected Climates," *Symposium on Thermal Insulation Materials and Systems*, Dallas, TX., December 2-6, 1984.

24. Burch, D. M., Krintz, D. F. and Spain, R. S., "The Effect of Wall Mass on Winter Heating Loads and Indoor Comfort-An Experimental Study," *ASHRAE Transactions*, Vol. 90, part 2, 1984, pp.94-121.

25. Burch, D. M., Johns, W. L., Jacobsen, T., Walton, G. N. and Reeve, C. P., "The Effect of Thermal Mass on Night Temperature Setback Savings," *ASHRAE Transactions*, Vol. 90, part 2, 1984, pp.94-121.

26. ASHRAE. *Handbook of Fundamentals*. New York American Society of Heating, Refrigeration and Air Conditioning Engineers, 1977.

27. ASHRAE. *Handbook of Fundamentals*. New York American Society of Heating, Refrigeration and Air Conditioning Engineers, 1981.

28. ASHRAE. *Handbook of Fundamentals*. New York American Society of Heating, Refrigeration and Air Conditioning Engineers, 1985.

29. Wang, F.S., "Mathematical Modeling and Computer Simulation of Insulated Systems in Below Grade Applications", *Proceedings of the ASHRAE/DoE-ORNL Conference, Thermal*

Performance of the Exterior Envelopes of Buildings, Orlando, FL, Dec. New York: American Society of Heating, Refrigerating, and Air-Conditioning Engineers.

30. McQuiston, F. C. and Parker J. D., *Heating, Ventilating, and Air Conditioning*, John Wiley and Sons, second edition, 1982.

31. Mitalas, G. P., "Calculation of Basement Heat Loss," *ASHRAE Transactions*, Vol. 89, part 1B, 1983, pp. 420-437.

32. Kusuda, T. and Bean, J. W., "Simplified Methods for Determining Seasonal Heat Loss From Uninsulated Slab-On-Grade Floors," *ASHRAE Transactions*, Vol. 90, part 1B, 1984, pp.611-632.

33. Yard, D. C., Morton-Gibson, M. and Mitchell, J. W., "Simplified Dimensionless Relations for Heat Loss From Basements," *ASHRAE Transactions*, Vol. 90, part 1B, 1984, pp.633-643.

34. Perry, E. H., Cunningham, G. T. and Scessa, S., "An Analysis of Heat Losses Through Residential Floor Slabs," *ASHRAE Transactions*, Vol. 91, part 2, 1985, pp.127-136.

35. Kusuda, T. and Achenbach, P. R., "Earth Temperature and Thermal Diffusivity at Selected Stations in the United States," *ASHRAE Transactions*, Vol. 71, part 1, 1965, pp.61-75.

36. Grimsrud, D. T., Modera, M. P. and Sherman, M. H., "A Predictive Air Infiltration Model-Long-Term Field Test Validation," *ASHRAE Transactions*, Vol. 88, part 1, 1982, pp.1351-1371.

37. Liddament. M. and Allen, C., "The Validation And Comparison of Mathematical Models of Air Infiltration," *Air Infiltration Center*, Berkshire, Great Britain, Technical Note A/C 11, Sept. 1983.

38. Jackman, P. J., "A Study of Natural Ventilation of Tall Office Buildings." *Inst. Heat Vent. Eng.*, Vol. 38, pp. 103-118, 1970.

39. Sander, D. M., "Fortran 4 Program to Calculate Air Infiltration in Buildings." *Division of Building Research, National Research Council of Canada.*, DBR Computer Program No. 37, 1974.

40. Kusuda, T., "NBSLD, the Computer Program for Heating and Cooling in Buildings." *NBS Building Science Series*, Vol. 69, 1974.

41. De Gids, W. F., "Calculation Method for the natural Ventilation of Buildings." *TNO Research Institute for Environmental Hygiene*, Delft, Netherlands, 1977.

42. Irving, S. J., "The Computer Simulation of Smoke Movement During Building Fires." *Fire Prevention Science and Technology*, No. 22, pp. 3-8, 1979.

43. Etheridge, D. W. and Alexander, D. K., "The British Gas Multi-cell Model for Calculating Ventilation." *ASHRAE Transactions*, Vol. 86, Part 2, pp. 808-821, 1980.

44. Etheridge, D. W. and Gale, R., "Theoretical and Experimental Techniques for Ventilation Research in Buildings." *Proc. 1983 International Gas Research Conference*, London, UK.

45. Larsen, B. T., "Energy Consumption of Residential Buildings. The Computer Program ENCORE. Part 1: User's Manual and Part 2: Documentation." *Norwegian Building Research Institute*, 1979.

46. Cole, J. T., Kinast, J. A., Zawacki, T. S., Elkins, R. H. and Macris, R. A., "Development and Field Verification of a Model of House Air Infiltration for Single Family Residences." *Gas Research Institute*, Final report, June 1981.

47. Warren, P. R. and Webb, B. C., "The Relationship Between Tracer Gas and Pressurization Techniques in Dwellings." *AIC Conference 'Instrumentation and Measuring Techniques'*, Windsor, UK, 1980.

48. Cole, J. T., et al, "Application of a Generalized Model of Air Infiltration to Existing Homes." *ASHRAE Transactions*, Vol. 86, Part 2, pp. 765-777, 1980.

49. *Procedure For Determining Heating and Cooling Loads For Computerizing Energy Calculations*,Compiled and Published by The ASHRAE Task Group on Energy Requirements for Heating and Cooling of Building of Buildings, 1976.

50. Tamura, G. T., "Computer Analysis of Smoke Movement in Tall Buildings."*ASHRAE Transactions*, Vol. 75, Part 2, pp. 81-93, 1969.

51. Sander, D. M. and Tamura, G. T., "A Fortran IV Program to Simulate Air Movement in Multi-Storey Buildings." *National Research Council of Canada*, Division of Building Research, DBR Computer Program No. 35, March 1973.

52. Balcomb, J. D. and Yamaguchi, K., "Heat Distribution by Natural Convection," *Eighth National Passive Solar Conference*,, Santa Fe, New Mexico, September 1983, pp.289-294.

53. Kimura, K. and Stephenson, D. G., "Theoretical Study of Cooling Load Caused by lights," *ASHRAE Transactions*, Vol. 74, part 2, 1968, pp.189-197.

54. Barakat, S. A. and Sander, D. M., "The Utilization of Internal Heat Gains," *ASHRAE Transactions*, Vol. 92, part 1, 1986.

55. Mitalas, G. P. and Stephenson, G. P., "Room Thermal Response Factors," *ASHRAE Transactions*, Vol. 73, 1967, pp.3-2.1-2.10.

56. Muncey, R., Spencer, J. and Gupta, C., "Method For Thermal Calculations Using Total Building Response Factors," *U.S. National Bureau of Standards, Building Science Series*,, Vol. 39, 1971, pp.111-116.

57. Kusuda, T., "Calculation of Building Thermal Response Factors as Wiener Coefficients," *U.S. National Bureau of Standards, Building Science Series*,, Vol. 39, 1971, pp.117-126.

58. Sonderegger, R. C., "Diagnostic Tests Determining the Thermal Response of a House," *ASHRAE Transactions*, Vol. 84, part 1, 1978, pp. 691-702.

59. Wilson, N. W., Colborne, W. G. and Ganesh, R., "Determination of Thermal Parameters for an Occupied House," *ASHRAE Transactions*, Vol. 90, part 2B, 1984, pp. 39-50.

60. Crawford, R. R. and Woods, J. E., "A Method for Deriving a Dynamic System Model From Actual Building Performance Data," *ASHRAE Transactions*, Vol. 91, part 2, 1985, pp.127-136.

61. Franklin, G. F. and Powell, J. D., *Digital Control of Dynamic Systems*, Addison-Wesley Publishing Company, 1980.

62. Harrison, H. L., Hansen, W. S., and Zelenski, R. E., "Development of a Room Transfer Function Model for Use in the Study of Short-Term Transient Response," *ASHRAE Transactions*, Vol. 74, part 2, 1968, pp.198-210.

63. Nelson, L. W., "The Analog Computer as a Product Design Tool," *ASHRAE Journal*, Vol. 7, No 7-12, 1965, pp. 37-45.

64. Kaya, A., "Analytical Techniques For Controller Design," *ASHRAE Journal*, Vol. 18, No 7-12, 1976, pp. 35-39.

65. Mehta, D. P., "Dynamic Thermal Response of Buildings and Systems," Thesis (PhD), Iowa State University, 1980.

66. Mehta, D. P. and Woods, J. E., "An Experimental Validation of a Rational Model for Dynamic Responses of Buildings," *ASHRAE Transactions*, Vol. 86, part 2, 1980, pp.497-520.

67. Hittle, D. C., *The Building Loads Analysis and System Thermodynamics (BLAST) Program, Users Manual, Version 2.0, Volumes 1 and 2.*,Technical Report E-153, U.S. Army Const. Eng. Res. Lab. (CERL), Champaign , IL, 1979.

68. *DOE-2 Reference Manual*, Group WX-4, Program Support, Los Alamos Scientific Laboratory Report LA-7689-M, 1979

69. Diamond, S. C., Hunn, B. D. and Mcdonald, T. E., "DOE-1 Verification Program Plan," *Los Alamos Scientific Laboratory Report*, LA-7552-MS (November, 1978).

70. *Building Energy Analysis Group*,Lawrence Berkeley Laboratory, DOE-2 User's Guide, LBL-8689, February, 1979.

71. Kusuda, T. *NBSLD-National Bureau Of Standards Heating and Cooling Load Determination Program*, NBS SS 69, July 1976.

72. Walton, G. N., "Thermal Analysis Research Program Reference Manual,"*U. S. National Bureau of Standards Intermemo Report* , March, 1983, NBSIR 83-2655.

73. Yuill, G. K. and Phillips, E. G., "Comparison of Blast Program Predictions with the Energy Consumptions of Two Buildings," *ASHRAE Transactions*, Vol. 87, part 1, 1981, pp. 1200-1206.

74. Diamond, S. C. and Hunn, B. D., "Comparison of DOE-2 Computer Program Simulations to Metered Data for Seven Commercial Buildings," *ASHRAE Transactions*, Vol. 87, part 1, 1981, pp. 1222-1231.

75. Alreza, T. and Hovander, L., " A Micro Evaluation," *ASHRAE Journal*, December, 1985, pp.34-37.

76. Diamond, S. C., Capiello, C. C. and Hunn, B. D., "User-Effect Validation Tests on the DOE-2 Building Energy Analysis Computer Program," *ASHRAE Transactions*, Vol. 91, part 2, 1985, pp.127-136.

77. Robertson, D. K. and Christian, J. E., "Comparisons of Four Computer Models With Experimental Data from Test Buildings in Northern New Mexico," *ASHRAE Winter Meeting, San-Francisco*, January, 1986.

78. Sorrel, F. Y., Luckenbach, T. J. and Phelps, T. L., "Validation of Hourly Building Energy Models for Residential Buildings," *ASHRAE Winter Meeting, San-Francisco*, January, 1986.

79. Yuill, G. K., "The BLAST Verification," *ASHRAE Journal*, January, 1986, pp.62-70.

80. Burch, D. M., Peavy, B. A. and Powell, F. J., "Comparison Between Measured Computer-Predicted Hourly Heating and Cooling Energy Requirements for an Instrumented Wood Framed Townhouse Subjected to Laboratory Tests," *ASHRAE Transactions*, Vol. 81, part 2, 1975.

81. Kusuda, T. and Bean, J. W., "Comparison of Calculated Hourly Cooling Load and Indoor Temperature With Measured Data For a High Mass Building Tested in an Environmental Chamber," *ASHRAE Transactions*, Vol. 87, part 1, 1981, pp.1232-1240.

82. Kusuda, T., Pierce, E. T. and Bean, J. W., "Comparison of Calculated Hourly Cooling Load and Attic Temperature With Measured Data For a Houston Test House," *ASHRAE Transactions*, Vol. 87, part 1, 1981, pp.1185-1199.

83. Borresen, B. A., "Thermal Room Models for Controller Analysis," *ASHRAE Transactions*, Vol. 87, part 2, 1981, pp. 251-261.

84. Sullivan, R., Huang, Y. J., Bull, J. C., Turiel, I., Ristchard, R. L. and Selkowitz, S. E., "Thermal Analysis of Buildings-Configuration Perturbation and Observed Climate Interface," *ASHRAE Transactions*, Vol. 92, part 1, 1986.

85. Hackner, R. J., Mitchell, J. W. and Beckman, W. A., "HVAC System Dynamic and Energy Use in Buildings-part 2," *ASHRAE Transactions*, Vol. 91, part 1, 1985.

86. Goldman, C. A., "Measured Results of Energy Conservation Retrofits in Residential Buildings," *ASHRAE Winter Meeting, San-Francisco*, January, 1986.

87. Lau, A. S., Beckman, W. A. and Mitchell, J. W., "Development of Computerized Control Strategies for a Large Chilled Water Plant," *ASHRAE Transactions*, Vol. 91, part 1, 1985.

88. Peavy, B. A., Powell, F. J. and Burch, D. M., "Dynamic Thermal Performance of an Experimental Masonry Building," *U.S. National Bureau of Standards, Building Science Series,*, Vol. 45, 1973.

89. Hittle, D. C., *Calculating Building Heating and Cooling Loads Using the Frequency Response of Multilayered Slabs*, Ph.D. Thesis, University of Illinois, Urban, Illinois, 1981 and Technical Manuscript E-169, U.S. Army Construction Engineering Research Laboratory, Champaign, Illinois, 1981.

90. Thomas, W. C. and Reed, K. T., "Effect of Infrared Irradiance on Collector Thermal Performance," *ASME Paper No. 84-WA/Sol-8*, 1984.

91. Haghighat, F., Unny, T. E. and Chandrashekar, M., "Stochastic Modeling of Transient Heat Flow Through Walls," *Transactions of the ASME, Journal of Solar Energy Engineering*, Vol. 107, August, 1985, pp.202-207.

92. Richard, O. E., "Evaluating Design Temperature For HVAC Applications in Extreme Climates," *ASHRAE Transactions*, Vol. 88, part 1, 1982, pp.747-756.

93. Kusuda, T. and Ishii, K., "Hourly Solar Radiation Data for Vertical and Horizontal Surfaces on Average Days in the United States and Canada," *U.S. National Bureau of Standards, Building Science Series,*, Vol. 96, 1977.

94. Tye, R. P. and Spinney, S. C., "Measurement of the Specific Heat of Building Materials," *ASHRAE Transactions*, Vol. 84, part 1, 1978, pp. 675-685.

95. Hoagland, L. C., DeWinter, F. and Reti, A. R., *Transactions ISA*, Vol. 6, part 2, 1967, pp.111.

96. ASTM C 351 A. S. T. M. Standards, 1973.

97. Churchill, R.V., Brown, J.W., and Verhey, R.F. *Complex Variables and Applications*, McGraw-Hill Book Company, third edition 1974.

98. Gerald, C. F. and Wheatly, P. O., *Applied Numerical Analysis*, third edition, Addison-Wesley Publishing Company, 1984, Chapter 1 and 2.

99. Walton, G. N., "A New Algorithm for Radiant Interchange in Room Loads Calculations," *ASHRAE Transactions*, Vol. 86, part 2, 1980.

100. Carroll, J. A., "An MRT Method of Computing Radiant Energy Exchange in Rooms," *Proceedings of the 2nd Systems Simulation & Economic Analysis Conference*, San Diego, 1980, pp. 343-348.

101. Carroll, J. A., "A Comparison of Radiant Interchange Algorithms," *Proceedings of the 2nd Systems Simulation & Economic Analysis Conference*, San Diego, 1980, pp. 399-407.

102. Thomas, W. C., "Finite Difference Algorithms for Single- And Multi-layer Slabs," *Personal Communication*, M E Department, Virginia Tech, 1986.

103. Rohsenow, W. M., Hartnet, J. P. and Ganic, E. N., *Handbook of Heat Transfer Applications*, second edition, McGraw-Hill Book Company, 1985, Chapter 9, pp. 9.1-9.55.

104. Niles, P. W. and Haggard, K. L., *Passive Solar Handbook*, California Energy Commission, 1980.

105. *Handbook of Air Conditioning System Design*, Carrier Air Conditioning Company, McGraw-Hill Book Company, 1965.

APPENDIX A INVERSION TO THE TIME DOMAIN

The inversion of Eq. 3.68 in Chapter 3 is required in the inversion of the elements of matrix $\bar{K}_i$ to the time domain. Rewriting Eq. 3.68 from Chapter 3.

$$
\begin{aligned}
L^{-1}[\bar{X}_i] = X_i &= \lim_{s \to 0} \frac{d}{ds}\left[\frac{s^2\bar{\varphi}De^{st_i}}{B}\right] + \sum_{k=1}^{\infty}\left[\frac{\bar{\varphi}De^{st_i}}{\frac{dB}{ds}}\right]_{s=-\beta_k} \\
L^{-1}[\bar{Y}_i] = Y_i &= \lim_{s \to 0} \frac{d}{ds}\left[\frac{s^2\bar{\varphi}e^{st_i}}{B}\right] + \sum_{k=1}^{\infty}\left[\frac{\bar{\varphi}e^{st_i}}{\frac{dB}{ds}}\right]_{s=-\beta_k} \qquad (A-1) \\
L^{-1}[\bar{Z}_i] = Z_i &= \lim_{s \to 0} \frac{d}{ds}\left[\frac{s^2\bar{\varphi}Ae^{st_i}}{B}\right] + \sum_{k=1}^{\infty}\left[\frac{\bar{\varphi}Ae^{st_i}}{\frac{dB}{ds}}\right]_{s=-\beta_k}
\end{aligned}
$$

where the β 's are the roots (poles) of the following equation:

$$B(s = -\beta_k) = 0 \ , \qquad k = 1, 2, ..., \infty \qquad (A-2)$$

Since the overall transmission matrix is the product of the individual transmission matrices (each matrix correspond to a single layer of the slab), the above variables must be determined at the individual matrices first. Rewriting Eq. 3.50 of Chapter 3,

$$\begin{bmatrix} A & B \\ C & D \end{bmatrix} = \begin{bmatrix} A_1 & B_1 \\ C_1 & D_1 \end{bmatrix} \begin{bmatrix} A_2 & B_2 \\ C_2 & D_2 \end{bmatrix} \cdots \begin{bmatrix} A_{n-1} & B_{n-1} \\ C_{n-1} & D_{n-1} \end{bmatrix} \qquad (A-3)$$

The derivative of the general matrix is

$$\begin{aligned} \frac{d}{ds}\begin{bmatrix} A & B \\ C & D \end{bmatrix} = &\begin{bmatrix} \frac{dA_1}{ds} & \frac{dB_1}{ds} \\ \frac{dC_1}{ds} & \frac{dD_1}{ds} \end{bmatrix} \begin{bmatrix} A_2 & B_2 \\ C_2 & D_2 \end{bmatrix} \cdots \begin{bmatrix} A_{n-1} & B_{n-1} \\ C_{n-1} & D_{n-1} \end{bmatrix} \\ &+ \begin{bmatrix} A_1 & B_1 \\ C_1 & D_1 \end{bmatrix} \begin{bmatrix} \frac{dA_2}{ds} & \frac{dB_2}{ds} \\ \frac{dC_2}{ds} & \frac{dD_2}{ds} \end{bmatrix} \cdots \begin{bmatrix} A_{n-1} & B_{n-1} \\ C_{n-1} & D_{n-1} \end{bmatrix} \\ &+ \;.\;.\;.\;.\;. \\ &+ \;.\;.\;.\;.\;. \\ &+ \;.\;.\;.\;.\;. \\ &+ \begin{bmatrix} A_1 & B_1 \\ C_1 & D_1 \end{bmatrix} \begin{bmatrix} A_2 & B_2 \\ C_2 & D_2 \end{bmatrix} \cdots \begin{bmatrix} \frac{dA_{n-1}}{ds} & \frac{dB_{n-1}}{ds} \\ \frac{dC_{n-1}}{ds} & \frac{dD_{n-1}}{ds} \end{bmatrix} \end{aligned} \qquad (A-4)$$

Next, the derivation of the elements of the transmission matrix for the general layer i is presented. Rewriting Eq. 3.33 of Chapter 3

$$\begin{aligned} A_i &= \cosh(\Delta x_i \sqrt{s/\alpha_i}) \\ B_i &= \frac{1}{k_i\sqrt{s/\alpha_i}} \sinh(\Delta x_i \sqrt{s/\alpha_i}) \\ C_i &= k_i\sqrt{s/\alpha_i} \sinh(\Delta x_i \sqrt{s/\alpha_i}) \\ D_i &= \cosh(\Delta x_i \sqrt{s/\alpha_i}) \end{aligned} \qquad (A-5)$$

The derivative of each variable with respect to s is therefore

$$\frac{dA_i}{ds} = \frac{\Delta x_i}{2\sqrt{s\alpha_i}} \sinh(\Delta x_i \sqrt{s/\alpha_i})$$

$$\frac{dB_i}{ds} = \frac{\Delta x_i}{2sk_i} \cosh(\Delta x_i \sqrt{s/\alpha_i}) - \frac{1}{2k_i\alpha_i(\sqrt{s/\alpha_i})^3} \sinh(\Delta x_i \sqrt{s/\alpha_i}) \qquad (A-6)$$

$$\frac{dC_i}{ds} = \frac{\Delta x_i k_i}{2\alpha_i} \cosh(\Delta x_i \sqrt{s/\alpha_i}) + \frac{k_i}{2\sqrt{s\alpha_i}} \sinh(\Delta x_i \sqrt{s/\alpha_i})$$

$$\frac{dD_i}{ds} = \frac{\Delta x_i}{2\sqrt{s\alpha_i}} \sinh(\Delta x_i \sqrt{s/\alpha_i})$$

Rewriting $\frac{dA_i}{ds}$ from Eq. A-6

$$\frac{dA_i}{ds} = \frac{\Delta x_i^2}{2\alpha_i} \quad \frac{\sinh(\Delta x_i \sqrt{s/\alpha_i})}{\Delta x_i \sqrt{s/\alpha_i}} \qquad (A-7)$$

since

$$\lim_{y \to 0} \frac{\sinh(y)}{y} = 1 \qquad (A-8)$$

Taking limits as s → 0

$$\lim_{s \to 0} \frac{dA_i}{ds} = \frac{\Delta x_i^2}{2\alpha_i} \qquad (A-9)$$

Rewriting $\frac{dB_i}{ds}$ from Eq. A-6

$$\frac{dB_i}{ds} = \left(\frac{\Delta x_i^2}{2\alpha_i}\right)\left(\frac{\Delta x_i}{k_i}\right)\left[\frac{\cosh(\Delta x_i \sqrt{s/\alpha_i})}{(\Delta x_i \sqrt{s/\alpha_i})^2} - \frac{\sinh(\Delta x_i \sqrt{s/\alpha_i})}{(\Delta x_i \sqrt{s/\alpha_i})^3}\right] \qquad (A-10)$$

Simplifying

$$\frac{\cosh(\Delta x_i \sqrt{s/\alpha_i})}{(\Delta x_i \sqrt{s/\alpha_i})^2} - \frac{\sinh(\Delta x_i \sqrt{s/\alpha_i})}{(\Delta x_i \sqrt{s/\alpha_i})^3} = \frac{\cosh Z}{Z^2} - \frac{\sinh Z}{Z^3} \qquad (A-11)$$

Substituting the series representation of the hyperbolic sine and cosine,

$$\frac{\cosh Z}{Z^2} - \frac{\sinh Z}{Z^3} = \frac{1}{Z^2}\left[1 + \frac{Z^2}{2!} + \frac{Z^4}{4!} + \cdots - \frac{1}{Z}(Z + \frac{Z^3}{3!} + \frac{Z^5}{5!} + \cdots)\right]$$

$$= \frac{1}{2} - \frac{1}{6} + (\frac{1}{Z^2} - \frac{1}{Z^2} + \frac{Z^2}{4!} - \frac{Z^2}{5!} + \cdots) \qquad (A-12)$$

$$= \frac{1}{3} \qquad as \quad Z \to 0$$

Equation A-10 becomes

$$\lim_{s \to 0} \frac{dB_i}{ds} = \frac{\Delta x_i^2}{6\alpha_i} R_i \qquad (A-13)$$

Similarly

$$\frac{dC_i}{ds} = (\frac{\Delta x_i^2}{2\alpha_i})(\frac{k_i}{\Delta x_i})\left[\frac{\sinh(\Delta x_i \sqrt{s/\alpha_i})}{\Delta x_i \sqrt{s/\alpha_i}} + \cosh(\Delta x_i \sqrt{s/\alpha_i})\right] \qquad (A-14)$$

Taking the limit as s → 0

$$\lim_{s \to 0} \frac{dC_i}{ds} = (\frac{\Delta x_i^2}{\alpha_i})(\frac{1}{R_i}) \qquad (A-15)$$

and

$$\lim_{s \to 0} \frac{dD_i}{ds} = \lim_{s \to 0} \frac{dA_i}{ds} = \frac{\Delta x_i^2}{2\alpha_i} \qquad (A-16)$$

Evaluating the elements of the transmission matrix as s → 0.

$$\lim_{s \to 0}\begin{bmatrix} A_i & B_i \\ C_i & D_i \end{bmatrix} = \lim_{s \to 0}\begin{bmatrix} \cosh(\Delta x_i\sqrt{s/\alpha_i}) & \dfrac{1}{k_i\sqrt{s/\alpha_i}}\sinh(\Delta x_i\sqrt{s/\alpha_i}) \\ k_i\sqrt{s/\alpha_i}\,\sinh(\Delta x_i\sqrt{s/\alpha_i}) & \cosh(\Delta x_i\sqrt{s/\alpha_i}) \end{bmatrix} \qquad (A-17)$$

Equation A-17 is evaluated similarly to Eq. 3.39 in Chapter 3 as s → 0

$$\lim_{s \to 0}\begin{bmatrix} A_i & B_i \\ C_i & D_i \end{bmatrix} = \begin{bmatrix} 1 & R_i \\ 0 & 1 \end{bmatrix} \qquad (A-18)$$

Using Eq. A-3 for n-1 multilayer slab

$$\lim_{s \to 0}\begin{bmatrix} A & B \\ C & D \end{bmatrix} = \begin{bmatrix} 1 & R_1 \\ 0 & 1 \end{bmatrix}\begin{bmatrix} 1 & R_2 \\ 0 & 1 \end{bmatrix} \cdots \begin{bmatrix} 1 & R_{n-1} \\ 0 & 1 \end{bmatrix} \qquad (A-19)$$

Expanding the right hand side leads to the following important characteristic of the overall transmission matrix

$$\lim_{s \to 0}\begin{bmatrix} A & B \\ C & D \end{bmatrix} = \begin{bmatrix} 1 & R_1 + R_2 + \cdots + R_{n-1} \\ 0 & 1 \end{bmatrix} = \begin{bmatrix} 1 & \dfrac{1}{U} \\ 0 & 1 \end{bmatrix} \qquad (A-20)$$

where U is the overall heat transfer coefficient of the multilayer (n-1 layers) slab.

Next, the elements and their derivatives of the individual transmission matrix of layer i (A, B, C, D and dA/ds, dB/ds, dC/ds, dD/ds) are evaluated at $s=-\beta_1$, $s=-\beta_2$, $s=-\beta_3$, etc. This result is needed in order to evaluate the second part of Eq. A-1. Substituting into Eq. A-5

$$A_i = \left[\cosh(\Delta x_i\sqrt{s/\alpha_i})\right]_{s=-\beta_k} = \cosh(\Delta x_i\, j\,\sqrt{\beta_k/\alpha_i}) \qquad (A-21)$$

where $j = \sqrt{-1}$. Using

$$\begin{aligned} \sinh(j\,u) &= j\,\sin(u) \\ \cosh(j\,u) &= \cos(u) \end{aligned} \qquad (A-22)$$

Eq. A-21 becomes

$$A_i = \cos(\Delta x_i \sqrt{\beta_k/\alpha_i}) \qquad (A-23)$$

Similarly

$$\begin{aligned} B_i &= \left[\frac{1}{k_i\sqrt{s/\alpha_i}}\,\sinh(\Delta x_i \sqrt{s/\alpha_i})\right]_{s=-\beta_k} \\ &= \frac{1}{j}\,\frac{1}{k_i\sqrt{\beta_k/\alpha_i}}\,j\,\sin(\Delta x_i \sqrt{\beta_k/\alpha_i}) \\ &= \frac{1}{k_i\sqrt{\beta_k/\alpha_i}}\,\sin(\Delta x_i \sqrt{\beta_k/\alpha_i}) \end{aligned} \qquad (A-24)$$

and

$$\begin{aligned} C_i &= \left[k_i\sqrt{s/\alpha_i}\,\sinh(\Delta x_i \sqrt{s/\alpha_i})\right]_{s=-\beta_k} \\ &= j\,k_i\sqrt{\beta_k/\alpha_i}\;j\,\sin(\Delta x_i \sqrt{\beta_k/\alpha_i}) \\ &= -\,k_i\sqrt{\beta_k/\alpha_i}\,\sin(\Delta x_i \sqrt{\beta_k/\alpha_i}) \end{aligned} \qquad (A-25)$$

$$\left[D_i\right]_{s=-\beta_k} = \left[A_i\right]_{s=-\beta_k} = \cos(\Delta x_i \sqrt{\beta_k/\alpha_i}) \qquad (A-26)$$

By setting $s = -\beta_k$ and making use of the hyperbolic relations given in Eq. A-22, the following relations are obtained:

$$
\begin{aligned}
&as \quad S = -\beta_k \\
&\frac{dA_i}{ds} = \frac{\Delta x_i}{2\sqrt{\beta_k \alpha_i}} \sin(\Delta x_i \sqrt{\beta_k/\alpha_i}) \\
&\frac{dB_i}{ds} = \frac{1}{2k_i\alpha_i(\sqrt{\beta_k/\alpha_i})^3} \sin(\Delta x_i \sqrt{\beta_k/\alpha_i}) - \frac{\Delta x_i k_i}{2\beta_k k_i} \cos(\Delta x_i \sqrt{\beta_k/\alpha_i}) \qquad (A-27) \\
&\frac{dC_i}{ds} = \frac{\Delta x_i k_i}{2\alpha_i} \cos(\Delta x_i \sqrt{\beta_k/\alpha_i}) + \frac{k_i}{2\sqrt{\beta_k \alpha_i}} \sinh(\Delta x_i \sqrt{\beta_k/\alpha_i}) \\
&\frac{dD_i}{ds} = \frac{\Delta x_i}{2\sqrt{\beta_k \alpha_i}} \sin(\Delta x_i \sqrt{\beta_k/\alpha_i})
\end{aligned}
$$

Therefore, Eq. A-1 can be evaluated

$$
\begin{aligned}
X_i &= \lim_{s \to 0} \frac{d}{ds}\left[\frac{s^2 \bar{\varphi} D e^{st_i}}{B}\right] + \sum_{k=1}^{\infty}\left[\frac{\bar{\varphi} D e^{st_i}}{\frac{dB}{ds}}\right]_{s=-\beta_k} \\
Y_i &= \lim_{s \to 0} \frac{d}{ds}\left[\frac{s^2 \bar{\varphi} e^{st_i}}{B}\right] + \sum_{k=1}^{\infty}\left[\frac{\bar{\varphi} e^{st_i}}{\frac{dB}{ds}}\right]_{s=-\beta_k} \qquad (A-1) \\
Z_i &= \lim_{s \to 0} \frac{d}{ds}\left[\frac{s^2 \bar{\varphi} A e^{st_i}}{B}\right] + \sum_{k=1}^{\infty}\left[\frac{\bar{\varphi} A e^{st_i}}{\frac{dB}{ds}}\right]_{s=-\beta_k}
\end{aligned}
$$

Examining the first term on the right hand side of the equation for X_i and substituting into Eq. 3.60 of Chapter 3

$$\lim_{s \to 0} \frac{d}{ds}\left[\frac{s^2\overline{\varphi}De^{st_i}}{B}\right] =$$

$$\begin{cases} \lim_{s \to 0} \frac{d}{ds}\left[\frac{\frac{D}{\delta}e^{st_i}}{B}\right] & 0 < t_i \leq \delta \\ \lim_{s \to 0} \frac{d}{ds}\left[\frac{\frac{D}{\delta}(1 - 2e^{-s\delta})e^{st_i}}{B}\right] & \delta < t_i \leq 2\delta \\ \lim_{s \to 0} \frac{d}{ds}\left[\frac{\frac{D}{\delta}(1 - e^{-s\delta})^2 e^{st_i}}{B}\right] & t_i > 2\delta \end{cases} \qquad (A - 28)$$

Carrying out the differentiations and taking the limits as s → 0, Eq. A-28 becomes

$$\lim_{s \to 0} \frac{d}{ds}\left[\frac{s^2\overline{\varphi}De^{st_i}}{B}\right] =$$

$$\begin{cases} \left[\frac{D}{B} + \left(\frac{1}{\delta B}\right)\left(\frac{dD}{ds}\right) - \left(\frac{D}{\delta B^2}\right)\left(\frac{dB}{ds}\right)\right]_{s=0} & 0 < t_i \leq \delta \\ \left[\frac{D}{\delta B^2} - \left(\frac{1}{\delta B}\right)\left(\frac{dD}{ds}\right)\right]_{s=0} & \delta < t_i \leq 2\delta \\ 0 & t_i > 2\delta \end{cases} \qquad (A - 29)$$

Applying the same procedure for Y_i *and* Z_i in Eq. A-1 leads to

$$\lim_{s \to 0} \frac{d}{ds}\left[\frac{s^2\overline{\varphi}e^{st_i}}{B}\right] =$$

$$\begin{cases} \left[\frac{1}{B} - \left(\frac{1}{\delta B^2}\right)\left(\frac{dB}{ds}\right)\right]_{s=0} & 0 < t_i \leq \delta \\ \left[\frac{1}{\delta B^2}\right]_{s=0} & \delta < t_i \leq 2\delta \\ 0 & t_i > 2\delta \end{cases} \qquad (A - 30)$$

and

$$\lim_{s \to 0} \frac{d}{ds}\left[\frac{s^2 \bar{\varphi} A e^{st_i}}{B}\right] =$$

$$\begin{cases} \left[\frac{A}{B} + \left(\frac{1}{\delta B}\right)\left(\frac{dA}{ds}\right) - \left(\frac{A}{\delta B^2}\right)\left(\frac{dB}{ds}\right)\right]_{s=0} & 0 < t_i \leq \delta \\ \left[\frac{A}{\delta B^2} - \left(\frac{1}{\delta B}\right)\left(\frac{dA}{ds}\right)\right]_{s=0} & \delta < t_i \leq 2\delta \\ 0 & t_i > 2\delta \end{cases} \qquad (A-31)$$

Substituting Eq. 3.60 into the second term of the right hand side of the expression for X_i in Eq. A-1 leads to

$$\sum_{k=1}^{\infty}\left[\frac{\bar{\varphi} D e^{st_i}}{\frac{dB}{ds}}\right]_{s=-\beta_k} =$$

$$\begin{cases} \sum_{k=1}^{\infty}\left[\left(\frac{e^{-\beta_k \delta}}{\delta \beta^2}\right) \frac{D}{\frac{dB}{ds}}\right]_{s=-\beta_k} & 0 < t_i \leq \delta \\ \sum_{k=1}^{\infty}\left[\left(\frac{(1-2e^{\beta_k \delta})e^{-2\beta_k \delta}}{\delta \beta^2}\right) \frac{D}{\frac{dB}{ds}}\right]_{s=-\beta_k} & \delta < t_i \leq 2\delta \\ \sum_{k=1}^{\infty}\left[\left(\frac{(1-e^{\beta_k \delta})^2 e^{-(i+1)\beta_k \delta}}{\delta \beta^2}\right) \frac{D}{\frac{dB}{ds}}\right]_{s=-\beta_k} & t_i = i\delta > 2\delta \end{cases} \qquad (A-32)$$

Similarly for Y_i

$$\sum_{k=1}^{\infty}\left[\frac{\bar{\varphi}e^{st_i}}{\frac{dB}{ds}}\right]_{s=-\beta_k} =$$

$$\sum_{k=1}^{\infty}\left[\left(\frac{e^{-\beta_k\delta}}{\delta\beta^2}\right)\ \frac{1}{\frac{dB}{ds}}\right]_{s=-\beta_k} \qquad 0 < t_i \leq \delta$$

$$\sum_{k=1}^{\infty}\left[\left(\frac{(1-2e^{\beta_k\delta})e^{-2\beta_k\delta}}{\delta\beta^2}\right)\ \frac{1}{\frac{dB}{ds}}\right]_{s=-\beta_k} \qquad \delta < t_i \leq 2\delta \qquad (A-33)$$

$$\sum_{k=1}^{\infty}\left[\left(\frac{(1-e^{\beta_k\delta})^2e^{-(i+1)\beta_k\delta}}{\delta\beta^2}\right)\ \frac{1}{\frac{dB}{ds}}\right]_{s=-\beta_k} \qquad t_i = i\delta > 2\delta$$

and for Z_i

$$\sum_{k=1}^{\infty}\left[\frac{\bar{\varphi}Ae^{st_i}}{\frac{dB}{ds}}\right]_{s=-\beta_k} =$$

$$\sum_{k=1}^{\infty}\left[\left(\frac{e^{-\beta_k\delta}}{\delta\beta^2}\right)\ \frac{A}{\frac{dB}{ds}}\right]_{s=-\beta_k} \qquad 0 < t_i \leq \delta$$

$$\sum_{k=1}^{\infty}\left[\left(\frac{(1-2e^{\beta_k\delta})e^{-2\beta_k\delta}}{\delta\beta^2}\right)\ \frac{A}{\frac{dB}{ds}}\right]_{s=-\beta_k} \qquad \delta < t_i \leq 2\delta \qquad (A-34)$$

$$\sum_{k=1}^{\infty}\left[\left(\frac{(1-e^{\beta_k\delta})^2e^{-(i+1)\beta_k\delta}}{\delta\beta^2}\right)\ \frac{A}{\frac{dB}{ds}}\right]_{s=-\beta_k} \qquad t_i = i\delta > 2\delta$$

By combining Eqs. A-29 and A-32 for X_i, Eqs. A-30 and A-33 for Y_i, and Eqs. A-31 and A-34 for Z_i and substituting into the original Eq. A-1, the following coefficients, called "RESPONSE FACTORS," are obtained

Response Factors X :

$$X_0 = \left[\frac{D}{B} + \left(\frac{1}{\delta B}\right)\left(\frac{dD}{ds}\right) - \left(\frac{D}{\delta B^2}\right)\left(\frac{dB}{ds}\right)\right]_{s=0} + \sum_{k=1}^{\infty}\left[\left(\frac{e^{-\beta_k\delta}}{\delta\beta^2}\right) \quad \frac{D}{\frac{dB}{ds}}\right]_{s=-\beta_k}$$

$$X_1 = \left[\frac{D}{\delta B^2} - \left(\frac{1}{\delta B}\right)\left(\frac{dD}{ds}\right)\right]_{s=0} + \sum_{k=1}^{\infty}\left[\left(\frac{(1-2e^{\beta_k\delta})e^{-2\beta_k\delta}}{\delta\beta^2}\right) \quad \frac{D}{\frac{dB}{ds}}\right]_{s=-\beta_k} \quad (A-35)$$

$$X_i = \sum_{k=1}^{\infty}\left[\left(\frac{(1-e^{\beta_k\delta})^2 e^{-(i+1)\beta_k\delta}}{\delta\beta^2}\right) \quad \frac{D}{\frac{dB}{ds}}\right]_{s=-\beta_k} \qquad i = 2, 3, 4, \ldots$$

Response Factors Y :

$$Y_0 = \left[\frac{1}{B} - \left(\frac{1}{\delta B^2}\right)\left(\frac{dB}{ds}\right)\right]_{s=0} + \sum_{k=1}^{\infty}\left[\left(\frac{e^{-\beta_k\delta}}{\delta\beta^2}\right) \quad \frac{1}{\frac{dB}{ds}}\right]_{s=-\beta_k}$$

$$Y_1 = \left[\frac{1}{\delta B^2}\right]_{s=0} + \sum_{k=1}^{\infty}\left[\left(\frac{(1-2e^{\beta_k\delta})e^{-2\beta_k\delta}}{\delta\beta^2}\right) \quad \frac{1}{\frac{dB}{ds}}\right]_{s=-\beta_k} \quad (A-36)$$

$$Y_i = \sum_{k=1}^{\infty}\left[\left(\frac{(1-e^{\beta_k\delta})^2 e^{-(i+1)\beta_k\delta}}{\delta\beta^2}\right) \quad \frac{1}{\frac{dB}{ds}}\right]_{s=-\beta_k} \qquad i = 2, 3, 4, \ldots$$

Response Factors Z :

$$Z_0 = \left[\frac{A}{B} + \left(\frac{1}{\delta B}\right)\left(\frac{dA}{ds}\right) - \left(\frac{A}{\delta B^2}\right)\left(\frac{dB}{ds}\right)\right]_{s=0} + \sum_{k=1}^{\infty}\left[\left(\frac{e^{-\beta_k\delta}}{\delta\beta^2}\right) \quad \frac{A}{\frac{dB}{ds}}\right]_{s=-\beta_k}$$

$$Z_1 = \left[\frac{A}{\delta B^2} - \left(\frac{1}{\delta B}\right)\left(\frac{dA}{ds}\right)\right]_{s=0} + \sum_{k=1}^{\infty}\left[\left(\frac{(1-2e^{\beta_k\delta})e^{-2\beta_k\delta}}{\delta\beta^2}\right) \quad \frac{A}{\frac{dB}{ds}}\right]_{s=-\beta_k} \quad (A-37)$$

$$Z_i = \sum_{k=1}^{\infty}\left[\left(\frac{(1-e^{\beta_k\delta})^2 e^{-(i+1)\beta_k\delta}}{\delta\beta^2}\right) \quad \frac{A}{\frac{dB}{ds}}\right]_{s=-\beta_k} \qquad i = 2, 3, 4, \ldots$$

APPENDIX B ROOTS AND RESPONSE FACTORS OF TYPICAL WALLS

The roots are the poles of the characteristic equation (Eq. 3.69), or equation B of the overall transmission matrix. As noted in Eq. 3.68, the functions X_i, Y_i, and Z_i are not analytic when B is zero. Therefore, the roots are needed in the residue theorem used to invert the solution from the Laplace to the time domain. It has been noted by Hittle and Bishop [16] that determining the roots of equation B tends to be tedious for thermally massive walls. A simple way to explain how these roots are calculated is by using an illustrative figure. In Fig. 71, the characteristic equation $B(\beta)$ is plotted versus β for a 0.2 ft (0.061 m) layer (slab) of insulation. Obviously, the roots are the β's corresponding to the characteristic equation being zero. The common procedure for finding these roots has been to take small steps of β's, starting with zero, and calculating the equation $B(\beta)$. When ever the sign changes, a root has been passed, and is located using some type of a root finding procedure. The procedure employed in this thesis is the Interval Halving Method [98]. It should be noted here that Newton's Method presented some difficulties when applied to find the roots. The slope needed in Newton's method was projected sometimes far, passing over some of the roots.

The important contribution of reference 16 was in proving that each root of the characteristic equation $B(\beta)$ must be always followed by a root of the characteristic equation $A(\beta)$. Equation $A(\beta)$ is the first element of the overall transmission matrix. The procedure for determining the roots is that for each step along the β axis, $A(\beta)$ *and* $B(\beta)$ are evaluated. When a change of sign of $B(\beta)$ occurs, a root has been passed. The root is determined using the Interval Halving Method. Also, the number of times $A(\beta)$ had a reversal of sign is checked after determining each root. If the number of sign changes of $A(\beta)$ is one, no roots have been passed over. If the number of sign changes of $A(\beta)$ is n, n-1 roots have been passed. Therefore, the roots of $A(\beta)$ are calculated in order to reevaluate the increments needed along the β axis to locate the remaining roots of equation $B(\beta)$.

Five different walls are used in examining the behavior of response factors and roots. A description of the five walls is given in Table 22. The five walls will be addressed by numbers 1 through 5.

The roots are examined first. Figures 72 through 76 are the roots of each wall case. In each figure, 45 roots are plotted versus their values. Figure 72 shows the root distribution of wall 1 (single insulation layer). The range of the 45 roots was from 0 to 3000. It should be noted here that in the calculation of response factors, the variable $e^{-\delta\eta_k}$ is used throughout and summed over k. Since $e^{-50.0} \cong 0.0$ and for $\delta = 1.0\,h$, all the roots above 50.0 are not needed in the calculations. In Fig. 75 (wall 2), the range of the numerical value of the 45 roots decreased to 1200. As the wall mass increased, the range of roots decreased sharply, 0 to 600 for wall 3, 0 to 400 for wall 4, and 0 to 220 for wall 5. Therefore, in calculating roots, extreme care should be placed if the wall is thermally massive.

As noted earlier, the roots of $B(\beta)$ are always between the roots of $A(\beta)$. This is shown in Figs. 77 through 81 for walls 1 through 5, respectively. As expected, the characteristic equations intersected the β axis in smaller intervals for the thermally massive walls compared

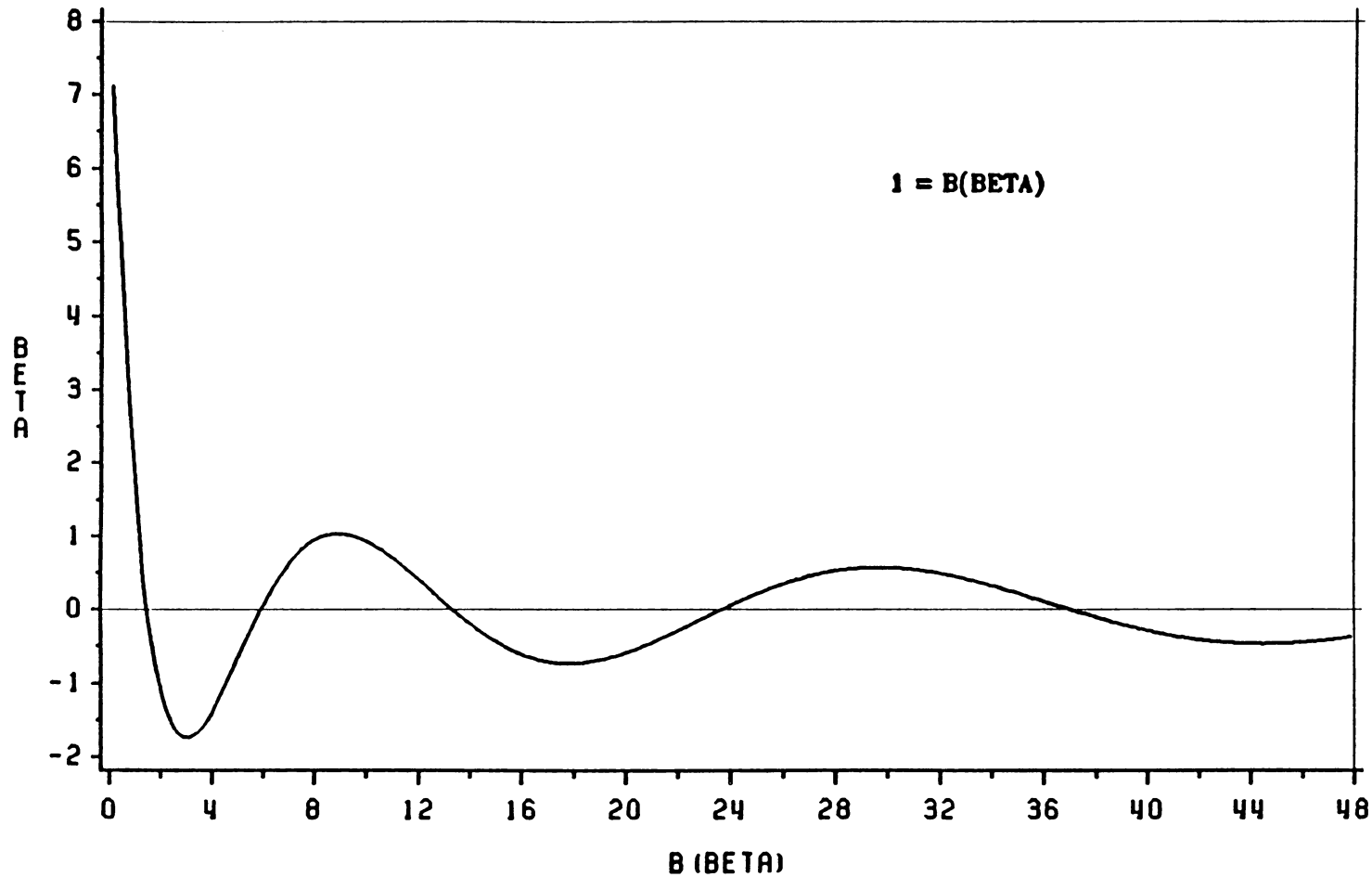

Figure 71. Characteristic Equation for a 0.2 ft (0.061 m) of Insulation

Table 22. Description of the Five Walls

DESCRIPTION OF LAYERS	LAYER No.	ΔX (ft)	k (Btu/h.ft.F)	ρ (lb/ft^3)	C_p (Btu/lb.F)
Insulation	1	0.2	0.025	13.0	0.32
Concrete	2	0.3	1.0	140.0	0.2
Brick	3	0.3	0.76	130.0	0.195
Concrete	4	0.3	1.0	140.0	0.2
Insulation	5	0.2	0.025	13.0	0.32

wall 1 consisits of layer 1 only
wall 2 consisits of layers 1 and 2
wall 3 consisits of layers 1, 2, and 3
wall 4 consisits of layers 1, 2, 3, and 4
wall 5 consisits of layers 1, 2, 3, 4, and 5

English to SI conversion:
1 ft = 0.3048 m
1 Btu/h.ft.F = 1.7307 W/m.C
1 lb/ft^3 = 16.018 kg/m^3
1 Btu/lb.F = 4.1869 kJ/kg.C

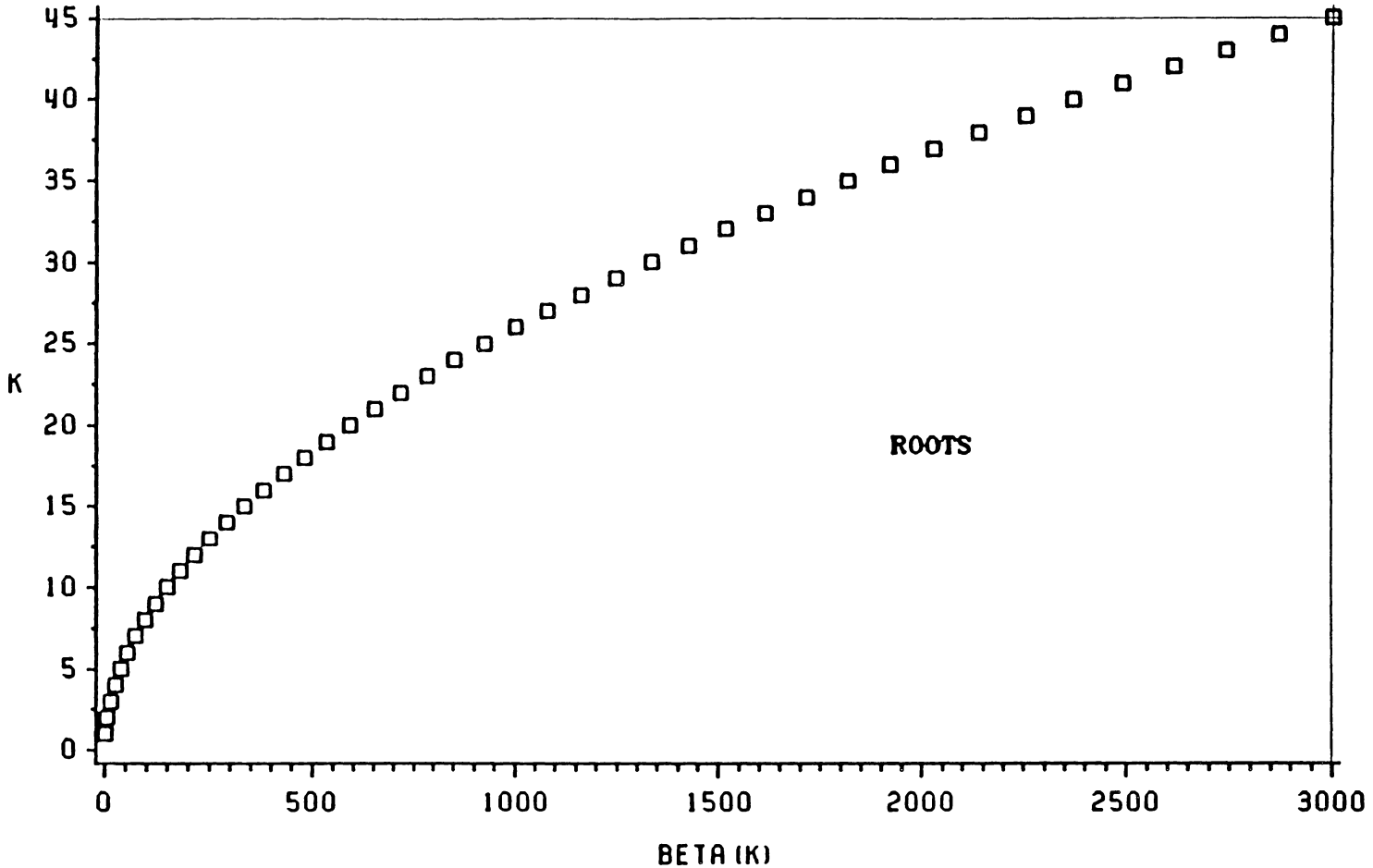

Figure 72. Root Distribution of Wall 1

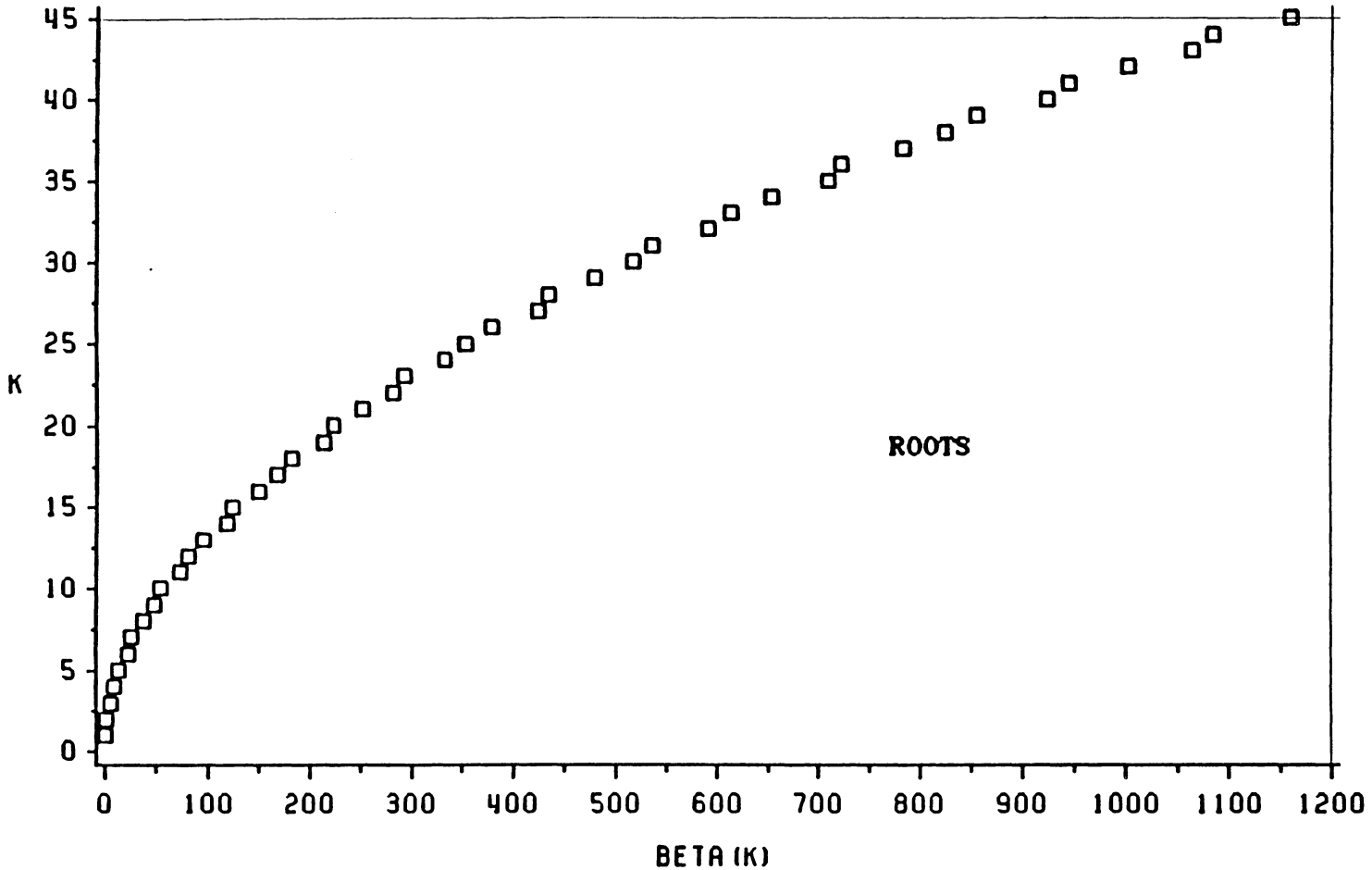

Figure 73. Root Distribution of Wall 2

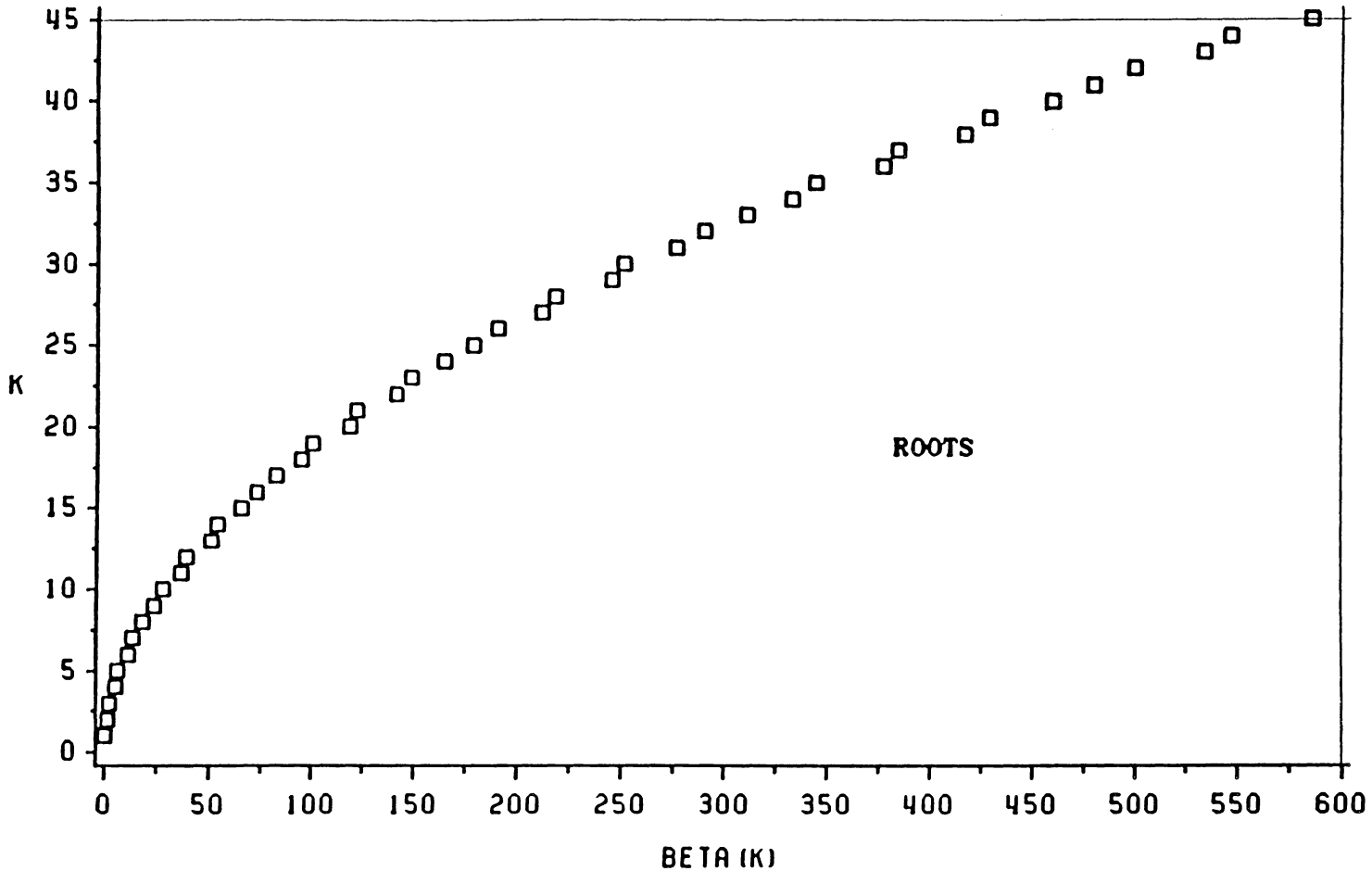

Figure 74. Root Distribution of Wall 3

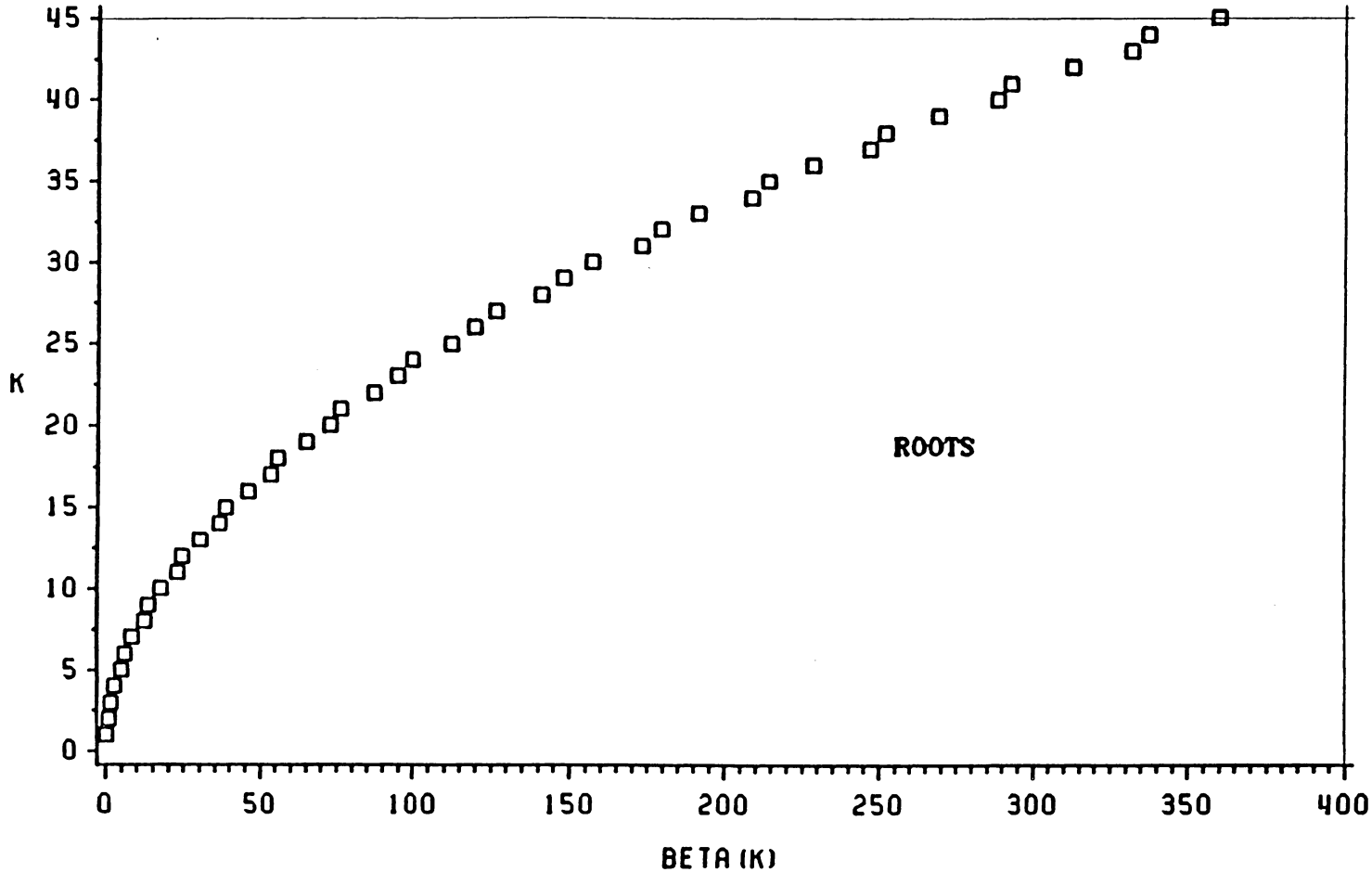

Figure 75. Root Distribution of Wall 4

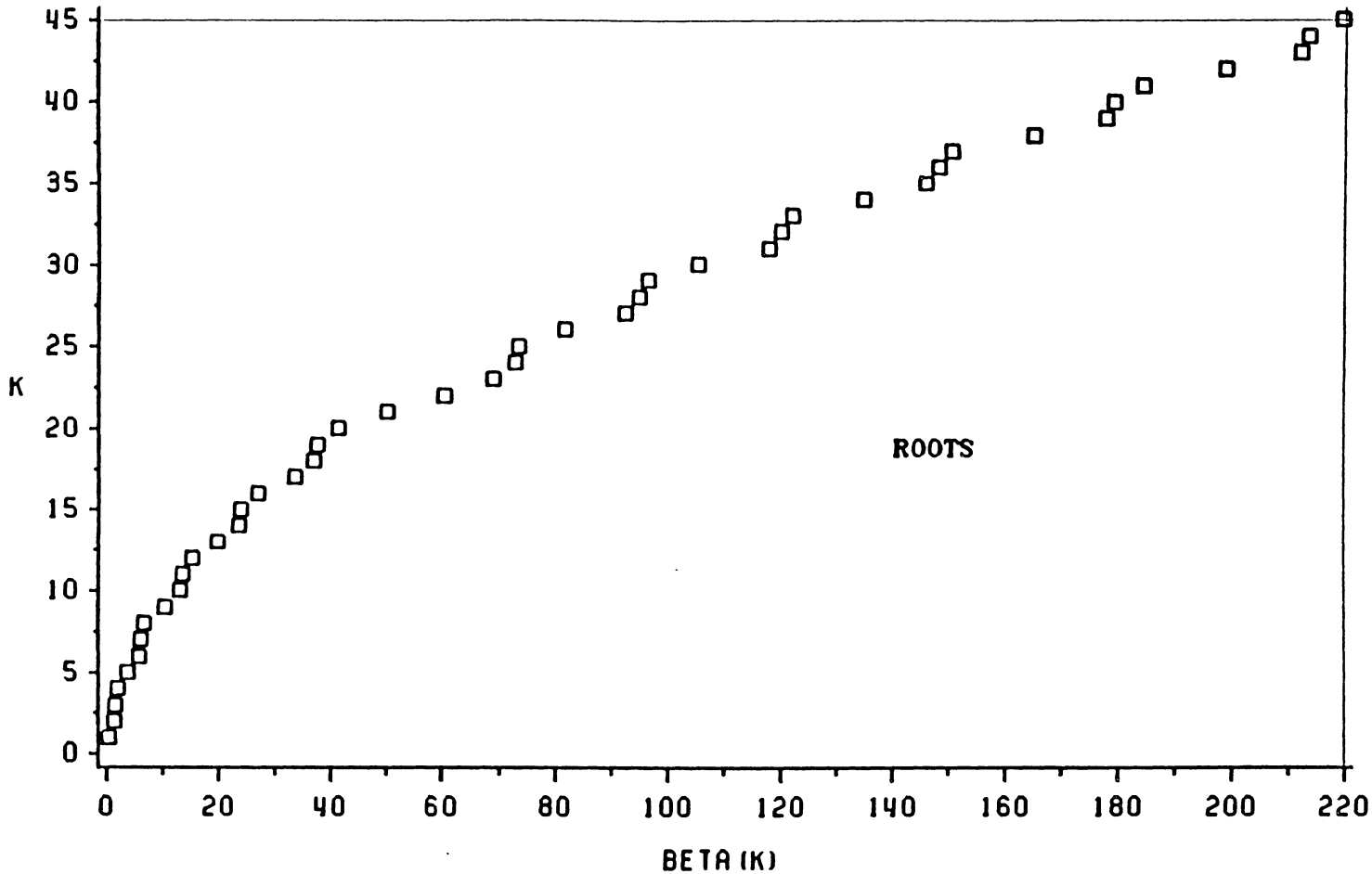

Figure 76. Root Distribution of Wall 5

to the light walls. It is noted that the characteristic curves are not symmetric for the thermally massive walls. It is also obvious that equation B overlapped equation A consistently.

The response factors are presented for the same five walls. All six orders of response factors are given for each wall. Tables 23 through 25 are the response factors X, Y, and Z of wall 1, respectively. It is obvious that the first order response factors could be used in the calculations since only 10 terms are numerically significant. The higher order response factors reduced significantly more the number of terms for thermally massive walls as given in Tables 26 through 37.

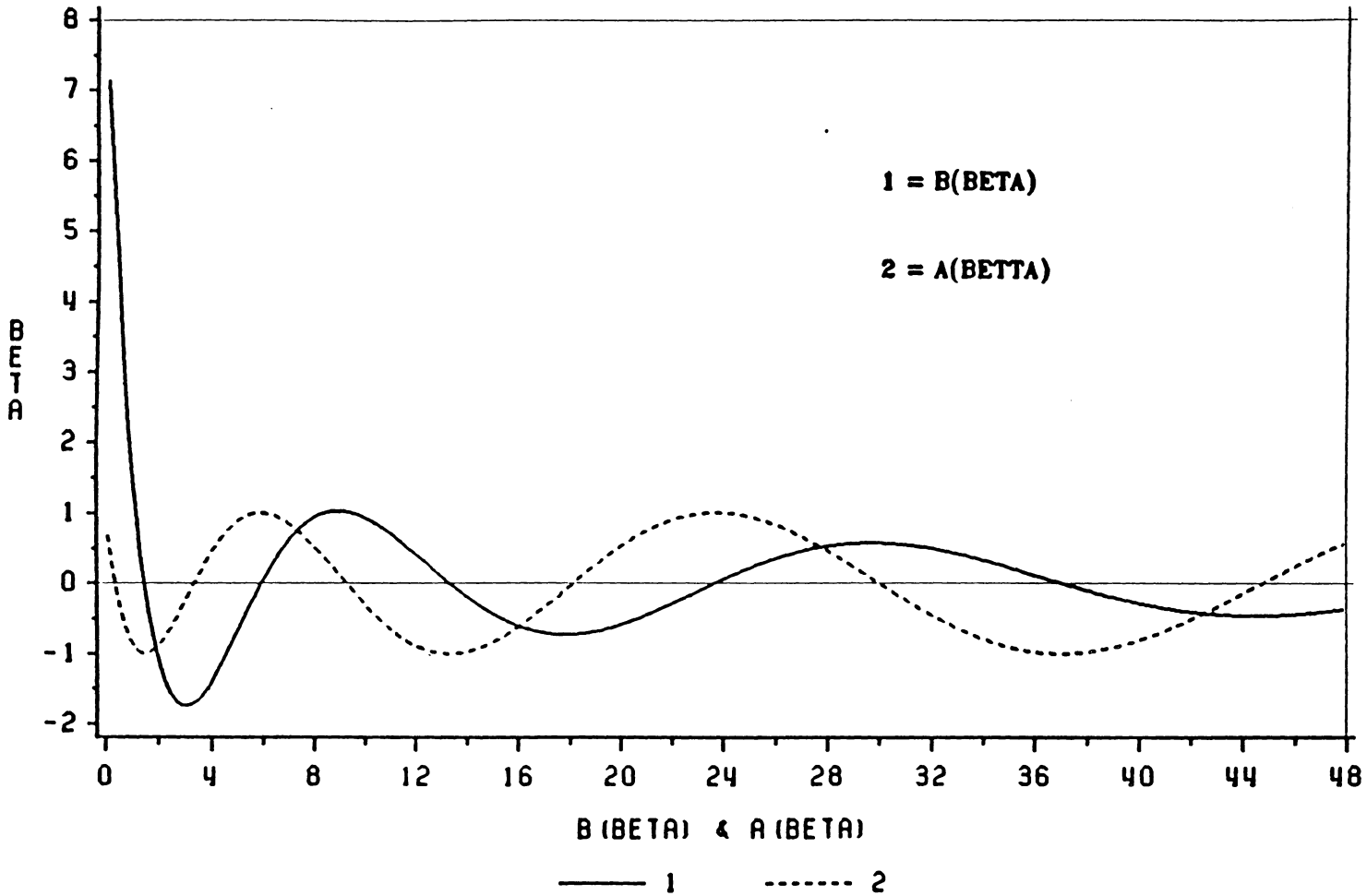

Figure 77. Characteristic Equations A and B of Wall 1

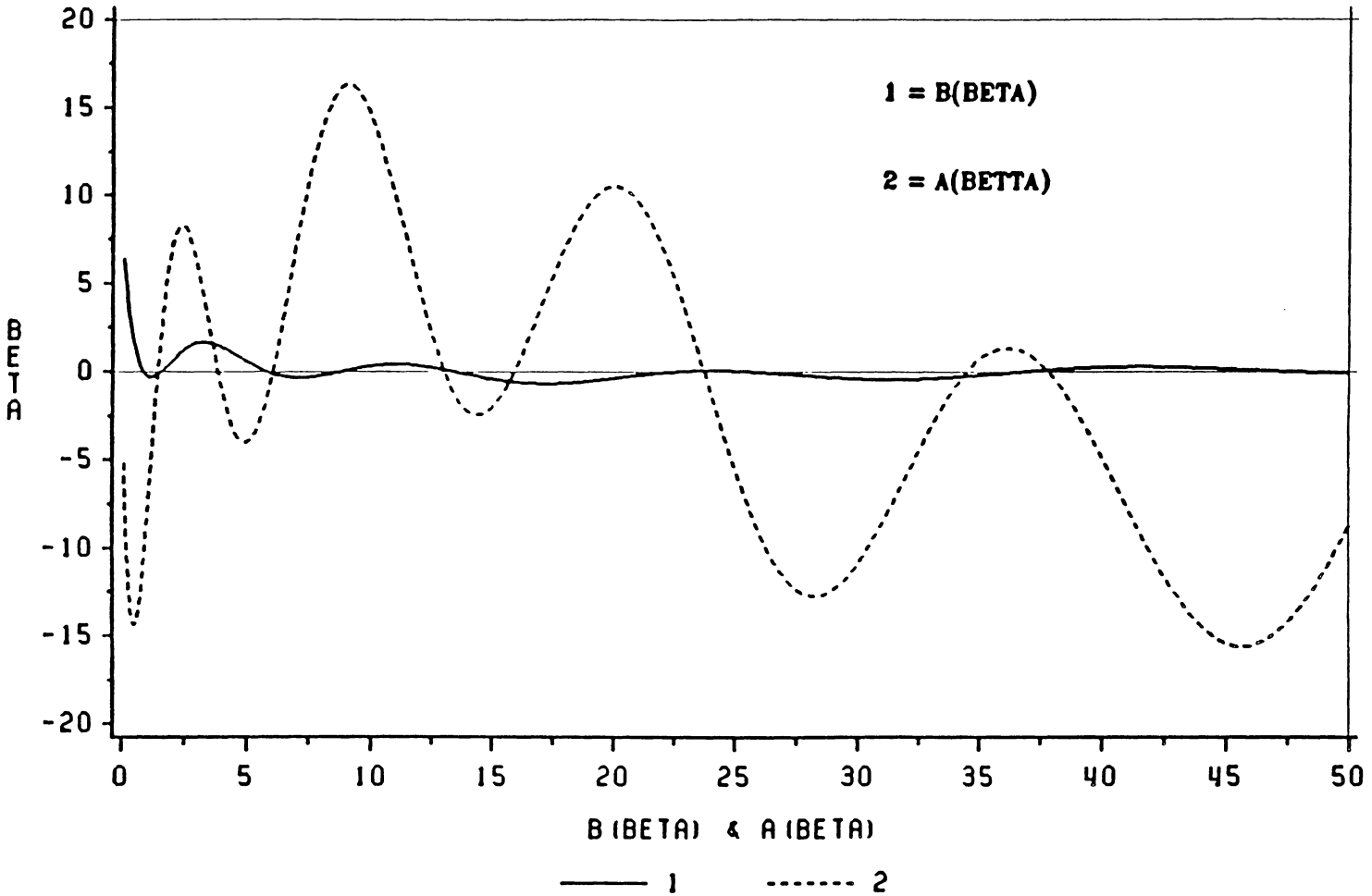

Figure 78. Characteristic Equations A and B of Wall 2

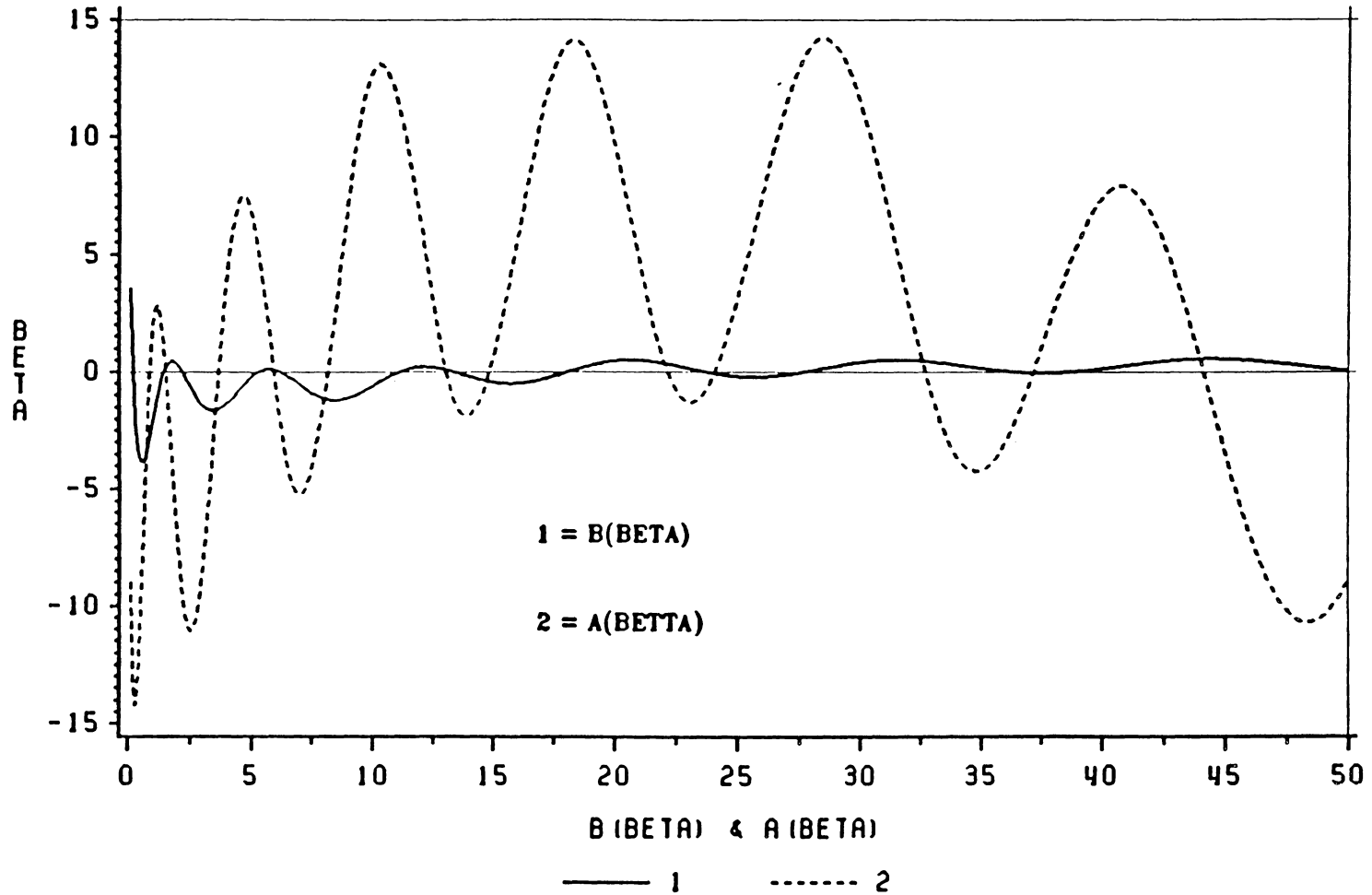

Figure 79. Characteristic Equations A and B of Wall 3

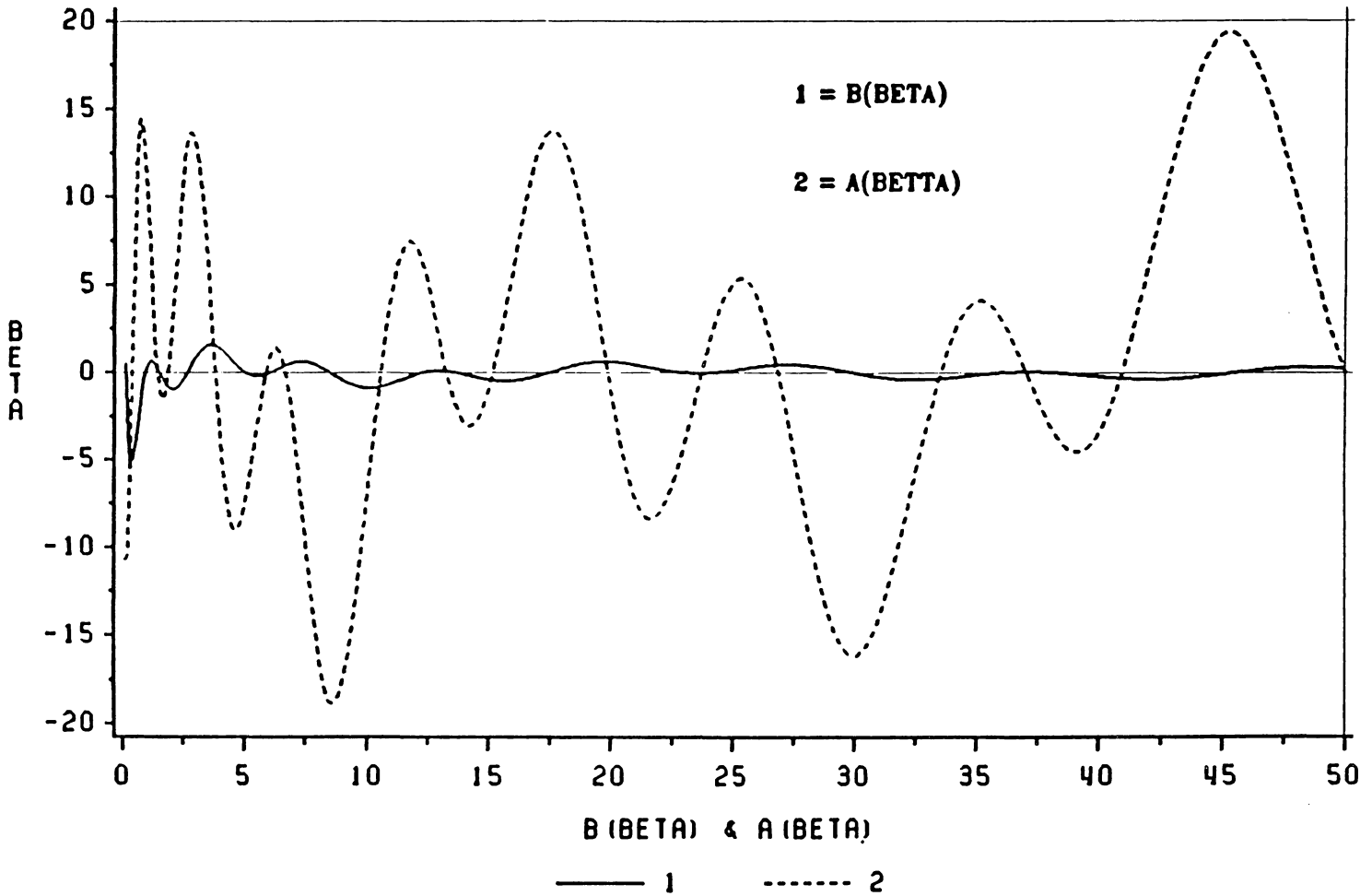

Figure 80. Characteristic Equations A and B of Wall 4

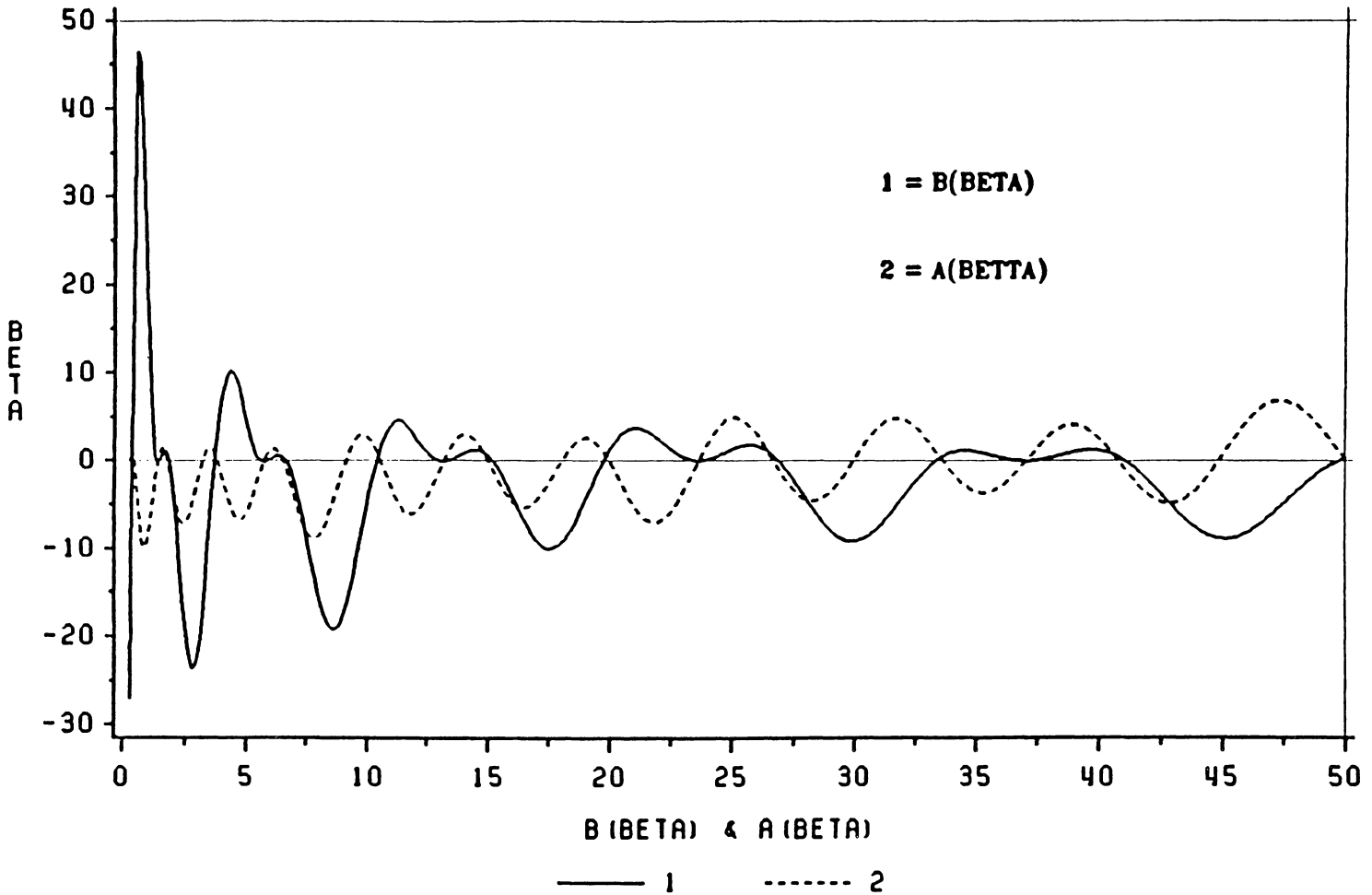

Figure 81. **Characteristic Equations A and B of Wall 5**

Table 23. Response Factors X for Wall 1

i	$X_{i,1}$	$X_{i,2}$	$X_{i,3}$	$X_{i,4}$	$X_{i,5}$	$X_{i,6}$
1	0.3642407	0.3642407	0.3642407	0.3642407	0.3642407	0.3642407
2	-0.2094467	-0.2923251	-0.2933014	-0.2933020	-0.2933020	-0.2933020
3	-0.0230401	0.0246169	0.0254004	0.0254009	0.0254009	0.0254009
4	-0.0052172	0.0000253	-0.0000407	-0.0000407	-0.0000407	-0.0000407
5	-0.0011870	0.0000001	-0.0000000	0.0000000	0.0000000	0.0000000
6	-0.0002701	0.0000000	-0.0000000	0.0000000	0.0000000	0.0000000
7	-0.0000615	0.0000000	-0.0000000	-0.0000000	-0.0000000	-0.0000000
8	-0.0000140	0.0000000	-0.0000000	-0.0000000	-0.0000000	-0.0000000
9	-0.0000032	0.0000000	0.0000000	0.0000000	0.0000000	0.0000000
10	-0.0000007	0.0000000	0.0000000	0.0000000	0.0000000	0.0000000
11	-0.0000002	-0.0000000	-0.0000000	-0.0000000	-0.0000000	-0.0000000
12	-0.0000000	0.0000000	0.0000000	0.0000000	0.0000000	0.0000000
13	-0.0000000	0.0000000	0.0000000	0.0000000	0.0000000	0.0000000
14	-0.0000000	-0.0000000	-0.0000000	-0.0000000	-0.0000000	-0.0000000
15	-0.0000000	0.0000000	0.0000000	0.0000000	0.0000000	0.0000000

$X_{i,j}$ = $Btu/ft^2h.F$

Table 24. Response Factors Y for Wall 1

i	$Y_{i,1}$	$Y_{i,2}$	$Y_{i,3}$	$Y_{i,4}$	$Y_{i,5}$	$Y_{i,6}$
1	0.0244219	0.0244219	0.0244219	0.0244219	0.0244219	0.0244219
2	0.0710099	0.0654530	0.0653875	0.0653875	0.0653875	0.0653875
3	0.0228150	0.0066576	0.0064821	0.0064820	0.0064820	0.0064820
4	0.0052166	0.0000253	0.0000075	0.0000074	0.0000074	0.0000074
5	0.0011870	0.0000001	0.0000000	0.0000000	0.0000000	0.0000000
6	0.0002701	0.0000000	0.0000000	-0.0000000	-0.0000000	-0.0000000
7	0.0000615	0.0000000	0.0000000	0.0000000	0.0000000	0.0000000
8	0.0000140	0.0000000	0.0000000	0.0000000	0.0000000	0.0000000
9	0.0000032	0.0000000	-0.0000000	-0.0000000	-0.0000000	-0.0000000
10	0.0000007	0.0000000	0.0000000	0.0000000	0.0000000	0.0000000
11	0.0000002	0.0000000	0.0000000	0.0000000	0.0000000	0.0000000
12	0.0000000	-0.0000000	0.0000000	-0.0000000	-0.0000000	-0.0000000
13	0.0000000	-0.0000000	-0.0000000	-0.0000000	-0.0000000	-0.0000000
14	0.0000000	0.0000000	0.0000000	0.0000000	0.0000000	0.0000000
15	0.0000000	-0.0000000	-0.0000000	-0.0000000	-0.0000000	-0.0000000

$Y_{i,j}$ = $Btu/ft^2h.F$

Table 25. Response Factors Z for Wall 1

i	$Z_{i,1}$	$Z_{i,2}$	$Z_{i,3}$	$Z_{i,4}$	$Z_{i,5}$	$Z_{i,6}$
1	0.3642407	0.3642407	0.3642407	0.3642407	0.3642407	0.3642407
2	-0.2094467	-0.2923251	-0.2933014	-0.2933020	-0.2933020	-0.2933020
3	-0.0230401	0.0246169	0.0254004	0.0254009	0.0254009	0.0254009
4	-0.0052172	0.0000253	-0.0000407	-0.0000407	-0.0000407	-0.0000407
5	-0.0011870	0.0000001	-0.0000000	0.0000000	0.0000000	0.0000000
6	-0.0002701	0.0000000	-0.0000000	0.0000000	0.0000000	0.0000000
7	-0.0000615	0.0000000	-0.0000000	-0.0000000	-0.0000000	-0.0000000
8	-0.0000140	0.0000000	-0.0000000	-0.0000000	-0.0000000	-0.0000000
9	-0.0000032	0.0000000	0.0000000	0.0000000	0.0000000	0.0000000
10	-0.0000007	0.0000000	0.0000000	0.0000000	0.0000000	0.0000000
11	-0.0000002	-0.0000000	-0.0000000	-0.0000000	-0.0000000	-0.0000000
12	-0.0000000	0.0000000	0.0000000	0.0000000	0.0000000	0.0000000
13	-0.0000000	0.0000000	0.0000000	0.0000000	0.0000000	0.0000000
14	-0.0000000	-0.0000000	-0.0000000	-0.0000000	-0.0000000	-0.0000000
15	-0.0000000	0.0000000	0.0000000	0.0000000	0.0000000	0.0000000

$Z_{i,j}$ = *Btu/ft²h.F*

Table 26. Response Factors X for Wall 2

i	$X_{i,1}$	$X_{i,2}$	$X_{i,3}$	$X_{i,4}$	$X_{i,5}$	$X_{i,6}$
1	0.3642340	0.3642340	0.3642340	0.3642340	0.3642340	0.3642340
2	-0.2098917	-0.3592154	-0.4324315	-0.4335046	-0.4335567	-0.4335573
3	-0.0243728	0.0616757	0.1338830	0.1351570	0.1352190	0.1352197
4	-0.0064716	0.0035204	-0.0088773	-0.0092717	-0.0092910	-0.0092913
5	-0.0019551	0.0006981	-0.0000096	0.0000166	0.0000179	0.0000179
6	-0.0006612	0.0001403	0.0000000	0.0000000	0.0000000	0.0000000
7	-0.0002429	0.0000282	0.0000000	0.0000000	0.0000000	0.0000000
8	-0.0000939	0.0000057	0.0000000	0.0000000	0.0000000	0.0000000
9	-0.0000374	0.0000011	0.0000000	0.0000000	0.0000000	0.0000000
10	-0.0000151	0.0000002	0.0000000	0.0000000	0.0000000	0.0000000
11	-0.0000061	0.0000000	0.0000000	0.0000000	0.0000000	0.0000000
12	-0.0000025	0.0000000	0.0000000	0.0000000	0.0000000	0.0000000
13	-0.0000010	0.0000000	0.0000000	0.0000000	0.0000000	0.0000000
14	-0.0000004	0.0000000	0.0000000	0.0000000	0.0000000	0.0000000
15	-0.0000002	0.0000000	0.0000000	0.0000000	0.0000000	0.0000000
16	-0.0000001	0.0000000	0.0000000	0.0000000	0.0000000	0.0000000
17	0.0000000	0.0000000	0.0000000	0.0000000	0.0000000	0.0000000
18	0.0000000	0.0000000	0.0000000	0.0000000	0.0000000	0.0000000
19	0.0000000	0.0000000	0.0000000	0.0000000	0.0000000	0.0000000
20	0.0000000	0.0000000	0.0000000	0.0000000	0.0000000	0.0000000

$X_{i,j}$ = $Btu/ft^2h.F$

Table 27. Response Factors Y for Wall 2

i	$Y_{i,1}$	$Y_{i,2}$	$Y_{i,3}$	$Y_{i,4}$	$Y_{i,5}$	$Y_{i,6}$
1	0.0015772	0.0015772	0.0015772	0.0015772	0.0015772	0.0015772
2	0.0295576	0.0289110	0.0285940	0.0285894	0.0285891	0.0285891
3	0.0426585	0.0305409	0.0247294	0.0246451	0.0246410	0.0246410
4	0.0255139	0.0080254	0.0018862	0.0018134	0.0018098	0.0018098
5	0.0120849	0.0016251	0.0000119	0.0000063	0.0000060	0.0000060
6	0.0052811	0.0003267	0.0000000	0.0000000	0.0000000	0.0000000
7	0.0022307	0.0000657	0.0000000	0.0000000	0.0000000	0.0000000
8	0.0009277	0.0000132	0.0000000	0.0000000	0.0000000	0.0000000
9	0.0003830	0.0000027	0.0000000	0.0000000	0.0000000	0.0000000
10	0.0001575	0.0000005	0.0000000	0.0000000	0.0000000	0.0000000
11	0.0000647	0.0000001	0.0000000	0.0000000	0.0000000	0.0000000
12	0.0000265	0.0000000	0.0000000	0.0000000	0.0000000	0.0000000
13	0.0000109	0.0000000	0.0000000	0.0000000	0.0000000	0.0000000
14	0.0000045	0.0000000	0.0000000	0.0000000	0.0000000	0.0000000
15	0.0000018	0.0000000	0.0000000	0.0000000	0.0000000	0.0000000
16	0.0000008	0.0000000	0.0000000	0.0000000	0.0000000	0.0000000
17	0.0000003	0.0000000	0.0000000	0.0000000	0.0000000	0.0000000
18	0.0000001	0.0000000	0.0000000	0.0000000	0.0000000	0.0000000
19	0.0000001	0.0000000	0.0000000	0.0000000	0.0000000	0.0000000
20	0.0000000	0.0000000	0.0000000	0.0000000	0.0000000	0.0000000
21	0.0000000	0.0000000	0.0000000	0.0000000	0.0000000	0.0000000
22	0.0000000	0.0000000	0.0000000	0.0000000	0.0000000	0.0000000

$X_{i,1}$ = $Btu/ft^2h.F$

Table 28. Response Factors Z for Wall 2

i	$Z_{i,1}$	$Z_{i,2}$	$Z_{i,3}$	$Z_{i,4}$	$Z_{i,5}$	$Z_{i,6}$
1	5.8570240	5.8570240	5.8570240	5.8570240	5.8570240	5.8570240
2	-4.1601200	-6.5613040	-7.7386460	-7.7559020	-7.7567400	-7.7567490
3	-0.9538267	0.7516830	2.0705950	2.0933950	2.0945050	2.0945160
4	-0.3720887	0.0189481	-0.1321505	-0.1382509	-0.1385505	-0.1385536
5	-0.1487591	0.0037848	-0.0000240	0.0003653	0.0003851	0.0003853
6	-0.0602255	0.0007607	0.0000000	0.0000000	0.0000000	0.0000000
7	-0.0245375	0.0001529	0.0000000	0.0000000	0.0000000	0.0000000
8	-0.0100288	0.0000307	0.0000000	0.0000000	0.0000000	0.0000000
9	-0.0041053	0.0000062	0.0000000	0.0000000	0.0000000	0.0000000
10	-0.0016818	0.0000012	0.0000000	0.0000000	0.0000000	0.0000000
11	-0.0006892	0.0000002	0.0000000	0.0000000	0.0000000	0.0000000
12	-0.0002825	0.0000001	0.0000000	0.0000000	0.0000000	0.0000000
13	-0.0001158	0.0000000	0.0000000	0.0000000	0.0000000	0.0000000
14	-0.0000475	0.0000000	0.0000000	0.0000000	0.0000000	0.0000000
15	-0.0000195	0.0000000	0.0000000	0.0000000	0.0000000	0.0000000
16	-0.0000080	0.0000000	0.0000000	0.0000000	0.0000000	0.0000000
17	-0.0000033	0.0000000	0.0000000	0.0000000	0.0000000	0.0000000
18	-0.0000013	0.0000000	0.0000000	0.0000000	0.0000000	0.0000000
19	-0.0000005	0.0000000	0.0000000	0.0000000	0.0000000	0.0000000
20	-0.0000002	0.0000000	0.0000000	0.0000000	0.0000000	0.0000000
21	-0.0000001	0.0000000	0.0000000	0.0000000	0.0000000	0.0000000
22	0.0000000	0.0000000	0.0000000	0.0000000	0.0000000	0.0000000

$X_{i,j}$ = *Btu/ft²h.F*

Table 29. Response Factors X for Wall 3

i	$X_{i,1}$	$X_{i,2}$	$X_{i,3}$	$X_{i,4}$	$X_{i,5}$	$X_{i,6}$
1	0.3642340	0.3642340	0.3642340	0.3642340	0.3642340	0.3642340
2	-0.2098938	-0.5064575	-0.5936446	-0.6343886	-0.6362350	-0.6369908
3	-0.0244328	0.1464653	0.2676966	0.3341031	0.3373188	0.3386391
4	-0.0067387	0.0131547	-0.0219048	-0.0518500	-0.0535436	-0.0542436
5	-0.0024565	0.0030302	-0.0001186	0.0023317	0.0025945	0.0027056
6	-0.0012854	0.0007147	-0.0000106	0.0000026	-0.0000092	-0.0000146
7	-0.0008767	0.0001699	-0.0000012	0.0000000	0.0000000	0.0000000
8	-0.0006733	0.0000405	-0.0000001	0.0000000	0.0000000	0.0000000
9	-0.0005385	0.0000097	0.0000000	0.0000000	0.0000000	0.0000000
10	-0.0004361	0.0000023	0.0000000	0.0000000	0.0000000	0.0000000
11	-0.0003546	0.0000006	0.0000000	0.0000000	0.0000000	0.0000000
12	-0.0002885	0.0000001	0.0000000	0.0000000	0.0000000	0.0000000
13	-0.0002349	0.0000000	0.0000000	0.0000000	0.0000000	0.0000000
14	-0.0001913	0.0000000	0.0000000	0.0000000	0.0000000	0.0000000
15	-0.0001557	0.0000000	0.0000000	0.0000000	0.0000000	0.0000000
16	-0.0001268	0.0000000	0.0000000	0.0000000	0.0000000	0.0000000
17	-0.0001032	0.0000000	0.0000000	0.0000000	0.0000000	0.0000000
18	-0.0000841	0.0000000	0.0000000	0.0000000	0.0000000	0.0000000
19	-0.0000684	0.0000000	0.0000000	0.0000000	0.0000000	0.0000000
20	-0.0000557	0.0000000	0.0000000	0.0000000	0.0000000	0.0000000
21	-0.0000454	0.0000000	0.0000000	0.0000000	0.0000000	0.0000000
22	-0.0000369	0.0000000	0.0000000	0.0000000	0.0000000	0.0000000

Table 29. (continued)

i	$X_{i,1}$	$X_{i,2}$	$X_{i,3}$	$X_{i,4}$	$X_{i,5}$	$X_{i,6}$
23	-0.0000301	0.0000000	0.0000000	0.0000000	0.0000000	0.0000000
24	-0.0000245	0.0000000	0.0000000	0.0000000	0.0000000	0.0000000
25	-0.0000199	0.0000000	0.0000000	0.0000000	0.0000000	0.0000000
26	-0.0000162	0.0000000	0.0000000	0.0000000	0.0000000	0.0000000
27	-0.0000132	0.0000000	0.0000000	0.0000000	0.0000000	0.0000000
28	-0.0000108	0.0000000	0.0000000	0.0000000	0.0000000	0.0000000
29	-0.0000088	0.0000000	0.0000000	0.0000000	0.0000000	0.0000000
30	-0.0000071	0.0000000	0.0000000	0.0000000	0.0000000	0.0000000
31	-0.0000058	0.0000000	0.0000000	0.0000000	0.0000000	0.0000000
32	-0.0000047	0.0000000	0.0000000	0.0000000	0.0000000	0.0000000
33	-0.0000039	0.0000000	0.0000000	0.0000000	0.0000000	0.0000000
34	-0.0000031	0.0000000	0.0000000	0.0000000	0.0000000	0.0000000
35	-0.0000026	0.0000000	0.0000000	0.0000000	0.0000000	0.0000000
36	-0.0000021	0.0000000	0.0000000	0.0000000	0.0000000	0.0000000
37	-0.0000017	0.0000000	0.0000000	0.0000000	0.0000000	0.0000000
38	-0.0000014	0.0000000	0.0000000	0.0000000	0.0000000	0.0000000
39	-0.0000011	0.0000000	0.0000000	0.0000000	0.0000000	0.0000000
40	-0.0000009	0.0000000	0.0000000	0.0000000	0.0000000	0.0000000
41	-0.0000007	0.0000000	0.0000000	0.0000000	0.0000000	0.0000000
42	-0.0000006	0.0000000	0.0000000	0.0000000	0.0000000	0.0000000
43	-0.0000005	0.0000000	0.0000000	0.0000000	0.0000000	0.0000000
44	-0.0000004	0.0000000	0.0000000	0.0000000	0.0000000	0.0000000
45	-0.0000003	0.0000000	0.0000000	0.0000000	0.0000000	0.0000000

Table 30. Response Factors Y for Wall 3

i	$Y_{i,1}$	$Y_{i,2}$	$Y_{i,3}$	$Y_{i,4}$	$Y_{i,5}$	$Y_{i,6}$
1	0.0000108	0.0000108	0.0000108	0.0000108	0.0000108	0.0000108
2	0.0020347	0.0020259	0.0020233	0.0020221	0.0020221	0.0020220
3	0.0104435	0.0087869	0.0083019	0.0080756	0.0080653	0.0080611
4	0.0155453	0.0070421	0.0049387	0.0040101	0.0039691	0.0039524
5	0.0152050	0.0025478	0.0008622	0.0003097	0.0002894	0.0002811
6	0.0130909	0.0007108	0.0001009	0.0000045	0.0000029	0.0000023
7	0.0108402	0.0001815	0.0000113	0.0000000	0.0000000	0.0000000
8	0.0088709	0.0000447	0.0000013	0.0000000	0.0000000	0.0000000
9	0.0072337	0.0000108	0.0000001	0.0000000	0.0000000	0.0000000
10	0.0058924	0.0000026	0.0000000	0.0000000	0.0000000	0.0000000
11	0.0047983	0.0000006	0.0000000	0.0000000	0.0000000	0.0000000
12	0.0039069	0.0000002	0.0000000	0.0000000	0.0000000	0.0000000
13	0.0031811	0.0000000	0.0000000	0.0000000	0.0000000	0.0000000
14	0.0025901	0.0000000	0.0000000	0.0000000	0.0000000	0.0000000
15	0.0021089	0.0000000	0.0000000	0.0000000	0.0000000	0.0000000
16	0.0017171	0.0000000	0.0000000	0.0000000	0.0000000	0.0000000
17	0.0013981	0.0000000	0.0000000	0.0000000	0.0000000	0.0000000
18	0.0011383	0.0000000	0.0000000	0.0000000	0.0000000	0.0000000
19	0.0009268	0.0000000	0.0000000	0.0000000	0.0000000	0.0000000
20	0.0007546	0.0000000	0.0000000	0.0000000	0.0000000	0.0000000
21	0.0006144	0.0000000	0.0000000	0.0000000	0.0000000	0.0000000
22	0.0005003	0.0000000	0.0000000	0.0000000	0.0000000	0.0000000

Table 30. (continued)

i	$Y_{i,1}$	$Y_{i,2}$	$Y_{i,3}$	$Y_{i,4}$	$Y_{i,5}$	$Y_{i,6}$
23	0.0004073	0.0000000	0.0000000	0.0000000	0.0000000	0.0000000
24	0.0003317	0.0000000	0.0000000	0.0000000	0.0000000	0.0000000
25	0.0002700	0.0000000	0.0000000	0.0000000	0.0000000	0.0000000
26	0.0002199	0.0000000	0.0000000	0.0000000	0.0000000	0.0000000
87	0.0001790	0.0000000	0.0000000	0.0000000	0.0000000	0.0000000
28	0.0001458	0.0000000	0.0000000	0.0000000	0.0000000	0.0000000
29	0.0001187	0.0000000	0.0000000	0.0000000	0.0000000	0.0000000
30	0.0000966	0.0000000	0.0000000	0.0000000	0.0000000	0.0000000
31	0.0000787	0.0000000	0.0000000	0.0000000	0.0000000	0.0000000
32	0.0000641	0.0000000	0.0000000	0.0000000	0.0000000	0.0000000
33	0.0000522	0.0000000	0.0000000	0.0000000	0.0000000	0.0000000
34	0.0000425	0.0000000	0.0000000	0.0000000	0.0000000	0.0000000
35	0.0000346	0.0000000	0.0000000	0.0000000	0.0000000	0.0000000
36	0.0000282	0.0000000	0.0000000	0.0000000	0.0000000	0.0000000
37	0.0000229	0.0000000	0.0000000	0.0000000	0.0000000	0.0000000
38	0.0000187	0.0000000	0.0000000	0.0000000	0.0000000	0.0000000
39	0.0000152	0.0000000	0.0000000	0.0000000	0.0000000	0.0000000
40	0.0000124	0.0000000	0.0000000	0.0000000	0.0000000	0.0000000
41	0.0000101	0.0000000	0.0000000	0.0000000	0.0000000	0.0000000
42	0.0000082	0.0000000	0.0000000	0.0000000	0.0000000	0.0000000
43	0.0000067	0.0000000	0.0000000	0.0000000	0.0000000	0.0000000
44	0.0000054	0.0000000	0.0000000	0.0000000	0.0000000	0.0000000
45	0.0000044	0.0000000	0.0000000	0.0000000	0.0000000	0.0000000

Table 31. Response Factors Z for Wall 3

i	$Z_{i,1}$	$Z_{i,2}$	$Z_{i,3}$	$Z_{i,4}$	$Z_{i,5}$	$Z_{i,6}$
1	4.8870810	4.8870810	4.8870810	4.8870810	4.8870810	4.8870810
2	-2.8138640	-6.7929840	-7.9628110	-8.5094910	-8.5342640	-8.5444060
3	-0.4628685	1.8282130	3.4542580	4.3449970	4.3881320	4.4058430
4	-0.2913765	0.0854965	-0.3521253	-0.7385267	-0.7605516	-0.7696582
5	-0.2258349	0.0114073	-0.0090581	0.0303315	0.0340751	0.0356535
6	-0.1821195	0.0017580	-0.0009726	0.0000407	-0.0001131	-0.0001838
7	-0.1479717	0.0003122	-0.0001086	0.0000002	0.0000000	0.0000002
8	-0.1204177	0.0000626	-0.0000121	0.0000000	0.0000000	0.0000000
9	-0.0980319	0.0000136	-0.0000014	0.0000000	0.0000000	0.0000000
10	-0.0798157	0.0000031	-0.0000002	0.0000000	0.0000000	0.0000000
11	-0.0649861	0.0000007	0.0000000	0.0000000	0.0000000	0.0000000
12	-0.0529123	0.0000002	0.0000000	0.0000000	0.0000000	0.0000000
13	-0.0430818	0.0000000	0.0000000	0.0000000	0.0000000	0.0000000
14	-0.0350777	0.0000000	0.0000000	0.0000000	0.0000000	0.0000000
15	-0.0285607	0.0000000	0.0000000	0.0000000	0.0000000	0.0000000
16	-0.0232545	0.0000000	0.0000000	0.0000000	0.0000000	0.0000000
17	-0.0189341	0.0000000	0.0000000	0.0000000	0.0000000	0.0000000
18	-0.0154163	0.0000000	0.0000000	0.0000000	0.0000000	0.0000000
19	-0.0125522	0.0000000	0.0000000	0.0000000	0.0000000	0.0000000
20	-0.0102201	0.0000000	0.0000000	0.0000000	0.0000000	0.0000000
21	-0.0083213	0.0000000	0.0000000	0.0000000	0.0000000	0.0000000
22	-0.0067753	0.0000000	0.0000000	0.0000000	0.0000000	0.0000000

Table 31. (continued)

i	$Z_{i,1}$	$Z_{i,2}$	$Z_{i,3}$	$Z_{i,4}$	$Z_{i,5}$	$Z_{i,6}$
23	-0.0055166	0.0000000	0.0000000	0.0000000	0.0000000	0.0000000
24	-0.0044916	0.0000000	0.0000000	0.0000000	0.0000000	0.0000000
25	-0.0036572	0.0000000	0.0000000	0.0000000	0.0000000	0.0000000
26	-0.0029777	0.0000000	0.0000000	0.0000000	0.0000000	0.0000000
27	-0.0024245	0.0000000	0.0000000	0.0000000	0.0000000	0.0000000
28	-0.0019740	0.0000000	0.0000000	0.0000000	0.0000000	0.0000000
29	-0.0016073	0.0000000	0.0000000	0.0000000	0.0000000	0.0000000
30	-0.0013087	0.0000000	0.0000000	0.0000000	0.0000000	0.0000000
31	-0.0010655	0.0000000	0.0000000	0.0000000	0.0000000	0.0000000
32	-0.0008676	0.0000000	0.0000000	0.0000000	0.0000000	0.0000000
33	-0.0007064	0.0000000	0.0000000	0.0000000	0.0000000	0.0000000
34	-0.0005751	0.0000000	0.0000000	0.0000000	0.0000000	0.0000000
35	-0.0004683	0.0000000	0.0000000	0.0000000	0.0000000	0.0000000
36	-0.0003813	0.0000000	0.0000000	0.0000000	0.0000000	0.0000000
37	-0.0003105	0.0000000	0.0000000	0.0000000	0.0000000	0.0000000
38	-0.0002528	0.0000000	0.0000000	0.0000000	0.0000000	0.0000000
39	-0.0002058	0.0000000	0.0000000	0.0000000	0.0000000	0.0000000
40	-0.0001676	0.0000000	0.0000000	0.0000000	0.0000000	0.0000000
41	-0.0001364	0.0000000	0.0000000	0.0000000	0.0000000	0.0000000
42	-0.0001111	0.0000000	0.0000000	0.0000000	0.0000000	0.0000000
43	-0.0000905	0.0000000	0.0000000	0.0000000	0.0000000	0.0000000
44	-0.0000736	0.0000000	0.0000000	0.0000000	0.0000000	0.0000000
45	-0.0000600	0.0000000	0.0000000	0.0000000	0.0000000	0.0000000

Table 32. Response Factors X for Wall 4

i	$X_{i,1}$	$X_{i,2}$	$X_{i,3}$	$X_{i,4}$	$X_{i,5}$	$X_{i,6}$
1	0.3642340	0.3642340	0.3642340	0.3642340	0.3642340	0.3642340
2	-0.2098938	-0.5362275	-0.6833667	-0.7655049	-0.7922307	-0.7948185
3	-0.0244328	0.1636205	0.3802397	0.5343454	0.5905146	0.5961431
4	-0.0067410	0.0151495	-0.0509480	-0.1366957	-0.1759035	-0.1800989
5	-0.0024703	0.0035692	-0.0025507	0.0089386	0.0189687	0.0202184
6	-0.0013254	0.0008879	-0.0005540	0.0000212	-0.0006346	-0.0007694
7	-0.0009529	0.0002346	-0.0001241	0.0000009	-0.0000007	0.0000038
8	-0.0007869	0.0000668	-0.0000279	0.0000001	0.0000000	0.0000000
9	-0.0006843	0.0000207	-0.0000063	0.0000000	0.0000000	0.0000000
10	-0.0006061	0.0000069	-0.0000014	0.0000000	0.0000000	0.0000000
11	-0.0005406	0.0000025	-0.0000003	0.0000000	0.0000000	0.0000000
12	-0.0004834	0.0000009	-0.0000001	0.0000000	0.0000000	0.0000000
13	-0.0004327	0.0000004	0.0000000	0.0000000	0.0000000	0.0000000
14	-0.0003876	0.0000001	0.0000000	0.0000000	0.0000000	0.0000000
15	-0.0003472	0.0000001	0.0000000	0.0000000	0.0000000	0.0000000
16	-0.0003110	0.0000000	0.0000000	0.0000000	0.0000000	0.0000000
17	-0.0002787	0.0000000	0.0000000	0.0000000	0.0000000	0.0000000
18	-0.0002497	0.0000000	0.0000000	0.0000000	0.0000000	0.0000000
19	-0.0002237	0.0000000	0.0000000	0.0000000	0.0000000	0.0000000
20	-0.0002004	0.0000000	0.0000000	0.0000000	0.0000000	0.0000000
21	-0.0001796	0.0000000	0.0000000	0.0000000	0.0000000	0.0000000
22	-0.0001609	0.0000000	0.0000000	0.0000000	0.0000000	0.0000000

Table 32. (continued)

i	$X_{i,1}$	$X_{i,2}$	$X_{i,3}$	$X_{i,4}$	$X_{i,5}$	$X_{i,6}$
23	-0.0001441	0.0000000	0.0000000	0.0000000	0.0000000	0.0000000
24	-0.0001291	0.0000000	0.0000000	0.0000000	0.0000000	0.0000000
25	-0.0001157	0.0000000	0.0000000	0.0000000	0.0000000	0.0000000
26	-0.0001037	0.0000000	0.0000000	0.0000000	0.0000000	0.0000000
27	-0.0000929	0.0000000	0.0000000	0.0000000	0.0000000	0.0000000
28	-0.0000832	0.0000000	0.0000000	0.0000000	0.0000000	0.0000000
29	-0.0000745	0.0000000	0.0000000	0.0000000	0.0000000	0.0000000
30	-0.0000668	0.0000000	0.0000000	0.0000000	0.0000000	0.0000000
31	-0.0000598	0.0000000	0.0000000	0.0000000	0.0000000	0.0000000
32	-0.0000536	0.0000000	0.0000000	0.0000000	0.0000000	0.0000000
33	-0.0000480	0.0000000	0.0000000	0.0000000	0.0000000	0.0000000
34	-0.0000430	0.0000000	0.0000000	0.0000000	0.0000000	0.0000000
35	-0.0000386	0.0000000	0.0000000	0.0000000	0.0000000	0.0000000
36	-0.0000345	0.0000000	0.0000000	0.0000000	0.0000000	0.0000000
37	-0.0000310	0.0000000	0.0000000	0.0000000	0.0000000	0.0000000
38	-0.0000277	0.0000000	0.0000000	0.0000000	0.0000000	0.0000000
39	-0.0000248	0.0000000	0.0000000	0.0000000	0.0000000	0.0000000
40	-0.0000223	0.0000000	0.0000000	0.0000000	0.0000000	0.0000000
41	-0.0000199	0.0000000	0.0000000	0.0000000	0.0000000	0.0000000
42	-0.0000179	0.0000000	0.0000000	0.0000000	0.0000000	0.0000000
43	-0.0000160	0.0000000	0.0000000	0.0000000	0.0000000	0.0000000
44	-0.0000143	0.0000000	0.0000000	0.0000000	0.0000000	0.0000000
45	-0.0000129	0.0000000	0.0000000	0.0000000	0.0000000	0.0000000

Table 33. Response Factors Y for Wall 4

i	$Y_{i,1}$	$Y_{i,2}$	$Y_{i,3}$	$Y_{i,4}$	$Y_{i,5}$	$Y_{i,6}$
1	0.0000000	0.0000000	0.0000000	0.0000000	0.0000000	0.0000000
2	0.0001078	0.0001078	0.0001078	0.0001078	0.0001078	0.0001078
3	0.0016748	0.0015782	0.0015346	0.0015103	0.0015024	0.0015017
4	0.0050774	0.0035769	0.0029393	0.0025932	0.0024824	0.0024717
5	0.0076449	0.0030958	0.0016509	0.0009881	0.0007978	0.0007801
6	0.0086010	0.0017516	0.0005009	0.0001287	0.0000562	0.0000505
7	0.0085371	0.0008310	0.0001235	0.0000105	0.0000011	0.0000007
8	0.0080131	0.0003643	0.0000286	0.0000008	0.0000000	0.0000000
9	0.0073330	0.0001537	0.0000065	0.0000001	0.0000000	0.0000000
10	0.0066335	0.0000636	0.0000015	0.0000000	0.0000000	0.0000000
11	0.0059693	0.0000260	0.0000003	0.0000000	0.0000000	0.0000000
12	0.0053587	0.0000106	0.0000001	0.0000000	0.0000000	0.0000000
13	0.0048054	0.0000043	0.0000000	0.0000000	0.0000000	0.0000000
14	0.0043071	0.0000017	0.0000000	0.0000000	0.0000000	0.0000000
15	0.0038596	0.0000007	0.0000000	0.0000000	0.0000000	0.0000000
16	0.0034583	0.0000003	0.0000000	0.0000000	0.0000000	0.0000000
17	0.0030986	0.0000001	0.0000000	0.0000000	0.0000000	0.0000000
18	0.0027762	0.0000000	0.0000000	0.0000000	0.0000000	0.0000000
19	0.0024873	0.0000000	0.0000000	0.0000000	0.0000000	0.0000000
20	0.0022285	0.0000000	0.0000000	0.0000000	0.0000000	0.0000000
21	0.0019966	0.0000000	0.0000000	0.0000000	0.0000000	0.0000000
22	0.0017889	0.0000000	0.0000000	0.0000000	0.0000000	0.0000000

Table 33. (continued)

i	$Y_{i,1}$	$Y_{i,2}$	$Y_{i,3}$	$Y_{i,4}$	$Y_{i,5}$	$Y_{i,6}$
23	0.0016027	0.0000000	0.0000000	0.0000000	0.0000000	0.0000000
24	0.0014360	0.0000000	0.0000000	0.0000000	0.0000000	0.0000000
25	0.0012865	0.0000000	0.0000000	0.0000000	0.0000000	0.0000000
26	0.0011527	0.0000000	0.0000000	0.0000000	0.0000000	0.0000000
27	0.0010327	0.0000000	0.0000000	0.0000000	0.0000000	0.0000000
28	0.0009253	0.0000000	0.0000000	0.0000000	0.0000000	0.0000000
29	0.0008290	0.0000000	0.0000000	0.0000000	0.0000000	0.0000000
30	0.0007427	0.0000000	0.0000000	0.0000000	0.0000000	0.0000000
31	0.0006654	0.0000000	0.0000000	0.0000000	0.0000000	0.0000000
32	0.0005962	0.0000000	0.0000000	0.0000000	0.0000000	0.0000000
33	0.0005342	0.0000000	0.0000000	0.0000000	0.0000000	0.0000000
34	0.0004786	0.0000000	0.0000000	0.0000000	0.0000000	0.0000000
35	0.0004288	0.0000000	0.0000000	0.0000000	0.0000000	0.0000000
36	0.0003842	0.0000000	0.0000000	0.0000000	0.0000000	0.0000000
37	0.0003442	0.0000000	0.0000000	0.0000000	0.0000000	0.0000000
38	0.0003084	0.0000000	0.0000000	0.0000000	0.0000000	0.0000000
39	0.0002763	0.0000000	0.0000000	0.0000000	0.0000000	0.0000000
40	0.0002475	0.0000000	0.0000000	0.0000000	0.0000000	0.0000000
41	0.0002218	0.0000000	0.0000000	0.0000000	0.0000000	0.0000000
42	0.0001987	0.0000000	0.0000000	0.0000000	0.0000000	0.0000000
43	0.0001780	0.0000000	0.0000000	0.0000000	0.0000000	0.0000000
44	0.0001595	0.0000000	0.0000000	0.0000000	0.0000000	0.0000000
45	0.0001429	0.0000000	0.0000000	0.0000000	0.0000000	0.0000000

Table 34. Response Factors Z for Wall 4

i	$Z_{i,1}$	$Z_{i,2}$	$Z_{i,3}$	$Z_{i,4}$	$Z_{i,5}$	$Z_{i,6}$
1	5.9579040	5.9579040	5.9579040	5.9579040	5.9579040	5.9579040
2	-3.5729610	-8.9109170	-11.317725	-12.661289	-13.098453	-13.140782
3	-0.6190649	2.5821130	6.1818460	8.7341010	9.6631270	9.7561880
4	-0.3089279	0.2457204	-0.7973729	-2.1914370	-2.8323050	-2.9009590
5	-0.1935179	0.0832645	-0.0159988	0.1638163	0.3246140	0.3447365
6	-0.1412593	0.0321221	-0.0015142	0.0020937	-0.0099264	-0.0122327
7	-0.1137852	0.0127754	-0.0002009	0.0001406	-0.0000131	0.0000575
8	-0.0968195	0.0051258	-0.0000351	0.0000102	-0.0000001	0.0000000
9	-0.0846815	0.0020635	-0.0000072	0.0000007	0.0000000	0.0000000
10	-0.0750379	0.0008320	-0.0000016	0.0000001	0.0000000	0.0000000
11	-0.0668941	0.0003358	-0.0000003	0.0000000	0.0000000	0.0000000
12	-0.0597979	0.0001356	-0.0000001	0.0000000	0.0000000	0.0000000
13	-0.0535209	0.0000547	0.0000000	0.0000000	0.0000000	0.0000000
14	-0.0479297	0.0000221	0.0000000	0.0000000	0.0000000	0.0000000
15	-0.0429334	0.0000089	0.0000000	0.0000000	0.0000000	0.0000000
16	-0.0384624	0.0000036	0.0000000	0.0000000	0.0000000	0.0000000
17	-0.0344587	0.0000015	0.0000000	0.0000000	0.0000000	0.0000000
18	-0.0308726	0.0000006	0.0000000	0.0000000	0.0000000	0.0000000
19	-0.0276599	0.0000002	0.0000000	0.0000000	0.0000000	0.0000000
20	-0.0247816	0.0000001	0.0000000	0.0000000	0.0000000	0.0000000
21	-0.0222030	0.0000000	0.0000000	0.0000000	0.0000000	0.0000000
22	-0.0198926	0.0000000	0.0000000	0.0000000	0.0000000	0.0000000

Table 34. (continued)

i	$Z_{i,1}$	$Z_{i,2}$	$Z_{i,3}$	$Z_{i,4}$	$Z_{i,5}$	$Z_{i,6}$
23	-0.0178227	0.0000000	0.0000000	0.0000000	0.0000000	0.0000000
24	-0.0159681	0.0000000	0.0000000	0.0000000	0.0000000	0.0000000
25	-0.0143066	0.0000000	0.0000000	0.0000000	0.0000000	0.0000000
26	-0.0128179	0.0000000	0.0000000	0.0000000	0.0000000	0.0000000
27	-0.0114841	0.0000000	0.0000000	0.0000000	0.0000000	0.0000000
28	-0.0102892	0.0000000	0.0000000	0.0000000	0.0000000	0.0000000
29	-0.0092185	0.0000000	0.0000000	0.0000000	0.0000000	0.0000000
30	-0.0082593	0.0000000	0.0000000	0.0000000	0.0000000	0.0000000
31	-0.0073999	0.0000000	0.0000000	0.0000000	0.0000000	0.0000000
32	-0.0066299	0.0000000	0.0000000	0.0000000	0.0000000	0.0000000
33	-0.0059400	0.0000000	0.0000000	0.0000000	0.0000000	0.0000000
34	-0.0053219	0.0000000	0.0000000	0.0000000	0.0000000	0.0000000
35	-0.0047682	0.0000000	0.0000000	0.0000000	0.0000000	0.0000000
36	-0.0042720	0.0000000	0.0000000	0.0000000	0.0000000	0.0000000
37	-0.0038275	0.0000000	0.0000000	0.0000000	0.0000000	0.0000000
38	-0.0034292	0.0000000	0.0000000	0.0000000	0.0000000	0.0000000
39	-0.0030724	0.0000000	0.0000000	0.0000000	0.0000000	0.0000000
40	-0.0027527	0.0000000	0.0000000	0.0000000	0.0000000	0.0000000
41	-0.0024663	0.0000000	0.0000000	0.0000000	0.0000000	0.0000000
42	-0.0022096	0.0000000	0.0000000	0.0000000	0.0000000	0.0000000
43	-0.0019797	0.0000000	0.0000000	0.0000000	0.0000000	0.0000000
44	-0.0017737	0.0000000	0.0000000	0.0000000	0.0000000	0.0000000
45	-0.0015891	0.0000000	0.0000000	0.0000000	0.0000000	0.0000000

Table 35. Response Factors X for Wall 5

i	$X_{i,1}$	$X_{i,2}$	$X_{i,3}$	$X_{i,4}$	$X_{i,5}$	$X_{i,6}$
1	6.6310280	6.6310280	6.6310280	6.6310280	6.6310280	6.6310280
2	-6.5385450	-11.133199	-12.855314	-14.357156	-15.360315	-15.52185
3	-0.0238223	4.5067500	7.3981040	10.3096600	12.4816500	12.8558500
4	-0.0061364	0.0103701	-1.1600580	-2.8356320	-4.3953050	-4.6993780
5	-0.0018721	0.0023799	-0.0003133	0.2624248	0.6914066	0.7984835
6	-0.0007351	0.0005621	-0.0000560	0.0000150	-0.0396853	-0.0565291
7	-0.0003746	0.0001347	-0.0000113	0.0000014	-0.0000009	0.0009659
8	-0.0002269	0.0000326	-0.0000024	0.0000002	0.0000000	0.0000000
9	-0.0001493	0.0000080	-0.0000005	0.0000000	0.0000000	0.0000000
10	-0.0001015	0.0000020	-0.0000001	0.0000000	0.0000000	0.0000000
11	-0.0000698	0.0000005	0.0000000	0.0000000	0.0000000	0.0000000
12	-0.0000483	0.0000001	0.0000000	0.0000000	0.0000000	0.0000000
13	-0.0000334	0.0000000	0.0000000	0.0000000	0.0000000	0.0000000
14	-0.0000231	0.0000000	0.0000000	0.0000000	0.0000000	0.0000000
15	-0.0000160	0.0000000	0.0000000	0.0000000	0.0000000	0.0000000
16	-0.0000111	0.0000000	0.0000000	0.0000000	0.0000000	0.0000000
17	-0.0000077	0.0000000	0.0000000	0.0000000	0.0000000	0.0000000
18	-0.0000053	0.0000000	0.0000000	0.0000000	0.0000000	0.0000000
19	-0.0000037	0.0000000	0.0000000	0.0000000	0.0000000	0.0000000
20	-0.0000026	0.0000000	0.0000000	0.0000000	0.0000000	0.0000000
21	-0.0000018	0.0000000	0.0000000	0.0000000	0.0000000	0.0000000
22	-0.0000012	0.0000000	0.0000000	0.0000000	0.0000000	0.0000000

Table 36. Response Factors Y for Wall 5

i	$Y_{i,1}$	$Y_{i,2}$	$Y_{i,3}$	$Y_{i,4}$	$Y_{i,5}$	$Y_{i,6}$
1	-6.2667940	-6.2667940	-6.2667940	-6.2667940	-6.2667940	-6.2667940
2	6.3286520	10.6709200	12.2984400	13.7177900	14.6658500	14.8185200
3	-0.0006076	-4.3857440	-7.1570430	-9.9424810	-12.017746	-12.375030
4	-0.0005737	-0.0001527	1.1388490	2.7598260	4.2639510	4.5567230
5	-0.0004932	-0.0000957	-0.0000561	-0.2579907	-0.6755045	-0.7793813
6	-0.0003869	-0.0000452	-0.0000203	-0.0000076	0.0390219	0.0554783
7	-0.0002857	-0.0000176	-0.0000059	-0.0000013	-0.0000002	-0.0009508
8	-0.0002041	-0.0000061	-0.0000015	-0.0000002	0.0000000	0.0000000
9	-0.0001434	-0.0000020	-0.0000004	0.0000000	0.0000000	0.0000000
10	-0.0000999	-0.0000006	-0.0000001	0.0000000	0.0000000	0.0000000
11	-0.0000694	-0.0000002	0.0000000	0.0000000	0.0000000	0.0000000
12	-0.0000482	-0.0000001	0.0000000	0.0000000	0.0000000	0.0000000
13	-0.0000334	0.0000000	0.0000000	0.0000000	0.0000000	0.0000000
14	-0.0000231	0.0000000	0.0000000	0.0000000	0.0000000	0.0000000
15	-0.0000160	0.0000000	0.0000000	0.0000000	0.0000000	0.0000000
16	-0.0000111	0.0000000	0.0000000	0.0000000	0.0000000	0.0000000
17	-0.0000077	0.0000000	0.0000000	0.0000000	0.0000000	0.0000000
18	-0.0000053	0.0000000	0.0000000	0.0000000	0.0000000	0.0000000
19	-0.0000037	0.0000000	0.0000000	0.0000000	0.0000000	0.0000000
20	-0.0000026	0.0000000	0.0000000	0.0000000	0.0000000	0.0000000
21	-0.0000018	0.0000000	0.0000000	0.0000000	0.0000000	0.0000000
22	-0.0000012	0.0000000	0.0000000	0.0000000	0.0000000	0.0000000

Table 37. Response Factors Z for Wall 5

i	$Z_{i,1}$	$Z_{i,2}$	$Z_{i,3}$	$Z_{i,4}$	$Z_{i,5}$	$Z_{i,6}$
1	6.6310280	6.6310280	6.6310280	6.6310280	6.6310280	6.6310280
2	-6.5385450	-11.133199	-12.855314	-14.357156	-15.360315	-15.52185
3	-0.0238223	4.5067500	7.3981040	10.3096600	12.4816500	12.8558500
4	-0.0061364	0.0103701	-1.1600580	-2.8356320	-4.3953050	-4.6993780
5	-0.0018721	0.0023799	-0.0003133	0.2624248	0.6914066	0.7984835
6	-0.0007351	0.0005621	-0.0000560	0.0000150	-0.0396853	-0.0565291
7	-0.0003746	0.0001347	-0.0000113	0.0000014	-0.0000009	0.0009659
8	-0.0002269	0.0000326	-0.0000024	0.0000002	0.0000000	0.0000000
9	-0.0001493	0.0000080	-0.0000005	0.0000000	0.0000000	0.0000000
10	-0.0001015	0.0000020	-0.0000001	0.0000000	0.0000000	0.0000000
11	-0.0000698	0.0000005	0.0000000	0.0000000	0.0000000	0.0000000
12	-0.0000483	0.0000001	0.0000000	0.0000000	0.0000000	0.0000000
13	-0.0000334	0.0000000	0.0000000	0.0000000	0.0000000	0.0000000
14	-0.0000231	0.0000000	0.0000000	0.0000000	0.0000000	0.0000000
15	-0.0000160	0.0000000	0.0000000	0.0000000	0.0000000	0.0000000
16	-0.0000111	0.0000000	0.0000000	0.0000000	0.0000000	0.0000000
17	-0.0000077	0.0000000	0.0000000	0.0000000	0.0000000	0.0000000
18	-0.0000053	0.0000000	0.0000000	0.0000000	0.0000000	0.0000000
19	-0.0000037	0.0000000	0.0000000	0.0000000	0.0000000	0.0000000
20	-0.0000026	0.0000000	0.0000000	0.0000000	0.0000000	0.0000000
21	-0.0000018	0.0000000	0.0000000	0.0000000	0.0000000	0.0000000
22	-0.0000012	0.0000000	0.0000000	0.0000000	0.0000000	0.0000000

APPENDIX C VALIDATION OF THE TRFM

Validation of the response factors' Fortran code and TRFM method are presented next. The response factors code is validated initially with published response factors. Response factors of the roof examined in Chapter 3 were calculated by Kusuda [71]. The published and calculated first order response factors of the roof are given in Table 38. Also, response factors of numerous (almost 50) walls were calculated and the TRFM characteristics were satisfied for all walls.

Kusuda [12] presented an exact solution of a periodic heat transfer problem for a multilayer wall. The interior air temperature was fixed at 75 F. the exterior air temperature was varied over a range of 94 F (74 to 168 F). The wall description is presented in Table 39. The exact solution of this problem was presented with hourly values of the heat fluxes on both sides of the wall. The exact solution presented a good test case to compare the TRFM solution. Based on the given periodic boundary temperatures, the fluxes are calculated and compared to the exact solution at hourly time intervals. The boundary temperatures and the heat fluxes calculated by the TRFM and the exact solution are presented in Table 40. Good agreement between the exact and the TRFM solutions are judged.

Table 38. Response Factors for the Multilayer Roof

i	$X_{i,2}$ CURRENT	$X_{i,2}$ REF. 44	$Y_{i,2}$ CURRENT	$Y_{i,2}$ REF. 44	$Z_{i,2}$ CURRENT	$Z_{i,2}$ REF. 44
1	0.219334329	0.21934	0.000110325	0.00011	3.305132124	3.30513
2	-0.254849783	-0.25485	0.0050-40388	0.00504	-4.270850969	-4.27082
3	0.046502322	0.04650	0.010599759	0.01060	0.978861074	0.97885
4	0.008565659	0.00857	0.004933018	0.00493	0.008087608	0.00808
5	0.002240880	0.00224	0.001404264	0.00140	0.001039202	0.00104
6	0.000590256	0.00059	0.000373374	0.00037	0.000240995	0.00024
7	0.000155556	0.00016	0.000098504	0.00010	0.000062522	0.00006
8	0.000040997	0.00004	0.000025964	0.00003	0.000016448	0.00002
9	0.000010805	0.00001	0.000006843	0.00001	0.000004334	0.00000

Table 39. Description of the Multi-layered Wall From Reference 12

DESCRIPTION OF LAYERS	LAYER No.	ΔX (ft)	k (Btu/h.ft.F)	ρ (lb/ft^3)	C_p (Btu/lb.F)
Inside air film h = 1.2	1	-- --	-- --	-- --	-- --
Common Brick	2	0.333	0.42	110.0	0.2
Face Brick	3	0.333	0.77	137.0	0.195
Outside air Film h = 3.0	4	-- --	-- --	-- --	-- --

English to SI conversion:
1 ft = 0.3048 m
1 Btu/h.ft.F = 1.7307 W/m.C
1 lb/ft^3 = 16.018 kg/m^3
1 Btu/lb.F = 4.1869 kJ/kg.C

Table 40. **Heat Flux Calculations For the Periodic Heat Transfer Problem**

T_1 (F)	T_n (F)	Q_1 EXACT SOLUTION ($Btu/h \cdot ft^2$)	Q_1 R. F. SOLUTION ($Btu/h \cdot ft^2$)	Q_n EXACT SOLUTION ($Btu/h \cdot ft^2$)	Q_n R. F. SOLUTION ($Btu/h \cdot ft^2$)
75	76	-15.07	-15.08	27.90	28.39
75	76	-13.11	-13.12	25.02	24.84
75	75	-11.29	-11.30	19.94	20.27
75	74	-9.65	-9.66	19.08	18.77
75	74	-8.21	-8.22	17.11	17.42
75	76	-6.94	-6.95	14.46	14.34
75	82	-5.82	-5.83	-5.83	8.04
75	86	-4.86	-4.87	-4.76	-4.73
75	90	-4.13	-4.15	-10.75	-10.70
75	95	-3.73	-3.75	-16.17	-16.18
75	104	-3.65	-3.68	-23.32	-23.04
75	104	-3.86	-3.89	-28.51	-28.87
75	128	-4.04	-4.36	-32.97	-32.06
75	148	-5.05	-5.07	-76.34	-74.90
75	163	-6.06	-6.13	-98.80	-99.37
75	168	-7.82	-7.91	-111.45	-111.14
75	162	-10.45	-10.53	-101.46	-103.27
75	138	-13.72	-13.76	-72.88	-78.01
75	87	-17.10	-17.10	-20.15	-24.28
75	85	-20.00	-19.91	69.48	70.30
75	83	-21.48	-21.33	44.79	47.35
75	81	-20.90	-20.83	39.47	38.71
75	79	-19.20	-19.18	32.92	33.77
75	77	-17.15	-17.15	31.04	30.58

Results were also compared with a finite-difference code. The surface temperatures and fluxes of a wall with constant interior surface temperature and convection, solar load, and emission of infrared radiation to the surroundings were calculated by Thomas [102]. A simple one layer slab was used with 5 nodes. The slab was composed of a 0.725 W/mC conductivity, a 0.0045 m^2/h thermal diffusivity, and a 0.5 m thickness. The initial, interior surface, and outside air temperature of the slab were fixed at 23.0 C. A 9.0 C effective sky temperature, a 28.39 W/m^2C convective coefficient, an emissivity of 0.9, and a solar load of 300.0 W/m^2 were simulated. The energy balances performed on the outside surface of the wall to solve for that temperature are not given here since they are presented in Chapter 4. The calculations in this example proceeded until reaching steady-state. The exterior surface temperature is given in Table 41 for both methods. Both methods compared well and confirmed that when using typical solar load and temperature profiles, the error in the TRFM is small.

The validation of the energy balances along with the computer code implementing the analysis was further obtained by simulating a given solution of a more complicated energy balances problem. Kusuda [58] presented a TRFM solution of the surface temperatures of a multilayer roof with convection to a room temperature on the inside and a convection, solar load, and emission to the surroundings by the exterior surface. In Fig. 82, the profiles of the solar load, the inside and outside temperatures, the heat transfer through the roof, and the outside surface temperature of the roof are shown. The wall description was given earlier in Table 1. The inside and outside surface temperatures and the heat flux through the roof are calculated using the current TRFM code and are given in Fig. 83. Identical results were obtained between the published and present solution.

Table 41. Exterior Surface Temp. Using the TRFM and Finite Difference

i (hr)	T_n TRFM (C)	T_n FINITE DIFF. (C)
0	23.00	23.00
1	28.02	28.52
2	28.80	28.87
3	29.04	29.06
4	29.17	29.17
5	29.25	29.24
6	29.30	29.30
7	29.34	29.34
8	29.38	29.37
9	29.40	29.40
10	29.42	29.42
11	29.44	29.44
12	29.46	29.45
13	29.47	29.46
14	29.48	29.47
15	29.49	29.48
16	29.50	29.49
17	29.50	29.50
18	29.51	29.50
19	29.51	29.51
20	29.52	29.51
21	29.52	29.52
22	29.52	29.52
23	29.53	29.52
24	29.53	29.52
25	29.53	29.53
26	29.53	29.53
27	29.53	29.53
28	29.53	29.53
29	29.53	29.53
30	29.53	29.53

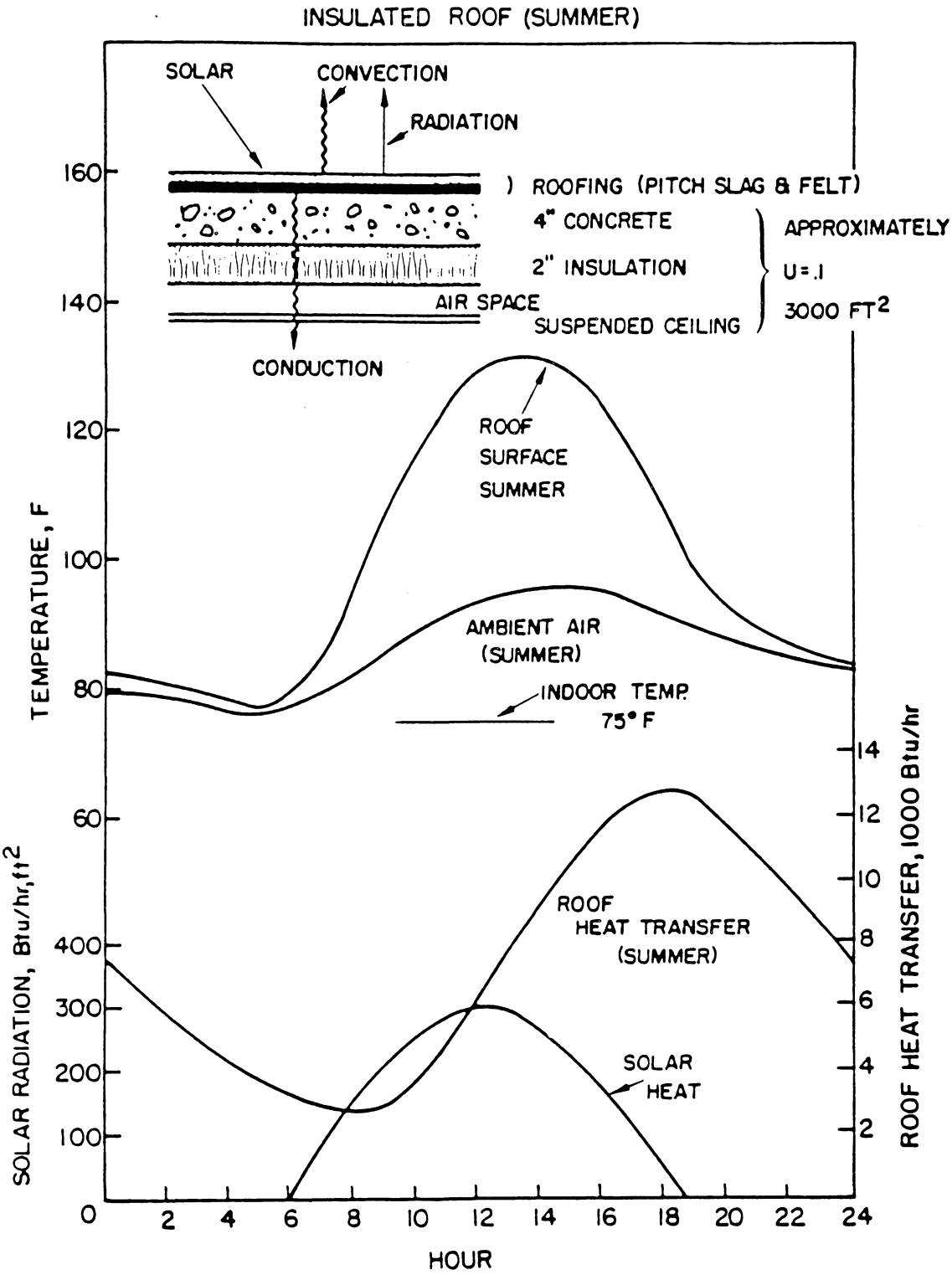

Figure 82. Solution of the Energy Balances of a Roof [71]

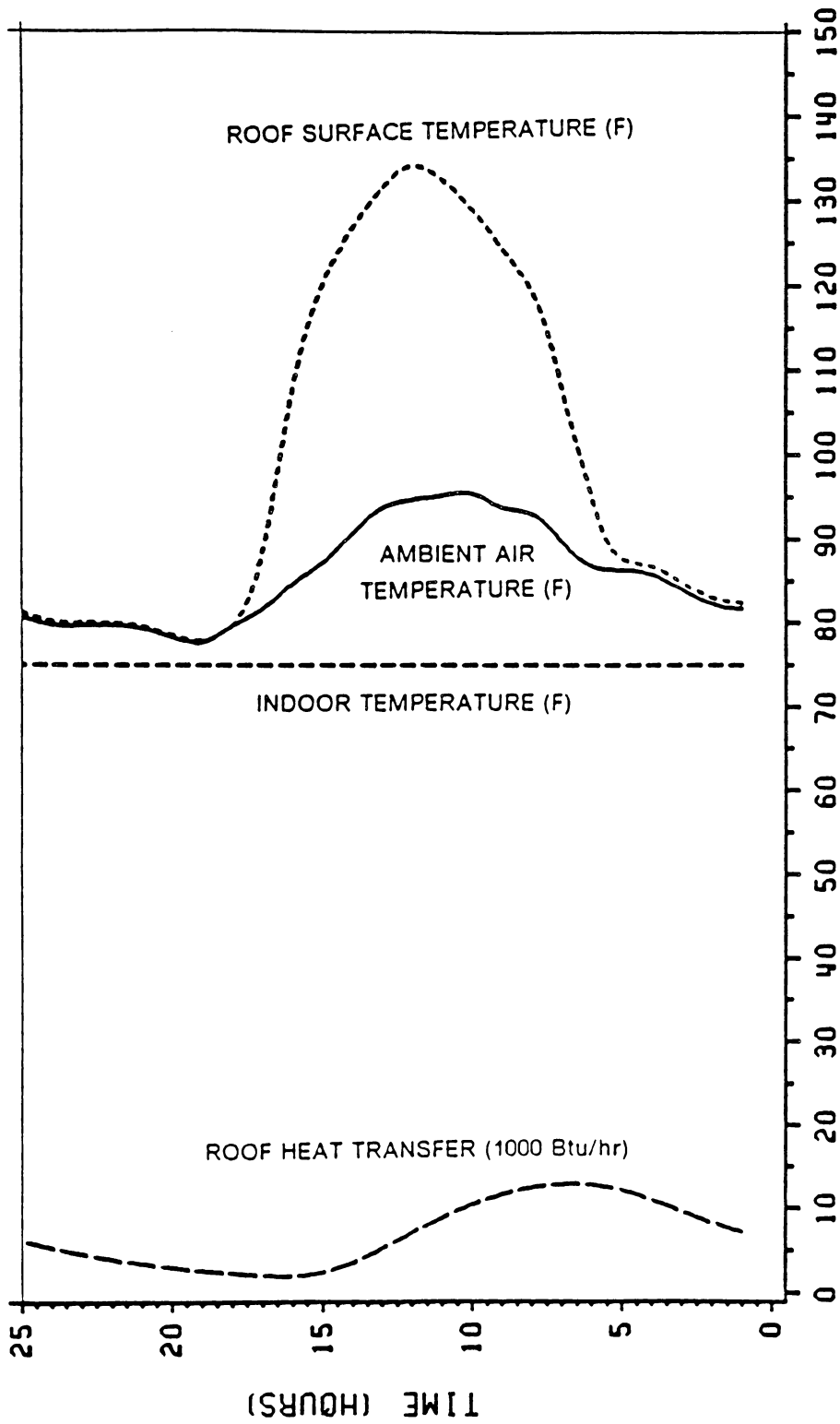

Figure 83. Solution of the Energy Balances of a Roof (present work)

APPENDIX D SOLAR LOAD

In determining the solar loads on exterior walls, the sun's position and intensity of direct, normal, and diffuse radiation are calculated. Transmitted, absorbed, and reflected solar loads by windows are also calculated. The following procedure was recommended by the ASHRAE task group on energy calculations [49].

Nomenclatures are introduced along with Figs. 84 and 85.

L_a = latitude of the structure, degrees (+ North and - south)

L_o = longitude of the structure, degrees (+ West and - East)

N_{tz} = time zone number (hours behind Greenwich time), dimensionless

τ = time from the beginning of the analysis, hours

t = time after midnight, hours (0-24)

ρ_g = ground reflectivity, dimensionless

C_n = clearness number, dimensionless

E_t = equation of time, hours

Time t is obtained from the overall time τ as follows

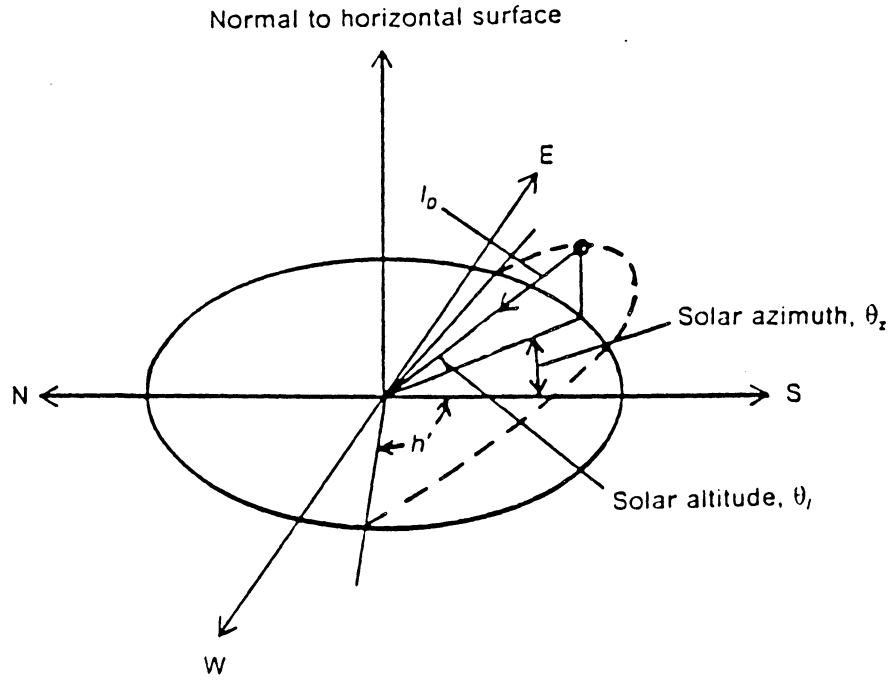

Figure 84. Solar Path and Variable Nomenclature: Nomenclature Used in Appendix A

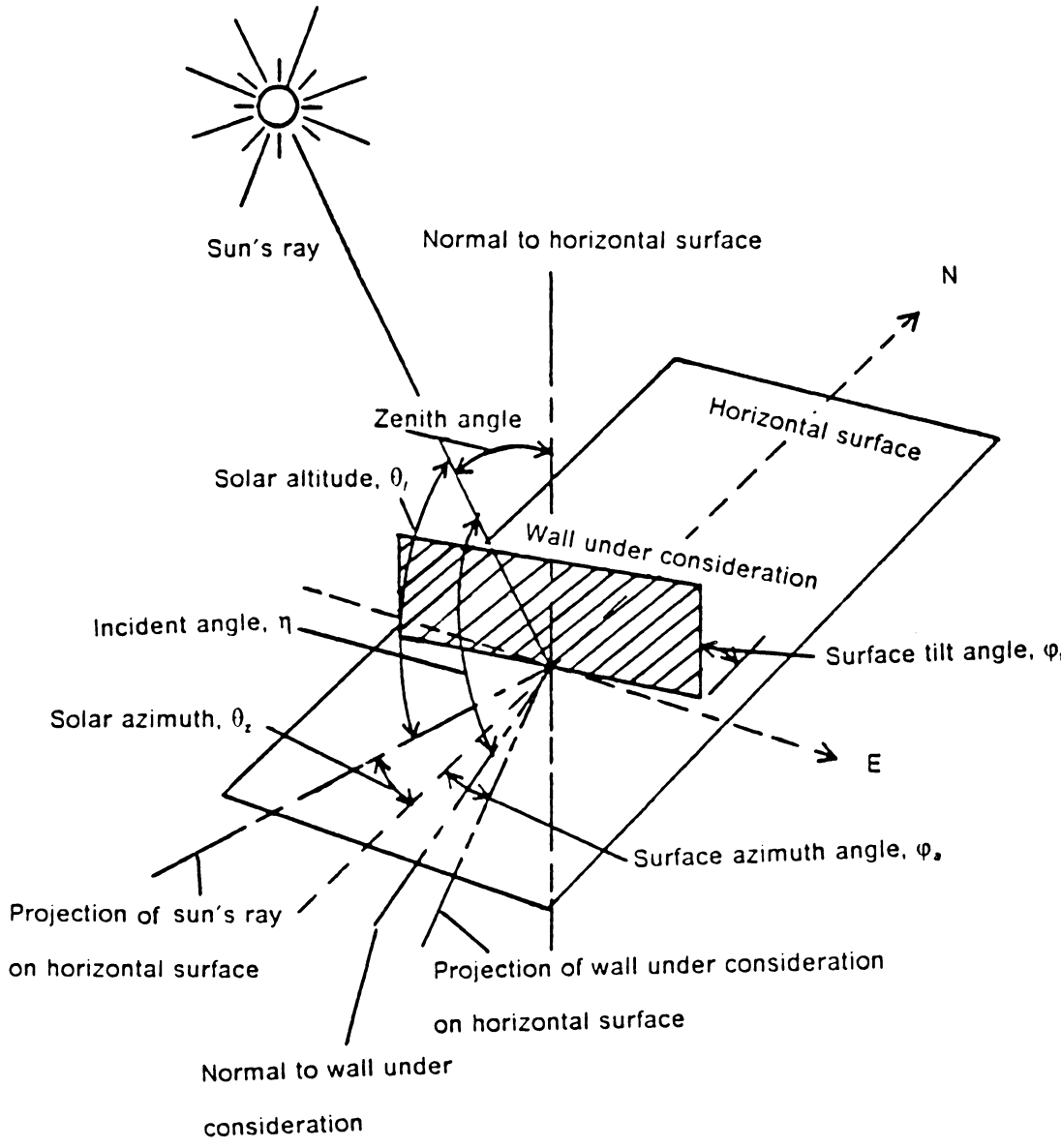

Figure 85. Definition of Solar Angles

$$N = INTEGER(\frac{\tau}{24})$$
$$t = \tau - 24N \qquad (D-1)$$

Therefore, the sunrise (t_{sr}) and sunset times (t_{ss}) , in hours, are

$$t_{sr} = 12 - Y - E_t - N_{tz} + \frac{L_o}{15}$$
$$t_{ss} = t_{sr} + 2Y \qquad (D-2)$$

where

$$Y = \frac{12\,h'}{\pi}$$
$$h' = \cos^{-1}[\, - tan(L_a)\, \tan(\delta)\,] \qquad (D-3)$$

In Tables 42 and 43, for the northern and southern hemisphere, respectively, the declination angle (δ, degrees), the equation of time (E_t, hours), the apparent solar constant (A, *Btu/hr ft²*), the atmospheric extinction coefficient (B, 1/air mass), and the sky diffuse factor (C, dimensionless) are presented.

The hour angle, h (radians), is

$$h = 15\,[\,t - 12 + N_{tz} + E_t\,] - L_o \qquad (D-4)$$

If $|h| > |h'|$, the remaining calculations are discontinued. The intensity of the direct, diffuse, and ground reflected radiation are set to zero. Since the actual time has surpassed the sunset time, solar related calculations are not needed. When solar loads are present, i.e., $|h| \leq |h'|$, the calculations of the direct, diffuse, and ground reflected radiations are obviously continued.

The direction cosines of the direct solar beam are

Table 42. Solar Variables, Northern Hemisphere

DATE	δ Degrees	E_t Hours	A *Btu/h*. ft	B 1/Air Mass	C
Jan. 21	-20.0	-0.190	390	0.142	0.058
Feb. 21	-10.8	-0.230	385	0.144	0.060
Mar. 21	0.0	-0.123	376	0.156	0.071
Apr. 21	11.6	0.020	360	0.180	0.097
May 21	20.0	0.060	350	0.196	0.121
June 21	23.4	-0.025	345	0.205	0.134
July 21	20.6	-0.103	344	0.207	0.136
Aug. 21	12.3	-0.051	351	0.201	0.122
Sept. 21	0.0	0.113	365	0.177	0.092
Oct. 21	-10.5	0.255	378	0.160	0.073
Nov. 21	-19.8	0.235	387	0.149	0.063
Dec. 21	-23.4	0.033	391	0.142	0.057

Table 43. Solar Variables, Southern Hemisphere

DATE	δ Degrees	E_t Hours	A *Btu/h.ft*	B 1/Air Mass	C
Jan. 21	-20.0	-0.190	390	0.207	0.136
Feb. 21	-10.8	-0.230	385	0.201	0.122
Mar. 21	0.0	-0.123	376	0.177	0.092
Apr. 21	11.6	0.020	360	0.160	0.073
May 21	20.0	0.060	350	0.149	0.063
June 21	23.4	-0.025	345	0.142	0.057
July 21	20.6	-0.103	344	0.142	0.058
Aug. 21	12.3	-0.051	351	0.144	0.060
Sept. 21	0.0	0.113	365	0.156	0.071
Oct. 21	-10.5	0.255	378	0.180	0.097
Nov. 21	-19.8	0.235	387	0.196	0.121
Dec. 21	-23.4	0.033	391	0.205	0.134

$$\begin{aligned} \cos(Z) &= \sin(L_a)\,\sin(\delta) + \cos(L_a)\,\cos(\delta)\,\cos(h) \\ \cos(W) &= \cos(\delta)\,\sin(h) \\ \cos(S) &= [1 - \cos^2(Z) - \cos^2(W)]^{1/2} \end{aligned} \qquad (D-5)$$

The sign for cos (S) is determined from the following conditions:

For $L_a \geq 0$

if $\cos(h) > [\frac{\tan(\delta)}{\tan(L_a)}]$, cos (S) is positive

if $\cos(h) \leq [\frac{\tan(\delta)}{\tan(L_a)}]$, cos (S) is negative.

For $L_a < 0$

if $\cos(h) > [\frac{\tan(\delta)}{\tan(L_a)}]$, cos (S) is negative.

if $\cos(h) \leq [\frac{\tan(\delta)}{\tan(L_a)}]$, cos (S) is positive

The solar altitude angle (radians) is

$$\theta_l = \sin^{-1}[\cos(Z)] \qquad (D-6)$$

and the solar azimuth angle (radians) is

$$\begin{aligned} \theta_z &= \sin^{-1}[\frac{\cos(W)}{\cos(\theta_l)}], & \cos(S) > 0 \\ \theta_z &= \pi - \sin^{-1}[\frac{\cos(W)}{\cos(\theta_l)}], & \cos(S) < 0 \end{aligned} \qquad (D-7)$$

The direct solar intensity for clear sky is

$$I_D = A\,C_n\,e^{[-B/\cos(Z)]} \qquad (D-8)$$

the diffuse sky radiation for a clear sky is

$$I_d = \frac{C\ I_D}{C_n^2} \qquad (D-9)$$

and the ground reflected radiation for a clear sky is

$$G_r = \rho_g [I_d + I_D \cos(Z)] \qquad (D-10)$$

The calculations of the overall incidence angles and direct, diffuse, and ground reflected intensities have been presented. Next, the above formulations are used to determine the solar loads (direct, diffuse, and ground reflected) on a given surface.

Defining φ_a (radians), as the Azimuth angle of a given surface measured from the south (+ if west of south and - if east of south) and φ_t (radians) as the Tilt angle measured from the horizontal surface (zero for the horizontal surface and $\pi/2$ for the vertical surface). The direction cosines of the normal to the surface under consideration are

$$\begin{aligned} \alpha &= \cos(\varphi_t) \\ \beta &= \sin(\varphi_a)\ \sin(\varphi_t) \\ \gamma &= \cos(\varphi_a)\ \sin(\varphi_t) \end{aligned} \qquad (D-11)$$

The cosine of the incident radiation on the surface is

$$\cos(\eta) = \alpha \cos(Z) + \beta \cos(W) + \gamma \cos(S) \qquad (D-12)$$

Therefore, the direct radiation on the surface is

$$\begin{aligned} I_{DS} &= I_D \cos(\eta) \qquad \cos(\eta) > 0 \\ I_{DS} &= 0 \qquad\qquad\ \cos(\eta) \leq 0 \end{aligned} \qquad (D-13)$$

The diffuse radiation is examined only for vertical and horizontal surfaces due to the lack of data for inclined surfaces. The diffuse radiation for a horizontal surface is

$$I_{ds} = I_d = \frac{C\,A}{C_n} e^{[-B/\cos(Z)]} \qquad (D-14)$$

and the diffuse radiation for a vertical surface is

$$I_{ds} = \kappa I_d + \frac{G_r}{2} \qquad (D-15)$$

Where

$$\begin{aligned} \lambda &= \cos(\eta) \\ IF \quad \lambda \leq -0.2 \quad & \kappa = 0.45 \\ IF \quad \lambda > -0.2 \quad & \kappa = 0.55 + 0.437\,\lambda + 0.313\,\lambda^2 \end{aligned} \qquad (D-16)$$

The diffuse radiation is known only for horizontal and vertical surfaces facing any direction. For tilted surfaces (i.e., $0 < \varphi_t < \pi/2$), the diffuse radiation is approximated between the two limits, horizontal and vertical.

Finally, the overall solar load on a given surface and a time step τ is

$$q_s(\tau) = I_{DS} + I_{ds} \qquad (D-17)$$

The solar load calculated in Eq. D-17 includes direct, diffuse, and ground reflected. It is obvious that for a horizontal surface, the ground reflected radiation is zero. The direct solar loads are calculated in terms of the surface location and tilt angles.

Window transmittance, absorptance, and reflectance are determined along with the solar load at every time step. The transmittance and reflectance for various extinction coefficients

of single- and double-pane windows are obtained from reference 98, expressed as polynomials of cos(η). Defining the following nomenclatures:

e_w = extinction coefficient of the window under consideration

Δx_w = thickness of the window under consideration, inches

$e_{l,w} = e_w \Delta x_w$

$\tau_{D,w}$ = window transmittance of direct solar radiation

$\tau_{d,w}$ = window transmittance of diffuse solar radiation

$\alpha_{D,w}$ = window absorptance of direct solar radiation

$\alpha_{d,w}$ = window absorptance of diffuse solar radiation

$\rho_{D,w}$ = window reflectance of direct solar radiation

$\rho_{d,w}$ = window reflectance of diffuse solar radiation

For single-pane windows, the transmittance and absorptance of direct solar radiation are, respectively

SINGLE – PANE WINDOWS

$$\tau_{D,w} = \sum_{j=1}^{6} B_j [\cos^j(\eta)] \qquad (D-18)$$

$$\alpha_{D,w} = \sum_{j=1}^{6} A_j [\cos^j(\eta)]$$

The transmittance and absorptance of diffuse radiation are, respectively

$$\tau_{d,w} = 2 \sum_{j=1}^{6} \left[\frac{B_j}{(j+2)}\right] \qquad (D-19)$$

$$\alpha_{d,w} = 2 \sum_{j=1}^{6} \left[\frac{B_j}{(j+2)}\right]$$

Coefficients A_j *and* B_j of Eqs. 18 and 19 are presented in Table 44. For double-pane windows, the transmittance and absorptance of the outer and inner pane of direct radiation are, respectively

Table 44. Window Coefficients, Single Glazed

$\varepsilon_{l,w}$	j	A_j	B_j
0.05 1/8" Sheet	1	0.01154	-0.00885
	2	0.77674	2.71235
	3	-3.94657	-0.62062
	4	8.57881	-7.07329
	5	-8.38135	9.75995
	6	3.01188	-3.89922
0.10	1	0.01636	-0.01114
	2	1.40783	2.39371
	3	-6.79030	0.42978
	4	14.37378	-8.98262
	5	-13.83357	11.51798
	6	4.92439	-4.52064
0.15 1/4" Reg. Plate	1	0.01837	-0.01200
	2	1.92497	2.13036
	3	-8.89134	1.13833
	4	18.40197	-10.07925
	5	-17.48648	12.44161
	6	6.17544	-4.83285
0.20	1	0.01902	-0.01218
	2	2.35417	1.90950
	3	-10.47151	1.61391
	4	21.24322	-10.64872
	5	-19.95978	12.83698
	6	6.99964	-4.95199

Table 44. (continued)

$\varepsilon_{l,w}$	j	A_j	B_j
0.40	1	0.01712	-0.01056
	2	3.50839	1.29711
	3	-13.86390	2.28615
	4	26.34330	-10.37132
	5	-23.84846	11.95884
	6	8.17372	-4.54880
0.60	1	0.01406	-0.00835
	2	4.15958	0.92766
	3	-15.06279	2.15721
	4	27.18492	-8.71429
	5	-23.88518	9.87152
	6	8.03650	-3.73328
0.80 50% Trans. H.A. Plate	1	0.01153	-0.00646
	2	4.55946	0.68256
	3	-15.43294	1.82449
	4	26.70568	-6.95325
	5	-22.87993	7.80647
	6	7.57795	-2.94454
1.00	1	0.00962	-0.00496
	2	4.81911	0.51403
	3	-15.47137	1.47607
	4	25.86516	-5.41985
	5	-21.69106	6.05546
	6	7.08714	-2.28162

DOUBLE – PANE WINDOWS

$$\tau_{D,w} = \sum_{j=1}^{6} C_j [\cos^j(\eta)]$$
$$\alpha_{D,o,w} = \sum_{j=1}^{6} D_{j,o} [\cos^j(\eta)] \qquad (D-20)$$
$$\alpha_{D,i,w} = \sum_{j=1}^{6} D_{j,i} [\cos^j(\eta)]$$

The transmittance and absorptance of the outer and inner pane of diffuse radiation are, respectively

$$\tau_{d,w} = 2 \sum_{j=1}^{6} \left[\frac{C_j}{(j+2)}\right]$$
$$\alpha_{d,o,w} = 2 \sum_{j=1}^{6} \left[\frac{D_{j,o}}{(j+2)}\right] \qquad (D-21)$$
$$\alpha_{d,i,w} = 2 \sum_{j=1}^{6} \left[\frac{D_{j,i}}{(j+2)}\right]$$

Coefficients C_j, $D_{j,o}$, *and* $D_{j,i}$ of Eqs. 20 and 21 are presented in Table 45. For double-pane windows

$$\alpha_{D,w} = \alpha_{D,o,w} + \alpha_{D,i,w}$$
$$\alpha_{d,w} = \alpha_{d,o,w} + \alpha_{d,i,w} \qquad (D-22)$$

The direct and diffuse solar loads, transmitted through the window to the room, are, respectively

$$q_{D,\tau} = S_a \, I_{DS} \, \tau_{D,w}$$
$$q_{d,\tau} = S_a \, I_{ds} \, \tau_{d,w} \qquad (D-23)$$

Table 45. Window Coefficients, Double Glased

$\varepsilon_{l,w}$	j	$D_{j,o}$	$D_{j,l}$	C_j
0.05 1/8″ Sheet	1	0.01407	0.00228	-0.00401
	2	1.06226	0.34559	0.74050
	3	-5.59131	-1.19908	7.20350
	4	12.15034	2.22366	-20.11763
	5	-11.78092	-2.05287	19.68824
	6	4.20070	0.72376	-6.74585
0.10	1	0.01819	0.00123	-0.00438
	2	1.86277	0.29788	0.57818
	3	-9.24831	-0.92256	7.42065
	4	19.49443	1.58171	-20.26848
	5	-18.56094	-1.40040	19.79706
	6	6.53940	0.48316	-6.79619
0.15 1/4″ Reg. Plate	1	0.01905	0.00067	-0.00428
	2	2.47900	0.26017	0.45797
	3	-11.74226	-0.72713	7.41367
	4	24.14037	1.14950	-19.92004
	5	-22.64299	-0.97138	19.40969
	6	7.89954	0.32705	-6.66603
0.20	1	0.01862	0.00035	-0.00401
	2	2.96400	0.22974	0.36698
	3	-13.48701	-0.58381	7.27324
	4	27.13020	0.84626	-19.29364
	5	-25.11877	-0.67666	18.75408
	6	8.68895	0.22102	-6.43968

Table 45. (continued)

$\varepsilon_{t,w}$	j	$D_{j,o}$	$D_{j,t}$	C_j
0.40	1	0.01423	-0.00009	-0.00279
	2	4.14384	0.15049	0.16468
	3	-16.66709	-0.27590	6.17715
	4	31.30484	0.25618	-15.84811
	5	-27.81955	-0.12919	15.28302
	6	9.36959	0.02859	-5.23666
0.60	1	0.01056	-0.00016	-0.00192
	2	4.71447	0.10579	0.08180
	3	-17.33454	-0.15035	4.94753
	4	30.91781	0.06487	-12.43481
	5	-26.63898	0.02759	11.92495
	6	8.79495	-0.02317	-4.07787
0.80 50% Trans. H.A. Plate	1	0.00819	-0.00015	-0.00136
	2	5.01768	0.07717	0.04419
	3	-17.21228	-0.09059	3.87529
	4	29.46388	0.00050	-9.59069
	5	-24.76915	0.06711	9.16022
	6	8.05040	-0.03394	-3.12776
1.00	1	0.00670	-0.00012	-0.00098
	2	5.18781	0.05746	0.02576
	3	-16.84820	-0.05878	3.00400
	4	27.90292	-0.01855	-7.33834
	5	-22.99619	0.06837	6.98747
	6	7.38140	-0.03191	-2.38328

where S_a is the sunlight area factor (for full shaded areas $S_a = 0.0$ and for full lighted areas $S_a = 1.0$).

APPENDIX E INFILTRATION LOAD

The following infiltration model was recommended by the ASHRAE task group on energy calculations [98]. Infiltration through an opening is expressed as:

$$Q_{i,A} = C\Delta P^{N} \qquad (E-1)$$

with $Q_{i,A}$ *in* ft^3, C is dimensionless, N is dimensionless, and ΔP in inches of water. C and N for typical windows, doors, and walls are given in Table 46 (some values of C are per unit crack area or length). The principle of conservation of mass is applied on every room in order to obtain an expression relating the pressure of that room to its surrounding pressures. Equations equalling the number of rooms in the building are obtained and solved simultaneously for the individual pressures. Equation E-1 is used to calculated the infiltration to each zone.

Applying the law of conservation of mass to room j,

$$\sum_{k=1}^{4} Q_{k,j,f} + Q_{s,j,f} - Q_{e,j,f} = 0 \qquad (E-2)$$

Table 46. Window Coefficients In Infiltration Calculations

DISCRIPTION	C	N
Double-hung wooden windows (locked)		
non-weatherstripped loose fit	6	0.66
average fit	2	0.66
weatherstripped loose fit	2	0.66
average fit	1	0.66
Window frames (per ft of linear crack length)		
masonry frame with no caulking	1.2	0.66
masonry frame with caulking	0.2	0.66
wooden frame	1	0.66
swinging doors (per unit area of wall surface)		
1/2 inch crack	160	0.5
1/4 inch crack	80	0.5
1/8 inch crack	40	0.5
Walls (per unit area of wall surface)		
8″ plain brick	1	0.8
8″ brick and plaster	0.01	0.8
13″ brick	0.8	0.8
13″ brick and plaster	0.004	0.7
13″ brick, furring, lath and plaster	0.03	0.9
frame wall, lath and plaster	0.01	0.55
24″ shingles on 1x6 boards on 14″ center	9	0.66
16″ shingles on 1x4 boards on 5″ center	5	0.66
24″ shingles on shiplap	3.6	0.7
16″ shingles on shiplap	1.2	0.66

where $Q_{k,j,f}$ is the infiltration from side k of the rooms, $Q_{s,j,f}$ is the air supplied, and $Q_{e,j,f}$ is the air returned from the room. Pressures outside the envelope of the building are determined next.

Two factors affect the pressure on the outside of buildings: wind and stack. The wind is characterized by its speed and direction. the stack is characterized by the difference of heights between two locations at different heights. Defining the following parameters:

V = wind speed measured at a 40 ft elevation, knots

α = wind direction measured clockwise from the north, degrees

β_k = surface direction measured clockwise from the north to the normal of the outside wall k, degrees

k = outside wall number. Designated numbers k=1, 2, 3 and 4 correspond to the north, south, east and west exterior wall of the building under consideration, respectively.

T_o = outside air temperature, F

$T_{r,j,f}$ = outside air temperature, F

f = floor location (f=1, first floor, ...)

P_b = barometric pressure, in Hg.

y_b = total height of the building, ft

y = floor height of the building, ft

$Q_{s,j,f}$ = supplied ventilation to zone j at floor f, ft^3

$Q_{e,j,f}$ = exhausted ventilation from zone j at floor f, ft^3

Changing units of the wind speed (knots to miles/hr), inside and outside temperatures (F to R), and the barometric pressure (in of Hg to psi),

$$\begin{aligned} V &= 1.153\,V \\ T_{r,j,f} &= T_{r,j,f} + 460.0 \\ T_o &= T_o + 460.0 \\ P_b &= 0.491\,P_b \end{aligned} \qquad (E-3)$$

The difference between the wind direction and the normal of the exterior surface of wall k is expressed as x_k:

$$x_k = \alpha - \beta_k \qquad (E-4)$$

where

x_k = 0, the wind is perpendicular to wall k (windward side).

x_k = 90 or 270, the wind is parallel to wall k (wind side).

x_k = 180, the wind is on the opposite side of wall k (leeward side).

The wind speed at the height of the building is

$$V(y) = 0.117\, V\,[1 + 2.81\ \ln(0.305\, y + 4.75)] \qquad (E-5)$$

The theoretical wind pressure on the outside surface of a building is

$$P_W(y) = 0.000482\,[V^2(y)] \qquad (E-6)$$

The wind pressure correction factor is introduced to correct the theoretical pressure to the actual pressure, taking into consideration the wind effect.

If wall k is on the windward side, $D_{w,k} = 1$

$$-45^\circ < x_k < 45^\circ$$

If wall k is on the leeward side, $D_{w,k} = 2$

$$90^\circ < x_k < 270^\circ$$

$$\text{or, } -90^\circ < x_k < -270^\circ$$

If wall k is on the wind side, $D_{w,k} = 3$

$$45^\circ < x_k < 90^\circ$$

$$\text{or, } -45^\circ < x_k < -90^\circ$$

The wind pressure correction factor is

$$
\begin{aligned}
D_{w,k} &= 1 \qquad P_{w,c}(k) = \cos\,(\,|x|\,) \\
D_{w,k} &= 2 \qquad P_{w,c}(k) = 1.0 \\
D_{w,k} &= 3 \qquad P_{w,c}(k) = \cos\,(\,|x|\,)
\end{aligned}
\qquad (E-7)
$$

The normal wind velocity pressure correction factor, $P_{w,n}(k)$, is given in Table 47. Therefore, the actual wind pressure on the wall under consideration is

$$P_{w,a}(k,y) = P_{w,n}(k)\, P_{w,c}(k)\, P_W(y) \qquad (E-8)$$

The stack effect pressure on the outside of the building at floor f is

$$P_s(y) = \frac{-0.52\, y\, P_b\, P_W(y)}{T_o} \qquad (E-9)$$

The total pressure on the outside surface of wall k at floor f is

$$P_t(k,y) = P_s(y) + P_{w,a}(k,y) \qquad (E-10)$$

The outside pressures are calculated at every floor level (y) on every side of the building (k). The inside room pressures are unknown. To determine their values, Eq. E-2 (mass balance) is used for each room to obtain an expression for its pressure in terms of the adjacent rooms' pressures. By solving this set of nonlinear equations iteratively, the pressures of all rooms are determined. Finally, Eq. E-1 is used for every wall and closed window and door to determine the infiltration from each room to the outside or an adjacent room. For a typical room, no infiltration through the ceiling, floor, or interior walls is present. The remaining infiltration sources are cracks in window frames, exterior walls, and gaps under closed doors. Convective heat transfer through large interior openings (doors, windows, and hallways) is determined as given in Chapter 5. Expanding Eq. E-2

Table 47. Pressure Correction Factors

$N_{s,b}$	$D_{w,k} = 1$	$D_{w,k} = 2$	$D_{w,k} = 3$
0.5	0.1	-0.3	-0.8
1.0	-0.1	-0.25	-0.5
2.0	0.1	-0.25	-0.4
3.0	0.1	-0.25	-0.4
5.0	0.25	-0.35	-0.6
∞	0.6	-0.35	-0.7

$N_{s,b}$	$D_{w,k} = 1$	$D_{w,k} = 2$	$D_{w,k} = 3$
0.5	-0.5	-0.25	-0.45
1.0	-0.5	-0.2	-0.3
2.0	0.0	-0.2	-0.3
3.0	0.1	-0.2	-0.35
5.0	0.25	-0.25	-0.45
∞	0.6	-0.35	-0.7

$N_{s,b}$	$D_{w,k} = 1$	$D_{w,k} = 2$	$D_{w,k} = 3$
0.5	0.5	0.45	0.45
1.0	0.45	0.3	0.3
2.0	0.45	0.1	0.1
3.0	0.45	0.0	0.0
5.0	0.5	-0.1	-0.1
∞	0.6	-0.35	-0.7

$$Q_{1,j,f} + Q_{2,j,f} + Q_{3,j,f} + Q_{4,j,f} + Q_{s,j,f} - Q_{e,j,f} = 0 \quad (E-11)$$

Substituting for the pressure expressions

$$C_1[P_1 - P_{j,f}]^{N_1} + C_2[P_2 - P_{j,f}]^{N_2} + C_3[P_3 - P_{j,f}]^{N_3} + C_4[P_4 - P_{j,f}]^{N_4} + Q_{s,j,f} - Q_{e,j,f} = 0 \quad (E-12)$$

In Eq. E-12, P_1 through P_4 are the pressures on the opposite four sides of the room. Equation E-12 is applied for every room in the building and the resulting system of nonlinear equations is solved iteratively for the room pressures. The infiltration rate to room j on floor f is

$$Q_{r,j,f} = Q_{1,j,f} + Q_{2,j,f} + Q_{3,j,f} + Q_{4,j,f} + Q_{s,j,f} - Q_{e,j,f} \quad (E-13)$$

where

$$\begin{aligned} Q_{1,j,f} &= C_1[P_1 - P_{j,f}]^{N_1} \\ Q_{2,j,f} &= C_2[P_2 - P_{j,f}]^{N_2} \\ Q_{3,j,f} &= C_3[P_3 - P_{j,f}]^{N_3} \\ Q_{4,j,f} &= C_4[P_4 - P_{j,f}]^{N_4} \end{aligned} \quad (E-14)$$

The infiltration load to this room at every time step τ is

$$\begin{aligned} Q_{i,j,f}(\tau) = {} & Q_{1,j,f}[T_1(\tau) - T_{r,j,f}(\tau)] + Q_{2,j,f}[T_2(\tau) - T_{r,j,f}(\tau)] \\ & + Q_{3,j,f}[T_3(\tau) - T_{r,j,f}(\tau)] + Q_{4,j,f}[T_4(\tau) - T_{r,j,f}(\tau)] \\ & + Q_{s,j,f}[T_s(\tau) - T_{r,j,f}(\tau)] + Q_{e,j,f}[T_{r,j,f}(\tau) - T_e(\tau)] \end{aligned} \quad (E-15)$$

APPENDIX F MRT METHOD

The Mean Radiative Temperature (MRT) method for calculating view factors between interior surfaces of rooms in buildings was developed by Carroll [100, 101]. The MRT view factor is calculated using a fictitious mean radiative temperature node located in the center of the network as shown in Fig. 86. Each boundary node in Fig. 86 represents an interior surface. The MRT node acts as a clearinghouse for all radiative interchanges in the room. That is, every surface emits all radiation to this node and are distributed by this node to the other surfaces. The MRT view factor of each surface i is calculated iteratively using the following equation:

$$F_i = \frac{1}{(1 - \frac{A_i F_i}{\sum_{k=1}^{6} A_k F_k})} \qquad (F - 1)$$

For example, F_1 is determined iteratively from the following equation:

$$F_1 = \frac{1}{(1 - \frac{A_1 F_1}{A_1 F_1 + A_2 F_2 + A_3 F_3 + A_4 F_4 + A_5 F_5 + A_6 F_6})} \qquad (F - 2)$$

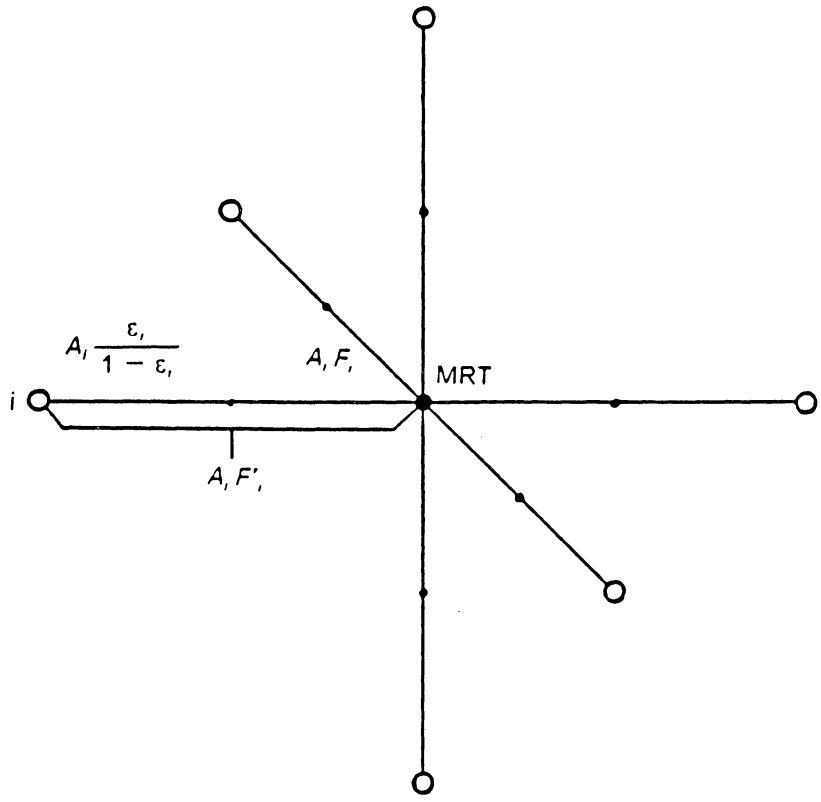

Figure 86. MRT Network for a Gray Surface

The effect of the surface emissivity is included in the MRT configuration factors by adding Oppenheim's surface resistance,

$$F'_i = \frac{1}{\left[\frac{1}{F_i} + \frac{(1 - e_i)}{e_i}\right]} \qquad (F - 3)$$

dissolving the MRT in a Y-Δ transformation to find the corresponding reciprocity relation, leads to

$$A_i F'_{ij} = \frac{A_i F'_i \; A_j F'_j}{\sum_{k=1}^{6} A_k F'_k} \qquad (F - 4)$$

The vita has been removed from the scanned document